University of Bristol

Variable Structure Control for Power Electronics

Limitations in the structured construction of sliding mode controllers

Author:

Georgios Kafanas
Department of Electrical and Electronic Engineering, University of Bristol

A dissertation submitted to the University of Bristol in accordance with the requirements of the degree of Doctor of Philosophy in the Faculty of Engineering.

October 7, 2019

Word count: 27400

Author's declaration

I declare that the work in this dissertation was carried out in accordance with the requirements of the University's Regulations and Code of Practice for Research Degree Programmes and that it has not been submitted for any other academic award. Except where indicated by specific reference in the text, the work is the candidate's own work. Work done in collaboration with, or with the assistance of, others, is indicated as such. Any views expressed in the dissertation are those of the author.

SIGNED: ..... DATE: .....

Acknowledgments

I would like to express my gratitude to my supervisors Dr Mike Jeffrey and Dr Xibo Yuan who have supported, encouraged, and coached me during my time as a PhD student. Under their supervision my time in the EEMG lab and research visits organized by the BCCS helped my develop as a researcher. I am also grateful to Sam Walder, Sam Williamson, Jeremy Dalton, Joanne Kitson, Appolo Charalampous, and all the students of the EEMG lab. I have learned a great deal from them through engaging conversations, and due to their practical knowledge and the excellent environment they cultivate in the EEMG lab.

I would also like to acknowledge the help of all the stuff of the BCCS and the EEMG. I would particularly like to thank Rich Walker, Enea Colleoni, Matthew Guppy, and Sophie Bennoit for their support and advice on administrative matters, and Steve Roome whose expertise in scientific computing has been instrumental in completing my research.

I could not have completed this thesis without the continued support of my family and friends. My mother, father, and sister have been an inexhaustible source of support during my PhD which I appreciate deeply. I am also deeply grateful to my friends Sofia, Kallia, Nikos, and Dimitris whose attitude has been a great source of inspiration and energy for me.

Abstract

This thesis analyzes the effects of the motion in the boundary layer of some sliding surfaces in the performance of sliding mode controllers for power electronic converters. In converters with multiple inputs and multiple internal states a sliding mode controller stabilizing the system imposes sliding on a manifold residing in the intersection of multiple switching surfaces. Systems sliding in the intersection of multiple surfaces can exhibit jitter, a phenomenon which causes abrupt changes in the sliding speed along the sliding manifold. But even in a system with a single sliding surface there can be distortion in the motion in the sliding layer due to unmodeled dynamics. Time delays introduced by sensors were reported to distort the motion in the boundary layer resulting in steady state drift and excessive ripple. Two converters were instigated to determine the effects of the motion in the sliding layer in the dynamics of the controlled system.

A sliding mode controller was designed for the voltage fed trans-Z-source DC-DC converter that can stabilize the full state of the system. The controller operates by imposing sliding in the intersection of two surfaces. Jitter was observed in the sliding motion for some hysteresis switching controllers. Two switching manifolds where tested. The dynamics on the sliding mode were found to be affected significantly by the selection of the switching manifold and the switching logic. An extended convex hull was used to describe the range of dynamical behaviors that can be expected for any switching manifold used to implement the sliding mode of the trans-Z-source converter.

To investigate the effects of the sensors on the motion in the sliding layer, a buck converter with sensors was analyzed. A model representing the sensors of power converters as first order integrators was used to model the non-ideal behavior of the sensors. The sliding mode in the resulting dynamics is proven to be unstable. Time domain simulations reveal a limit cycle that appears in steady state operation. A relation between the quality of the sensors and ripple in steady state operation is determined numerically. This relation allows for a less conservative selection of the sensors of the converter.

Many new methods are being developed for the design of sliding mode controllers. Applying the resulting controllers in power electronic converters requires a careful design of the switching algorithm. In converters with multiple switched inputs, a careful design of the switching surface and the switching logic can improve the performance of the controlled system. Unmodeled dynamical behavior such as the dynamics of sensors can also affect the performance of the converter significantly. Numerical simulations are a useful tool for detecting the viable designs with respect to the range of acceptable unmodeled behavior.

Contents

List of Figures

List of Tables

List of Algorithms

List of Symbols

$D_t x$	The derivative of the variable x with respect to the variable t.
$\partial_x v$	The partial derivative of the variable v with respect to the variable x.
$A \to B$	The set of functions from the set A to the set B.
$A \nrightarrow B$	The set of partial functions from the set A to the set B.
$f : A \to B$	A function from the set A to the set B.
$f : A \nrightarrow B$	A partial function from the set A to the set B.
∂A	The boundary of the set A.
A°	The interior of the set A.
$\|x\|$	The euclidean norm, defined for $x \in \mathbb{R}^n$ as $\|x\| = (x^T \cdot x)^{\frac{1}{2}}$.

Chapter 1

Introduction

Improvements in the performance of power converters facilitated their use in an extensive range of applications. New topologies are being developed constantly in an effort to improve performance. However, the dynamics of a new family of topologies, the impedance source converters, significantly complicate the design of the converter controller. Sliding mode controllers with their ability to reject any disturbance outside the sliding surface and their order reduction property provide significant advantages when used in impedance source converters in terms of performance and simplicity in the design and analysis.

The aim of this thesis is to design a sliding mode controller for an impedance source converter. Sliding mode controllers for impedance source converters work by imposing sliding in the intersection of multiple sliding surfaces. An algorithm is proposed in this thesis which given some control objectives in the form of invariant surfaces it constructs the switching function enforcing the invariants within finite time. The methods is applied in the design of a sliding mode controller for the voltage fed trans-Z-source DC-DC converter. However, in impedance source converters the dynamics of the control system are sensitive to the modulation algorithm.

When a system slides in the intersection of multiple surfaces, the motion of the system in the boundary layer of the sliding surface determines the sliding speed. The dynamics in the directions perpendicular to the sliding surface operate in much faster time scale as the boundary layer vanishes. In the limit, the instantaneous sliding speed for any point in the sliding surface is determined by the limiting behavior of the boundary layer dynamics. In some systems bifurcations in the dynamics of boundary layer motion cause abrupt variations to the sliding speed as the system moves along the sliding surface, a phenomenon called jitter. In this thesis it is proven that impedance source converters satisfy the necessary conditions for jitter to appear in the sliding motion. Numerical simulations where used to study this behavior in a practical converter design. To our knowledge this is the first time that jitter was demonstrated in a practical power electronic circuit.

The sliding mode controlled trans-Z-source converter displays jitter for various hysteresis modulation algorithms. For hysteresis modulated converters, the boundary layer is formed by the hysteresis zone. Switching based of two co-dimension one surfaces, and one co-dimension surface was investigated for enforcing the sliding mode. Numerical simulations demonstrate that it is possible to stabilize the trans-Z-source converter using both hysteresis modulation approaches, but some steady state drift is introduced due to the variation in the sliding speed

caused by the jitter. More sophisticated switching algorithms could potentially control the variation in the sliding speed as well, but such a control would require an analysis of the speed in the boundary layer beyond within boundary layer of finite size.

The numerical analysis of the boundary layer dynamics is a potent tool in explaining deviations from the expected behavior on the sliding mode. The dynamics in the hysteresis region are significantly affected by non-ideal dynamics such as delays in the sensors. The numerical analysis framework for modeling the dynamics in the sliding layer is extended to model the dynamics of electrical sensors, and to determine their effect on the steady state ripple of a buck converter. The resulting framework is more computationally intensive than analytical approaches, but it offers a detailed range of admissible sensor performance in applications where direct measurement is impossible, such electrically isolated converters.

1.1 Power electronics converters

Power electronic converters are used in a range of applications to precisely regulate the energy flow in electric devices. Electronic loads in particular depend on converters for power delivery. With power converters becoming more reliable, electronics replace conventional devices improving efficiency and reliability. A typical example is LED lamps which are replacing incandescent and florescent lamps [1]. The accurate power delivery of power electronic converters is also exploited in driving more conventional grid connected loads such as motors in order to improve the overall efficiency of the system. Off-grid traction applications, such as electric and hybrid cars, rely on power converters for charging batteries and controlling electric motors [2]. Furthermore, power converters are playing an increasingly important role in the grid in recent years. In distributed energy generation converters are used to interface electrical energy sources with the grid [3]–[5] and regulate the power extraction [6]–[11]. In the power system itself converters are used to move power over long distances through high voltage direct current systems [12], and in the transmission and distribution grid nodes to regulate the power flow [13].

Performance improvements achieved through the development of new topologies, passive elements, and semiconductor devices are facilitating the increasingly widespread use of converters. The introduction of wide band-gap semiconductor switches [14], [15] enabled higher switching frequencies by reducing switching losses, and lead to more compact and efficient converter designs [16]. Optimization methods applied in the design of the passive elements of the converter [17]–[20] and the packing of the semiconductor switches [21], improve thermal performance and thus allow for further size reductions. To fully exploit the improvements in individual passive components however, new topologies are required.

1.2 Advances in converter topologies and impedance source networks

New topologies typically extend conventional designs such as the buck, boost, and buck boost converters for DC-DC conversion, or the voltage and current source converters for DC-AC conversion, and can be broadly classified into two design approaches according to the method

used to extend the conventional conversion cells. Multilevel designs increase the number of available network configuration by increasing the number of switches. The design are derived by iteratively merging basic cells [22], or combining them in a modular manner such as the modular multilevel converter [23] and its various extensions [24]. By increasing the number of output states multilevel designs allow a finer control of the output which reduces noise and overcomes limitations of components, such as the maximum blocking voltage of semiconductor switches and capacitors [25]. On the other hand, impedance source designs use networks of passive elements within each individual cell in order to extend the range of possible dynamical responses achievable by a given set of configuration for the switches [26]. The two approaches are also combined in modular topologies with cell containing impedance networks [27], [28].

The rich dynamics of the impedance networks have been exploited in a variety of applications [29]–[31]. A typical example is DC-AC power conversion, depicted in fig. 1.1. The conventional voltage source topology cannot boost the voltage of the source, requiring a DC-DC boost converter stage when the voltage gain in its output is greater than one. The Z-source converter has a theoretically infinite range of voltage gains thus eliminating the DC-DC stage [26]. This reduction in conversion stages reduces the number of active switching elements and has the potential to simplify the design. However, the dynamics of the impedance network often complicate the design of the controller and thus reduce the benefit form using an impedance network in simplifying the overall design of the converter.

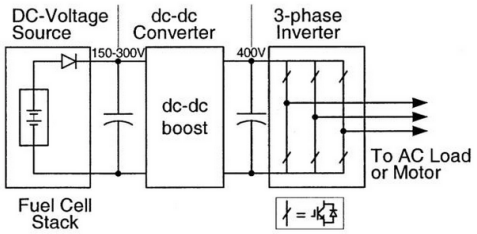

(a) Back to back converters

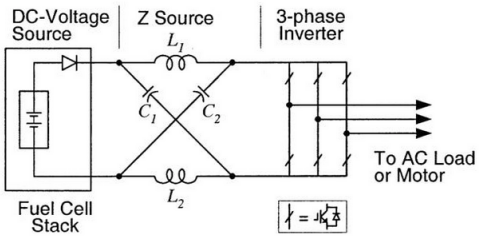

(b) Z-source converter

Figure 1.1: An application of impedance source converters in power inversion (images from [26]). Conventional voltage source inverters cannot boost the voltage of the source, requiring a DC-DC inverter. A Z-source converter boost the voltage internally, reducing the number of conversion stages and the number of active switches.

1.3 The optimal control design problem in power electronics and sliding modes

The design of a converter and its controller is a constrained optimal design problem with multiple objectives [32]. Models of the electrical, magnetic, and thermal dynamical behaviors are used to capture all the aspects of the converter performance that are relevant to the design requirements [32]–[34]. When there are weak interactions between a set of components, their design is decoupled into independent sub-problems to improve the solver efficiency [35]–[39]. Problems with convex objective and constraint functions are solved efficiently by convex optimization algorithms [40], [41]. For the majority of problems however, heuristic methods are required to derive good solutions efficiently.

Various heuristic optimization methods are applied in the design of power electronics depending on the requirements of the problem. Methods such as pattern search [41] and Tabu search [42] are used to reduce the number of times computationally expensive performance objectives or constraints are evaluated. Genetic algorithms have been used in problems with non-smoothly varying performance measures, such as the optimization of designs with discrete choices [43]. Logic and relational leaning algorithms, are applied in non-smooth problems as well [44]–[50]. By restricting the search space to set of designs that can be constructed according to a set of rules, these algorithms trade some of the potential performance of the resulting converter design for providing better control over the design process. The search for the optimal solution can be directed to designs that are expected to perform well, by encoding background knowledge in the search rules.

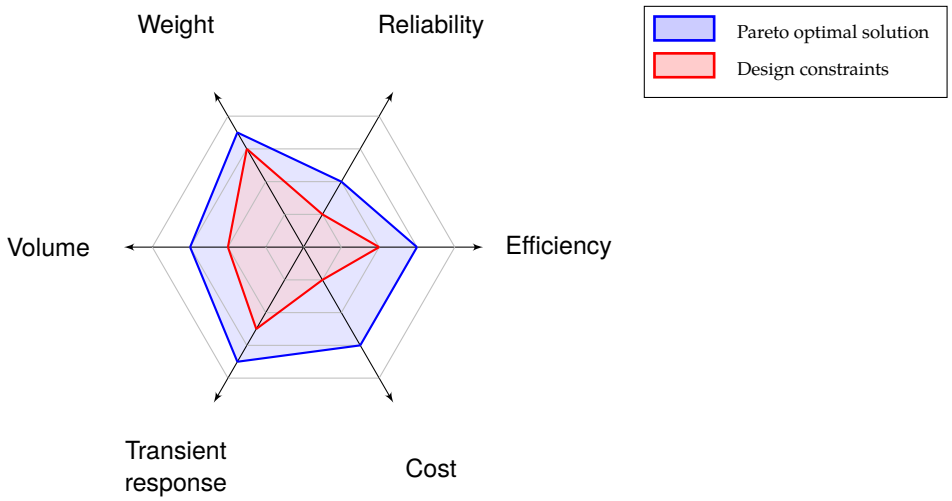

Figure 1.2: Typical objective functions of the constraint optimal control design problem in power electronics. The optimal performance with respect to each objective function defines a Pareto front. Furthermore, there are often constraints in the minimum acceptable performance which define a set of performance requirements that the converter must satisfy simultaneously.

Quite often in the design of power electronics there are constraints or objective functions which are linked to the dynamical behavior of the converter and thus require the optimization of the transient response of the controller. The transient response of the converter is optimized in harmonic filtering of the line [51], [52] or in active power filtering of the DC-bus [53]. Most

design approaches in this case simply ensure the local stability of the generated solution by tuning the gains of a fixed linear controller [41], [49]. However, strict specification for the transient response of the controller require the solution of a constraint optimal control design problem, whose solution is in general computationally difficult [54]. In some applications of linear controllers, such as shunt harmonic filtering, the optimal control problem can be solved analytically [51], [52]. In most cases though time domain simulations of the circuit are required [54], [55] which are computationally expensive.

Sliding mode controllers can significantly simplify the controller design in the new impedance source topologies. Sliding mode controllers are completely determined by the selection of the sliding surface, and the global behavior of the controlled converter is captured by the dynamics on the sliding mode [56]. When using sliding surfaces from a parametrized family, the design of the sliding controller is simplified significantly and involves optimizing a few parameters in order to select the optimal sliding surface, and a large range of control responses can be achieved by relatively few parameters. The transient response of sliding mode control algorithms solving the tracking problem are optimized in [57] using a genetic optimization algorithm, and in [58], [59] using particle swarm optimization.

A sliding mode controller design for impedance source converters can therefore allow the application of similar methods to impedance source converters. Constraint optimal control design algorithms are used to construct controllers achieving the theoretically optimal performance of a topology. Exploring the performance limits of new topologies is more challenging due to their dynamical behavior, but it is necessary to prove their performance advantages over conventional design. Due to the many efficient optimization algorithms that have been developed for sliding mode controllers, these controllers are a promising tool for constructing efficient impedance source converter designs. However, the classes of sliding mode controllers that have been developed for impedance source converters cannot be optimized with the existing tools.

1.4 Sliding mode control for impedance source converters

The sliding mode controllers that have been developed for impedance source converters impose sliding either on the state of the impedance network or the converter output, but not both. A sliding mode controller developed in [60] uses hysteresis modulation for the output current, and energy transfer states are inserted in the zero states of the hysteresis modulation according to a pulse width modulated signal. Conversely, in [61] and [62] sliding mode controllers are used for the impedance network and active states are inserted in the zero states of the modulation of the impedance network. In [63] and [64] integral sliding mode controllers are introduced for the impedance network that ensure asymptotic convergence to the sliding surface, and can be implemented with any pulse width modulation. The integral sliding mode is thus combined with an averaged controller for the output of the converter, and the switching signal is generated by any pulse width modulation scheme for impedance source converters [28], [65]–[71].

Optimization algorithms for sliding mode controllers however require all the control objectives to be enforced by a sliding surface. Hysteresis modulation can enforce sliding on multiple surfaces, and furthermore ensure finite time convergence to the sliding surface. Imposing a constraint that couples the state of the impedance network with the output of the converter, a sliding

mode controller for the full system is constructed in [72]. However this controller is limited, as it cannot be used in applications such as active power filtering that require independent control of the impedance network from the converter output. Two independent switching surfaces are required for an impedance source converter to decouple the input and output voltages. With hysteresis modulation, the modulation of the two surfaces interfere, and a careful selection of the surfaces is required to ensure that the system converges to the intersection in finite time.

1.5 Main aims and objectives

The aim of this thesis is the design and simulation of a sliding mode controller for an impedance source converter regulating both the output and the state of the impedance network. Current approaches for the sliding mode control of impedance source converters are effectively hybrid approaches, combining a sliding mode with averaged controllers. The sliding mode controller proposed in this thesis uses a sliding surface for each control objective, thus ensuring the benefits of sliding modes such as finite time convergence to an invariant manifold and the rejection of all unmatched disturbances outside the invariant manifold.

For simplicity the control of a DC-DC converter is considered, where the control objective is the stabilization of the state of the converter to a predetermined value. To design the controller a sliding surface is first constructed so that the desired steady state is a fixed point of the resulting sliding motion. Then, a method for selecting the switching surfaces that impose stable sliding in the desired manifold is developed. Due to the convergence of the state of the system on the sliding surface, the motion of the controlled system is of reduced order. To determine the performance of resulting controller the sliding dynamics are determined. The ideal response of the system is determined by a closed form solution, but the dynamics in practical implementations are difficult to evaluate due to dynamical phenomena in the boundary layer of the sliding motion.

In systems that slide on the intersection of multiple sliding surfaces, the sliding speed is determined by dynamics in the boundary layer. The minimal convex hull theorem that describes the range of possible dynamical behaviors in the sliding mode predicts a range of possible sliding speeds. In implementations of the sliding mode based on hysteresis modulation, the sliding speed is determined by the dynamics in this boundary layer. To ensure that the designed sliding mode dynamics successfully stabilize the system at the required state, the effects of the boundary layer motion steady state drift in the sliding dynamics are quantified numerically.

Non-models dynamics can also have significant effects in the boundary layer motion. In some applications such as electrically isolated converters, it is difficult to use observers to counteract the effects of the sensors. Numerical methods can be extended to model parasitic dynamics of components such as sensors in order to evaluate their effect in the steady state drift. To demonstrate the effectiveness of numerical methods in evaluating the sliding vector field in systems with complex dynamics in the boundary layer, a method is developed to determine the admissible range of admissible sensor dynamics for a given steady state deviation in a buck converter.

1.6 Challenges in designing a hysteresis modulated sliding mode controller for impedance source converters

The non-linearity of the impedance source converters with respects to their control input complicates the hysteresis modulation of these topologies. When a system slides on the intersection of a number of sliding surfaces, the convex hull method [73], [74] determines the dynamics of sliding motion based on the full order dynamics of the system in some boundary layer around the sliding manifold. The dynamics of the sliding motion are not always unique. Sliding can be enforced by various control algorithms, and for the input of each algorithm a unique solution for the sliding dynamics arises.

The effects of the ambiguity in the sliding dynamics are captured in a number of phenomena described in the literature. In the sliding mode control of dynamical systems with continuous control inputs, ambiguous sliding dynamics can appear in planar systems when the control inputs are non-linear. The planar system

$$\begin{cases} D_t x_1 = 0.3x_2 + ux_1, & \text{(1.6.1a)} \\ D_t x_2 = -0.7x_2 + 4u^3 x_1, & \text{(1.6.1b)} \end{cases}$$

with a continuous control input u introduced in [56], demonstrates opposite sliding dynamics on the same sliding surface depending on the control input that enforces sliding, as depicted in fig. 1.3. More pertinent to power electronics where the control inputs are discrete, convex hulls resulting in multiple solutions for the sliding dynamics appear in systems of three-dimensions or more that are non-linear with respect to a discontinuous control input. An example is the system introduced in [74, §1.2],

$$\begin{cases} D_t x_1 = 1 - 2u_1, & \text{(1.6.2a)} \\ D_t x_2 = 1 - 2u_2, & \text{(1.6.2b)} \\ D_t x_3 = (1 - 2u_1)(1 - 2u_2), & \text{(1.6.2c)} \end{cases}$$

with switching surfaces

$$H_1 = x_1, \qquad H_2 = x_2, \qquad \text{(1.6.3)}$$

and discrete control input $u \in \{0, 1\} \times \{0, 1\}$. The convex hull for of the hysteresis modulated dynamics has a non-unique intersection with the sliding manifold line $H = 0$ as depicted in fig. 1.4. The resulting dynamics on the sliding mode depend on the exact implementation of the hysteresis modulation.

In hysteresis modulation the hysteresis boundaries form a layer around the sliding manifold where the systems state is constrained when the system is sliding. Inside this hysteresis layer the motion of the system converges to some attractor with respect to dimensions perpendicular to the sliding manifold, and the projection of this attractor in the full space determines the sliding speed. The motion of a system in the intersection of multiple hysteresis layers was studied in [75], where it was demonstrated that there is always a unique attracting limit cycle in the projected dynamics of the system as the size of the hysteresis layers tends to zero. The sliding speed in

systems with hysteresis modulation depends on the limit cycle that appears in the hysteresis region. In systems such as systems that slide on a surface of co-dimension one, the sliding solution is unique and the limit cycle in the hysteresis region can be easily constructed. When the sliding solution is not unique however, the limit cycle can only be detected by numerical simulation.

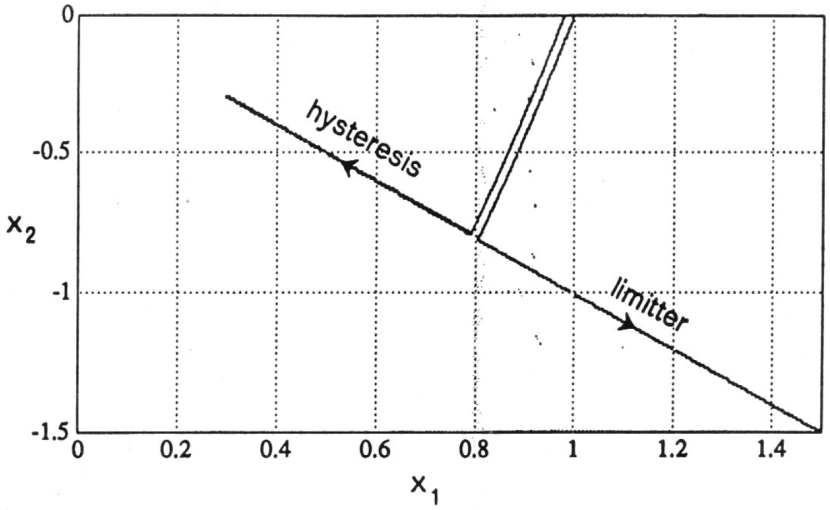

Figure 1.3: The sliding dynamics of the system in relation (1.6.1), where the control input is continuous, demonstrate a qualitatively different behavior depending on the implementation of the control input that enforces sliding. Image taken from [56].

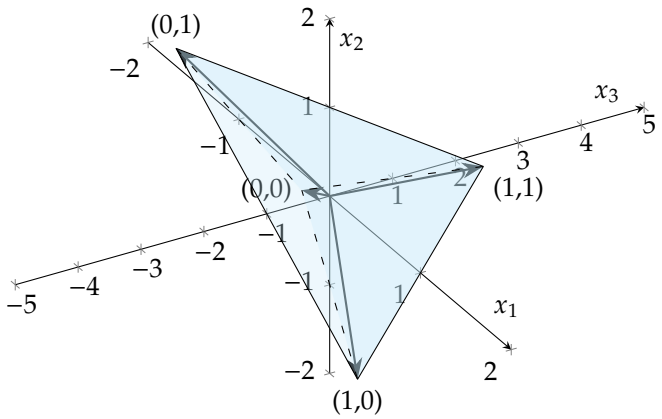

Figure 1.4: Convex hull of the hysteresis modulated system of relation (1.6.2). There are multiple intersections with the x_3 axis indicating multiple solutions for the sliding dynamics when sliding on the x_3 axis.

The sliding dynamics of hysteresis modulated systems with non-unique sliding solutions were analyzed in [76] using numerical simulations. As the system moves along the sliding surface, the attracting limit cycle varies smoothly and also undergoes bifurcations. As a result, the value of the sliding speed along the sliding surface varies erratically and is difficult to predict, unlike when the system slides on a single sliding surface. The resulting fast changes in the sliding speed as the system moves along the sliding surface are called jitter. Jitter is a phenomenon distinct from chatter. Chatter is the fast changes in the control input required

to maintain sliding. In hysteresis switching fast changes in the switches maintain the system state within the boundaries of the hysteresis layer. Jitter however is a phenomenon affecting the speed along the sliding surface and not the motion inside the hysteresis boundary layer. Apart from hysteresis, time delay in the switching was also shown to display a similar pattern of jitter in the variation of the sliding speed [76].

1.6.1 Implications of jitter in the design of sliding mode controllers

The sliding dynamics of hysteresis modulated impedance source converters are not unique according the convex hull method. Jitter is expected to appear in sliding mode controlled converters with hysteresis switching which can have detrimental effects for the stabilization of the converter. Stabilization usually requires the converter state to be driven and fixed at a specific point in the state space, and the converter to display a well defined dynamical response to disturbances along the sliding surface. However, due to the unpredictable variation of the sliding vector fields withing the range predicted by the minimal convex hull method, drift appears in the steady state of the converter. Furthermore, the dynamical response of the converter to displacements along the sliding surface can vary. It is thus important for impedance source converters to analyze and rectify the effects of the modulation algorithm on the sliding dynamics. The hysteresis modulation algorithms used in the implementation of the sliding mode must be tested to ensure that they maintain a small variation of the sliding speed within the limits required for the stability of the converter.

Jitter caused by hysteresis modulation is a complex dynamical behavior. The dynamics within the hysteresis layer are not observable in the temporal scale and the magnitude of sliding motion, but nevertheless they determine the sliding dynamics. The sliding dynamics are not chaotic, in the sense that they do not display sensitivity to initial conditions and can be predicted well into the future. However, any prediction relies on numerical simulation in the boundary layer in order to determine the sliding solution, and these numerical simulations are computationally expensive. Thus the construction of the sliding dynamics lies in the intersection of problems that are computationally tractable and problems that are simple enough so that the information describing their dynamical behavior can be compressed in an algebraic formula.

1.6.2 Effects of the dynamics in the boundary layer in the sliding motion of power converters

The dynamics of the sliding motion in the boundary layer of the hysteresis region have a significant effect in the performance of converters. Conventionally in power electronics the dynamics of the boundary layer are studied to determine the effects of chatter in the switching frequency. Power electronics use passive filter to reduce the noise in their output, and these filters tend to operate optimally in a specific range of frequencies. Variable switching frequencies are problematic as the filters must then be designed to operate in a wider range of frequencies increasing the weight, size and losses of the converter. Using an integral sliding mode controller with pulse width modulation the switching frequency can be controlled accurately. However, there are integral sliding mode controllers do not offer the order reduction of conventional sliding modes which is useful in optimizing the transient behavior of the controller. As a result,

methods where developed to stabilize the switching frequency of hysteresis modulated sliding mode controllers.

There is a number of hysteresis modulation algorithms for power electronics that modify the dynamics in the sliding layer which aim to achieve a constant switching frequency. The switching frequency is regulated by controlling the width of the hysteresis zone. In [77] an adaptive hysteresis zone is used to maintain a constant switching frequency. A different approach to the problem is the zero averaged control [78]. In this method the hysteresis boundary is not determined explicitly; instead the system is using a fixed switching frequency and the duty ratios are selected in each period so that the linear approximation of the switching function achieves an average value of zero during the period [79]. The zero averaged controllers are quasi-sliding controllers, since the width of their boundary layer is not predetermined and depends on the dynamics of the system.

In the impedance source converter however, the dynamics in the hysteresis layer directly influence the sliding dynamics. The hysteresis regions form the boundary layer of the sliding motion. There are two distinct time scales in the analysis of the sliding motion. The motion inside the sliding layer can be interpreted as happening in a timescale that is fast enough so that the state along the sliding surface can be assumed to be constant as the converter converges to an attractor. In the attractor the system spends a specific time in each of the available modes. The percentage of time spent in each mode then determines the system speed along the sliding surface. As the system moves along the sliding surface the limit cycle for the sliding motion can vary smoothly, or undergo bifurcations. These bifurcations are the cause of the jitter in the sliding dynamics.

1.7 Contributions

The main contribution of this thesis is the introduction of a systematic method for constructing hysteresis modulated sliding mode controllers for impedance source converters and analyzing the dynamics in the resulting sliding mode. Numerical analysis of the dynamics in the sliding layer is used to determine the sliding dynamics. The efficacy of numerical approach is evaluated in one more design problem, the determination of the effects of sensor dynamics in the stability of a sliding mode controlled buck converter. The dynamics of the sensors are not modeled during the design of the system, but can deteriorate the performance of sliding mode controllers. Therefore, the thesis introduces a model of the dynamics of the sensors in the design of the sliding mode. Given a parameterized model of the sensor dynamics, the range of parameters for the sensor that results in acceptable performance is determined through numerical simulations.

The analysis in this thesis focuses on the voltage fed trans-Z-source converter, a type of impedance source converter with a coupled inductor [80], [81]. This converter achieves in practice lower losses for high voltage gains by using the transformer turn ration to boost the voltage. More significantly, the trans-Z-source converter is a fully actuated system due to the magnetic coupling in the transformer. Most impedance source topologies are under-actuated. In the sliding mode control of such converters the state of the converter is allowed to vary freely on some subspace [82]. For instance in the conventional voltage fed Z-source inverter circular currents can flow in the impedance network. The voltage fed trans-Z-source inverter in

contrast requires one less capacitor and eliminates the circular current significantly simplifying its numerical analysis.

In this thesis a methodology is developed for designing and analyzing hysteresis modulated sliding mode controllers for impedance source converters. The control objective is to enforce sliding on a set of invariant surfaces, one for the output of the converter and one for the impedance network. The proposed method then constructs a set of switching surfaces so that in their intersection the system slides in the intersection of the invariant surfaces. The methodology is applied in the construction of a sliding mode control algorithm for a voltage fed trans-Z-source DC-DC converter. The sliding dynamics resulting by two hysteresis modulation algorithms are determined for the proposed sliding mode controller.

Numerical simulations suggest that the impedance source converters display jitter. Even though jitter appears in many switched topologies [76], this is the first demonstration of jitter in a practical power electronic topology. The dynamics in the sliding layer are analyzed and the effect of the modulation algorithm in the steady state drift and variation of the sliding speed are numerically quantified. A strong dependence of the jitter to the design of the switching surface is detected.

The specific contributions of this thesis are summarized as follows:

- Designed a method for generating a class of hysteresis modulation algorithms for the sliding mode control of power converters with multiple inputs (chapter 3).
- Simulated a hysteresis modulation algorithm for a converter with two control inputs using a box and an elliptical switching surface (chapter 3).
- Described conditions under which jitter can degrade the performance of hysteresis modulation algorithms for power electronics, and used an extended minimal convex hull to determine the range of possible sliding dynamics in system with a finite hysteresis width (chapter 3).
- Presented a numerical methodology for incorporating models of non-ideal sensor dynamics in the design of sliding mode controllers for power electronic converters (chapter 4).
- Demonstrated the methodology by determining the range of acceptable sensor performance for a buck converter controlled by a hysteresis modulated sliding mode controller so that design constraints in the ripple and switching frequency are satisfied (chapter 4).

1.8 Publications

As part of the work for this thesis the following two articles were published.

[76] M. R. Jeffrey, G. Kafanas, and D. J. W. Simpson, "Jitter in piecewise-smooth dynamical systems with intersecting discontinuity surfaces", *International Journal of Bifurcation and Chaos*, vol. 28, no. 06, pp. 1–22, 2018.

[83] G. Kafanas, M. R. Jeffrey, and X. Yuan, "Variable structure control for active power decoupling topologies", in *IET International Conference on Power Electronics, Machines and Drives*, Apr. 2016, pp. 1–6.

1.9 Thesis outline

The rest of the thesis is organized as follows. In chapter 2 the tools for the analysis and design of sliding mode controllers for impedance source converters are presented. The modeling framework is established, and methods for determining the ideal sliding dynamics to simplify the design of the sliding mode are discussed. In chapter 3 the sliding dynamics of a tarns-Z-source converter sliding in the intersection of two sliding surfaces are analyzed. The converter is linearized and the equivalent control method is used to design the sliding manifold. Then a model for the dynamics of the converter with non-ideal components is derived and it is demonstrated that the resulting convex hull results in a range of sliding solutions. Then a new method for designing the switching surfaces that enforce sliding on the desired manifold is developed and used to construct two controllers for the converter with hysteresis modulation. Numerical simulations indicate the presence of jitter which induces steady state drift in the constructed controllers. An extension of the convex hull method is then introduced to explain the magnitude of the drift. In chapter 4 the effects of the dynamics of the sensors on the sliding dynamics are analyzed. A model for the dynamics of sensors in power electronic converters is proposed. A methodology is developed for systematically introducing the dynamics of the sensors in the design of the sliding mode. A parameterized model of the sensor dynamics in DC-DC buck converter is then numerically simulated, and the sensor configurations that maintain the output ripple within an admissible range are determined. Finally, in chapter 5 the results of the thesis are summarized and few suggestions are made on how to approach the design of controllers for the dynamics of the motion in the sliding layer, in order to control the sliding speed.

Chapter 2

Variable structure control and sliding modes in power electronics

This chapter provides an overview of the models used for designing controller for power electronics. Due to the use of switched mode power electronics, power converters are non-smooth dynamical systems. The dynamical behavior of systems with non-smooth dynamics is in general captured by hybrid automata. However, simplified models such as variable structure systems are used for the designing of controllers for power converters. Sliding, a dynamical behavior appearing in ideal variable structure systems, has been used extensively for control design. Modulation algorithms that enforce sliding display a rich dynamical behavior in the boundary layer of the sliding mode requiring a full hybrid automaton representation to determine the dynamics of the controlled system. The minimum convex hull theorem simplifies the process by determining the range of possible sliding dynamics as practical controllers approach the behavior of the ideal variable structure system. Methods such as the equivalent control method provide algebraic solutions of the sliding dynamics for specific classes of variable structure systems. Algebraic methods are particularly useful design tools, as they provide a computationally efficient method to evaluate the dynamics of the controlled system.

2.1 Dynamics of power electronic converters

Power electronics converters are electrical energy conversion systems characterized by a continuous state and relatively abrupt changes in their dynamical behavior. A converter consists of a network of passive elements and semiconductor switches. The topology of the network is controlled by the state of the switches which is discrete. The state of the passive elements is continuous and varying smoothly for each topological configuration. Changes in the state of the switches instantaneous reconfigure the topology of the system and change the dynamics that determine the variation of the continuous state.

Semiconductor switches for power electronic are continuous dynamical systems with nonlinear dynamics that are approximated accurately by discrete models in control problems. A typical example is the diode [84], [85] whose circuit diagram is depicted in fig. 2.1a. The dynamical behavior of the diode is captured by the IV curve of the device. An idealized IV curve

is used for the design of the converter depicted in fig. 2.1b. This model is accurate in the region where power electronics operate, but there are subtle differences between the idealized model and the exact IV characteristic for the steady state operation of the diode depicted in fig. 2.1c. Focusing on the current axis, there is a voltage drop when the diode conducts. For reverse voltage above the maximum blocking voltage the diode conducts negative currents. The device also has some internal dynamics; for instance the current flows in the reverse direction through the diode for short periods of time as depicted in fig. 2.1d. However, due to the timescale in which the internal dynamical phenomena occur, they are treated with other non-ideal behavior as disturbances in the design of controllers for power electronics.

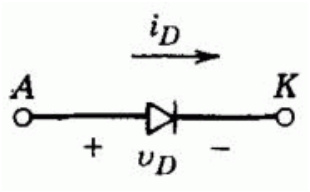

(a) Circuit digram of a diode.

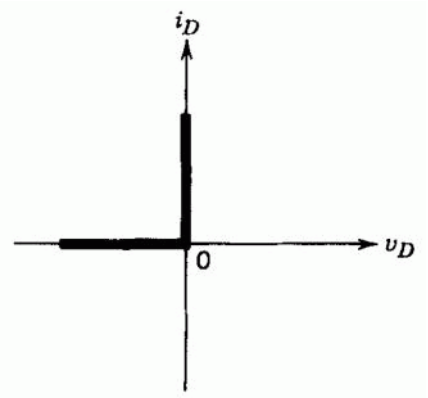

(b) The IV characteristic for a diode idealized in the region of operation of power electronic converters.

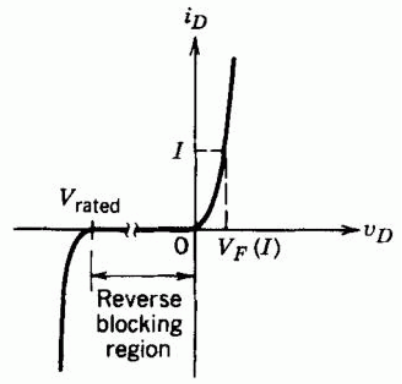

(c) Details of the actual static IV characteristic of a diode.

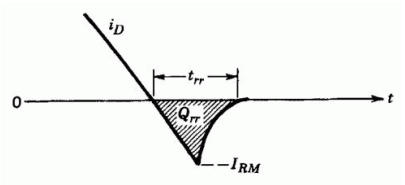

(d) Reverse recovery current. The current in the diode is momentarily negative as the internal capacitance of the device charges.

Figure 2.1: The dynamical model of a semiconductor diode. The circuit diagram in fig. 2.1a displays the voltage and current in the device. The idealized static response of the device is depicted in fig. 2.1c, and the non-ideal static response of the device is given in the detailed view of fig. 2.1d. The dynamical response of the diode is depicted in fig. 2.1d. Images from [84].

In semiconductor switches with three terminals, operation in intermediate states is actively avoided in switched mode power electronics. The IV characteristic response in three terminal devices is regulated by the input to a special control terminal. The MOSFET, whose circuit diagram depicted in fig. 2.2a, is a typical example of a three terminal device [84], [85]. The ideal IV response of the MOSFET, shown in fig. 2.2b, is controlled by the voltage in the gate terminal.

The IV curves used in power electronics correspond to an on state where the MOSFET allows current to pass with ideally no voltage drop, and an off state where the MOSFET fully blocks any current flow. Intermediate states are also available. By appropriately controlling the input to the gate terminal the MOSFET can operate in other IV curves, demonstrated in the vicinity of the voltage axes in fig. 2.2c. However, when at least one of the current or the voltage across the MOSFET are not zero, power is dissipated in the switch. Since the objective of power electronic circuits is to convert energy without excessive losses, in switched mode power electronics the input to the control terminal ensures that the switch is either fully on or fully off only, and the transition is designed to be as fast as possible to minimize losses [84], [85]. Some modern designs actively control the transient dynamical response of the switches with a modulation system for the input to the third terminal of the switch which limits losses and the effects of other phenomena associated with switching transitions such as electromagnetic emissions [86], [87]. Thus, with respect to the design of controllers for power electronic converters, the change in the state of the switches is effectively instantaneous.

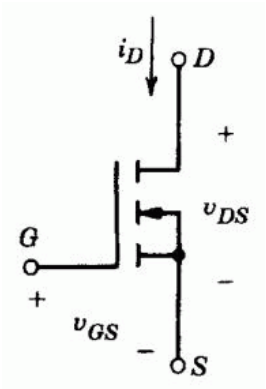

(a) Circuit digram of an N-channel MOSFET.

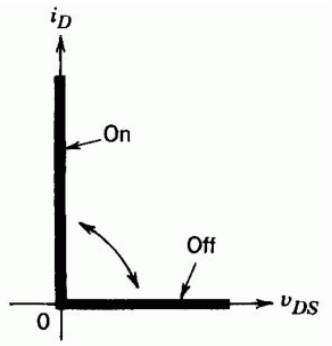

(b) The idealized IV characteristic for a MOSFET.

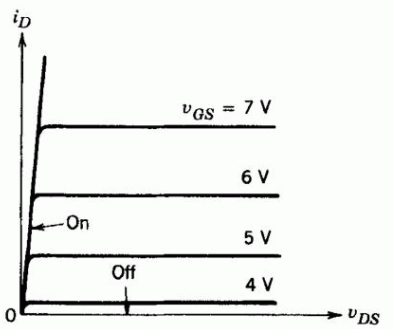

(c) Detail of the IV characteristic close to the off state.

Figure 2.2: The dynamical model of a MOSFET, a three terminal semiconductor switch. The circuit diagram in fig. 2.2a displays the voltages and currents in the device. The switch operates either in the on or off state as shown in fig. 2.2b, but unlike the diode, the state is now controllable by the voltage applied to the gate. The switch can also operate in intermediate states some of which are depicted in fig. 2.2c. However these are avoided in power electronics as they incur losses. Images from [84].

Due to the dynamics of semiconductor switches, the state of power converters can be sep-

arated in discrete and continuous states. Physical quantities corresponding to the states of passive elements, such as currents in the inductors and voltages in the capacitors, evolve according to dynamics described by ordinary differential equations. Control inputs change the state of switches in power electronics and reconfigure the network of passive elements resulting in different dynamics for the continuous variables. Since the change in the topology happens effectively instantaneously in the time scale where the controller operates, the changes are approximated accurately by discrete transitions, and hybrid systems are used extensively to model power converters [56], [88]–[95].

2.2 Computational models for power electronics

A number of computational models have been developed for hybrid dynamical systems, which combine discrete and continuous states in their dynamics. The computational models can be broadly classified as hybrid automata [96], and constrained difference and differential inclusions [97], [98]. Hybrid automata were developed primarily for the verification of real time systems [99]. The hybrid automaton as a generic model for systems with hybrid dynamics was introduced in [100], where it was used to construct symbolic methods for solving the reachability problem. A slightly extended model, the generalized hybrid automation introduced in [96], allows for simpler notation and simplifies operation such as composition of hybrid systems. The constrained difference and differential inclusions computational model is a variation of the hybrid automaton models that was developed explicitly for the study of dynamical systems [98], and often allows for simpler representation. The two families of computational models are equivalent representations, as any system can be translated from one representation to the other without changing its semantics [97].

The *generalized hybrid automaton* model will be used to succinctly describe control algorithms as it is simple, expressive and allows various operations on hybrid systems such as composition to be performed efficiently. The formal definition of generalized hybrid automata found in [96] is as follows.

Definition 2.2.1 (Generalized hybrid automaton)**.** A *generalized hybrid automaton* is a tuple $(Q, \Omega, L, \Sigma, R, \mathrm{Act})$ where

- Q is a countable set of discrete states,
- $\Omega \subset \mathbb{R}^n$ for some $n \in \mathbb{N}$ is the continuous state space where the continuous state takes values,
- L is the discrete communication space, a countable set of labels that are used as input to control discrete state transitions,
- $\Sigma \subset \mathbb{R}^m$ for some $m \in \mathbb{N}$ is the continuous communications space,
- R is a set of transitions such that

$$R \subset (Q \times \Omega) \times (L \times \Sigma) \times (Q \times \Omega)\,, \tag{2.2.1}$$

- and $\text{Act} : Q \rightarrow (\Omega \times \mathbb{R}^n \times \Sigma \rightarrow \mathbb{R}^n)$ is a mapping that assigns to each discrete state $q \in Q$ a differential algebraic equation determined by $\text{Act}_q : \Omega \times \mathbb{R}^n \times \Sigma \rightarrow \mathbb{R}^n$, as

$$\text{Act}_q\left(x, D_t x, s\right) = 0. \tag{2.2.2}$$

The operational semantics of the generalized hybrid automaton are determined by the transition set R. The automaton can jump from state q_0 to state q_1 and the continuous state from x_0 to x_1, if the continuous communication variable $s \in \Sigma$, and the discrete communication variable $\ell \in L$ satisfy

$$\left(q_0, x_0, \ell, s, q_1, x_1\right) \in R. \tag{2.2.3}$$

For $q = q_0 = q_1$ the automaton may remain in the state q, which must be enabled explicitly by R. Depending on the definition of the transition set, the operational semantics are undefined if

$$\forall q_0, q_1 \in Q, x_0, x_1 \in \Omega, \ell \in L, s \in \Sigma : \left(q_0, x_0, \ell, s, q_1, x_1\right) \notin R, \tag{2.2.4}$$

or they can be non-deterministic if for some t and any $q_0, q_1, q_2 \in Q$ such that $q_1 \neq q_2$ there are some continuous states x_0, x_1, x_2 and for some $\ell \in L, s \in \Sigma$ such that

$$\left(q_0, x_0, \ell, s, q_1, x_1\right) \in R \textbf{ and } \left(q_0, x_0, \ell, s, q_2, x_2\right) \in R. \tag{2.2.5}$$

Despite the fact that these kind of behaviors are undesirable in a practical controller, they are useful in idealized models of the converter behavior for the analysis and design of the controller. Quite often in the design of a controller, a guard relation with few restrictions is first generated and then refined to ensure that the controller can be implemented in practice. For instance, in [101] a guard relation is generated to satisfy liveness constraints, and then refined to ensure that the resulting controller is well defined and deterministic.

The semantics of hybrid systems are based on extensions of the notion of trajectories for systems with continuous dynamics. The computation performed by a hybrid system is defined as the trajectory traced by the evaluation of the corresponding hybrid automaton in [99]. The evaluation takes place over a totally order set, the *time structure*, and the evolution of the discrete and continuous state of the system is described by the *hybrid trace*. Unlike conventional trajectories, in a hybrid trace multiple consecutive transitions in the discrete and continuous states can occur during the same time instance. The time structure differentiates between the occurrence of such events by maintaining a counter for the number of discrete transitions. A similar solution structure is used in constrained difference and differential inclusions [97]. The notion of a trajectory for a hybrid automaton is also formalized in [100] where it is called a *run*, and is used to construct a symbolic model for the execution of hybrid automata. Symbolic reasoning has been used to prove reachability [100] and stability [91] properties for certain classes of hybrid systems.

Further refinements made to the trajectory structures allow solutions of systems displaying behavior such as consecutive Zeno limit points. Conventional trajectories of hybrid automata, such as the hybrid traces defined in [99], are called *executions* in [102], [103] and they are classified into three classes: finite executions, where the finite automaton trajectory terminates after finite time and a finite number of steps, infinite executions where there is a countably infinite number

of steps taking up infinite time, and Zeno executions where there are a countably infinite number of steps taking a finite amount of time. In some practical cases it is desirable that the solution of the hybrid system continues past a Zeno execution which converges to an accumulation point. Generalized hybrid domains are introduced in [104], [105] to allow solution trajectories with up to a countably infinite number of Zeno accumulation points to be defined.

The semantics of the generalized hybrid automata that are used to describe controllers in this work are determined by their trajectories. The following definition for the trajectory of a generalized hybrid automaton is taken from [96]. In the definition of the trajectories, the set of positive rational numbers, $\mathbb{R}_{\geq 0}$, is defined as

$$\mathbb{R}_{\geq 0} = \{x \in \mathbb{R} : x \geq 0\}, \tag{2.2.6}$$

and the set of all the partial functions from set A to set B is denoted by $A \nrightarrow B$. Finally for any partial function $f : A \nrightarrow B$ the set range(f) is defined as

$$\text{range}(f) = \left\{x \in A : \left(\exists y \in B : \left(x, y\right) \in f\right)\right\}. \tag{2.2.7}$$

Definition 2.2.2 (Trajectory)**.** A *trajectory* of a generalized hybrid automaton $(Q, \Omega, L, \Sigma, \text{Act})$ is a finite or infinite sequence

$$\tau : \mathbb{N} \nrightarrow Q \times L \times \mathbb{R}_{\geq 0} \times (\mathbb{R}_{\geq 0} \nrightarrow \Omega) \times (\mathbb{R}_{\geq 0} \nrightarrow \Sigma), \tag{2.2.8}$$

such that

$$\text{range}(\tau) \in \mathcal{N}, \tag{2.2.9}$$

where

$$\mathcal{N} = \{\{n \in \mathbb{N} : n < N\} : N \in \mathbb{N}\} \cup \{\mathbb{N}\}. \tag{2.2.10}$$

Furthermore, any $n \in \text{range}(\tau)$, such that $\tau_n = (q, \ell, \delta, x, s)$ must satisfy

- $q \in Q$, $\ell \in L$, $\delta \geq 0$, $x : \Delta_*(\delta) \to \Omega$, and $s : \Delta_*(\delta) \to \Sigma$,
- $\left(q, x(t), \ell, s(t), q, x(t)\right) \in R$ for all $t \in \Delta(\delta)$, and
- $\text{Act}_q\left(x(t), D_t x(t), s(t)\right) = 0$ for almost all $t \in \Delta(\delta)$, with exceptions the points of discontinuity of s,

where

$$\Delta_*(\delta) = \begin{cases} [0, +\infty), & \text{if } \forall k \in \text{range}(\tau) : k \leq n \\ [0, \delta], & \text{otherwise,} \end{cases} \tag{2.2.11}$$

and

$$\Delta(\delta) = \begin{cases} (0, +\infty), & \text{if } \forall k \in \text{range}(\tau) : k \leq n \\ (0, \delta), & \text{otherwise,} \end{cases} \tag{2.2.12}$$

and for any $n \in \text{range}(\tau)$ such that $(n+1) \in \text{range}(\tau)$, $\tau_n = (q_n, \ell_n, \delta_n, x_n, s_n)$ and $\tau_{n+1} =$

$(q_{n+1}, \ell_{n+1}, \delta_{n+1}, x_{n+1}, s_{n+1})$ must satisfy

$$\big(q_n, x_n(\delta_n), \ell_n, s_n(\delta_n), q_{n+1}, x_{n+1}(0)\big) \in R. \tag{2.2.13}$$

Apart from power electronics, there are multiple phenomena where physical systems display non-smooth dynamical behavior. A number of application specific representations has been developed. One such representation that is used extensively to model physical phenomena is piecewise smooth systems [106]. Physical phenomena modeled by piecewise smooth systems include impacts [107]–[109], dry friction [110], [111], and discontinuous control inputs [112], [113]. Similar models have been developed for power electronics, but there are subtle differences as switching is often controllable in power electronics while it is often no controllable in other physical systems.

2.2.1 Models for controllers of power electronics

Using a hybrid automaton to model both the circuitry and the control of the converter obscures the details of the internal structure of power converters. For each topological configuration of the passive element network the dynamics of the network are described by some differential equation with a continuous right hand side. The topological configuration of the passive element network is determined by the state of the switches. Power conversion circuits are designed so that the topological configurations result in a range of dynamical behaviors, allowing the controller of the circuit to regulate the dynamics of the passive elements by selecting the appropriate configuration. Most models separate the dynamics of the passive elements that are continuous, from the dynamics of the control input that are discrete due the nature of semiconductor switches.

To separate the dynamics of the power circuit from those of the controller, the dynamics of the passive element network are modeled by a switched system. In switched systems the dynamics of the continuous states are selected from a family of vector fields with the selection being determined by a discrete control input. A switched system model for the circuit dynamics forms the basis of many models used in the design of controllers for power converters, most notably the variable structure model with discrete control inputs [56], [92]–[95]. The switched system model is also used to derive other models for the converter dynamics such as the averaged dynamics of power converters that are used in the design of linear controllers [88]–[90]. The following definition is found in [114, §1.1.2]. Without loss of generality, it is assumed that the family of switched systems is autonomous.

Definition 2.2.3 (Family of switched systems)**.** A *family of switched systems* for some finite set P and $\Omega \subset \mathbb{R}^n$, is a function $f : \Omega \times P \to \mathbb{R}^n$, where

$$D_t x = f(x, u), \tag{2.2.14}$$

where x is the continuous state of the system, u is the control input, and and f is smooth in x for all $u \in P$.

Various classes of control algorithms with discrete input have been developed for families of switched systems, and many of them found application in the control of power electronics.

Control objectives in switched systems are often formalized as enforcing a series of transitions along a constrained region in the state space. Discrete controllers enforcing such trajectories have been developed in [115] by combining solutions to reach control subproblem, and in [91] where the control objective of stabilizing a boost converter was described as following a trajectory in the state space and a controller was developed to enforce such a trajectory. Many controller designs for power electronics directly enforce convergence to a desired operating point by selecting a control input that reduces a suitable selected Lyapunov function to zero monotonically [116]–[118]. The methods for designing the Lyapunov function and selecting the control input for power converters that have been developed include passivity based control [54], [119]–[121], and direct numerical methods [122].

2.2.2 Variable structure control

A specially kind of controllers for systems with discrete input is discrete variable structure controllers that change their control signal when the system crosses surfaces in the state space [74], [112]. In general, variable structure controllers allow for a continuous control input. Without loss of generality the variable structure controller is defined for autonomous systems. The following definition is found in [74].

Definition 2.2.4 (Variable structure system)**.** A *variable structure system* with a state space $\Omega \subset \mathbb{R}^n$, is a dynamical system

$$D_t x = f(x, u), \tag{2.2.15}$$

where $f : \Omega \times \mathbb{R}^m \to \mathbb{R}^n$ is continuous in all its inputs for some $m < n$, x is the continuous state of the system, and the control input u is determined by

$$u_i = \begin{cases} u_i^+(x), & S_i(x) < 0 \\ u_i^-(x), & S_i(x) > 0, \end{cases} \tag{2.2.16}$$

for $i = 1, \ldots, m$, where $u^+, u^-, S : \mathbb{R}^n \to \mathbb{R}^m$ are smooth functions. The functions S_i for $i = 1, \ldots, m$, are called the *switching functions* of the system, and the corresponding sets

$$\mathcal{S}_i = \{x \in \mathbb{R}_i : S_i(x) = 0\}, \tag{2.2.17}$$

are the *switching surfaces*.

In power electronics however, the control input can only take discrete values. Usually only two control input values are attainable, corresponding to the on and off states of the switches. Thus in the design of most sliding mode controllers for power converters the dynamics of the *variable structure system* are modeled by an autonomous family of switched systems, such that

$$D_t x = f(x, u), \tag{2.2.18}$$

where the discrete control input is provided by

$$u_i = \begin{cases} u_i^+, & S_i(x) < 0 \\ u_i^-, & S_i(x) > 0, \end{cases} \tag{2.2.19}$$

for some vectors of constants $u^+, u^- \in \mathbb{R}^m$. Since there are only two states available for the switches, in most models used in the design of discrete variable structure controllers for power electronics, each input u_i, receives values 0 and 1 corresponding to the off and on states of the switch [78], [93]–[95], [123]–[132]. Thus, the control input is further simplified to

$$u_i = \begin{cases} 1, & S_i(x) < 0 \\ 0, & S_i(x) > 0. \end{cases} \tag{2.2.20}$$

The variable structure control is an ideal model. Direct implementations of variable structure controllers lead to dynamical behaviors with infinite frequency switching, such as Zeno dynamics and ideal sliding [106]. However, the ideal control input is still useful as an analysis and design tool. Sliding in particular finds many applications in the design of controllers, as it has been proven that the dynamics of systems controlled by hybrid controllers tend to an ideal limit that can be evaluated analytically. In switched systems, this limit appears as the controller limits the state close to the switching surface of a variable structure controller.

2.3 Sliding modes in variable structure systems

A dynamical structure that often appears in variable structure systems and is particularly useful in control applications is *sliding modes* [112]. To completely define the dynamics of a *variable structure system*, the vector fields on all the points of the state space must be determined, so that the trajectory of any initial point in the state space can be constructed. Outside the *switching surfaces*, function f is Lipschitz continuous as the control inputs are smooth functions, and the solution of the system in definition 2.2.4 is well defined. However, the control input is not determined on the switching surfaces themselves.

Sliding modes appear when extending the dynamics on the switching surfaces so that trajectories can be defined in the whole state space. In regions of the state space where vector fields direct the state of the system on the intersection of multiple switching surfaces, the solution of the system is selected so that the state moves along the intersection. The range of possible sliding speeds along the intersection is determined by the minimal convex hull method developed by Filippov and Utkin [73], [74]. The dynamics on the switching surfaces are now defined for a class of variable structure systems where the gradients of the switching functions are linearly independent [133].

Definition 2.3.1 (Variable structure system with linearly independent switching surfaces)**.** A *variable structure system* with control input given by

$$u_i = \begin{cases} 1, & S_i(x) < 0 \\ 0, & S_i(x) > 0. \end{cases} \tag{2.3.1}$$

for some smooth function $S : \mathbb{R}^n \to \mathbb{R}^m$ where $m < n$, has *linearly independent switching surfaces* if the set

$$\{\partial_x S_i : i = 1, \ldots, m\} \tag{2.3.2}$$

is linearly independent for any $x \in \mathbb{R}^n$.

Sliding modes appear when extending the definition of the vector field on the switching surfaces. To formalize the definition of the vector field, the flow function of the system that maps every point of the state space to its trajectory is introduced, and the control input is defined so that the flow satisfies the following properties. There are three cases regarding the dynamics close to points of a switching surface $\mathcal{S}_i$ [113], [134]:

- if vector fields in opposite sides of the switching surface point to the same side of the surface, trajectories starting close to the switching surface cross the surface changing from one flow to the other;
- if vector fields in both sides point towards the switching surface, trajectories starting close to the switching surface reach the surface in finite time since the closing speed is finite, and then move along the surface; the resulting motion is called *stable sliding* and the surface where sliding occurs is called the *sliding surface*;
- if vector fields point away from the switching surface, trajectories staring on the switching surface follow any of the two vector fields in either side of the surface.

In general, points on the switching surface where the dynamics in each side point to opposite directions are not reachable in practical systems. The definition is formalized using the *flow function* of the system. Flow functions are defined locally on the switching surfaces $\mathcal{S}_i$ by relaxing the requirement that the control input is discrete on the switching surface, and on each of the regions

$$\mathcal{S}_i^+ = \{x \in \mathbb{R}^n : S_i(x) > 0\}, \qquad \mathcal{S}_i^- = \{x \in \mathbb{R}^n : S_i(x) < 0\}. \tag{2.3.3}$$

The overall flow is then constructed by connecting the flows in each individual region.

2.3.1 The minimal convex hull method and semantics of the ideal sliding dynamics

The minimal convex hull method, developed originally by Filippov and Utkin [73], [74], determines an ideal set of solutions to the sliding dynamics. To construct the minimal convex hull for a point on the sliding surface, the vector fields for all available control inputs in a vanishing vicinity of the point are first determined. The convex hull of all the vector fields is constructed, and the set of solutions for the sliding dynamics at the point of the sliding surface are the vector fields in the convex hull that are tangent to the sliding surface. Combining the vector fields determined by the convex hull with the dynamics in other sectors of the state space, the flow functions of the system are defined over the whole state space as the solution of a set of constrained differential inclusions, so that trajectories of the complete solution are constructed by combining trajectories from individual domains [134].

Definition 2.3.2 (Flow function)**.** Let $f : \Omega \to \mathbb{R}^n$ be a smooth function for some open set $\Omega \subset \mathbb{R}^n$. The flows of the system

$$D_t x = f(x), \tag{2.3.4}$$

is a function $\phi : \mathbb{R}^n \times \mathbb{R} \to \mathbb{R}^n$, such that for any $x_0 \in \Omega$

$$D_t \phi(x_0, t) = f(\phi(x_0, t)). \tag{2.3.5}$$

Flow functions of autonomous systems with a smooth right hand side satisfy the properties in the following proposition; a detailed discussion of flows and proofs of their properties can be found in [135, §6].

Proposition 2.3.1 (Properties of flow functions)**.** *Let $f : \Omega \to \mathbb{R}^n$ be a smooth function for some open set $\Omega \subset \mathbb{R}^n$. The flows of the system*

$$D_t x = f(x), \tag{2.3.6}$$

have the following two properties,

$$\forall x_0 \in \mathbb{R}^n : \phi(x_0, 0) = x_0, \tag{2.3.7}$$

and

$$\forall x_0 \in \mathbb{R}^n, t_0, t_1 \in \mathbb{R} : \phi(x_0, t_0 + t_1) = \phi(\phi(x_0, t_0), t_1). \tag{2.3.8}$$

According to the chain rule, the time derivative of a smooth function $S_i : \mathbb{R}^n \to \mathbb{R}$ is

$$D_t S_i = \partial_x S_i(x) \cdot f(x, u). \tag{2.3.9}$$

Using this notation, the flows in a region of the state space separated by a single switching function are defined as follows. The dynamics on a switching surface where sliding appears, are determined according to the *minimal convex hull method* [73], [74]. In this method, a solution is selected from the minimal convex hull generated by the vector fields for all the available control inputs, so that the resulting flow remains on the surface. In the special case of variable structure systems with discrete control inputs, the construction of the minimal convex hull is straight forward, and the details of the process can be found in [74, §3]. In the following definition, $A \to B$ denotes the set of functions from set A to set B.

Definition 2.3.3 (Minimal convex hull in variable structure systems with discrete control input)**.** The minimal convex hull of a *variable structure system with discrete control input*, generated by a set of control inputs $\mathcal{U}$ at some $x \in \Omega$ is

$$\mathcal{H}_{\mathcal{U}}(x) = \left\{ \sum_{u \in \mathcal{U}} \gamma_u f(x, u) : \gamma \in C \right\}, \tag{2.3.10}$$

where

$$C = \left\{ \gamma \in (\mathcal{U} \to \mathbb{R}) : \left(\forall u \in \mathcal{U} : 0 \le \gamma_u \le 1 \right) \textbf{ and } \sum_{u \in \mathcal{U}} \gamma_u = 1 \right\}. \tag{2.3.11}$$

Definitions of the minimal convex hull for more general classes of systems can be found in [73], [136]. In the following definitions the set $\mathcal{H}$ denotes the minimal convex hull, and $\mathcal{T}$ is the set of tangent vector to sliding surface according to the notation introduced in [136].

Definition 2.3.4 (Flow functions in variable structure systems with sliding)**.** Consider a *variable structure system with linearly independent switching surfaces*

$$D_t x = f(x, u), \tag{2.3.12}$$

where $f : \Omega \times \mathbb{R} \to \mathbb{R}^n$ and a switching function $S : \mathbb{R}^n \to \mathbb{R}$. For any $x_0 \in \Omega$ such that $S(x_0) \neq 0$, the flow $\phi(x_0, t)$ is the solution of the constraint differential equation:

1. $D_t x = f(x, 0), S(x) \geq 0$ if $S(x_0) > 0$,
2. $D_t x = f(x, 1), S(x) \leq 0$ if $S(x_0) < 0$.

If $S(x_0) = 0$, the flow $\phi(x_0, t)$, is the solution of:

$$D_t x = f(x, 0), S(x) \geq 0 \text{ if } D_t S(x_0, 0) > 0 \textbf{ and } D_t S(x_0, 1) > 0, \tag{2.3.13}$$

$$D_t x = f(x, 1), S(x) \leq 0 \text{ if } D_t S(x_0, 0) < 0 \textbf{ and } D_t S(x_0, 1) < 0, \tag{2.3.14}$$

$$D_t x = f(x, u), (2u - 1)S(x) \leq 0 \text{ if } D_t S(x_0, 0) > 0 \textbf{ and } D_t S(x_0, 1) > 0, \tag{2.3.15}$$

where either $u = 0$ or $u = 1$, and

$$D_t x \in \mathcal{F}(x), S(x) = 0 \text{ if } D_t S(x_0, 0) < 0 \textbf{ and } D_t S(x_0, 1) < 0, \tag{2.3.16}$$

where

$$\mathcal{F}(x) = \mathcal{H}_{\{0,1\}}(x) \cap \mathcal{T}(x) \tag{2.3.17}$$

for the convex hull $\mathcal{H}_{\{0,1\}}(x)$ and the set of tangent vector fields

$$\mathcal{T}(x) = \left\{ v \in \mathbb{R}^2 : \partial_x S(x) \cdot v = 0 \right\}. \tag{2.3.18}$$

The vector field is thus defined in all the state space and the flow functions of the system are constructed by concatenating flow functions from the various regions. Points where the flows of the vector fields are tangent to the switching surfaces are not considered in this definition. A number of methods have been proposed for defining the flow in tangency point [133], [134]. Defining the flow in points where one or more of the vector fields are tangent to the switching surface is not crucial in the design of sliding mode controllers for power electronics, as ambiguous behavior is avoided by an appropriate selection of the controller parameters. Tangency points affect some aspects of the performance of the controller, as they determine the boundaries of the region on the sliding surface where sliding is stable.

The analysis of the vector field that enforces sliding is more involved when sliding in the intersection of multiple surfaces of co-dimension one [137]–[141]. For instance, stable sliding may exist in the intersection of two surfaces without stable sliding existing in each of the two surfaces individually [142]. The sliding solution is easier to define in the intersection of co-dimension one surfaces if all the intersecting surfaces are attracting [143]. A detailed description on how the flow functions of each region are combined can be found in [133, §4.2].

Definition 2.3.5 (Stability of a sliding surface)**.** Stable sliding exists for a set of control inputs $\mathcal{U}$ in the intersection $\mathcal{I}_s \subset \{0, \ldots, m\}$ of a variable structure system with linearly independent switching surfaces, if there exists a map $\sigma : \mathcal{I}_s \to \{0, \ldots, m\}$ defining the function $S^\sigma : \mathbb{R}^n \to \mathbb{R}^{|\mathcal{I}_s|}$, where

$$S_i^\sigma(x) = S_{\sigma(i)}(x) \tag{2.3.19}$$

for $i = 1, \ldots, |\mathcal{I}_s|$, such that

$$\forall x, y \in \mathcal{I}_s : \sigma(x) = \sigma(y) \Rightarrow x = y, \tag{2.3.20}$$

and there exists a continuous and continuously differentiable function $V : \mathbb{R}^{|\mathcal{I}_s|} \to \mathbb{R}$, such that

1. $\forall s \in \mathbb{R}^m : V(s) \geq 0$, and
2. $\forall s \in \mathbb{R}^m : V(s) = 0 \Rightarrow x = 0$,

and

$$\forall y \in \mathcal{U} : D_t(V \circ S^\sigma)(x_0, u) < 0. \tag{2.3.21}$$

A definition of the sliding vector fields for systems with discrete control input and multiple switching surfaces follows. The notation

$$\text{step}(s) = \begin{cases} 1, & s > 0 \\ 0, & s < 0 \end{cases} \tag{2.3.22}$$

is used for the partial step function, and the notation

$$\text{sing}(s) = \begin{cases} 1, & s > 0 \\ -1, & s < 0 \end{cases} \tag{2.3.23}$$

is used for the partial sign function. Furthermore, let $\mathcal{I} \subset \{1, \ldots, m\}$ be a finite collection of sliding surface indexes; the intersection of the surfaces with indices in $\mathcal{I}$ is defined as

$$\mathcal{S}_\mathcal{I} = \bigcap_{i \in \mathcal{I}} \mathcal{S}_i. \tag{2.3.24}$$

Definition 2.3.6 (Sliding in the intersection of attracting co-dimension one surfaces)**.** Consider a *variable structure system with linearly independent switching surfaces*

$$D_t x = f(x, u), \tag{2.3.25}$$

where $f : \Omega \times \mathbb{R}^m \to \mathbb{R}^n$ and a switching function $S : \mathbb{R}^n \to \mathbb{R}^m$ for some $m < n$, and let $\mathcal{I}$ be the maximal subset of $\{1, \ldots, m\}$ such that $x_0 \in \mathcal{S}_\mathcal{I}$. A sliding solution is then defined on any $\mathcal{S}_{\mathcal{I}_s}$, for some $\mathcal{I}_s \subset \mathcal{I}$, where $\mathcal{I}_s$ satisfies

$$\begin{aligned} \forall i \in \mathcal{I} : ((\forall u \in \{0,1\}^m : u_i = 0 \Rightarrow D_t S_i(x_0, u) < 0) \ \textbf{and} \\ (\forall u \in \{0,1\}^m : u_i = 1 \Rightarrow D_t S_i(x_0, u) < 0)) \Rightarrow i \in \mathcal{I}_s, \end{aligned} \tag{2.3.26}$$

if stable sliding exists on the intersection of $\mathcal{I}_s$ for $\mathcal{U}$, where the sliding solution on the surface $\mathcal{S}_{\mathcal{I}_s}$ is the solution of the constrained differential inclusion

$$D_t x \in \mathcal{F}(x), x \in \mathcal{S}_{\mathcal{I}_s} \cap \mathcal{B}(x_0) \tag{2.3.27}$$

where

$$\mathcal{F}(x) = \mathcal{H}_\mathcal{U}(x) \cap \mathcal{T}(x), \tag{2.3.28}$$

for the convex hull $\mathcal{H}_{\mathcal{U}}(x)$, the set of tangent vector fields

$$\mathcal{T}(x) = \{v \in \mathbb{R}^m : (\forall i \in \mathcal{I}_s : \partial_x S_i(x) \cdot v = 0)\}. \tag{2.3.29}$$

and

$$\mathcal{U} = \left\{u \in \{0,1\}^m : (\forall i \in \{1,\ldots,n\} \backslash \mathcal{I}_s : u_i = \mathcal{G}_1(i, x_0))\right\}, \tag{2.3.30}$$

$$\mathcal{B}(x_0) = \bigcap_{i \in \{1,\ldots,n\}\backslash \mathcal{I}_s} \mathcal{G}_2(i, x_0), \tag{2.3.31}$$

where

$$\mathcal{G}(i, x_0) = \begin{cases} \left\{\left(\text{step}\left(-S_i(x_0)\right), \left\{x \in \Omega : \text{sign}\left(S_i(x_0)\right) S(x) \geq 0\right\}\right)\right\}, & S_i(x_0) \neq 0 \\ \{(1, \{x \in \Omega : S_i(x) \leq 0\})\}, & S_i(x_0) = 0 \textbf{ and } \texttt{cross}_+(i, x_0) \\ \{(0, \{x \in \Omega : S_i(x) \geq 0\})\}, & S_i(x_0) = 0 \textbf{ and } \texttt{cross}_-(i, x_0) \\ \{(0, \{x \in \Omega : S_i(x) \geq 0\}), (1, \{x \in \Omega : S_i(x) \leq 0\})\}, & S_i(x_0) = 0 \textbf{ and } \texttt{diverge}(i, x_0) \end{cases} \tag{2.3.32}$$

where

$$\texttt{cross}_+(i, x_0) = \left(\forall u \in \{0,1\}^m : u_i = 0 \Rightarrow D_t S_i(x_0, u) > 0\right) \textbf{ and } \left(\forall u \in \{0,1\}^m : u_i = 1 \Rightarrow D_t S_i(x_0, u) > 0\right), \tag{2.3.33}$$

$$\texttt{cross}_-(i, x_0) = \left(\forall u \in \{0,1\}^m : u_i = 0 \Rightarrow D_t S_i(x_0, u) < 0\right) \textbf{ and } \left(\forall u \in \{0,1\}^m : u_i = 1 \Rightarrow D_t S_i(x_0, u) < 0\right), \tag{2.3.34}$$

and

$$\texttt{diverge}(i, x_0) = \left(\forall u \in \{0,1\}^m : u_i = 0 \Rightarrow D_t S_i(x_0, u) > 0\right) \textbf{ and } \left(\forall u \in \{0,1\}^m : u_i = 1 \Rightarrow D_t S_i(x_0, u) < 0\right). \tag{2.3.35}$$

2.3.2 Practical implementations of sliding modes and regularization theorems

The variable structure system is an ideal model that does not capture the details of switching; it is used in conjunction with idealized dynamics on attracting switching surfaces to define the system trajectories. However, due to the discontinuity in the control signal of variable structure systems at either side of the switching surface, direct use of the variable structure control signal for the control of a family of switched systems leads to high frequency switching between the control inputs. The resulting high frequency oscillation in the control input is called *chatter* [144], and its frequency is determined by unmodeled dynamical behavior in the system. In some applications, such as mechanical actuators, chatter is undesirable [145], [146]. Sliding mode controllers for power electronics rely on switching to impose sliding, but there are constraints in the resulting switching frequency [132].

The switching frequency in power electronics is constrained within some finite range de-

termined by the topology and components in the power circuit. The high frequency switching cased by chatter increases losses and electromagnetic emissions. Electromagnetic interference with control signals in particular can cause the circuit to enter temporary in unsafe configurations increasing the probability of failure [147]. A typical example is short circuits in the phase bridge of voltage source converters. As a result, the modulation algorithm enforces a finite switching frequency. Due to the finite switching frequency the state of the system varies in the boundary region of the sliding manifold. This variation is persistent even during steady state operation, when a limit cycle appears in the dynamics of the boundary layer. The resulting variation in the continuous states of the converter due to the modulation is called *ripple*. The ripple adversely affects the stability of systems connected to the coveter output, so it is often attenuated using filters [84]. However, the losses in the filter and the physical size of the filter increase with the ripple [84], [85]. As a result the switching frequency is kept sufficiently high to maintain a low ripple in the converter output. Overall, the switching frequency is regulated by a modulation algorithm, and it is kept fixed within a predetermined range.

A set of models for systems with non-smooth control inputs are now proposed to model the details of the switching process. In these models, the control input for the system dynamics is provided by a hybrid automaton according to a switching function. The hybrid automaton has access to the system state through the output of the switching function. Two classes of algorithms implementing the control signal are defined: a generic class with a non-smooth control signal, and a class with a discrete control signal.

Definition 2.3.7 (Variable structure system with non-smooth control signal)**.** A variable structure system with non-smooth control signal over a state space $\Omega \subset \mathbb{R}^n$, is a dynamical system

$$D_t x = f(x, u), \tag{2.3.36}$$

where $f : \Omega \times \mathbb{R}^m \to \mathbb{R}^n$ is continuous in all its inputs for some $m < n$, x is the continuous state of the system, and u the control input, together with a smooth function $S : \mathbb{R}^n \to \mathbb{R}^m$ such that the set

$$\{\partial_x S_i : i = 1, \ldots, m\} \tag{2.3.37}$$

is linearly independent for any $x \in \mathbb{R}^n$. The algorithm generating the control signal is a hybrid automaton $(Q, \Omega, L, \Sigma_{\text{sys}} \times \Sigma_{\text{ctrl}}, R, \text{Act})$ such that

- $L = \varnothing$,
- $\Sigma_{\text{sys}} = \Sigma_{\text{ctrl}} = \mathbb{R}^m$,

and the continuous communication variable of the automaton is given by the pair of the switching function and the control input $(S(x), u)$.

Definition 2.3.8 (Variable structure system with discrete control signal)**.** A variable structure system with discrete control signal over a state space $\Omega \subset \mathbb{R}^n$, is a dynamical system

$$D_t x = f(x, u), \tag{2.3.38}$$

where $f : \Omega \times \mathbb{R}^m \to \mathbb{R}^n$ is continuous in all its inputs for some $m < n$, x is the continuous state of the system, and u the control input, together with a smooth function $S : \mathbb{R}^n \to \mathbb{R}^m$ such that

the set

$$\{\partial_x S_i : i = 1, \ldots, m\} \tag{2.3.39}$$

is linearly independent for any $x \in \mathbb{R}^n$. The algorithm generating the control signal is a hybrid automaton $(Q, \Omega, L, \Sigma_{\text{sys}}, R, \text{Act})$ such that

- $L = \{0, 1\}^m$,
- $\Sigma_{\text{sys}} = \mathbb{R}^m$,

and the continuous communication variable of the automaton is given by $S(x)$, where as the discrete communication variable provides the control input u.

Typical examples of modulation algorithms for generic variable structure systems include the saturation (fig. 2.3), hysteresis (fig. 2.4b), and their combination [113]. In variable structure systems with discrete control inputs the selection of control signal is more restricted; for instance saturation cannot be used as it requires a continuously varying control signal. Hysteresis controllers are used in power electronics as their discrete control output can be used directly as input for the semiconductor switches. In hysteresis controllers, the width of the hysteresis zone is used to regulate the switching frequency. For a fixed hysteresis width, the switching frequency varies along the sliding surface. However, the range of frequency variation is determined by the hysteresis width, simplifying the design of passive filters as the filter performance is optimized only for the range of switching frequencies expected in steady state operation.

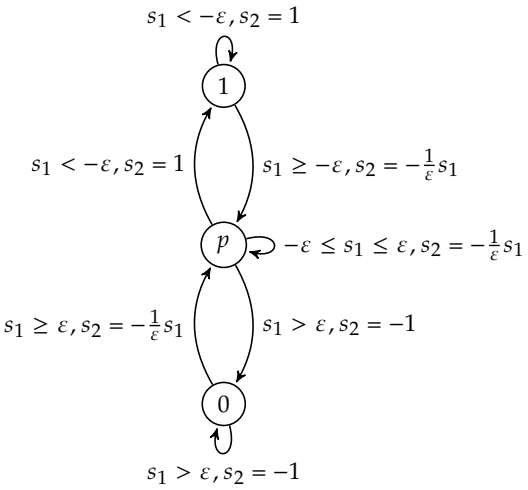

Figure 2.3: A saturation algorithm for the control signal. Given a continuous input by some switching function $s_1 = S(x)$, it produces a continuous control signal $u = s_2$. The control signal is normalized in the interval $u \in [-1, 1]$. Continuous control inputs cannot be used directly for the control of power semiconductor switches.

Practical switching algorithms constrain the state of the converter in a region close to the sliding surface and not exactly on the surface. The definition of stable sliding is extended to practical controllers by formally defining the stability of domains of the sliding manifold [74, §4.1]. For a sliding domain $\mathcal{S}$ stable sliding is defined in a neighborhood of $\mathcal{S}$. The sliding domain $\mathcal{S}$ is stable, if given a δ neighborhood of the sliding domain, an ε neighborhood exists such that any solution starting at an $x_0 \in \mathbb{R}^n$ inside the ε neighborhood can only exit the δ

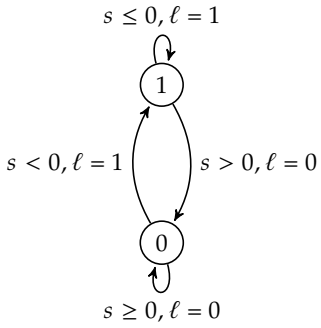

(a) An ideal sliding mode controller for a switched system. Solutions of the system with ideal control are not well defined, and in practical implementations the ideal control signal leads to chatter.

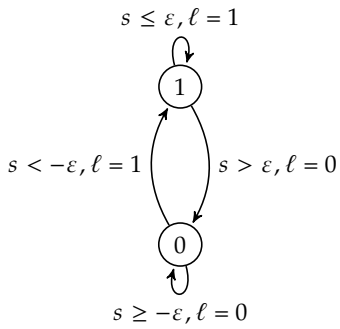

(b) A realistic hysteresis switching algorithm. A hysteresis width of $\varepsilon > 0$ is used to avoid chatter.

Figure 2.4: Hysteresis switching for variable structure systems with discrete input. An ideal and a realistic switching algorithm are depicted. The value of the continuous input $s = S(x)$ is provided by the switching function, and the value of the discrete control input of the switched system is provided by the discrete communication variable $u = \ell$.

neighborhood from a δ neighborhood of a boundary point of $\mathcal{S}$. This idea is formalized in definition 2.3.9. The diagram in fig. 2.5 displays the key components for defining when a sliding surface is stable in a domain $\mathcal{S}$. The ε neighborhood $B(x, \varepsilon)$ of a point $x \in \mathbb{R}^n$ is defined for $\varepsilon > 0$ as

$$B(x, \varepsilon) = \{y \in \mathbb{R}^n : \|y - x\| < \varepsilon\}, \tag{2.3.40}$$

where $\|x\| = \left(x^T \cdot x\right)^{\frac{1}{2}}$ is the Euclidean norm in $\mathbb{R}^n$. The notion of the ε neighborhood is extended to sets by defining the neighborhood of any set S as

$$\mathcal{B}(S, \varepsilon) = \bigcup_{x \in S} B(x, \varepsilon). \tag{2.3.41}$$

The set ∂S is the boundary of S, and S° is the interior of S. The definition of stable sliding in [74, §4.1] is now formally presented.

Definition 2.3.9 (Stability of a sliding surface)**.** Let $\phi_{C(\delta)} : \mathbb{R}^n \times \mathbb{R} \to \mathbb{R}^n$ be the flow induced by a family of switched systems for a controlling hybrid automaton C parametrized by δ. Let $H : \mathbb{R}^m \to \mathbb{R}^n$ be a smooth function for $m < n$ such that the set

$$\{\partial_x H_i : i = 1, \ldots, m\} \tag{2.3.42}$$

is linearly independent, and define

$$\mathcal{M} = \{x \in \mathbb{R}^n : H(x) = 0\}. \tag{2.3.43}$$

Let $\mathcal{D} \subset \mathcal{M}$ be a connected set. The hybrid automaton controller C enforces sliding on $\mathcal{D}$ if

$$\exists \eta > 0, \forall \delta > 0 : \delta < \eta \Rightarrow (\exists \varepsilon > 0, \forall x_0 \in \mathbb{R}^n : x_0 \in \mathcal{B}(\mathcal{D}, \varepsilon) \Rightarrow \texttt{sliding}(x_0, \delta, \mathcal{D})). \tag{2.3.44}$$

where

$$\texttt{sliding}(x_0, \delta, S) = \forall t \geq 0 : \left(\phi_{C(\delta)}(x_0, t) \notin \mathcal{B}(S, \delta) \Rightarrow \texttt{exit}(t, x_0, \delta, S)\right), \tag{2.3.45}$$

$$\texttt{exit}(t_f, x_0, \delta, S) = \exists t_e \in (0, t_f) : \phi_{C(\delta)}(x_0, t_e) \in \mathcal{E}(S, \delta) \textbf{ and } \texttt{slided}(t_e, x_0, \delta, S), \tag{2.3.46}$$

$$\mathcal{E}(S, \delta) = \partial\mathcal{B}(\partial S, \delta) \backslash \mathcal{B}(S^\circ, \delta), \tag{2.3.47}$$

and

$$\texttt{slided}(t_e, x_0, \delta, S) = \forall t \in (0, t_e) : \phi_{C(\delta)}(t, x_0) \in \mathcal{B}(S, \delta). \tag{2.3.48}$$

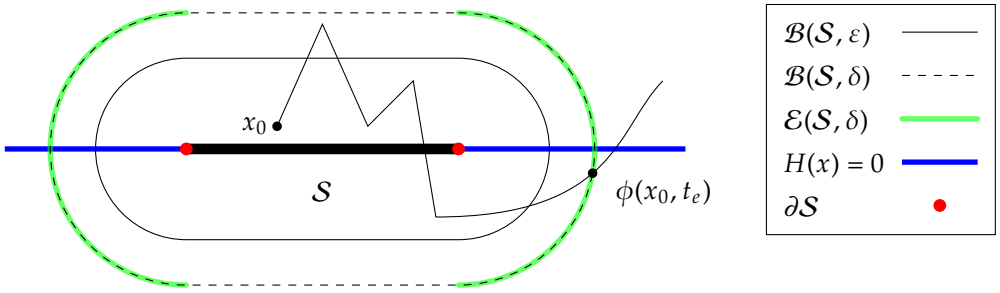

Figure 2.5: The diagram displays the key components for defining when a domain of a sliding surface is stable. The stability of the sliding surface requires that all trajectories leave any neighborhood of the sliding domain from neighborhoods of the boundary points of the domain, given that they start in a sufficiently small neighborhood of the domain. Thus, trajectories cannot leave the vicinity of the sliding surface except from the boundaries of the sliding domain.

2.3.3 Boundary layer dynamics and regularization theorems

The dynamics of variable structure systems where the control input is provided by a practically implemented controller in the limit as the controller restricts the system closer to a sliding surface of the system are determined by various regularization theorems [74]. In regularization the ideal control input is replaced by a more accurate model of the controller. The regularized control input then constraints the system locally in a region around the manifold where sliding occurs. The region where the system is constrained by the control algorithm is called the *boundary layer*. A boundary layer of width Δ around a sliding manifold

$$S(x) = 0 \tag{2.3.49}$$

is defined as the set of points $x \in \mathbb{R}^n$ such that

$$\|S(x)\| \leq \Delta, \tag{2.3.50}$$

where $\|s\| = \left(s^T \cdot s\right)^{\frac{1}{2}}$. Given any neighborhood of a domain of the sliding surface, a boundary layer exists so that it is fully contained within the neighborhood, up to the neighborhood of the boundaries of the sliding domain. Thus, any controller that maintains the system in the boundary layer as the boundary layer shrinks around the sliding domain, enforces stable sliding. The exact sliding solution is then determined by the resulting motion along the direction of the sliding surface.

The minimal convex hull determines the range of possible dynamical behaviors that can be achieved by regularized systems. For various classes of controllers for variable structure systems it has been proven that the dynamics of the controller converge to some dynamics within the minimal convex hull as the size of the boundary layer δ tends to zero. Proofs have been developed for systems, such as in systems linear with respect to their control input [74, §2.3], and systems with a step scalar control input [74, §3.1.1]. In some cases, such as systems that are linear with respect to their control input, the minimal convex hull contains a unique solution, and thus all regularized controllers converge to the same solution. The minimal convex hull however does not always contain a unique solution.

The minimal convex hull method determines the range of possible solutions for the sliding dynamics [73], [74]. The minimal convex hull is constructed of all available vector fields in the vicinity of a given point on the sliding surface. Then, the set of vectors in the convex hull that are tangent to the sliding surface give all the possible sliding vector fields at the given point of the sliding surface. In some systems, the minimal convex hull results in a set of solutions. For instance, systems with a discrete control signal that are non-linear with respect to their control input have a continuum of sliding solutions [74, §3.1.2].

When the solution predicted by the minimum convex hull is not unique, the exact solution depends by the details of the switching algorithm. The switching algorithm enforces some trajectory within the boundary layer, and as the boundary layer vanishes the limiting behavior of the trajectory is determine by the regularization process. For some switching algorithms the solution in the boundary layer converges to a unique value. For instance, in systems that slide in the intersection of two switching surfaces, where there is a switching surface for each switch and the control signal for the switch is generated independently from other switches by hysteresis switching with respect to the corresponding surface, it has been proven in [75] that the resulting dynamics converge to a unique sliding solution. However, in other hysteresis switching controllers it has been demonstrated that there is no unique regularization limit. For instance, in algorithms where there are interactions between the modulation of the switches the solution where the sliding dynamics converge depends on parameters such as the initial conditions [139]. In systems with a non-unique regularization limit all regularized sliding vector field are within the range determined by the minimal convex hull, but the regularization process does not produce well defined sliding dynamics to which all practical implementations converge.

2.3.4 Stability of a sliding surface in a practical controller

Given a variable structure system with a practical control algorithm, sliding may appear in any of the switching surfaces of the system and their intersections over some sliding domain. Sufficient conditions for stable sliding to appear on the intersection of a set of switching surfaces for system linear with respect to their control input were provided in [74, §4]. In some special cases it can be proven that a controller that enforced stable sliding on a domain of an arbitrary sliding manifold can be constructed. For instance in an intersection of multiple switching surfaces where all vector fields point to the intersection in a node like structure, a vector field can always be chosen that ensures that the system moves towards the intersection [122], [138], [140]. This construction is formalized in the following theorem, and a depiction of the construction process

can be seen in fig. 2.6.

Proposition 2.3.2 (Stability of node like intersection)**.** *Let the dynamics of a variable structure system with discrete input be given by*

$$D_t x = f(x, u) \tag{2.3.51}$$

for some function $f : \Omega \times \mathbb{R}^m \to \mathbb{R}^n$ witch is smooth on all its inputs, and let $\Omega \subset \mathbb{R}^n$ where $n > m$. Furthermore, let $\mathcal{M}$ be a sliding manifold defined by the function H, and define $V : \mathbb{R}^n \to \mathbb{R}$ where

$$V(x) = \frac{1}{2}\left(H(x)\right)^T \cdot H(x). \tag{2.3.52}$$

If for a sliding domain $\mathcal{D}$,

$$\exists \delta > 0, \forall \varepsilon > 0 : \varepsilon < \delta \Rightarrow (\forall x \in \mathcal{B}(\mathcal{D}, \varepsilon), \exists u \in \{0,1\}^m : D_t V(x,u) < 0) \tag{2.3.53}$$

then for any $x^* \in \mathcal{D}$ a control input exists that enforces sliding on $\mathcal{D}$ in a neighborhood of x^*.

Proof. Let $x^* \in \mathcal{D}$. Using the Taylor expansion of H on x^*,

$$H(x) = \partial_x H \cdot (x - x^*) + O\left(\|x - x^*\|^2\right) \tag{2.3.54}$$

in a sufficiently small neighborhood of x^*. Then in the same neighborhood

$$V(x) = \frac{1}{2}(x - x^*)^T \cdot A \cdot (x - x^*) + O\left(\|x - x^*\|^3\right) \tag{2.3.55}$$

where

$$A = (\partial_x H)^T \cdot \partial_x H. \tag{2.3.56}$$

Choosing a sufficiently small $\varepsilon_D > 0$ so that H is approximated sufficiently accurately by the linear term of the Taylor expansion, define the sliding domain

$$\mathcal{D}_s = \mathcal{D} \cap B(x^*, \varepsilon_D). \tag{2.3.57}$$

According to the definition of stability of a sliding domain, $\mathcal{D}_s$ is stable if the system trajectories exit the $\mathcal{B}(\mathcal{D}_s, \varepsilon_D)$ only through the neighborhoods of the boundary points of $\mathcal{D}_s$. Thus, it is sufficient to demonstrate that for a given control input the system never crosses points that are only in the boundary of the neighborhood of internal points of $\mathcal{D}_s$.

The row vectors of $\partial_x H$ are linearly independent, thus the null space of $\partial_x H$,

$$\text{null}(\partial_x H) = \{x \in \mathbb{R}^n : \partial_x H \cdot x = 0\} \tag{2.3.58}$$

has dimensionality $n - m$. Similarly since the rows of $\partial_x H$ are linearly independent, the column space of $(\partial_x H)^T$,

$$\text{column}((\partial_x H)^T) = \left\{(\partial_x H)^T \cdot c : x \in \mathbb{R}^m\right\} \tag{2.3.59}$$

has dimensionality m. Therefore, there exist orthonormal matrices $B_{\mathcal{M}} \in \mathbb{R}^{n \times (n-m)}$, and $B_H \in \mathbb{R}^{n \times m}$ that form a basis with their column vectors for $\text{null}(\partial_x H)$ and $\text{column}((\partial_x H)^T)$ respectively.

Furthermore, according to the rank-nullity theorem, the column vectors of the matrix

$$B = \begin{pmatrix} B_{\mathcal{M}} & B_H \end{pmatrix} \tag{2.3.60}$$

form a basis for $\mathbb{R}^n$, and since the column vectors of $B_{\mathcal{M}}$ are orthogonal to the column vectors of B_H, the basis is orthonormal.

To prove the sliding stability of $\mathcal{D}_s$ it will be demonstrated that for some $\varepsilon_s > 0$ such that $\varepsilon_s < \varepsilon_D$ the system trajectories do not cross $\mathcal{B}(\mathcal{D}_s, \varepsilon_s)$ through the set of points that are only in the boundary of the neighborhood of internal points of $\mathcal{D}_s$,

$$\mathcal{T} = \partial\mathcal{B}(\mathcal{D}_s, \varepsilon_s) \backslash \partial\mathcal{B}(\partial\mathcal{D}_s, \varepsilon_s). \tag{2.3.61}$$

An explicit form for $\mathcal{T}$ is derived; it is then proven that for any $x \in \mathcal{T}$ there exists a $y \in \mathbb{R}^{n-m}$ and a $z \in \mathbb{R}^m$ with $B_{\mathcal{M}} \cdot y + x^* \in \mathcal{D}_s$ and $\|z\| = \varepsilon_s$ such that

$$B_{\mathcal{M}} \cdot y + B_H \cdot z + x^* = x. \tag{2.3.62}$$

The column vectors of matrix B form a basis for $\mathbb{R}^n$, so any x can be written in the form of relation (2.3.62) uniquely. Let $x \in \mathcal{T}$, then for some unique $y \in \mathbb{R}^{n-m}$ and a $z \in \mathbb{R}^m$,

$$x = B_{\mathcal{M}} \cdot y + B_H \cdot z + x^*. \tag{2.3.63}$$

The projection of x along $\text{null}(\partial_x H) + x^*$ is then $B_{\mathcal{M}} \cdot y + x^*$. If $B_{\mathcal{M}} \cdot y + x^* \in \mathcal{D}_s$, then the minimum distance of x from $\mathcal{D}_s$ is

$$\left\| x - (B_{\mathcal{M}} \cdot y + x^*) \right\| = \|B_H \cdot z\| \tag{2.3.64}$$

$$= \|z\|. \tag{2.3.65}$$

Thus the point x is on $\mathcal{T}$ if and only if $\|z\| = \varepsilon_s$. If $B_{\mathcal{M}} \cdot y + x^* \notin \mathcal{D}_s$, then x cannot be in the boundary of an internal point. The set $\overline{\mathcal{D}_s} = \mathcal{D}_s \cup \partial\mathcal{D}_s$ is a complete and totally bounded set, thus the continuous function $\|x - x^*\|$ attains a minimum value in $\overline{\mathcal{D}_s}$. Since $x \in \mathcal{T}$,

$$\min_{x \in \overline{\mathcal{D}_s}} \|x - x^*\| = \varepsilon_s. \tag{2.3.66}$$

Let

$$x_m = B_{\mathcal{M}} \cdot y_m + x^* \tag{2.3.67}$$

be the point for which the minimum distance is attained. Since $B_{\mathcal{M}} \cdot y + x^* \notin \mathcal{D}_s$, the point $B_{\mathcal{M}} \cdot y_m + x^*$ has to be a boundary point of $\mathcal{D}_s$, and thus the x must be in the neighborhood of a boundary point. If x_m is not a boundary point, there exists $\varepsilon_m > 0$ such that

$$x_m + \varepsilon_m B_{\mathcal{M}} \cdot (y - y_m) \in \mathcal{D}_s. \tag{2.3.68}$$

Then

$$\|x - x_m\| = \left\| B_{\mathcal{M}} \cdot (y - y_m) + B_H \cdot z \right\| \tag{2.3.69}$$

$$= \left(\left\| y - y_m \right\|^2 + \|z\|^2 \right)^{\frac{1}{2}} \tag{2.3.70}$$

$$= \varepsilon_s, \tag{2.3.71}$$

by definition of x_m, where as

$$\left\| x - \left(x_m + \varepsilon_m B_{\mathcal{M}} \cdot (y - y_m) \right) \right\| = \left\| B_{\mathcal{M}} \cdot (y - y_m)(1 - \varepsilon_m) + B_H \cdot z \right\| \tag{2.3.72}$$

$$= \left((1 - \varepsilon_m)^2 \left\| y - y_m \right\|^2 + \|z\|^2 \right)^{\frac{1}{2}} \tag{2.3.73}$$

$$< \varepsilon_s. \tag{2.3.74}$$

This is a contradiction, so x is not on the boundary of the neighborhood of an internal point. Thus overall,

$$\mathcal{T} = \left\{ B_{\mathcal{M}} \cdot y + B_H \cdot z + x^* : \|z\| = \varepsilon_s \textbf{ and } B_{\mathcal{M}} \cdot y + x^* \in \mathcal{D}_s \right\}. \tag{2.3.75}$$

It will now be demonstrated that the function V can be used to ensure that the state of the system is withing $\mathcal{B}(\mathcal{D}_s, \varepsilon_s)$. The matrix $A \in \mathbb{R}^{n \times n}$ is Hermitian, and thus it is diagonalizable with real eigenvalues. Thus there exists a matrix E whose column vectors are eigenvectors that form a basis for $\mathbb{R}^n$, and a diagonal matrix of eigenvalues $\Lambda = \text{diag}(\lambda_1, \ldots, \lambda_n)$, where some eigenvalue may repeat such that

$$A = E^{-1} \Lambda E. \tag{2.3.76}$$

Then for any $x = B_{\mathcal{M}} \cdot y_m + x^*$,

$$V(x) = \frac{1}{2} (x - x^*)^T (\partial_x H)^T \partial_x H \, (x - x^*) + O\left(\|x - x^*\|^3 \right) \tag{2.3.77}$$

$$= \frac{1}{2} \left(B_{\mathcal{M}} y + B_H z \right)^T (\partial_x H)^T \partial_x H \left(B_{\mathcal{M}} y + B_H z \right) + O\left(\|x - x^*\|^3 \right) \tag{2.3.78}$$

$$= \frac{1}{2} z^T {B_H}^T (\partial_x H)^T \partial_x H B_H z + O\left(\|x - x^*\|^3 \right) \tag{2.3.79}$$

$$= \frac{1}{2} z^T {B_H}^T A B_H z + O\left(\|x - x^*\|^3 \right) \tag{2.3.80}$$

$$= \frac{1}{2} z^T {B_H}^T E^{-1} \Lambda E B_H z + O\left(\|x - x^*\|^3 \right), \tag{2.3.81}$$

where relation (2.3.79) follows from the fact that the column vectors of $B_{\mathcal{M}}$ form a basis for the null space of $\partial_x H$. For a diagonal matrix $\Lambda = \text{diag}(\lambda_1, \ldots, \lambda_n)$, and any vector $x \in\in \mathbb{R}^n$,

$$x^T \cdot \Lambda \cdot x = \sum_{i=1}^{n} \lambda_i x_i^2 < n \left(\max_{i \in \{1, \ldots, n\}} \lambda_i \right) \|x\|^2. \tag{2.3.82}$$

Therefore, an upper bound for the value of V is

$$V(x) < K \|E B_H z\|^2 + O\left(\|x - x^*\|^3 \right) \tag{2.3.83}$$

$$= K \left(z^T {B_H}^T E^{-1} E B_H z \right) + O\left(\|x - x^*\|^3 \right) \tag{2.3.84}$$

$$= K \|z\|^2 + O\left(\|x - x^*\|^3 \right), \tag{2.3.85}$$

where

$$K = \frac{1}{2} n \max \{\lambda_i : i \in \{1, \ldots, n\}\}. \tag{2.3.86}$$

Thus, a constant $\varepsilon_V > 0$ can be chosen so that for all $y \in \mathbb{R}^{n-m}$ such that $B_{\mathcal{M}} \cdot y + x^* \in \mathcal{D}_s$,

$$V(B_{\mathcal{M}} y + B_H z + x^*) < \varepsilon_V \Rightarrow \|z\| < \varepsilon_s. \tag{2.3.87}$$

The final step in the proof is to show that there is a control input so that the state does not cross $\mathcal{T}$ except after exiting $\mathcal{B}(\mathcal{D}_s, \varepsilon_s)$. Assume that for some $x = B_{\mathcal{M}} \cdot y + B_H \cdot z + x^*$,

$$V(x) = \varepsilon_V. \tag{2.3.88}$$

Then, by assumption there exists a control input $u \in \{0,1\}^m$ such that

$$D_t V(x, u) < 0. \tag{2.3.89}$$

Let the control algorithm select such a control input, and let $\phi : \mathbb{R}^n \times \mathbb{R} \to \mathbb{R}^n$ be a flow function of the system. Then, since the derivative is negative, and using the Taylor expansion of the smooth function $V \circ \phi$,

$$V(\phi(x,t)) = \varepsilon_V + D_t V(x,u)t + O(t^2), \tag{2.3.90}$$

and thus $V(\phi(x,t)) \leq \varepsilon_V$, for any sufficiently small t. Therefore, the system cannot cross $V(x) = \varepsilon_V$, and thus it cannot cross $\mathcal{T}$ unless it exits through the neighborhood of a boundary point of $\mathcal{D}_s$ first. □

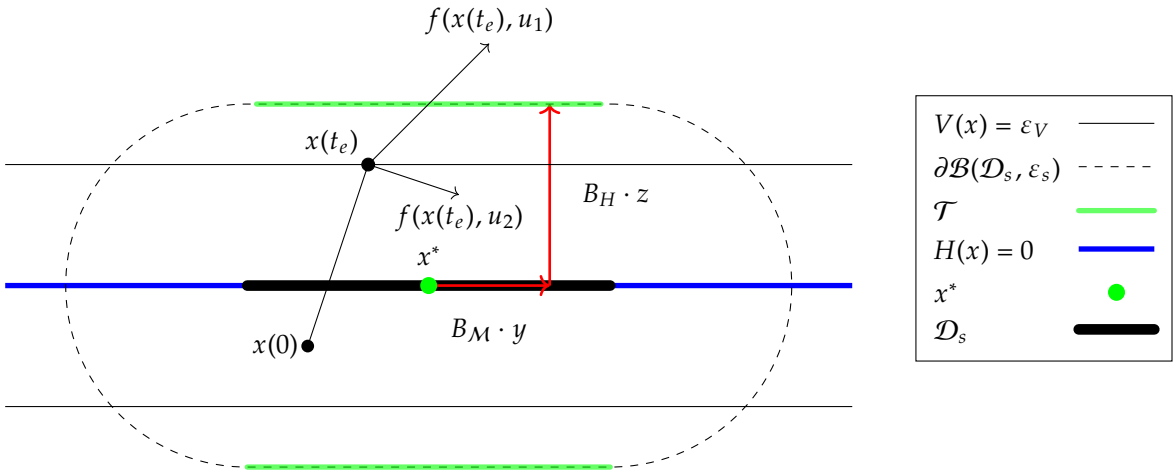

Figure 2.6: Control input selection for nodal stability. The figure depicts the boundary for the neighborhoods of internal points $\mathcal{T}$. Any point $x \in \mathcal{T}$ can be decomposed in coordinates y and z such that $x = B_{\mathcal{M}} \cdot y + B_H \cdot z + x^*$ such that $\|z\| = \varepsilon_s$ and $B_{\mathcal{M}} \cdot y + x^* \in \mathcal{D}_s$. By selecting an appropriately small ε_V the set of points $\{x \in \mathbb{R}^n : V(x) < \varepsilon_V\}$ does not cross $\mathcal{T}$. Selecting at every $x(t_e)$ for which $V(x(t_e)) = \varepsilon_V$ the control input that decreases V, for instance the control input u_2 in the figure, the trajectory $x(t)$ does not cross $\mathcal{T}$.

2.4 Sliding mode control

Sliding motion is a useful tool in the design of variable structure controllers. Due to the contraction of the system in the neighborhood of a restricted manifold in the state space, sliding mode algorithms offer a number of advantages over conventional linear controllers, such as global stability [148], complete rejection of disturbances outside an invariant surface [112], [113], and simple implementation of large signal stabilization [112]. These benefits lead to applications of sliding modes in the control of power electronics soon after sliding mode control theory became widely known [149].

As systems on the sliding mode remain on the sliding manifold, the sliding manifold becomes a topological invariant of the system. Thus the controlled system completely rejects any disturbance outside the sliding manifold up to saturation of the control input. Furthermore, as the flows in each side of a sliding manifold approach the manifold with a finite speed, the sliding manifold is reached in finite time. Thus by appropriately selecting switching manifolds, a control invariant can be enforced in finite time.

2.4.1 Sliding mode control for stabilization

Sliding mode controllers are a class of control algorithms that exploit the properties of the sliding motion. The objective of the stabilization problem for the *autonomous variable structure system* is to move and maintain the converter state on some point $x^* \in \mathbb{R}^n$ in the state space of the system. Sliding mode controllers achieve this objective by forcing the state of the system to slide on a surface in the state space. Thus the operation of the controller can be partitioned in two distinct phases [113], [144], [148]:

(i) a *reaching mode*, a phase where the full order dynamics of some of the switch modes of the system determine the flow of the system, and

(ii) a *sliding mode*, a phase where after reaching a sliding surface $\mathcal{S}$ of the system, the state of the system moves along the sliding surface according to some reduced order dynamics determined by the minimal convex hull method.

In order to stabilize the converter on the state $x^* \in \mathbb{R}^n$ the sliding surface must be chosen so that the state is on the sliding surface $x^* \in \mathcal{S}$, and furthermore, x^* must be a fixed point of the sliding dynamics.

Definition 2.4.1 (Sliding manifold)**.** A *sliding manifold* of a variable structure system with a variable structure controller is a manifold defined by the null space of a smooth function $H : \mathbb{R}^n \to \mathbb{R}^m$ for $m < n$,

$$\mathcal{M} = \{x \in \mathbb{R}^n : H(x) = 0\}, \tag{2.4.1}$$

such that the set

$$\{\partial_x H_i : i = 1, \ldots, m\} \tag{2.4.2}$$

is linearly independent.

The sliding manifold is thought of in this thesis as a control objective, and it is independent from the switching surfaces. It is an invariant condition that the switching algorithm of the

converter enforces. A sliding mode controller enforces sliding on a manifold $\mathcal{M}$ if the system state $x \in \mathbb{R}^n$ of the controlled system if

- x reaches $\mathcal{M}$ in finite time, and
- stable sliding is established on $\mathcal{M}$.

In general the sliding manifold is not identical to the switching surfaces of the system so a different symbol is used for the sliding manifold and the sliding surfaces. Defining the manifolds

$$\mathcal{M}_i = \{x \in \mathbb{R}^n : H_i(x) = 0\}, \tag{2.4.3}$$

for $i = 1, \ldots, m$, sliding may not occur in any manifold individually, or in any partial intersection

$$\mathcal{M}_{\mathcal{I}} = \bigcap_{i \in \mathcal{I}} \mathcal{M}_i, \tag{2.4.4}$$

where $\mathcal{I} \subset \{0, \ldots, m\}$ such that $\mathcal{I} \neq \{0, \ldots, m\}$. However, sliding must occur in the intersection of all manifolds

$$\mathcal{M} = \bigcap_{i=1}^{m} \mathcal{M}_i. \tag{2.4.5}$$

The design of a sliding mode controller usually starts with the selection of a sliding manifold $\mathcal{M}$. The range of the expected dynamics on the sliding mode is determined by the minimal convex hull or some regularization method, and the sliding manifold is selected so that the sliding dynamics satisfy the control objectives. In order to enforce sliding in the selected manifold $\mathcal{M}$, the ideal switching surfaces of a variable structure system are selected so that for some subset $\mathcal{I}$ of the switching surfaces, sliding exists on the intersection of the surfaces $\mathcal{S}_{\mathcal{I}}$, and furthermore $\mathcal{M}$ coincides with the intersection $\mathcal{M} = \mathcal{S}_{\mathcal{I}}$. Finally, an algorithm for generating the switching signal is constructed to implement the sliding mode.

2.5 Evaluating the vector fields of the sliding dynamics

The design of a sliding mode controller for the trans-Z-source converter requires the evaluation of the sliding dynamics on arbitrary sliding manifolds. The design is based on a parametrized family of sliding manifolds. The sliding dynamics are chosen by adjusting the parameter determining the sliding surface. Thus in order to select the parameter a method is required to determine the dynamics on the sliding surface, and provide a relation between the parameter of the sliding surface and the sliding vector field.

Notation is now introduced that simplifies the analysis of switched systems such as power converter and the derivation of the sliding vector field. The convex hull of switched systems is constructed using the scalar combination of the available vector fields. A notation for the scalar combination of the available vector fields is first introduced. Then the convex hull is defined, and a set of constraints is introduced that describe the sliding dynamics solutions predicted by the convex hull.

Definition 2.5.1 (Scalar combination of vector fields)**.** Given the dynamics of a variable structure system,

$$D_t x = f(x, u) \tag{2.5.1}$$

where $f : \Omega \times \mathbb{R}^m \rightarrow \mathbb{R}^n$ for $m < n$, $\Omega \subset \mathbb{R}^n$, and f is smooth on all it inputs, the scalar combination of the vector fields is the vector field

$$D_t x = f_s(x, \gamma) \tag{2.5.2}$$

where

$$f_s(x, \gamma) = \sum_{w \in U} \gamma_w f(x, w), \tag{2.5.3}$$

$U = \{0, 1\}^m$ is the finite set of binary discrete inputs, and $\gamma : U \rightarrow \mathbb{R}$.

Any control input of the original system is translated to a control input for the scalar system by an appropriate mapping to scalar combinations of vector fields. Given any $u \in U$, the control input $\gamma : U \rightarrow \mathbb{R}$ for the scalar combination of vector fields given by

$$\gamma_i = \begin{cases} 1, & i = u \\ 0, & \text{otherwise} \end{cases} \tag{2.5.4}$$

results in

$$f_s(x, \gamma) = f(x, u), \tag{2.5.5}$$

which is the dynamics of the variable structure system with discrete inputs, for the control input u. Thus, in general the mapping $m : U \times U \rightarrow \mathbb{R}$, given by

$$m_i(u) = \begin{cases} 1, & i = u \\ 0, & \text{otherwise} \end{cases} \tag{2.5.6}$$

maps the control input for the variable structure system with discrete inputs to the control input of a scalar combination of vector fields that displays the same dynamical behavior.

2.5.1 The minimal convex hull

The most generic method for evaluating the sliding vector field is the minimal convex hull method. The solutions of the minimal convex hull are determined by the set of all collections of scalar multipliers that enforce sliding. The solutions may not be unique, and they do not provide a mechanism for implementing the sliding solution. It will be later demonstrated for the case of the trans-Z-source converter how optimization algorithms can be used to determine the range of possible sliding vector fields. The range of sliding solutions is important in the control design problems as it determines whether any practical controller can achieve the desired dynamical response for the controlled system.

Definition 2.5.2 (Minimal convex hull for a scalar combination of vector fields)**.** Given a *scalar combination of vector fields* and a *sliding surface* $\mathcal{M}$ defined by a function H, if stable sliding exists on the surface H the dynamics of the system are determined by

$$f_s(x) = \sum_{u \in U} \gamma_u f(x, u) \tag{2.5.7}$$

for any $\gamma : U \to \mathbb{R}$ that satisfies the constraints

$$\begin{cases} \partial_x H \cdot f_s(x) = 0, & \text{(2.5.8a)} \\ \sum_{u \in U} \gamma_u = 1, & \text{(2.5.8b)} \\ \forall u \in U : 0 \leq \gamma_u \leq 1. & \text{(2.5.8c)} \end{cases}$$

The minimal convex hull definition provides a set of possible dynamical responses for every point on the sliding surface. The performance that sliding mode controllers achieve for a given surface can then be determined by determining the optimal solutions over the convex hull by any quadratic optimization algorithm. The condition in relation (2.5.8a) requires that the system remains on the sliding surface, and can be expressed in terms of γ as

$$\partial_x H \cdot f_s(x) = 0 \tag{2.5.9}$$

$$\Leftrightarrow \quad \partial_x H \cdot \left(\sum_{u \in U} \gamma_u f(x, u) \right) = 0 \tag{2.5.10}$$

$$\Leftrightarrow \quad \sum_{u \in U} \gamma_u \left(\partial_x H \cdot f(x, u) \right) = 0. \tag{2.5.11}$$

The controller for the converter is implemented by switching in the vicinity of the sliding surface. A number of m switching surfaces is enough to define a sliding manifold of co-dimension $(n - m)$. The sliding dynamics f_s, are parameterized by $\gamma : U \to \mathbb{R}$, which are $|U| = 2^m$ parameters, whereas there are $(m + 1)$ equality constraints in the minimal convex hull. Thus except for $m = 1$, the convex hull describes a set of possible solutions. In cases where for some $x \in \mathcal{M}$ the set

$$\{ f(x, u) : u \in U \} \tag{2.5.12}$$

is not linearly independent, there is not a one-to-one correspondence between sets of scalar multipliers γ and the sliding dynamics in relation (2.5.7). Thus unique sliding solutions may arise even when there are multiple solution for the scalar multipliers. A typical example is systems that are linear in their control input [74, §2]. When multiple solutions exist, the flow function for the ideal dynamics of the variable structure systems are given by differential inclusions. In practical implementations of the controller the flow is deterministic and depends on the exact implementation of the control algorithm providing the switched control signal.

The notation in the convex hull solution provides some intuition about the meaning of scalar multipliers. The parameter γ_u for each mode u, is the portion that mode u contributes in the sliding motion. For instance, in hysteresis switching where the limit of the regularized dynamics exists, γ_u tends to the time the system spends on mode u on average as the hysteresis width tends to zero. Regularization theorems, such as those for hysteresis controllers, prove the convergence of the fraction of time that the solution spends in each mode as the boundary layer vanishes. The scalar multipliers are determined by the time fractions and are then used to evaluate the sliding vector field in relation (2.5.7). In some cases the time fractions do not converge to a unique value. For instance, in some cases the resulting sliding vector field depends on the initial conditions inside the boundary layer. However, even if the sliding dynamics are not unique the sliding vector field is always located in the minimal convex hull.

2.5.2 Sliding dynamics for a continuous control input

In the design of sliding mode controllers it is quite often easy to construct an ideal continuous control input that maintains the system state on the sliding surface. Given such a control input, the resulting sliding dynamics are then determined to ensure that the dynamics on the sliding mode display the desired behavior. For systems linear with respect to their control input, regular forms and the accompanying reduction methods are formalized in various textbooks such as [74, §6.4], and simplify the process of deriving the sliding dynamics. The regularization methods are extended to handle generic systems that can be non-linear with respect to their control input. The discussion focuses on linear switching surfaces which are later used for the sliding mode control of trans-Z-source converters. A process is described that given any sliding manifold $\mathcal{M}$, defined by a function H, and a control input u enforcing sliding on $\mathcal{M}$, constructs the sliding dynamics.

Let the sliding manifold $\mathcal{M}$ be defined by the function H, and let the dynamics of a variable structure system while it slides on $\mathcal{M}$ be defined as

$$D_t x = f(x, u),\ x \in \mathcal{M} \tag{2.5.13}$$

for some control input u resulting in sliding, and some function $f : \Omega \times \mathbb{R}^m \to \mathbb{R}^m$, where $m < n$, $\Omega \subset \mathbb{R}^n$, and f is smooth on all its inputs. While the system slides on the surface $\mathcal{M}$, the system state $x \in \Omega$ satisfies the relation

$$H(x) = 0, \tag{2.5.14}$$

and therefore the dynamics must also satisfy

$$D_t H = 0. \tag{2.5.15}$$

Expanding the time derivative according the chain rule,

$$\begin{aligned} D_t H &= \partial_x H \cdot D_t x && (2.5.16)\\ &= \partial_x H \cdot f(x, u), && (2.5.17) \end{aligned}$$

where the dynamics of x were substituted from relation (2.5.13).

A mapping from the sliding manifold $\mathcal{M}$ to the vector space $\mathbb{R}^n$ is now constructed for the special case where H is a linear affine function. The sliding surface function $H : \mathbb{R}^n \to \mathbb{R}^m$ determines the sliding surface $\mathcal{M}$ by its null space

$$\mathcal{M} = \{x \in \mathbb{R}^n : H(x) = 0\}. \tag{2.5.18}$$

When H is a linear affine function, then

$$H(x) = A \cdot x + c \tag{2.5.19}$$

for some $A \in \mathbb{R}^{m \times n}$ that has full rank and $c \in \mathbb{R}^m$. Furthermore, since H defines a sliding surface, the set

$$\{\partial_x H_i : i = 1, \ldots, m\} \tag{2.5.20}$$

is linearly independent, and thus

$$A = \partial_x H \tag{2.5.21}$$

has full rank. Defining a matrix

$$B_{\mathcal{M}} = \begin{pmatrix} b_1 & \dots & b_{n-m} \end{pmatrix} \tag{2.5.22}$$

whose columns $b_1, \dots, b_{n-m} \in \mathbb{R}^n$ form a basis for $\text{null}(\partial_x H)$ where

$$\text{null}(\partial_x H) = \{x \in \mathbb{R}^n : \partial_x H \cdot x = 0\}. \tag{2.5.23}$$

Then given any $x^* \in \mathbb{R}^n$ on the sliding surface such that $H(x^*) = 0$, the function $M : \mathbb{R}^{n-m} \to \mathbb{R}^n$ where

$$M(y) = B_{\mathcal{M}} \cdot y + x^* \tag{2.5.24}$$

provides a map from $\mathbb{R}^{n-m}$ to $\mathcal{M}$. Indeed for any $y \in \mathbb{R}^{n-m}$,

$$\begin{aligned} H(M(y)) &= H(B_{\mathcal{M}} \cdot y + x^*) && (2.5.25)\\ &= A \cdot \left(B_{\mathcal{M}} \cdot y + x^*\right) + c && (2.5.26)\\ &= (A \cdot B_{\mathcal{M}}) \cdot y + (A \cdot x^* + c) && (2.5.27)\\ &= (A \cdot B_{\mathcal{M}}) \cdot y + H(x^*) && (2.5.28)\\ &= 0, && (2.5.29) \end{aligned}$$

since $H(x^*) = 0$ by definition, and $A \cdot B_{\mathcal{M}} = 0$ as the column vectors of $B_{\mathcal{M}}$ span $\text{null}(\partial_x H) = \text{null}(A)$.

To determine the dynamics of the system on the sliding mode it is enough to determine the dynamics of $y \in \mathbb{R}^{n-m}$. For any $y \in \mathbb{R}^{n-m}$ there exists an $x \in \mathcal{M}$ such that

$$x = M(y). \tag{2.5.30}$$

Therefore,

$$\begin{aligned} & D_t x = D_t M(y) && (2.5.31)\\ \Rightarrow \quad & f(x,u) = B_{\mathcal{M}} \cdot D_t y && (2.5.32) \end{aligned}$$

where the last equality follows from relation (2.5.24), and the dynamics of x. Since the column vectors of $B_{\mathcal{M}}$ are linearly independent, a matrix $\overline{B}_{\mathcal{M}} \in \mathbb{R}^{(n-m)\times n}$ can be constructed by the Gram-Schmidt process [150], such that

$$\overline{B}_{\mathcal{M}} \cdot B_{\mathcal{M}} = I_{n-m}, \tag{2.5.33}$$

where $I_{n-m} \in \mathbb{R}^{(n-m)\times(n-m)}$ is the identity matrix. Therefore,

$$\begin{aligned} & B_{\mathcal{M}} \cdot D_t y = f(x,u) && (2.5.34)\\ \Rightarrow \quad & D_t y = \overline{B}_{\mathcal{M}} \cdot f(x,u) && (2.5.35)\\ \Rightarrow \quad & D_t y = \overline{B}_{\mathcal{M}} \cdot f(M(y),u), && (2.5.36) \end{aligned}$$

where in the last equality the fact that $x = M(y)$ was used. The problem of evaluating $\overline{B}_{\mathcal{M}}$ can be simplified in terms of computational complexity by selecting an orthonormal base for $B_{\mathcal{M}}$, in which case $\overline{B}_{\mathcal{M}} = {B_{\mathcal{M}}}^T$.

2.6 Algebraic methods for evaluating the sliding dynamics

When a sliding solution exists, algebraic methods significantly simplify the evaluation of the sliding manifold. In the design of a sliding mode controller where the sliding manifold is selected from a family of sliding manifolds, the sliding dynamics must be evaluated for every member of the family. Algebraic method can efficiently generate closed form solutions for the sliding dynamics. Two methods are explored, the equivalent control and the canopy method.

2.6.1 Equivalent control

The equivalent control is defined on the sliding surface of systems linear to their control input [74]. The dynamics of an autonomous variable structure system which is linear with respect to its control input are

$$D_t x = f(x) + g(x) \cdot u \tag{2.6.1}$$

where $f : \mathbb{R}^n \to \mathbb{R}^n$, $g : \mathbb{R}^n \to \mathbb{R}^{n\times m}$ are smooth functions, and $u \in \mathbb{R}^m$ is the control input. Given a sliding manifold $\mathcal{M}$ defined by the function H, the equivalent control method allows the construction of an ideal continuous feedback control function u_{eq} on the manifold $\mathcal{M}$, such that for any trajectory $x : \mathbb{R} \to \mathbb{R}^n$ solving

$$D_t x = f(x) + g(x) \cdot u_{\text{eq}}, \tag{2.6.2}$$

if $x(t_0) \in \mathcal{S}$ then $x(t) \in \mathcal{S}$ for $t > t_0$. While $x \in \mathcal{M}$,

$$H(x) = 0. \tag{2.6.3}$$

Therefore, the solution x must also satisfy

$$D_t H = 0 \tag{2.6.4}$$

while on $\mathcal{S}$.

According to the chain rule, the time derivative of H is evaluated as follows.

$$\begin{aligned} D_t H &= \partial_x H \cdot D_t x && (2.6.5)\\ &= \partial_x H \cdot \big(f(x) + g(x) \cdot u\big) && (2.6.6)\\ &= \partial_x H \cdot f(x) + \partial_x H \cdot g(x) \cdot u, && (2.6.7) \end{aligned}$$

where the dynamics of x were substituted from relation (2.6.1). The Lie derivative defined as

$$\mathcal{L}_f H = \partial_x H \cdot f(x). \tag{2.6.8}$$

can simplify the notation in relation (2.6.7). So using the Lie derivative notation the time

derivative of H is

$$D_t H = \mathcal{L}_f H + \mathcal{L}_g H \cdot u. \tag{2.6.9}$$

Therefore, the equivalent control is defined as follows.

Definition 2.6.1 (Equivalent control)**.** The equivalent control input for variable structure system with dynamics defined by relation (2.6.2), on the sliding manifold $\mathcal{M}$ defined by a function H is the control input u_{eq} solving the equation

$$\mathcal{L}_f H + \mathcal{L}_g H \cdot u_{\text{eq}} = 0, \tag{2.6.10}$$

and is defined for any $x \in \mathcal{M}$.

To determine the dynamics on the sliding surface $\mathcal{M}$ defined by an affine function H under the equivalent control, the control input $u = u_{\text{eq}}$ is substituted in relation (2.5.36). The equivalent control is defined implicitly over the sliding manifold in relation (2.6.10) is a function of the system state, $u_{\text{eq}} : \mathcal{M} \to \mathrm{R}^m$. Let M be the mapping introduced for H in relation (2.5.24). Since $M(y) \in \mathcal{M}$ for all $y \in \mathbb{R}^{n-m}$, substituting the equivalent control input in relation (2.5.36) for the system in relation (2.6.1), the dynamics on the sliding mode under the equivalent control are

$$\begin{aligned} D_t y &= \overline{B}_{\mathcal{M}} \cdot \big(f(M(y)) + g(M(y)) \cdot u_{\text{eq}}\big) && (2.6.11)\\ &= \overline{B}_{\mathcal{M}} \cdot f(M(y)) + \overline{B}_{\mathcal{M}} \cdot g(M(y)) \cdot u_{\text{eq}}. && (2.6.12) \end{aligned}$$

Defining the function $g_s : \mathbb{R}^{n-m} \to \mathbb{R}^{n-m}$, where

$$g_s(y) = \overline{B}_{\mathcal{M}} \cdot f(M(y)) + \overline{B}_{\mathcal{M}} \cdot g(M(y)) \cdot u_{\text{eq}}, \tag{2.6.13}$$

the dynamics are then

$$D_t y = g_s(y). \tag{2.6.14}$$

The equivalent dynamics describe an autonomous system, not affected directly by the control input. The equivalent dynamics are however determined directly by the selection of the sliding surface, which implicitly determines the equivalent control input u_{eq}.

2.6.2 The canopy solution

In systems that are linear with respect to their control input, the equivalent control method can be used to construct an ideal control input enforcing sliding. However, the equivalent control method cannot be applied in systems non-linear with respect to their control input. In non-linear systems the convex hull intersection with the sliding surface can contain multiple points resulting in multiple sliding solutions. An extension of the equivalent control method, the *canopy method*, is introduced in [151] to algebraically construct a control input enforcing sliding in systems that are non-linear with respect to their control input.

The canopy is a subset of the convex hull defined by the intersection of a surface of co-dimension one with the sliding manifold. The canopy solutions are then defined as the intersections of the canopy with the sliding surface. For systems non-linear in their control input, the canopy results in a finite number of isolated solutions located inside the convex hull. Further-

more, when the convex hull is flat, the canopy coincides with the convex hull. In this case the canopy method results in the same unique sliding speed predicted by the convex hull method and the equivalent control method. Canopy solutions are an ideal control input like the equivalent control and they provide no information on how to implement them. However, the canopy solutions are a useful reference point when analyzing the convex hull, and they will be used in the analysis of the sliding dynamics of the trans-Z-source converter.

For a variable structure system and a sliding manifold $\mathcal{M}$ defined by some function H, the canopy solution for the sliding dynamics is determined by

$$f_{\text{cp}}(x) = \sum_{u \in U} \left(\prod_{i=1}^{m} \mu_i^{u_i} \right) f(x, u) \tag{2.6.15}$$

where for all $i = 1, \ldots, m$,

$$0 \leq \mu_i \leq 1, \tag{2.6.16}$$

and

$$\mu_i^1 = \mu_i, \qquad \mu_i^0 = 1 - \mu_i, \tag{2.6.17}$$

such that the vector μ satisfies the equation

$$\partial_x H \cdot \left(\sum_{u \in U} \left(\prod_{i=1}^{m} \mu_i^{u_i} \right) f(x, u) \right) = 0 \tag{2.6.18}$$

or equivalently

$$\sum_{u \in U} \left(\prod_{i=1}^{m} \mu_i^{u_i} \right) \left(\partial_x H \cdot f(x, u) \right) = 0. \tag{2.6.19}$$

The canopy equations result in a finite number of isolated solutions in the convex hull. Let M be the mapping introduced for H in relation (2.5.24). Since $M(y) \in \mathcal{M}$ for all $y \in \mathbb{R}^{n-m}$ and given a specific solution for the canopy equation, $\mu_{\text{cp}} : \mathcal{M} \to \mathbb{R}^m$, the resulting sliding dynamics are determined by

$$D_t y = \overline{B}_{\mathcal{M}} \cdot \left(\sum_{u \in U} \left(\prod_{i=1}^{m} \mu_{\text{cp}_i}^{u_i}(M(y)) \right) f(x, u) \right). \tag{2.6.20}$$

Defining the function $g_{\text{cp}} : \mathbb{R}^{n-m} \to \mathbb{R}^{n-m}$,

$$g_{\text{cp}}(y) = \overline{B}_{\mathcal{M}} \cdot \left(\sum_{u \in U} \left(\prod_{i=1}^{m} \mu_{\text{cp}_i}^{u_i}(M(y)) \right) f(x, u) \right), \tag{2.6.21}$$

the dynamics of the sliding mode according to the canopy solution are

$$D_t y = g_{\text{cp}}(y). \tag{2.6.22}$$

2.7 Concluding remarks

The section introduced the main constructs required for the design of a sliding mode controller for the trans-Z-source converter. Power electronic converters are modeled as variable structure systems with discrete inputs. Variable structure systems are an ideal model where a dynamical behavior called the sliding appears on a surface where ideal switching occurs, when the surface satisfies some stability conditions. The solutions for variable structure systems with discrete inputs were then defined using the minimal convex hull. The dynamics of actual implementation tend to the dynamics within the convex hull as the non-ideal behavior in the implementation vanishes.

Controllers for variable structure systems are designed by selecting the sliding surface of the system to enforce the desired dynamics on the sliding mode. Algebraic methods simplify the derivation of the sliding dynamics. The resulting solutions do not provide an implementation of the required control input, but they provide a computationally efficient method for determining the dynamics of the controlled system. In some cases where the sliding dynamics of algebraic solution such as the equivalent control can be enforced, there are regularization proofs for some classes of controllers proving that the resulting sliding dynamics tend to the dynamics predicted by the algebraic solution.

Chapter 3

Sliding mode control and jitter in the trans-Z-source converter

Designing a sliding mode controller for impedance source converters is a challenging problem. In this section, a stabilizing sliding mode controller is designed for the DC-DC voltage source trans-Z-source converter, a member of the impedance source converter family with a coupled inductor. As part of the design process, a sliding manifold is selected, and two switching algorithms are constructed that enforce sliding. The sliding manifold of the impedance source converter lies in the intersection of two switching surfaces. The minimal convex hull method predicts the existence of a continuum of sliding solutions for certain systems sliding on the intersection of multiple switching surfaces. In the boundary layer of the intersection defining the sliding manifold, the system converges into some limit cycle; bifurcations in this limit cycle as the system moves along the sliding surface lead to discontinuous changes in the rate of change of the sliding speed, a phenomenon called jitter. It is demonstrated in this chapter that jitter appears in the trans-Z-source converter. This is to our knowledge the first demonstration of jitter in a practical power electronic circuit.

3.1 Introduction

The impedance source family of converters is a set of converter topologies that introduces a network of passive elements between the source and the output bridge. The dynamics of the impedance network were first used in power inversion where impedance source inverters overcome some of the fundamental limitations of conventional voltage source and current source inverters [26], [81], [152], [153]. In the conventional voltage source inverter, the maximum output voltage is less than the input voltage and a dead-time in the switching devices of each phase leg is required to prevent an accidental shoot-through. Conversely, in the conventional current source inverter, the output voltage can only be higher than the input voltage and an overlap time between the phase legs is required to avoid an accidental open-circuit between the high and low voltage output terminals of the phase bridge. By storing energy in the impedance network, impedance source converters provide a theoretically unlimited voltage gain range in their output, and furthermore they are tolerant to both shoot-through and open-circuits in the

phase bridge eliminating the need for programming dead-time in the modulation signal [29].

Impedance source topologies have found many applications apart from single level power inversion. Variations of the basic topology have been developed including galvanically isolated converters [154]–[156], multilevel converters [27], and DC-DC converters [29], [72]. Impedance source converter topologies can be broadly classified as voltage and current fed converters depending on the type of the power source with topologies appearing in symmetrical pairs of current and voltage fed topologies [153]. Due to this symmetry the following discussion focuses on voltage fed topologies only.

3.1.1 Control and modulation of impedance source converters

Impedance source converters are characterized by non-minimum phase response to their control input. The impedance network modifies the dynamical behavior compared to conventional converters allowing new topological configuration in output phase bridge. In addition to the zero and active modes an energy transfer mode is available in impedance source converters, which are the short-circuits of the phase bridge (shoot-through) in voltage fed converters and the open-circuits in current fed converters. The impedance network is a form of a bilinear network [124] where the transfer of energy during shoot-through modes boosts the output voltage. However, shoot-through states are identical to the zero state of the converter during which there is no control of the output resulting in non-minimum phase behavior [69].

Averaged controllers are extensively used in impedance source converters. Nested feedback control loops are required to ensure stability due to the non-minimum phase response of the converter to their control input. Early designs used linear control with gain scheduling due to its simplicity [157]. However, gain scheduling does not regulate accurately the impedance network, where transients in high power applications cause large voltage spikes across switches. This problem is rectified in dual loop controllers that directly control the filter current [158]–[161]. More accurate control of the bridge peek voltage is achieved by combining the feedback with direct feed-forward control of the bridge voltage [162]. In an effort to improve the performance of the control algorithms in regulating the transient response and ensure global stability, averaged non-linear control methods have been developed. To control the peak DC-link voltage, a fuzzy logic controller is introduced in [163], and a unified controller of the output and impedance network voltages based on space vector modulation in [164].

The continuous control signal produced by averaged controllers is converted to the discrete input that drives the switches by a pulse width modulation algorithm. Pulse width modulation schedules the active and shoot-through states according to a predetermined series of transitions in the system topology. Modulation schemes have been developed in an effort to regulate and balance voltage stresses in the output bridge switches and the maximum voltage gain of the converter [69]–[71]. The basic pulse width modulation schemes for impedance source converters are constant boost modulation [67] which minimizes voltage stress, maximum boost modulation [66] that maximizes the voltage gain, and maximum constant boost modulation [65] that provides a balance between voltage gain and voltage stress in the switches. Space vector pulse width modulation algorithms dynamically determine the series of state transitions offering superior transient response [164]. Space vector modulation schemes for the reduction of switching losses [68], and the control of multilevel impedance source topologies have been

developed [28]. However, pulse width modulation cannot be used with every controller. Many sliding mode controllers rely in hysteresis modulation to ensure stable sliding.

3.1.2 Sliding mode control for impedance source converters

Sliding mode control algorithms have been explored for impedance source converters. Advantages of sliding mode controllers over averaged control designs include global stability [148], complete rejection of disturbances outside an invariant surface [112], [113], and a structured and computationally efficient design of the controller by the selection of a sliding manifold [112]. Furthermore, due to the restriction of the state on the sliding manifold the dynamics of the controlled system are of reduced order, simplifying the analysis and the design of the controller. The designs developed for impedance source converters however, impose sliding either on the state of the impedance network or the converter output, but not both.

The main obstacle in constructing implementing sliding mode controllers for impedance source converters is that in hysteresis modulation there is interference between the modulation of the output and the impedance network. A sliding mode controller developed in [60] uses hysteresis modulation for the output current, and shoot-through states are inserted in the zero states of the hysteresis modulation according to a pulse width modulated signal. Conversely, in [61] and [62] sliding mode controllers are used for the impedance network and shoot-through states are inserted in the zero states of the modulation of the impedance network. Integral sliding modes ensure asymptotic convergence to the control objective while maintaining the state of the system on the sliding surface at all times. As there is no reaching phase, integral sliding modes provide a continuous control signal that can be implemented with pulse width modulation. Integral sliding mode controllers for the impedance network introduced in [63] and [64] are thus used directly with averaged controllers for the output of the converter, and the switching signal is generated by any of the available pulse width modulation schemes for impedance source converters.

Sliding mode controllers able to control impedance source converters in the full range of their dynamical behavior have not yet been developed. In hybrid approaches the advantages of sliding modes, such as the complete rejection of disturbances outside the sliding manifold and reduced order dynamics are not realized for the control objectives that are not enforced using sliding modes. As a result, the performance of the controller is poorer than a controller enforcing all control objectives using sliding modes, and the analysis of the response of the controlled system is more computationally complex as a dynamical system of higher order is analyzed. Sliding mode control algorithms using a single sliding surface have been developed for DC-DC impedance source converters in special applications to overcome the constraints of hybrid approaches. In such applications however, additional constrains are placed in the control of impedance network. For instance, in the controller developed in [72] the network operates in maximum boost mode; as a result the input and output power are coupled and the converter cannot be used in application such as active power filtering. To fully exploit the dynamics of impedance source converters and the advantages of sliding modes, a sliding mode controller with two independent switching surfaces is required.

3.1.3 Designing a sliding mode controller for impedance source converters

A sliding mode controller is proposed for the control of impedance source converters. The controller uses two invariant surfaces to track a desired state in the impedance network and the converter output. The intersection of the two invariant surfaces forms the sliding manifold. Two hysteresis algorithms are designed to enforce sliding. The first algorithm uses sliding on the intersection of two switching surfaces. Sliding is imposed on a surface whenever it is reached, and the sliding dynamics in each surface are designed so that the state of the systems converges in their intersection. A method for selecting the switching surfaces for a given sliding manifold is also developed. The selected switching surfaces are optimal with respect to their ability to impose sliding under perturbation in the parameters of the system. The second algorithm imposes sliding to the desired manifold, by imposing sliding on manifolds of progressively higher co-dimension. Sliding is initially imposed on a conventional co-dimension one surface, and when a desired co-dimension two manifold is reached in this initial surface, sliding is imposed on the manifold. To enforce sliding on the co-dimension two manifold, a modulation algorithm where switching occurs with hysteresis with respect to a co-dimension two manifold is used.

The design of the control algorithm focuses on the voltage fed trans-Z-source converter, a type of DC-DC impedance source converter with a coupled inductor in its impedance network [80], [81]. Converters with coupled inductors are preferred in applications with high voltage gain where by using the transformer turns ratio to boost the voltage, the converter reduces the switching losses associated with high peak currents. Furthermore, the trans-Z-source converter is a fully actuated system that simplifies the design of the controller. Most impedance source topologies are under-actuated, and circular currents can appear in the impedance network. In the sliding mode control of such systems, the system state is allowed to vary freely on some subspace [82], and thus a transformation of the coordinate system is required. Impedance source converters with coupled inductors, such as the trans-Z-source converter, are however fully actuated systems due to the magnetic coupling of the inductor thus eliminating the need for a state transformation.

3.1.4 Jitter and its effects on the controller performance

Sliding mode controllers regulating the whole state of the Z-source inverter require sliding along a manifold of co-dimension higher than one. When the sliding is implemented using hysteresis modulation, the dynamics of the motion in the hysteresis layer determine the speed along the sliding surface. If the system is sliding on the intersection of two switching surfaces, a regularization process introduced in [75] determines the sliding dynamics in the ideal limit where the hysteresis layer vanishes. As the hysteresis layer vanishes, the dynamics of the system are effectively linearized and projected on a plane perpendicular to the sliding surface. A limit cycle appears in the projected system that determines the resulting sliding speed [75]. As the system moves along the sliding surface bifurcations appear in the limit cycle; the resulting variation in the sliding speed called *jitter* was analyzed in [76].

In a system sliding on a manifold of co-dimension two, the modulation uses switching with hysteresis with respect to the co-dimension two sliding manifold. The resulting trajectory in the sliding manifold does not always converge to a well defined limit cycle. When applying the

regularization process in hysteresis layer around a manifold of co-dimension two, the resulting trajectory in the projected dynamics may be chaotic or may converge to a limit cycle dependent on the initial state. Thus the existence of limit of the regularization process cannot be proven in every system [139]. Nevertheless, the resulting sliding dynamics are within the range determined by the minimal convex hull method. If the convex hull is sufficiently restrictive the performance of a stabilizing controller using hysteresis modulation around a co-dimension two manifold may be sufficient. Thus the evaluation of the convex hull is necessary.

3.1.5 Contributions

In this section it is demonstrated that jitter appears in hysteresis modulated trans-Z-source converter used for DC-DC voltage conversion. To our knowledge, this is the first time this behavior has been detected in a practical power conversion circuit. To determine the effects that jitter has on the design of a hysteresis modulated controller regulating both the output current of the converter and the state of the impedance network, the sensitivity of the jitter in the non-ideal dynamics present in the converter and the selection of the hysteresis manifold are investigated. It is demonstrated that non-ideal equivalent series resistance in the switches of the converter result in jitter. The convex hull in practice is not flat due to parasitic dynamics, resulting in multiple sliding solutions according to the minimal convex hull theory, and thus allowing for the appearance of jitter. Jitter appears in hysteresis modulated controllers, with independent modulation of the switches, and it is much more sensitive to the size and shape of the hysteresis layer than to non-ideal component dynamics. Finally, based on these findings some recommendations are made on how to select a switching algorithm that does not display jitter in a sliding mode control systems with a co-dimension two sliding surface. The section is organized as follows:

- In section 3.2 the dynamics of the system are introduced, the dynamics of an ideal system are linearized with respect to the control input, and a steady state analysis is performed to show that it is equivalent to the averaged methods conventionally used in the analysis of Z-source topologies.
- In section 3.3 a sliding surface is constructed based on the equivalent control method. The convex hull of the system solutions of the system are constructed and it is demonstrated that infinitely many solutions exist in systems with non-ideal dynamics. The canopy method is then used to construct a solution which is used as the reference solution in the analysis of the sliding dynamics.
- Section 3.4 introduces a method for the construction of the switching surface, and constructs two switching manifolds for the hysteresis modulation of the trans-Z-source converter.
- Section 3.5 demonstrates the appearance of jitter in the DC-DC trans-Z-source converter, and introduces the concept of the extended convex hull that explains the magnitude of the jitter.
- Section 3.6 concludes the chapter and provides a few thoughts on how the selection of the sliding surface can potentially eliminate the jitter in the trans-Z-source converter.

3.2 Dynamics of the trans-Z-source converter

The trans-Z-source family of inverters was first introduced in [80] and the topology was later generalized in [81]. The trans-Z-source inverters employ a non-isolated transformer to offer greater voltage gain with a smaller shoot through duty ratio than equivalent conventional Z-source topologies. This improves the efficiency of the power conversion, as the peak current in the impedance network of Z-source inverters increases with a larger shoot-through ratio. Furthermore, due to the coupling introduced by the transformer, one of the capacitors in the Z-source network is also eliminated simplifying the circuit.

The trans-Z-source inverter has a total of three state variables. Since jitter appears on system sliding on manifolds of co-dimension two or higher, three state variables is the minimum number of state variables required in a system to exhibit jitter. Other impedance network topologies with two capacitors have four state variables, and exhibit a richer dynamical behavior when the capacitor voltages are not balanced. These topologies can also display jitter, but the analysis of their sliding dynamics is more involved. The trans-Z-source network topology introduced in [80] was chosen to simulate a realistic system.

3.2.1 Converter model

The circuit diagram of the voltage fed quasi trans-Z-source converter with a full single phase bridge is depicted in fig. 3.1. In order to determine the dynamics of the circuit, the equivalent circuit model of the transformer is used in fig. 3.1b. In this model the transformer is represented by an ideal transformer with turns ratio n:1 and a magnetizing inductance L_m. The dynamics of the voltage fed trans-Z-source inverter are then derived according to the ideal transformer model. The state variables in this model are the magnetizing current of the transformer i_{L_m}, the output current i_L and the voltage of the capacitor in the filter v_C. The dynamics are determined by the system of differential equations

$$\begin{cases} D_t i_L = \dfrac{1}{L}\left(-E_2 + (u_+ - u_-)\left(v_C + \dfrac{1}{n}(v_C - E_1)\right)\right) \\ D_t i_{L_m} = \dfrac{1}{L_m}\left(s_D \dfrac{1}{n}(E_1 - v_C) + (1 - s_D)\, v_C\right) \\ D_t v_C = \dfrac{1}{C}\left(-(1 - s_D)\, i_{L_m} + s_D \dfrac{1}{n} i_{L_m} - (u_+ - u_-)\left(1 + \dfrac{1}{n}\right) i_L\right), \end{cases} \tag{3.2.1}$$

where the values of the switching variables $u_+, u_- \in \{0, 1\}$ are related to the input of the circuit switches s_i for $i = 1, \ldots, 4$ according to the relations

$$\begin{cases} u_+ = s_1 (1 - s_2)(1 - s_3)\, s_4, & \text{(3.2.2a)} \\ u_- = (1 - s_1)\, s_2 s_3 (1 - s_4). & \text{(3.2.2b)} \end{cases}$$

The input to the shoot-through switch s_D is not independent. In converters with unidirectional power flow from the source E_1 to the load E_2 only, the switch is implemented by a diode. When bidirectional power flow is required the switch s_D is implemented with an unidirectionally blocking voltage switch. Furthermore, in the converters with bidirectional power flow, the switch has to be closed during the shoot-through states otherwise a short-circuit occurs. Thus,

the value of s_D is determined by the input to the other switches as

$$s_D = 1 - u_+ u_-. \tag{3.2.3}$$

Thus, substituting in the dynamics of the converter, the resulting dynamical system,

$$\begin{cases} D_t i_L = \dfrac{1}{L}\left(-E_2 + (u_+ - u_-)\left(v_C + \dfrac{1}{n}(v_C - E_1)\right)\right) \\ D_t i_{L_m} = \dfrac{1}{L_m}\left((1 - u_+u_-)\dfrac{1}{n}(E_1 - v_C) + u_+u_-v_C\right) \\ D_t v_C = \dfrac{1}{C}\left(-u_+u_-i_{L_m} + (1 - u_+u_-)\dfrac{1}{n}i_{L_m} - (u_+ - u_-)\left(1 + \dfrac{1}{n}\right)i_L\right), \end{cases} \tag{3.2.4}$$

has only two control inputs, u_+ and u_-.

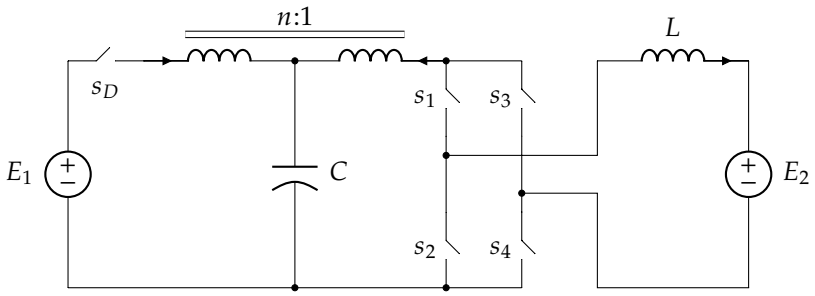

(a) Circuit digram.

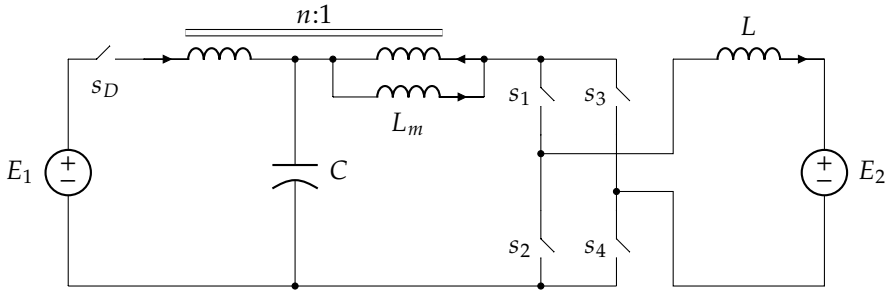

(b) Circuit diagram with the equivalent circuit of the transformer.

Figure 3.1: Single phase trans-Z-source inverter with a constant voltage source load with a transformer with magnetizing inductance L_m.

The model is expressed in vector form for conciseness. The state of the converter is

$$x = \begin{pmatrix} i_L \\ i_{L_m} \\ v_C \end{pmatrix} \tag{3.2.5}$$

and the discrete control input is determined by the vector,

$$u = \begin{pmatrix} u_+ \\ u_- \end{pmatrix} \tag{3.2.6}$$

where $u_+, u_- \in \{0, 1\}$. Therefore, the dynamics of an ideal circuit can then be expressed as

$$D_t x = f_{\text{id}}(x, u), \tag{3.2.7}$$

where

$$f_{\text{id}}(x, u) = \begin{pmatrix} \frac{1}{L}\left(-E_2 + (u_+ - u_-)\left(v_C + \frac{1}{n}(v_C - E_1)\right)\right) \\ \frac{1}{L_m}\left((1 - u_+u_-)\frac{1}{n}(E_1 - v_C) + u_+u_-v_C\right) \\ \frac{1}{C}\left(-u_+u_-i_{L_m} + (1 - u_+u_-)\frac{1}{n}i_{L_m} - (u_+ - u_-)\left(1 + \frac{1}{n}\right)i_L\right) \end{pmatrix}. \tag{3.2.8}$$

Since the product of the control inputs appears in the dynamics, the system is not linear with respect to its control input.

The values of the component parameters for the converter being analyzed are give in table 3.1. The passive elements values were taken from an inverter tested in [80], and the 3-phase bridge was replace by a single phase bridge for a bidirectional DC-DC converter. A turns ratio of 2:1 instead of 1:1 was chosen to improve the system transient stability at the expense of a higher magnetizing current [81]. A higher turns ratio can achieve the same voltage gain with a smaller shoot through duty ratio, allowing a larger portion of the duty cycle to be devoted to non-shoot through states. As the impedance source converters are minimum phase systems, they rely on non-shoot through states to control the output current. In conventional averaged controllers reducing to shoot through duty ratio increases the control bandwidth for the output current i_L. In sliding mode controllers the increase in the turns ratio increases stable sliding region on the sliding manifold.

Converter parameters	
L_m	1 mH
C	48 µF
n	2
L	1.5 mH
E_1	100 V
E_2	380 V
P_{out}	2.4 kW

Table 3.1: Parameters for the dynamics of the simulated voltage fed, DC-DC, trans-Z-source converter. The parameters were taken from [80], with a higher turns ratio being used to increase the region of stability of the sliding mode controller.

3.2.2 Steady state analysis

The averaged dynamics of the converter are useful in the design of averaged controllers and in the steady state analysis of the converter [85, §7]. In the design of stabilizing sliding mode controllers, the sliding surfaces for the stabilization of the converter output are selected from a family of surfaces that contain an ideal fixed point determined by the averaged analysis of the converter. The ideal fixed point is the fixed point of the converter for an ideal continuous control input and is selected so that it results in the desired output for the converter. To design the sliding mode controller, a sliding surface is selected so the ideal fixed point is a fixed point of the sliding dynamics. Linear affine switching surfaces are used for the control of the trans-Z-source

converter, so the family of surfaces passes from the ideal fixed point and is parametrized by an orientation vector.

Given the nominal output for the converter, the ideal fixed point that results in the desired output is evaluated using the averaged dynamics of the converter. An ideal continuous control input required to produce the desired output is evaluated in the process of determining the averaged steady state dynamics. This control input provides an insight in the operation of switching algorithms in the stead state of the converter. In pulse width modulation the ideal control input coincides with the steady state duty ratios. Similarly, in any stabilizing sliding mode controller, the value of the control input during steady state operation when it is filtered by a low pass filter tends to the ideal control input [144].

Nominal state parameters	
i_L^*	6.32 A
v_C^*	480 V

Table 3.2: Nominal steady state for the simulated voltage fed, DC-DC, trans-Z-source converter.

The nominal output for the simulated trans-Z-source converter is given in table 3.2. In the design of controllers for the voltage fed trans-Z-source converter, the nominal value the output current i_L and the nominal voltage of the capacitor in the impedance network v_C are known design parameters. The magnetizing current i_{L_m} in the ideal fixed point is then determined. Given the nominal values i_L^* for the output current and the voltage v_C^* for the capacitor voltage, the steady state analysis also determines the idealized continuous control input required so that in the fixed point of the resulting dynamics, the output current i_L and capacitor voltage v_C attain their nominal values. For the same ideal continuous control input, the averaged magnetizing current attains its nominal steady state value, $i_{L_m}^*$.

3.2.2.1 Control input linearization

A transformation that linearizes the system with respect to the control inputs greatly simplifies the algebraic analysis of the dynamics. The transformation conventionally used in the trans-Z-source inverters to linearize the dynamics with respect to the control input is

$$\begin{cases} m = u_+ - u_- & \text{(3.2.9a)} \\ D = u_+ u_-, & \text{(3.2.9b)} \end{cases}$$

where D is the *shoot through duty ratio* and m is the *modulation index* of the phase bridge. To translate the linearized control inputs m and D into inputs for the converter dynamics, the system of equations in (3.2.9) is solved. Using the substitution,

$$u_+ = u_- + m, \tag{3.2.10}$$

$$D = (u_- + m)\, u_- \tag{3.2.11}$$

$$\Rightarrow \quad {u_-}^2 + m u_- - D = 0. \tag{3.2.12}$$

Since $u_-, u_+ \in [0,1]$ the limits for the control inputs according to relation (3.2.9) are

$$m \in [-1,1], \qquad D \in [0,1]. \tag{3.2.13}$$

Furthermore, since $u_- \in [0,1]$, the only admissible solution of relation (3.2.12) is

$$u_- = \frac{1}{2}\left(-m + \sqrt{m^2+4D}\right). \tag{3.2.14}$$

Therefore, the inverse transformation is given by

$$\begin{cases} u_+ = \dfrac{1}{2}\left(m + \sqrt{m^2+4D}\right) & \text{(3.2.15a)} \\ u_- = \dfrac{1}{2}\left(-m + \sqrt{m^2+4D}\right), & \text{(3.2.15b)} \end{cases}$$

resulting in a one-to-one mapping between the linearized control input and the converter input. By defining the linearizing transformation $\ell : \mathbb{R}^2 \to \mathbb{R}^2$,

$$\ell\begin{pmatrix} m \\ D \end{pmatrix} = \begin{pmatrix} \frac{1}{2}\left(m + \sqrt{m^2+4D}\right) \\ \frac{1}{2}\left(-m + \sqrt{m^2+4D}\right) \end{pmatrix}, \tag{3.2.16}$$

the linearized dynamics are determined by

$$D_t x = f_{\mathrm{id}}(x, \ell(m, D)). \tag{3.2.17}$$

In component wise form, relation (3.2.17) corresponds to the system of ordinary differential equations

$$\begin{cases} D_t i_L = \dfrac{1}{L}\left(-E_2 + m\left(v_C + \dfrac{1}{n}\left(v_C - E_1\right)\right)\right), \\ D_t i_{L_m} = \dfrac{1}{L_m}\left(\left(1-D\right)\dfrac{1}{n}\left(E_1 - v_C\right) + D v_C\right), \\ D_t v_C = \dfrac{1}{C}\left(-D i_{L_m} + \left(1-D\right)\dfrac{1}{n} i_{L_m} - m\left(1 + \dfrac{1}{n}\right) i_L\right). \end{cases} \tag{3.2.18}$$

Note that in the resulting system the control inputs m and D are not independent, but they are related according to relation (3.2.9). Without this relation, the averaged control input may not realizable by the actual input for the switches, u_+ and u_-.

3.2.2.2 Nominal operating state

To determine the nominal operating state of the converter, a relation between the magnetizing current, the output current, and the filter capacitor voltage is derived. Given the nominal state

$$x^* = \begin{pmatrix} i_L^* \\ i_{L_m}^* \\ v_C^* \end{pmatrix}, \tag{3.2.19}$$

the ideal control input is found by solving the equation

$$f(x^*, \ell(m, D)) = 0. \tag{3.2.20}$$

Thus, a relation is derived by the idealized steady state operation, where the ideal continuous control input maintains the state of the system on the nominal state x^*. Therefore

$$\begin{aligned} & x = x^* && (3.2.21)\\ \Rightarrow \quad & D_t x = 0 && (3.2.22)\\ \Rightarrow \quad & f(x^*, \ell(m, D)) = 0. && (3.2.23) \end{aligned}$$

The steady state analysis also determines the relation between the nominal state and the resulting ideal averaged control input. The condition in relation (3.2.20) is equivalent to the capacitor voltage balance and inductor voltage second balance conditions used in the steady state analysis of pulse width modulated controller [81]. Analyzing this condition component wise and starting from the second component,

$$\begin{aligned} & f_2(x^*, \ell(m, D)) = 0 && (3.2.24)\\ \Rightarrow \quad & (1 - D)\left(E_1 - v_C^*\right) + nDv_C^* = 0 && (3.2.25)\\ \Rightarrow \quad & v_C^*\left(1 - (n+1)D\right) = (1 - D)E_1 && (3.2.26)\\ \Rightarrow \quad & v_C^* = \frac{1 - D}{1 - (n+1)D}E_1, && (3.2.27) \end{aligned}$$

where solving for the control input D,

$$D = \frac{v_C^* - E_1}{(n+1)v_C^* - E_1}. \tag{3.2.28}$$

Similarly,

$$\begin{aligned} & f_1(x^*, \ell(m, D)) = 0 && (3.2.29)\\ \Rightarrow \quad & -E_2 + m\left(v_C^* + \frac{1}{n}\left(v_C^* - E_1\right)\right) = 0 && (3.2.30)\\ \Rightarrow \quad & -nE_2 + m\left((n+1)v_C^* - E_1\right) = 0 && (3.2.31)\\ \Rightarrow \quad & m = \frac{nE_2}{(n+1)v_C^* - E_1}. && (3.2.32) \end{aligned}$$

Substituting v_C^* from relation (3.2.27), the two control inputs are related according to the equation

$$m = \frac{E_2}{E_1}\left(1 - (n+1)D\right). \tag{3.2.33}$$

Finally, the third component can be used to determine the magnetizing current of the transformer with respect to the control inputs and the load current,

$$f_3(x^*, \ell(m, D)) = 0 \tag{3.2.34}$$

$$\Rightarrow \quad -Di^*_{L_m} + (1-D)\frac{1}{n}i^*_{L_m} - m\left(1+\frac{1}{n}\right)i^*_L = 0 \tag{3.2.35}$$

$$\Rightarrow \quad i^*_{L_m} = \frac{(n+1)\,m}{1-(n+1)\,D}i^*_L. \tag{3.2.36}$$

Thus, the magnetizing current is an increasing function of the shoot-through duty ratio. To extract a relation for the steady state of the magnetizing current $i^*_{L_m}$ that depends only on the parameters of the converter, v^*_C is substituted from relation (3.2.27), resulting in

$$i^*_{L_m} = (n+1)\frac{E_2}{E_1}i^*_L = (n+1)\frac{P_{\text{out}}}{E_1}, \tag{3.2.37}$$

where

$$P_{\text{out}} = E_2 i^*_L, \tag{3.2.38}$$

is the nominal power output. The results of the steady state analysis are identical to the averaged analysis typically employed in the design of pulse width modulated controllers [80], [81].

3.3 Design of the sliding surface for a sliding mode controller

In this section a linear sliding manifold of co-dimension two is designed for a sliding mode controller for the trans-Z-source converter. A parametrized family of sliding manifolds is constructed for the converter. The family consists of linear manifolds passing through the averages steady state x^* and are parametrized by a direction vector. The equivalent control method is then used to select a sliding manifold from the family. The manifold is selected so that x^* is a stable fixed point of the sliding dynamics. Furthermore, to ensure a swift dynamical response the local rate of asymptotic convergence to x^* is selected to be sufficiently fast in the vicinity of x^*.

3.3.1 Designing a sliding surface family for the controller

In the designing of the sliding mode algorithm, the control objective is the stabilization of the system, so that in the averaged output of the converter at the steady state is

$$(i_L, v_C) = (i^*_L, v^*_C), \tag{3.3.1}$$

where i^*_L and v^*_C are given parameters. The averaged value of the magnetizing current in the steady state is determined by relation (3.2.37) for the given i^*_L and v^*_C. To achieve the control objective it is sufficient to stabilize the system on the nominal operating point x^* as defined in relation (3.2.19).

The main control objective of the trans-Z-source DC-DC converter is to regulate the output current to the load, i_L. Given that the value of the output current is known and constant, the invariant manifold capturing this control objective is

$$H_1(x) = 0, \tag{3.3.2}$$

where $H_1 : \mathbb{R}^3 \to \mathbb{R}$, and

$$H_1(x) = i_L - i_L^*, \tag{3.3.3}$$

with i_L^* being the desired load current. A controller solves the control problem for the output current when it drives and subsequently maintains at all times the state of the system on the manifold $H_1 = 0$. Using the surface $H_1 = 0$ as one of the sliding surfaces on a sliding mode controller ensures that $H_1 = 0$ is a control invariant. Since any disturbance is matched by the control input, all disturbances are completely rejected if sufficient control energy is available [144], [165]. Furthermore, for hysteresis modulated controllers the system attains the control objective in finite time $H_1 = 0$. Thus $H_1 = 0$ is selected as one of the sliding surfaces for the sliding mode controller.

The secondary control objective of the converter is to regulate the state of the impedance network. The nominal state of the network is given by $(i_{L_m}^*, v_C^*)$. Since this is an internal state of the converter, the target stabilization performance will be asymptotic convergence. Thus, the control objective is to ensure that the controlled dynamics converge to $(i_{L_m}^*, v_C^*)$ at least asymptotically. To achieve this secondary control objective, a sliding mode controller that imposes sliding on the surface

$$H_2(x) = 0, \tag{3.3.4}$$

where $H_2 : \mathbb{R}^3 \to \mathbb{R}$, and

$$H_2(x) = k\left(i_{L_m} - i_{L_m}^*\right) + v_C - v_C^*, \tag{3.3.5}$$

is used, where the sliding surface is parametrized by the control parameter $k \in \mathbb{R}$. The control objective is achieved when the sliding dynamics converge to x^*, and locally the convergence is a least linear. Thus, the second sliding surface for the controller is $H_2 = 0$. Sliding mode controllers using hysteresis switching to enforce sliding on $H_2 = 0$, require access to the magnetizing current in order to evaluate the switching function. Sensors, such as Hall effect sensors, can measure the magnetizing current directly from the transformer magnetic field, or the magnetizing current can be estimated by measuring other currents in the circuit.

Combining the two surfaces $H_1 = 0$ and $H_2 = 0$, the sliding mode controller enforces sliding on the manifold

$$H(x) = 0, \tag{3.3.6}$$

where $H : \mathbb{R}^3 \to \mathbb{R}^2$, and

$$H(x) = \begin{pmatrix} H_1(x) \\ H_2(x) \end{pmatrix}. \tag{3.3.7}$$

To simplify the notation, the expression determining the value of H is written in matrix form,

$$H(x) = K_H \cdot (x - x^*), \tag{3.3.8}$$

where

$$K_H = \begin{pmatrix} 1 & 0 & 0 \\ 0 & k & 1 \end{pmatrix}, \qquad x^* = \begin{pmatrix} i_L^* \\ i_{L_m}^* \\ v_C^* \end{pmatrix}. \tag{3.3.9}$$

The function H is a smooth function, and furthermore the set $\{\partial_x H_1, \partial_x H_2\}$ is linearly independent. Thus H defines a sliding manifold

$$\mathcal{M} = \left\{x \in \mathbb{R}^3 : H(x) = 0\right\}. \tag{3.3.10}$$

Overall, a sliding mode controller achieves the control objective when it enforces stable sliding on relation (3.3.6) and in the resulting sliding motion the nominal state x^* is a stable fixed point.

3.3.2 Sliding manifold stability

The stability of the sliding manifold is analyzed using the projection of the vector fields of the modes of the system on the range of H. The variable $z \in \mathbb{R}^2$ defined as

$$z = H(x) \tag{3.3.11}$$

is introduced to plot the projection of the vector fields. The time derivative of the sliding surface determines the projection of the vector field on the range of H, which according to the chain rule is

$$D_t H = \partial_x H \cdot f_{\text{id}}(x, u) \tag{3.3.12}$$

$$= K_H \cdot f_{\text{id}}(x, u). \tag{3.3.13}$$

Introducing the notation

$$v_H(u) = D_t H(x^*, u) = K_H \cdot f_{\text{id}}(x^*, u), \tag{3.3.14}$$

the dynamics around the the nominal operating point x^* when projected the range of H can be seen in fig. 3.2.

For the stabilization of the trans-Z-source converter, the sliding surface must be stable in a sliding domain $\mathcal{D} \subset \mathcal{M}$ in some neighborhood of x^*. The stability of the sliding manifold in the vicinity of x^* depends on the time derivative of H and thus on the value of the parameter k. Introducing the function $V : \mathbb{R}^3 \to \mathbb{R}$,

$$V(x) = \frac{1}{2}(H(x))^T \cdot H(x), \tag{3.3.15}$$

the system will be stable in the vicinity of x^* if there is a control input so that $D_t V$ is negative for any x sufficiently close to the sliding surface according to proposition 2.3.2. Furthermore, for a local result the requirement fir the negativity of $D_t V$ is reduced to a simpler condition. The time derivative of V is

$$D_t V = H(x) \cdot D_t H \tag{3.3.16}$$

$$= H(x) \cdot \partial_x H \cdot f_{\text{id}}(x, u) \tag{3.3.17}$$

$$= z \cdot \partial_x H \cdot f_{\text{id}}(x, u) \tag{3.3.18}$$

where the projection $z = H(x)$ is used. Sufficiently close to x^*

$$f_{\text{id}}(x, u) = f_{\text{id}}(x^*, u) + O(\|x - x^*\|^2) \tag{3.3.19}$$

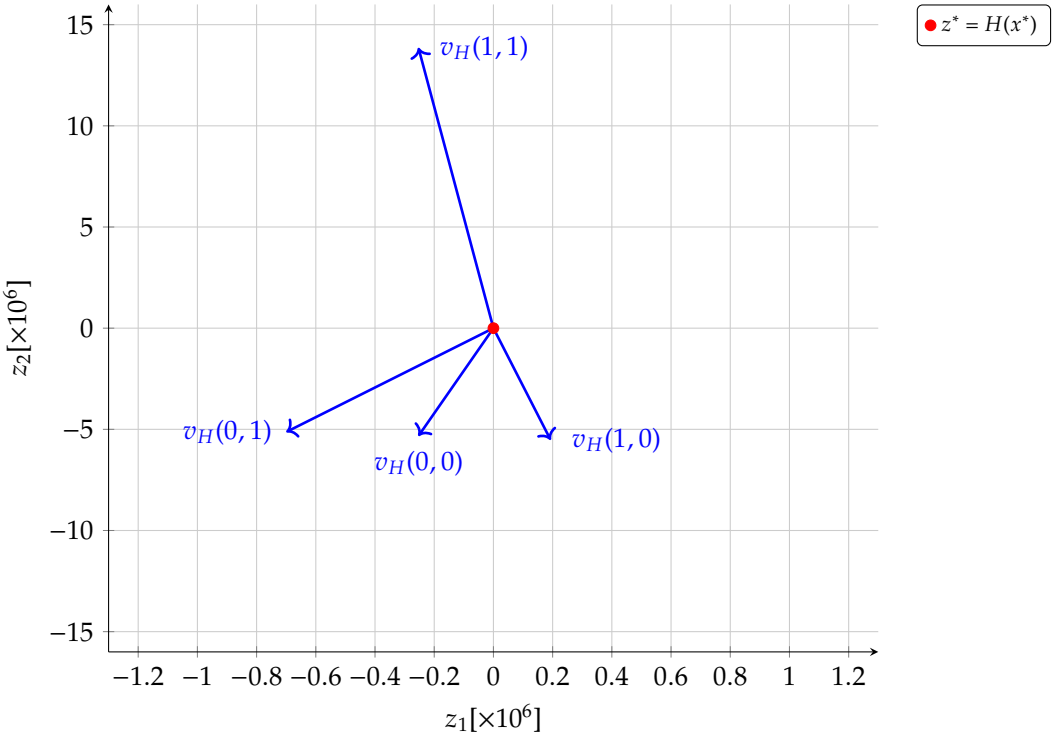

Figure 3.2: Projection of the vector fields on the range of H. The vector function $v_H(u) = K_H \cdot f_{\text{id}}(x^*, u)$ determines the vector field for each control input in the projected space.

since f is a smooth function. Thus,

$$D_t V = z \cdot \partial_x H \cdot f_{\text{id}}(x^*, u) + O(\|x - x^*\|^2). \tag{3.3.20}$$

Therefore, setting

$$z = \varepsilon \begin{pmatrix} \cos\varphi \\ \sin\varphi \end{pmatrix} \tag{3.3.21}$$

the system is stable if for a sufficiently small $\varepsilon > 0$, and for any $\varphi \in [0, 2\pi)$ there exists a control input u such that

$$D_t V = \varepsilon \begin{pmatrix} \cos\varphi \\ \sin\varphi \end{pmatrix} \cdot \partial_x H \cdot f_{\text{id}}(x^*, u) < 0. \tag{3.3.22}$$

The linearized control inputs are used in the proof form simplicity. The time derivative of H is

$$D_t H_1 = D_t i_L \tag{3.3.23}$$

$$= \frac{1}{L}\left(-E_2 + m\left(v_C + \frac{1}{n}(v_C - E_1)\right)\right). \tag{3.3.24}$$

and

$$D_t H_2 = k D_t i_{L_m} + D_t v_C \tag{3.3.25}$$

$$= \frac{k}{L_m}\left((1-D)\frac{1}{n}(E_1 - v_C) + D v_C\right)$$

$$+\frac{1}{C}\left(-Di_{L_m}+(1-D)\frac{1}{n}i_{L_m}-m\left(1+\frac{1}{n}\right)i_L\right). \tag{3.3.26}$$

Therefore, the time derivative of V at x^* for the linearized control inputs is

$$D_tV = m\varepsilon\left(\alpha_m\cos\varphi+\beta_m\sin\varphi\right)+D\varepsilon\left(k\beta_{kD}-\beta\right)\sin\varphi \tag{3.3.27}$$

$$+\varepsilon\left(-\alpha\cos\varphi-\left(k\beta_k-\beta\right)\sin\varphi\right). \tag{3.3.28}$$

where the constants

$$\alpha=\frac{E_2}{L}, \qquad \alpha_m=\frac{1}{L}\left(v_C^*+\frac{1}{n}\left(v_C^*-E_1\right)\right) \tag{3.3.29}$$

$$\beta=\frac{1}{nC}i_{L_m}^*, \qquad \beta_m=\frac{1}{C}\left(1+\frac{1}{n}\right)i_L^* \tag{3.3.30}$$

$$\beta_D=\frac{1}{C}\left(1+\frac{1}{n}\right)i_{L_m}^*, \qquad \beta_{kD}=\frac{1}{L_m}\left(v_C^*+\frac{1}{n}\left(v_C^*-E_1\right)\right), \qquad \beta_k=\frac{1}{nL_m}\left(v_C^*-E_1\right) \tag{3.3.31}$$

are all positive real numbers. Therefore, defining the function

$$p(\varphi,k,m,D)=m\varepsilon\left(\alpha_m\cos\varphi+\beta_m\sin\varphi\right)+D\varepsilon\left(k\beta_{kD}-\beta\right)\sin\varphi \tag{3.3.32}$$

$$+\varepsilon\left(-\alpha\cos\varphi-\left(k\beta_k-\beta\right)\sin\varphi\right), \tag{3.3.33}$$

the time derivative of V is

$$D_tV=\varepsilon p(\varphi,k,m,D). \tag{3.3.34}$$

According to the definition of the linearized control inputs in relation (3.2.9), the range of values for (m,D) is given by the set

$$\hat{U}=\{(0,0),(-1,1),(0,1),(1,1)\}. \tag{3.3.35}$$

Therefore, a given k is stable if the corresponding value of the function

$$\hat{p}(k)=\max_{\varphi\in[0,2\pi)}\min_{(m,D)\in\hat{U}}p(\varphi,k,m,D) \tag{3.3.36}$$

is positive. The plot of the function $\hat{p}$ can be seen in fig. 3.3. The sliding surface is stable for k sufficiently away from zero. It should be noted that the further away the value of $\hat{p}$ is from zero, the more resilient is the system to structural variation due to unmodeled dynamical behavior.

3.3.3 Sliding dynamics under the equivalent control

The dynamics on the sliding manifold $\mathcal{M}$ are now derived for the ideal trans-Z-source converter. Given the desired nominal operating point x^* and a matrix

$$B_{\mathcal{M}}=\begin{pmatrix}b\end{pmatrix} \tag{3.3.37}$$

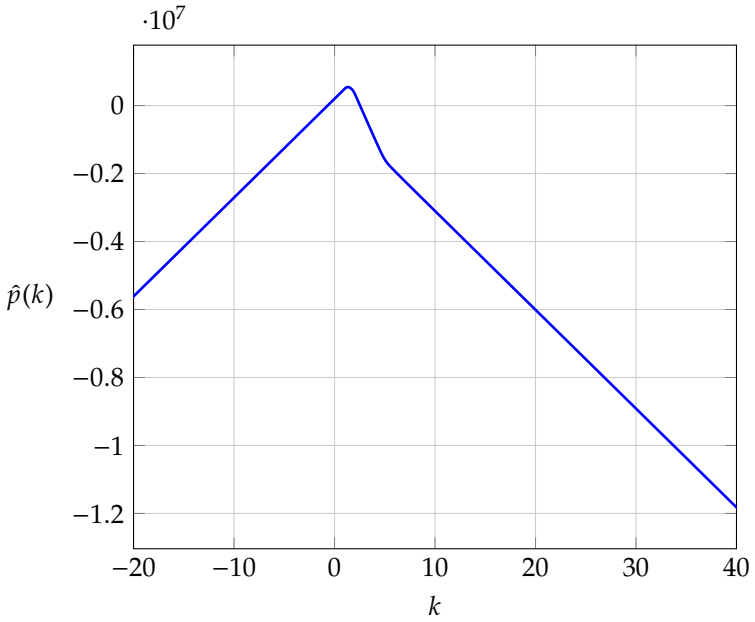

Figure 3.3: Stability analysis of the sliding surface with respect to the control parameter k. A controller stabilizing the surface can be constructed if $\hat{p}(k)$ is negative.

whose column $b \in \mathbb{R}^3$ is spanning null$(\partial_x H)$ and furthermore it is a unit vector,

$$\|b\| = 1, \tag{3.3.38}$$

a map is constructed from $\mathcal{M}$ to the state space $\mathbb{R}^3$, by the function $M : \mathbb{R} \to \mathbb{R}^3$ where

$$M(y) = B_{\mathcal{M}} \cdot y + x^*. \tag{3.3.39}$$

The Jacobian of the function H defining the sliding surface $\mathcal{M}$ is

$$\partial_x H = \begin{pmatrix} 1 & 0 & 0 \\ 0 & k & 1 \end{pmatrix}. \tag{3.3.40}$$

The null space null$(\partial_x H)$ is spanned by the unit vector

$$b = \alpha \begin{pmatrix} 0 \\ -1 \\ k \end{pmatrix}, \tag{3.3.41}$$

where

$$\alpha = \frac{1}{\sqrt{k^2 + 1}} \tag{3.3.42}$$

is a normalization constant. The sliding manifold can thus be constructed explicitly as

$$\mathcal{M} = \text{null}(\partial_x H) + x^* = \left\{ b \cdot y + x^* : y \in \mathbb{R} \right\}. \tag{3.3.43}$$

The equivalent control input to the trans-Z-source converter is defined for the system lin-

earized with respect to its control input. Thus substituting the linearizing transformation in relation (2.6.13), the sliding dynamics for the equivalent control input are

$$D_t y = g_{\mathrm{id}_s}(y), \tag{3.3.44}$$

where $g_{\mathrm{id}_s} : \mathbb{R} \to \mathbb{R}$ is defined as

$$g_{\mathrm{id}_s}(y) = \overline{B}_{\mathcal{M}} \cdot f(M(y), \ell(u_{\mathrm{eq}}(M(y)))), \tag{3.3.45}$$

where $u_{\mathrm{eq}} : \mathcal{M} \to \mathbb{R}^2$ is the linearized equivalent control input, and $\overline{B}_{\mathcal{M}} \in \mathbb{R}^{1\times 3}$ is a matrix satisfying the relation (2.5.33). Thus $\overline{B}_{\mathcal{M}}$ is constructed by finding a vector $\overline{b}$ such that

$$\overline{b} \cdot b = 1 \tag{3.3.46}$$

and setting

$$\overline{B}_{\mathcal{M}} = \left(\overline{b}\right). \tag{3.3.47}$$

Such a vector $\overline{b}$ is

$$\overline{b} = -\frac{1}{\alpha}\begin{pmatrix} 0 & 1 & 0 \end{pmatrix}, \tag{3.3.48}$$

and therefore, the sliding dynamics can be constructed given the linearized equivalent control input by substitution in relation (3.3.45).

To determine the sliding dynamics under the equivalent control, the time derivative of the sliding function is first evaluated. For any $x \in \mathcal{M}$, the first component results in

$$\begin{aligned}
& D_t H_1 = 0 && (3.3.49)\\
\Rightarrow\quad & D_t i_L = 0 && (3.3.50)\\
\Rightarrow\quad & -E_2 + m\left(v_C + \frac{1}{n}\left(v_C - E_1\right)\right) = 0 && (3.3.51)\\
\Rightarrow\quad & m = \frac{nE_2}{(n+1)\,v_C - E_1}. && (3.3.52)
\end{aligned}$$

Similarly for the second component,

$$\begin{aligned}
& D_t H_2 = 0 && (3.3.53)\\
\Rightarrow\quad & k D_t i_{L_m} + D_t v_C = 0 && (3.3.54)\\
\Rightarrow\quad & \frac{k}{L_m}\left((1-D)\frac{1}{n}\left(E_1 - v_C\right) + D v_C\right)\\
& \qquad + \frac{1}{C}\left(-D i_{L_m} + (1-D)\frac{1}{n} i_{L_m} - m\left(1 + \frac{1}{n}\right) i_L\right) = 0 && (3.3.55)\\
\Rightarrow\quad & D = \frac{\frac{k}{L_m}\left(v_C - E_1\right) + \frac{1}{C}\left(m\,(n+1)\,i_L - i_{L_m}\right)}{\frac{k}{L_m}\left((n+1)\,v_C - E_1\right) - \frac{1}{C}\,(n+1)\,i_{L_m}}. && (3.3.56)
\end{aligned}$$

Thus, the component of the linearized equivalent control input has been expressed in terms of the system state on the sliding surface.

The sliding dynamics can be evaluated by substituting the m and D input of the linearized

equivalent control in relation (3.3.45). However, it is simpler in the case of the trans-Z-source converter to evaluate the sliding dynamics from first principle using the linearized equivalent control input. For any $x \in \mathcal{M}$ there exists a $y \in \mathbb{R}$ such that

$$x = B_{\mathcal{M}} \cdot y + x^* = c \cdot y + x^*, \tag{3.3.57}$$

and thus multiplying across by $\overline{b}$

$$\overline{B}_{\mathcal{M}} \cdot x = \overline{B}_{\mathcal{M}} \cdot B_{\mathcal{M}} \cdot y + \overline{B}_{\mathcal{M}} \cdot x^* \tag{3.3.58}$$

$$= y + \overline{B}_{\mathcal{M}} \cdot x^*. \tag{3.3.59}$$

The dynamics on the manifold $\mathcal{M}$ are thus determined by

$$D_t y = \overline{B}_{\mathcal{M}} \cdot D_t x \tag{3.3.60}$$

$$= \overline{b} \cdot D_t x \tag{3.3.61}$$

$$= -\frac{1}{\alpha} D_t i_{L_m} \tag{3.3.62}$$

$$= -\frac{1}{\alpha L_m} \left((1-D) \frac{1}{n} (E_1 - v_C) + D v_C \right) \tag{3.3.63}$$

$$= -\frac{1}{\alpha n L_m} \left(D \left((n+1) v_C - E_1 \right) - (v_C - E_1) \right) \tag{3.3.64}$$

$$= -\frac{1}{\alpha n L_m} \left(D \left((n+1) \left(v_C^* + \alpha k y \right) - E_1 \right) - \left(v_C^* + \alpha k y - E_1 \right) \right), \tag{3.3.65}$$

where substituting all the state variables in terms of the sliding variable y in relations (3.3.52) and (3.3.56),

$$D = \frac{\frac{k}{L_m} \left(v_C^* + \alpha k y - E_1 \right) + \frac{1}{C} \left(m (n+1) i_L^* - \left(i_{L_m}^* - \alpha y \right) \right)}{\frac{k}{L_m} \left((n+1) \left(v_C^* + \alpha k y \right) - E_1 \right) - \frac{1}{C} (n+1) \left(i_{L_m}^* - \alpha y \right)}, \tag{3.3.66}$$

and

$$m = \frac{n E_2}{(n+1) \left(v_C^* + \alpha k y \right) - E_1}. \tag{3.3.67}$$

3.3.4 Selecting the switching surface parameter

Having constructed a sliding manifold family parameterized by $k \in \mathbb{R}$, the value of the parameter must now be chosen to ensure that the dynamics of y in relation (3.3.65) have a stable fixed point at $y = 0$. The dynamics are locally stable when the eigenvalue

$$\lambda(k) = \frac{\partial}{\partial y} \frac{dy}{dt} \bigg|_{y=0} \tag{3.3.68}$$

of the system is negative. The partial derivative of the dynamics is given by

$$\frac{\partial}{\partial y} \frac{dy}{dt} = -\frac{1}{\alpha n L_m} \left(\frac{\partial D}{\partial y} \left((n+1) \left(v_C^* + \alpha k y \right) - E_1 \right) + n D \alpha k \right), \tag{3.3.69}$$

where

$$\frac{\partial D}{\partial y} = \frac{\frac{\alpha k^2}{L_m} + \frac{1}{C}\left((n+1)\, i_L^* \frac{\partial m}{\partial y} + \alpha\right)}{\frac{k}{L_m}\left((n+1)\left(v_C^* + \alpha k y\right) - E_1\right) - \frac{1}{C}(n+1)\left(i_{L_m}^* - \alpha y\right)} - \frac{\left(\frac{\alpha k^2 (n+1)}{L_m} + \frac{\alpha (n+1)}{C}\right)\left(\frac{k}{L_m}\left(v_C^* + \alpha k y - E_1\right) + \frac{1}{C}\left(m\,(n+1)\, i_L^* - \left(i_{L_m}^* - \alpha y\right)\right)\right)}{\left(\frac{k}{L_m}\left((n+1)\left(v_C^* + \alpha k y\right) - E_1\right) - \frac{1}{C}(n+1)\left(i_{L_m}^* - \alpha y\right)\right)^2} \tag{3.3.70}$$

and

$$\frac{\partial m}{\partial y} = -\frac{n\,(n+1)\, E_2 \alpha k}{\left((n+1)\left(v_C^* + \alpha k y\right) - E_2\right)^2}. \tag{3.3.71}$$

Furthermore, the values of the control inputs and their derivatives at $y = 0$ are,

$$m|_{y=0} = \frac{n E_2}{(n+1)\, v_C^* - E_1}, \tag{3.3.72}$$

$$D|_{y=0} = \frac{\frac{k}{L_m}\left(v_C^* - E_1\right) + \frac{1}{C}\left(m|_{y=0}\,(n+1)\, i_L^* - i_{L_m}^*\right)}{\frac{k}{L_m}\left((n+1)\, v_C^* - E_1\right) - \frac{1}{C}(n+1)\, i_{L_m}^*}, \tag{3.3.73}$$

and

$$\left.\frac{\partial m}{\partial y}\right|_{y=0} = -\frac{n\,(n+1)\,\alpha k E_2}{\left((n+1)\, v_C^* - E_1\right)^2}, \tag{3.3.74}$$

$$D|_{y=0} = \frac{\frac{k}{L_m}\left(v_C^* - E_1\right) + \frac{1}{C}\left(m|_{y=0}\,(n+1)\, i_L^* - i_{L_m}^*\right)}{\frac{k}{L_m}\left((n+1)\, v_C^* - E_1\right) - \frac{1}{C}(n+1)\, i_{L_m}^*}, \tag{3.3.75}$$

$$\left.\frac{\partial D}{\partial y}\right|_{y=0} = \frac{\frac{\alpha k^2}{L_m} + \frac{1}{C}\left((n+1)\, i_L^* \left.\frac{\partial m}{\partial y}\right|_{y=0} + \alpha\right)}{\frac{k}{L_m}\left((n+1)\, v_C^* - E_1\right) - \frac{1}{C}(n+1)\, i_{L_m}^*} - \frac{\left(\frac{\alpha k^2 (n+1)}{L_m} + \frac{\alpha (n+1)}{C}\right)\left(\frac{k}{L_m}\left(v_C^* - E_1\right) + \frac{1}{C}\left(m\,(n+1)\, i_L^* - i_{L_m}^*\right)\right)}{\left(\frac{k}{L_m}\left((n+1)\, v_C^* - E_1\right) - \frac{1}{C}(n+1)\, i_{L_m}^*\right)^2} \tag{3.3.76}$$

respectively. Therefore, the function $\lambda(k)$ has two asymptotes. The first asymptote is located at the root of the denominator of $D|_{y=0}$, denoted by k_r.

$$\frac{k_r}{L_m}\left((n+1)\, v_C^* - E_1\right) - \frac{1}{C}(n+1)\, i_{L_m}^* = 0 \tag{3.3.77}$$

$$\Rightarrow \quad k_r = \frac{L_m\,(n+1)\, i_{L_m}^*}{C\left((n+1)\, v_C^* - E_1\right)} = -3.358, \tag{3.3.78}$$

for the selected parameters, and furthermore,

$$\lim_{k \to k_r} \lambda(k) = -\infty. \tag{3.3.79}$$

The second asymptote is approached by λ as $k \to \pm\infty$. Exploiting the fact that,

$$\lim_{k\to\pm\infty} \alpha k = \pm 1, \qquad \lim_{k\to\pm\infty} \frac{\alpha}{k} = 0, \tag{3.3.80}$$

the limits

$$\lim_{k\to\pm\infty} m|_{y=0} = \frac{nE_2}{(n+1)\,v_C^* - E_1}, \tag{3.3.81}$$

$$\lim_{k\to\pm\infty} D|_{y=0} = \frac{v_C^* - E_1}{(n+1)\,v_C^* - E_1}, \tag{3.3.82}$$

$$\lim_{k\to\pm\infty} \left.\frac{\partial m}{\partial y}\right|_{y=0} = \mp \frac{n\,(n+1)\,E_2}{\left((n+1)\,v_C^* - E_1\right)^2}, \tag{3.3.83}$$

$$\lim_{k\to\pm\infty} \left.\frac{\partial D}{\partial y}\right|_{y=0} = \pm \frac{nE_1}{\left((n+1)\,v_C^* - E_1\right)^2}, \tag{3.3.84}$$

are evaluated. Then, by substitution in relation (3.3.68),

$$\lim_{k\to\pm\infty} \frac{\lambda(k)}{k} = -\frac{\left(v_C^* - E_1\right)\left(n\left(v_C^* + E_1\right) + v_C^*\right)}{L_m\left((n+1)\,v_C^* - E_1\right)} < 0, \tag{3.3.85}$$

which is a negative constant. In fig. 3.4, the eigenvalue of the sliding dynamics is plotted as a function of the control parameter k.

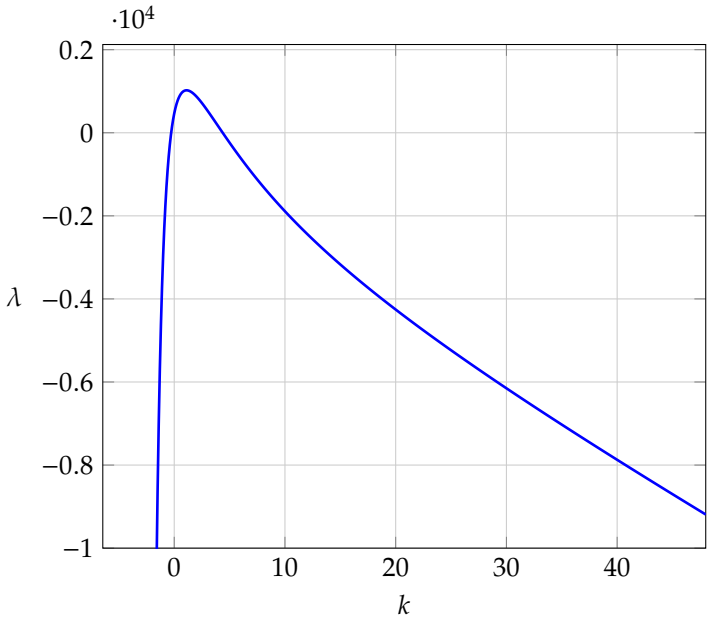

Figure 3.4: Stability analysis of the sliding dynamics with respect to the control parameter k. The eigenvalue λ of the sliding dynamics at $y = 0$ is plotted as a function of the control parameter k. The eigenvalue diverges to $-\infty$ at $k = -3.358$. For stable dynamics the eigenvalue must be negative.

The selection of the constant parameter k must ensure that the dynamics on the sliding

surface have a stable fixed point at x^*. This condition is satisfied if the eigenvalue of the sliding dynamics at x^* satisfies the constraint

$$\lambda(k) < 0. \tag{3.3.86}$$

According to the asymptotic analysis relation (3.3.85), the system is unstable for large negative values of k. Thus positive values of k are considered only.

In addition to the stability of the sliding dynamics, the sliding manifold itself must be stable. The sliding manifold $\mathcal{M}$ is stable in the neighborhood of x^* for sufficiently large $k > 0$ according to the analysis in section 3.3.2. A sufficiently large value of k is chosen,

$$k = 32, \tag{3.3.87}$$

to ensure that the sliding manifold is stable and that the eigenvalue of the system remains negative despite any variation in the system parameters that inevitably occurs in any implementation of the system. Overall, the parameters for the sliding surface of the sliding mode controller are given in table 3.4.

Control parameters	
i_L^*	6.32 A
$i_{L_m}^*$	72 A
v_C^*	480 V
k	32

Table 3.3: Parameters for the sliding mode controller of the simulated voltage fed, DC-DC, trans-Z-source converter.

3.3.5 Non-ideal dynamics for the trans-Z-source converter

The dynamics of the ideal trans-Z-source inverter are linearizable with respect to the control input, however when non-ideal dynamical behavior is introduced in the model the dynamics are no longer linearizable. As an example, the model of the dynamics is extended to include the resistance of the switches in the phase bridge legs. There are two paths through the phase bridge,

- the path through switches $s_1 s_4$ with resistance r_1, and
- the path through switches $s_2 s_3$ with resistance r_2.

The resistance of a semiconductor switch depends on the type of the switch and it often varies dynamically. However, switches such as MOSFETs are accurately modeled by fixed resistances, the on state drain to source resistance [84]. Assuming that MOSFET switches are used, let the resistance of the switches be r_{s_1}, r_{s_2}, r_{s_3} and r_{s_4} respectively. The circuit diagram of the converter including the parasitic resistances can be seen in fig. 3.5.

The parasitic resistance in the semiconductor switches affects the voltage across the output inductor. The resistance of the path $s_1 s_4$ is

$$r_1 = r_{s_1} + r_{s_4} \tag{3.3.88}$$

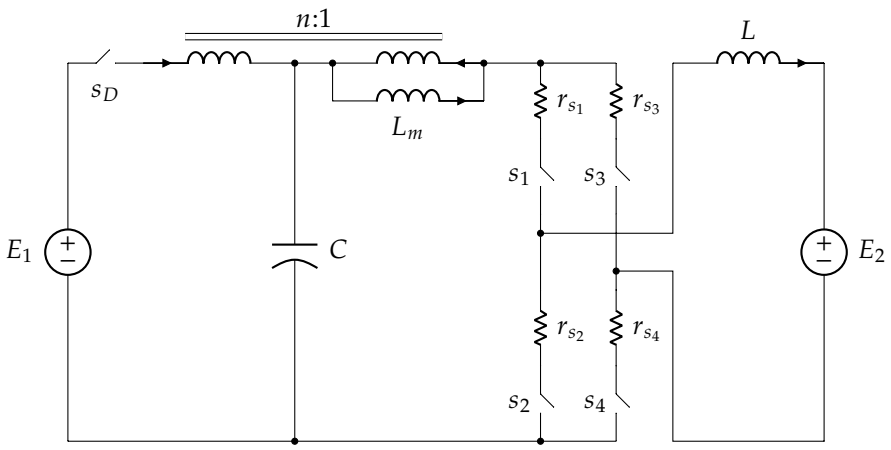

Figure 3.5: Circuit diagram of a trans-Z-source converter model including the on state drain to source resistance of MOSFET switches.

and the resistance of the path $s_2 s_3$ is

$$r_2 = r_{s_2} + r_{s_3}. \tag{3.3.89}$$

The resistance of a non-ideal circuit to current flowing across the the phase bridge is given by

$$r_H(u) = (1 - u_+)\, u_- r_1 + u_+ (1 - u_-)\, r_2 + u_+ u_- \frac{r_1 r_2}{r_1 + r_2}, \tag{3.3.90}$$

and depends on the value of the control input. The dynamics of the non-ideal converter are then determined by

$$D_t x = f(x, u), \tag{3.3.91}$$

where

$$f(x, u) = f_{\mathrm{id}}(x, u) + \begin{pmatrix} -r_H(u) i_L \\ 0 \\ 0 \end{pmatrix}. \tag{3.3.92}$$

It will be proven that due to the presence of extra multiplicative terms with respect to the control input in r_H, the dynamics are no longer linearizable. Some typical values for the resistance of the paths are derived for demonstration purposes.

The switches in the converter are chosen according to the maximum voltage they block and average current they conduct. The maximum voltage occurs in the zero state when all switches are off. During steady state operation the maximum blocking voltage is

$$v_C^* + \frac{1}{n}\left(v_C^* - E_1\right) = 650\,\mathrm{V}. \tag{3.3.93}$$

The maximum current being conducted is during the shoot through states

$$i_{L_m} = 57\,\mathrm{A}. \tag{3.3.94}$$

Silicon carbide MOSFETs achieve the required performance. For instance the CAB450M12XM3[1]

[1]Data sheets of the CAB450M12XM3 silicon carbide MOSFET half-bridge module: https://www.wolfspeed.com/cab450m12xm3

silicon carbide MOSFET provides blocking voltage of 1200 V and an average current of 450 A that are sufficient. The maximum on state drain to source resistance of this switch is

$$R_{\text{ds-on}} = 3.7\,\text{m}\Omega. \tag{3.3.95}$$

Thus, including parasitic resistances due to resistance in conductors, the resistance of the switches is assumed to be

$$r_{s_1} = r_{s_2} = r_{s_3} = r_{s_4} = 0.05\,\Omega. \tag{3.3.96}$$

The resulting values of the resistance of the paths across the phase bridge that induce a non-linear response in the converter are given in table 3.4.

Non-ideal disturbance	
r_1	$0.01\,\Omega$
r_2	$0.01\,\Omega$

Table 3.4: Typical values of non-ideal disturbances that induce non-linear dynamical response in the control input of the converter. These parameters were used in the simulation of the voltage fed, DC-DC, trans-Z-source converter. The disturbances are not available to the controller of the converter.

3.3.6 Convex hull solution

In any implementation of the converter the dynamics of the switches affect the performance of the controller. To analyze the effects of the switches, the convex hull of a hysteresis controlled converter is constructed for a trans-Z-source converter with the non-ideal dynamics of relation (3.3.91). The results indicate that multiple sliding solutions exist in the regularization limit. The sliding dynamics thus depend on the details of the switching control algorithm.

In a system with two discrete control inputs such as the trans-Z-source converter, there are four discrete control vectors,

$$U = \left\{ \begin{pmatrix} 0 \\ 0 \end{pmatrix}, \begin{pmatrix} 1 \\ 0 \end{pmatrix}, \begin{pmatrix} 0 \\ 1 \end{pmatrix}, \begin{pmatrix} 1 \\ 1 \end{pmatrix} \right\}. \tag{3.3.97}$$

Each one of these control vectors corresponds to a vector field for the corresponding mode of the converter. Defining the enumeration $\kappa : \{1, \ldots, 4\} \to U$, given by

$$\kappa_1 = \begin{pmatrix} 0 \\ 0 \end{pmatrix}, \qquad \kappa_2 = \begin{pmatrix} 1 \\ 0 \end{pmatrix}, \qquad \kappa_3 = \begin{pmatrix} 0 \\ 1 \end{pmatrix}, \qquad \kappa_4 = \begin{pmatrix} 1 \\ 1 \end{pmatrix}. \tag{3.3.98}$$

the available dynamical modes of the system are enumerated as

$$\mathcal{V}(x) = \left\{ f(x, \kappa_i) : i = 1, \ldots, 4 \right\}. \tag{3.3.99}$$

To analyze the convex hull of the trans-Z-source converter a matrix of the four vectors fields of each mode is defined

$$F(x) = \begin{pmatrix} f(x, \kappa_1) & f(x, \kappa_2) & f(x, \kappa_3) & f(x, \kappa_4) \end{pmatrix}, \tag{3.3.100}$$

according to the enumeration of the control inputs in relation (3.3.98). A vector is then constructed by the scalar multipliers $\gamma : U \to \mathbb{R}$

$$\gamma = \begin{pmatrix} \gamma_{\kappa_1} \\ \gamma_{\kappa_2} \\ \gamma_{\kappa_3} \\ \gamma_{\kappa_4} \end{pmatrix}. \tag{3.3.101}$$

Let $\mathbf{0}, \mathbf{1} \in \mathbb{R}^4$ be the vectors of zeros and unit entries respectively. The convex hull problem is expressed in vector form. The convex hull consists of all the vector fields

$$f_s(x) = F(x) \cdot \gamma, \tag{3.3.102}$$

such that

$$\begin{cases} (\partial_x H \cdot F(x)) \cdot \gamma = \mathbf{0}, & \text{(3.3.103a)} \\ \mathbf{1}^T \cdot \gamma = 1, & \text{(3.3.103b)} \\ \mathbf{0} \leq \gamma \leq \mathbf{1}, & \text{(3.3.103c)} \end{cases}$$

where the constraints in relations (2.5.11), (2.5.8b) and (2.5.8c) of the convex hull definition are written in vector form. Finally, the convex hull problem is formulated in matrix form by defining

$$A(x) = \begin{pmatrix} \partial_x H \cdot F(x) \\ \mathbf{1}^T \end{pmatrix}, \qquad c = \begin{pmatrix} 0 \\ 0 \\ 1 \end{pmatrix}. \tag{3.3.104}$$

Then the convex hull consists of all the vector fields

$$f_s(x) = F(x) \cdot \gamma, \tag{3.3.105}$$

such that

$$\begin{cases} A(x) \cdot \gamma = c, & \text{(3.3.106a)} \\ \mathbf{0} \leq \gamma \leq \mathbf{1}. & \text{(3.3.106b)} \end{cases}$$

Given that the matrix $A(x) \in \mathbb{R}^{3\times 4}$ has full rank for some $x \in \mathcal{M}$, the set of solutions to the equality constraint in relation (3.3.106a) forms an one-dimensional vector space. Thus the solutions generated by substituting the resulting scalar multipliers in relation (3.3.105) also span an one-dimensional vector space. The scalar multipliers and the sliding solutions are however furtherer constrained by the inequalities in relation (3.3.106b). To investigate the effects of the inequality constraint an explicit form of the solutions to relation (3.3.106a) is obtained. Let $\sigma \in \text{null}(A(x))$, be a non-zero vector. Since the null space is one dimensional, $\sigma \neq 0$ is a base for $\text{null}(A)$, and thus

$$\text{span}\,(\{\sigma\}) = \text{null}(A(x)). \tag{3.3.107}$$

Then, the equality constraint for γ is

$$A\gamma = c \tag{3.3.108}$$

$$\Rightarrow \quad A\gamma - c = 0. \tag{3.3.109}$$

Since A has a full column rank, there exists $c_A \in \mathbb{R}^4$ such that

$$c = Ac_A. \tag{3.3.110}$$

Such a vector can be constructed using the pseudo-inverse of A, the matrix $A^T(AA^T)^{-1}$ where (AA^T) is non-singular when A has full rank. A suitable vector c_A is given by

$$c_A = A^T(AA^T)^{-1}c. \tag{3.3.111}$$

Having constructed the vector c_A, the relation (3.3.109) is reduced to

$$A\left(\gamma - c_A\right) = 0. \tag{3.3.112}$$

Therefore, since σ is a base for the null space of A, the function $\gamma_{\text{eq}} : \mathbb{R} \to \mathbb{R}^4$ where

$$\gamma_{\text{eq}}(y) = y\sigma + c_A \tag{3.3.113}$$

can forms a bijection from $\mathbb{R}$ the solution space of relation (3.3.106a).

Thus, the set of vectors of scalar multiplier that satisfy the both the equality and inequality constraint in relation (3.3.106) is the set

$$S_{\text{cons}} = \{y \in \mathbb{R} : 0 \leq \gamma_{\text{eq}}(y) \leq 1\}. \tag{3.3.114}$$

Thus the solutions of the sliding dynamics are

$$f_s(x) = F(x) \cdot \gamma_{\text{eq}}(y), \ y \in S_{\text{cons}}. \tag{3.3.115}$$

An explicit definition of the set of admissible vectors of scalar multipliers, S_{cons}, is derived. Substituting γ_{eq} into the inequality constraint,

$$\begin{aligned}
& \mathbf{0} \leq \gamma_{\text{eq}}(y) \leq \mathbf{1} && (3.3.116)\\
\Rightarrow \quad & \mathbf{0} \leq y\sigma + c_A \leq \mathbf{1} && (3.3.117)\\
\Rightarrow \quad & 0 \leq y\sigma_i + c_{A_i} \leq 1, \text{ for all } i = 1, \ldots, 4 && (3.3.118)\\
\Rightarrow \quad & -\frac{c_{A_i}}{\sigma_i} \leq y \leq \frac{1 - c_{A_i}}{\sigma_i}, \text{ for all } i = 1, \ldots, 4 \text{ such that } \sigma_i \neq 0 && (3.3.119)\\
\Rightarrow \quad & m_{\text{cons}} \leq y \leq M_{\text{cons}}, && (3.3.120)
\end{aligned}$$

where

$$m_{\text{cons}} = -\max_{i=1,\ldots,4:\sigma_i \neq 0} \left\{ \frac{c_{A_i}}{\sigma_i} \right\}, \qquad M_{\text{cons}} = \min_{i=1,\ldots,4:\sigma_i \neq 0} \left\{ \frac{1 - c_{A_i}}{\sigma_i} \right\}, \tag{3.3.121}$$

and the condition

$$0 \leq c_{A_i} \leq 1 \tag{3.3.122}$$

must be satisfied for all i such that $\sigma_i = 0$. Therefore, given that a solution exists it is a linear segment

$$S_{\text{cons}} = \left\{ y\sigma + c_A : y \in [m_{\text{cons}}, M_{\text{cons}}] \right\}. \tag{3.3.123}$$

The corresponding vector fields for the sliding dynamics are then given by

$$L = \left\{ F(x) \cdot \left(y\sigma + c_A \right) : y \in [m_{\text{cons}}, M_{\text{cons}}] \right\}. \tag{3.3.124}$$

which is a linear segment on the one-dimensional sliding manifold.

The uniqueness of the solution of the minimal convex hull method depends on the set L in relation (3.3.124). For instance, in special cases where $m_{\text{cons}} = M_{\text{cons}}$ the resulting solution is unique. A simple geometrical criterion exists that provides a sufficient condition for the convex hull to result in a unique sliding solution. The convex hull is defined for any $x \in \mathcal{M}$ as

$$\mathcal{H}(x) = \left\{ F(x) \cdot \gamma : \mathbf{0} \leq \gamma \leq \mathbf{1} \textbf{ and } \mathbf{1}^T \cdot x = 1 \right\}, \tag{3.3.125}$$

and it is effectively a polyhedron whose vertices are defined by the four modes of the system, $\{f(x, \kappa_i) : i = 1, \ldots, 4\}$. The convex hull is called *flat* when all the vertices of the polyhedron defining the convex hull reside on the same affine hyperplane. In this case, there are some vectors $\alpha_1, \alpha_2, \beta \in \mathbb{R}^3$ defining a set

$$\mathcal{E} = \left\{ \alpha_1 y_1 + \alpha_2 y_2 + \beta : y_2, y_2 \in \mathbb{R} \right\}, \tag{3.3.126}$$

such that $f(x, \kappa_i) \in \mathcal{E}$ for $i = 1, \ldots, 4$. The volume of the convex hull $\mathcal{H}$ is evaluated as

$$\text{Vol}(\mathcal{H}(x)) = \frac{1}{2} \det(\Delta F(x)) \tag{3.3.127}$$

where ΔF is a matrix defined as

$$\Delta F(x) = \begin{pmatrix} f(x, \kappa_2) - f(x, \kappa_1) & f(x, \kappa_3) - f(x, \kappa_1) & f(x, \kappa_4) - f(x, \kappa_1) \end{pmatrix}. \tag{3.3.128}$$

When the convex hull is flat its volume is zero. Since in a flat hull $f(x, \kappa_i) \in \mathcal{P}$ for all $i = 1, \ldots, 4$, then

$$\Delta F_{*(i-1)}(x) = f(x, \kappa_i) - f(x, \kappa_1) \in \text{span}\left\{ \alpha_1, \alpha_2 \right\}, \tag{3.3.129}$$

for $i = 2, 3, 4$, where ΔF_{*j} is the j^{th} column vector of ΔF. Since the two vectors α_1 and α_2 span a two dimensional space, the three column vectors of $\Delta F(x)$ is a linearly dependent set, and thus $\det(\Delta F(x)) = 0$.

For a flat convex hull the sliding dynamics are unique given that a sliding solution exists. Letting $f(x, \kappa_i) \in \mathcal{E}$ for $i = 1, \ldots, 4$, the equality constraints of the convex hull solution are then expressed as

$$(\partial_x H \cdot F(x)) \cdot \gamma = \partial_x H \cdot \left(F(x) \cdot \gamma \right) \tag{3.3.130}$$

$$= \partial_x H \cdot \left(\sum_{i=1}^{4} \gamma_{\kappa_i} f(x, \kappa_i) \right) \tag{3.3.131}$$

$$= \partial_x H \cdot \left(\sum_{i=1}^{4} \gamma_{\kappa_i} \left(\alpha_1 y_1(i) + \alpha_2 y_2(i) + \beta \right) \right). \tag{3.3.132}$$

where $f(x, \kappa_i) = \alpha_1 y_1(i) + \alpha_2 y_2(i) + \beta$ for $i = 1, \ldots, 4$ for some $y_1(i)$ and $y_2(i)$ as the convex hull is spanned by a_1 and a_2. Therefore,

$$(\partial_x H \cdot F(x)) \cdot \gamma = c_1 (\partial_x H \cdot \alpha_1) + c_2 (\partial_x H \cdot \alpha_2) + \partial_x H \cdot \beta, \tag{3.3.133}$$

where

$$c_1 = \sum_{i=1}^{4} \gamma_{\kappa_i} y_1(i), \qquad c_2 = \sum_{i=1}^{4} \gamma_{\kappa_i} y_2(i), \tag{3.3.134}$$

and the fact that $\gamma_{\kappa_1} + \gamma_{\kappa_2} + \gamma_{\kappa_3} + \gamma_{\kappa_4} = 1$ was used. Therefore, the condition in relation (3.3.103a) is reduced to

$$c_1 (\partial_x H \cdot \alpha_1) + c_2 (\partial_x H \cdot \alpha_2) = -\partial_x H \cdot \beta. \tag{3.3.135}$$

Since all the vectors belong to $\mathbb{R}^2$, a unique solution exists for c_1, c_2. The resulting sliding speed is then,

$$f_s(x) = \sum_{i=1}^{4} \gamma_{\kappa_i} f(x, \kappa_i) \tag{3.3.136}$$

$$= \sum_{i=1}^{4} \gamma_{\kappa_i} \left(\alpha_1 y_1(i) + \alpha_2 y_2(i) + \beta \right) \tag{3.3.137}$$

$$= c_1 \alpha_1 + c_2 \alpha_2 + \beta, \tag{3.3.138}$$

which is unique. It should be noted that in the solution the sliding speed is unique even thought the duty ratio γ_{κ_i} of each mode is not.

Evaluating the convex hull of the trans-Z-source converter with non-ideal dynamics, the volume of the convex set for any $x \in \mathcal{M}$ is

$$\mathrm{Vol}(\mathcal{H}(x)) = -\frac{(n (i_{L_m} - v_C) + E_1 - v_C)(n+1) {i_L}^2 (r_1 + r_2)}{2n^2 L L_m C}, \tag{3.3.139}$$

which is non-zero when the parasitic resistances $r_1, r_2 \geq 0$ are non-zero. Therefore, in a non-ideal system given that the sliding dynamics converge in the limit where the controller restricts the state of the system closer to the sliding surface, there is a range of possible solutions for the sliding vector field.

3.3.7 Sliding solutions in a system with non-ideal dynamics

In the ideal dynamics of the trans-Z-source converter where there is no parasitic dynamics the convex hull of the solutions is flat. Thus, there is a unique solution where all the regularized control inputs tend to. However, in models that include the parasitic dynamics introduced by the semiconductor switches the convex hull may not be flat. Regularized solutions may converge anywhere within the set of solution inside the minimal convex hull that are tangent to the sliding surface or may not converge to a particular solution at all. In deterministic controllers where the

regularized solution is expected to converge, the limit depends on the details of the switching algorithm.

For the design of a controller, the the convex hull provides a description of the range of possible sliding dynamics solutions. Even if in some systems it is computationally difficult to predict the limit where regularized solutions converge, it is possible that the whole range of solutions results in sufficiently good performance. In order to plot the set of tangent solution within the convex hull over each point of the sliding surface, the canopy is used as a representative solution and the minimum and maximum possible sliding solutions are then plotted as tolerance region around the canopy solution. As the value of the canopy solution can vary significantly, plotting the upper and lower bounds of the convex hull separately preserves the information about the size of the convex hull, which would otherwise vanish in the scale of variation in the canopy solution.

To determine the canopy solution of the converter with non-ideal switches the equation introduced in section 2.6.2 is solved numerically. In the trans-Z-source converter, the canopy equation is

$$\partial_x H \cdot f_{\text{cp}}(x) = 0 \tag{3.3.140}$$

where

$$f_{\text{cp}}(x) = \sum_{u \in U} \left(\prod_{i=1}^{m} \mu_i^{u_i} \right) f(x, u) \tag{3.3.141}$$

and for all $i = 1, \ldots, 4$,

$$0 \leq \mu_i \leq 1. \tag{3.3.142}$$

Using the enumeration κ introduced in relation (3.3.98), the dynamics of the converter satisfy

$$\begin{aligned} f(x, \mu) = &\left(1 - \mu_1\right)\left(1 - \mu_2\right) f(x, \kappa_1) + \mu_1 \left(1 - \mu_2\right) f(x, \kappa_2) \\ &+ \left(1 - \mu_1\right) \mu_2 f(x, \kappa_3) + \mu_1 \mu_2 f(x, \kappa_4), \end{aligned} \tag{3.3.143}$$

and so the canopy equation is simplified in the case of the trans-Z-source converter to

$$\partial_x H \cdot f(x, \mu) = 0 \tag{3.3.144}$$

where for all $i = 1, \ldots, 4$,

$$0 \leq \mu_i \leq 1. \tag{3.3.145}$$

For the trans-Z-source converter with the non-ideal dynamics defined in relation (3.3.92), the canopy equation is solvable numerically over a range of values for the non-ideal parameters r_1 and r_2. The resulting solution on $\mathcal{M}$ determines the sliding dynamics on according to relation (2.6.22) for the mapping M introduced in relation (3.3.39), with the resulting sliding speed given by a function $g_{\text{cp}} : \mathbb{R} \to \mathbb{R}$. A plot of g_{cp} can be seen in fig. 3.6.

The minimum and maximum sliding speed solutions are derived converting the minimal convex problem into an optimization problem. Using the mapping M introduced in relation (3.3.39)

and substituting in relation (3.3.103) two optimization problems are defined,

$$g_{\min}(y) = \min_{\gamma \in \mathbb{R}^4} F(M(y)) \cdot \gamma, \tag{3.3.146a}$$

$$g_{\max}(y) = \max_{\gamma \in \mathbb{R}^4} F(M(y)) \cdot \gamma, \tag{3.3.146b}$$

subject to

$$\left(\partial_x H \cdot F(M(y))\right) \cdot \gamma = \mathbf{0}, \tag{3.3.146c}$$

$$\mathbf{1}^T \cdot \gamma = 1, \tag{3.3.146d}$$

$$\mathbf{0} \leq \gamma \leq \mathbf{1}. \tag{3.3.146e}$$

The solutions of these problems, then functions $g_{\min}, g_{\max} : \mathbb{R} \to \mathbb{R}$, determine the sliding solutions with the minimum and maximum sliding speeds respectively, with the dynamics of the solutions given by

$$D_t y = g_{\min}(y), \qquad D_t y = g_{\max}(y). \tag{3.3.147}$$

The difference of these solutions from the sliding speed is then defined as

$$\Delta g_{\max}(y) = g_{\max}(y) - g_{\text{cp}}(y), \qquad \Delta g_{\min}(y) = g_{\min}(y) - g_{\text{cp}}(y). \tag{3.3.148}$$

The differences are plotted in fig. 3.6. Both the maximum and minimum solutions start at the canopy solution for the minimum value of y for which the problem is feasible and their difference increases with y, meaning that the intersection of the convex hull with the sliding surface becomes larger.

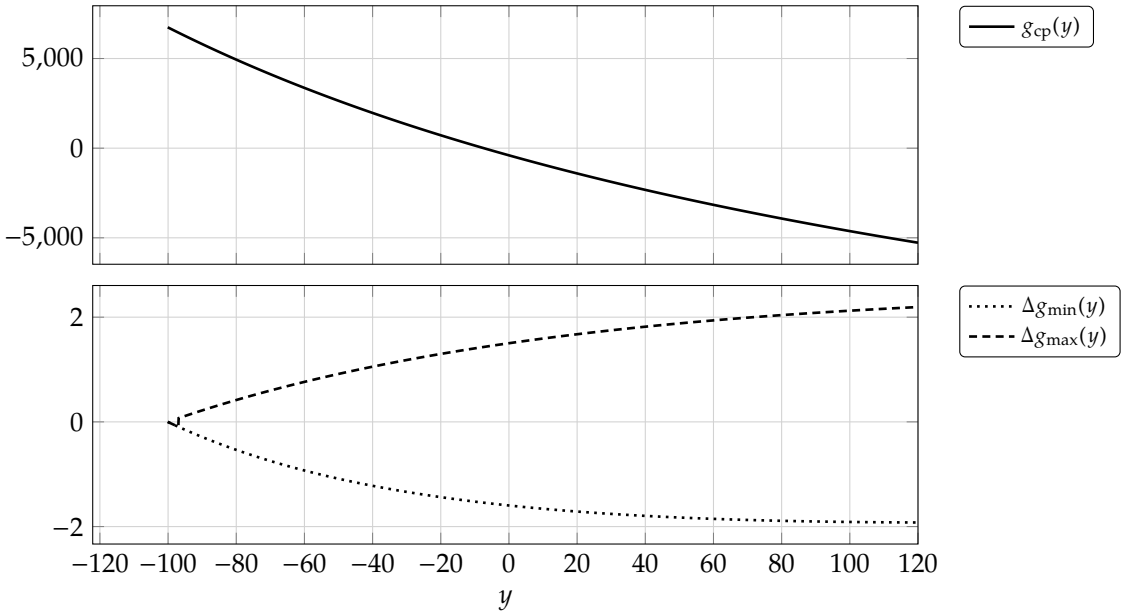

Figure 3.6: The canopy solution and the boundaries of the convex hull solutions for the sliding dynamics of a non-ideal trans-Z-source converter.

3.4 Designing the switching surfaces and logic

In order to implement the sliding mode controller for the trans-Z-source converter, switching algorithms are designed to enforce sliding on the manifold $\mathcal{M}$ defined by the function H in relation (3.3.7). The aim of the controllers is to enforce stable sliding on $\mathcal{M}$ on the vicinity of the desired averaged state $x^* \in \mathcal{M}$, and to ensure that the domain of $\mathcal{M}$ where stable sliding exists is reachable from every starting state. Switches are actuated on switching surfaces with some hysteresis.

A class of sliding mode control algorithms introduced in [148] is used to stabilized the trans-Z-source converter. This class of algorithms enforces sliding on the intersection of successively larger sets of switching surfaces to reach a given sliding manifold. To define the class, the notion of the cover in a partially order set is used. If $(\mathcal{P}, \subset)$ is a partially ordered set where $\mathcal{P}$ is a collection of sets, and $\subset$ relation, then an element $x \in \mathcal{P}$ *covers* and element $y \in \mathcal{P}$ if

$$y \subset x, \tag{3.4.1}$$

and

$$\nexists z \in \mathcal{P} : y \subset z \textbf{ and } z \subset x. \tag{3.4.2}$$

The family of control algorithms with partially ordered set of switching surfaces is now defined.

Definition 3.4.1 (Hierarchy of switching surfaces)**.** For a variable structure system

$$D_t x = f(x, u) \tag{3.4.3}$$

where $f : \Omega \times \mathbb{R}^m \to \mathbb{R}^n$ is a smooth function for some $\Omega \subset \mathbb{R}^n$ and $m < n$, and

$$u_i(x) = \begin{cases} 0, & S_i(x) > 0 \\ 1, & S_i(x) < 0, \end{cases} \tag{3.4.4}$$

let $S : \mathbb{R}^n \to \mathbb{R}^m$ be a switching function defining a set of *linearly independent switching surfaces*

$$\mathcal{S}_* = \{\mathcal{S}_1, \ldots, \mathcal{S}_m\}, \tag{3.4.5}$$

where

$$\mathcal{S}_i = \{x \in \mathbb{R}^n : S_i(x) = 0\} \tag{3.4.6}$$

for $i = 1, \ldots, m$. A hierarchy of switching surfaces is then a partially ordered set $(\mathcal{P}, \subset)$ such that

$$\mathcal{P} \in \{x : x \subset \mathcal{S}_*\} \tag{3.4.7}$$

and

$$\varnothing, \mathcal{S}_* \in \mathcal{P}. \tag{3.4.8}$$

Definition 3.4.2 (Enforcing sliding with a hierarchy of switching surfaces)**.** Let $\mathcal{M}$ be the sliding manifold defined by a function $H : \mathbb{R}^n \to \mathbb{R}^m$. A *hierarchy of switching surfaces* $(\mathcal{P}, \subset)$ enforces

sliding on $\mathcal{M}$ if

$$\mathcal{M} = \bigcap_{i=1}^{m} \mathcal{S}_i, \tag{3.4.9}$$

and

- for any $x \in \mathcal{P}$ the switching algorithm enforces stable sliding on the intersection of switching surfaces $\cap_{s \in x} s$, and
- for any $x \in \mathcal{P}$ the sliding motion reaches one of its covers in finite time.

The motion resulting by using a hierarchy as the sliding surfaces in a variable structure system is a composition of sling motions that slide in increasingly more restrictive intersections of the sliding surfaces in $\mathcal{S}_*$, and eventually reach $\mathcal{M}$. As an example, the switching surfaces for the trans-Z-source converter are considered. Let $S : \mathbb{R}^3 \to \mathbb{R}^2$ be a switching function with linearly independent switching surfaces such that

$$\mathcal{M} = \mathcal{S}_1 \cap \mathcal{S}_2, \tag{3.4.10}$$

where $\mathcal{M}$ is the sliding manifold defined in relation (3.3.7). Two hierarchies that switching algorithms can follow to enforce sliding on $\mathcal{M}$ are depicted in fig. 3.7. Algorithms such as those in fig. 3.7a follow any of the switching surfaces encountered first to slide into the intersection $\mathcal{S}_1 \cap \mathcal{S}_2$. Algorithms such as those in fig. 3.7b always slide into the intersection $\mathcal{S}_1 \cap \mathcal{S}_2$ through the surface $\mathcal{S}_1$.

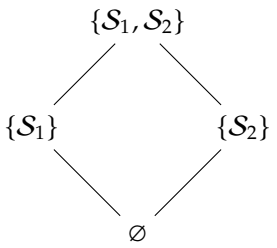

(a) The algorithm enforces sliding on the switching surface encountered first.

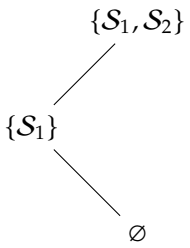

(b) The algorithm enforces sliding first on the surface $\mathcal{S}_1$.

Figure 3.7: Two switching algorithms enforcing sliding on $\mathcal{M} = \mathcal{S}_1 \cap \mathcal{S}_2$.

The following notation is used to describe succinctly the structure which a switching algorithm uses to enforce sliding.

- $\mathcal{S}_i \cap \mathcal{S}_j$: denotes sliding on the intersection of $\mathcal{S}_i$ and $\mathcal{S}_j$.
- $\mathcal{S}_i \to \mathcal{S}_j$: denotes chronologically sliding first in $\mathcal{S}_i$ before moving to sliding on $\mathcal{S}_j$.
- $\mathcal{S}_i | \mathcal{S}_j$: denotes sliding on any of the surface $\mathcal{S}_i$ or $\mathcal{S}_j$ that the system meets first.

For the trans-Z-source converter, a system with two switching surfaces, four different sliding mode control algorithms can be constructed using this method.

1. $\varnothing \to \mathcal{S}_1 \to \mathcal{S}_1 \cap \mathcal{S}_2$
2. $\varnothing \to \mathcal{S}_2 \to \mathcal{S}_1 \cap \mathcal{S}_2$

3. $\varnothing \rightarrow (\mathcal{S}_1 \rightarrow \mathcal{S}_1 \cap \mathcal{S}_2) \,|(\mathcal{S}_2 \rightarrow \mathcal{S}_1 \cap \mathcal{S}_2)$

4. $\varnothing \rightarrow \mathcal{S}_1 \cap \mathcal{S}_2$

In the fourth case the control input is selected so that the system converges monotonically to $\mathcal{S}_1 \cap \mathcal{S}_2$, but without monotonic convergence and sliding to either $\mathcal{S}_i$ individually. A discussion on how to implement such a controller is presented in [74], but such controllers will not be used in the control of the trans-Z-source converter. The design of the switching surfaces of the structures is now considered.

3.4.1 Constructing switching surfaces enforcing nodally attracting sliding

Nodally attracting switching surfaces is a partially ordered set of switching surfaces $(\mathcal{P}, \subset)$ such that $\mathcal{P}$ contains all the subsets of $\mathcal{S}_*$. In this structure sliding is enforced on any switching surface once it is encountered. For instance in the trans-Z-source converter, if sliding occurs on two switching surfaces $\mathcal{S}_1$ and $\mathcal{S}_2$ individually and the surfaces displaying nodal attractivity, then sliding occurs on their intersection $\mathcal{S}_1 \cap \mathcal{S}_2$ as well. To ensure that sliding is stable in the intersection $\mathcal{S}_1 \cap \mathcal{S}_2$, nodal attractivity requires that there is always a control input driving the state of the system towards the intersection.

3.4.1.1 Conditions for nodal attractivity

The requirements for nodal attractivity were discussed informally in [74]. A more formal and focused treatment is presented in [137], [138]. A definition for nodally attracting surfaces is provided here based on the treatment in [137], [138]. The definition is then successively reduced to a single structure that defines a nodally attracting switching surface. The next section provides a method for constructing this structure.

Definition 3.4.3 (Nodally attractive switching surface)**.** Let $S : \mathbb{R}^n \rightarrow \mathbb{R}^m$ be a switching function for a variable structure system with discrete inputs such that

$$\{\partial_x S_i : i = 1, \ldots, m\} \tag{3.4.11}$$

is a linearly independent set. The switching manifolds $\mathcal{S}_i = \{x \in \mathbb{R}^n : S_i(x) = 0\}$ are nodally attractive to the manifold

$$\mathcal{S} = \bigcap_{i=1}^{m} \mathcal{S}_i, \tag{3.4.12}$$

if S satisfies the attractivity condition,

$$\exists \varepsilon > 0, \forall x \in \mathbb{R}^n : 0 < \|S(x)\| < \varepsilon \Rightarrow \\ \left(\exists u \in \{0,1\}^m, \forall i \in \{1, \ldots, m\}, \exists \eta > 0 : D_t S_i(x,u) S_i(x) < -\eta\right). \tag{3.4.13}$$

A set of switching manifolds is thus nodally attractive if there is always a control input such that the absolute value of every switching function decreases monotonically and with a finite rate. For instance defining the function $V_{S_i} : \mathbb{R}^n \rightarrow \mathbb{R}$

$$V_{S_i}(x) = \frac{1}{2} S(x)^2, \tag{3.4.14}$$

the time derivative of V_{S_i} is

$$D_t V_{S_i}(x,u) = D_t S_i(x,u) S_i(x). \tag{3.4.15}$$

So in a nodally attracting system, there is always a control input so that V_{S_i} decrease for all $i = 1, \ldots, m$ with a finite rate. Since

$$|S_i| = \sqrt{S_i^2} = \sqrt{2V_{S_i}}, \tag{3.4.16}$$

it follows that every S_i will reach zeros within finite time, and thus the intersection $S = 0$ is reached within finite time.

The stability of sliding on the switching manifold is investigated in a neighborhood of $x^* \in \mathcal{S}$ which is the ideal fixed point of the system. Thus it is sufficient to prove that the manifold $\mathcal{S}$ is nodally attractive in a neighborhood of x^*. Considering the time derivative of the surface S_i in the vicinity of $x^* \in \mathcal{S}$, according to the dynamics of the variable structure system

$$D_t S_i = \partial_x S_i \cdot f(x,u) \tag{3.4.17}$$

$$= \partial_x S_i \cdot f(x^*,u) + O(\|x - x^*\|^2). \tag{3.4.18}$$

Thus, for a sufficiently small neighborhood of x^*, it is sufficient to demonstrate that

$$\exists \varepsilon > 0, \forall x \in \mathbb{R}^n : 0 < \|S(x)\| < \varepsilon \Rightarrow \\ \left(\exists u \in \{0,1\}^m, \forall i \in \{1,\ldots,m\}, \exists \eta > 0 : \left(\partial_x S_i \cdot f(x^*,u)\right) S_i(x) < -\eta\right), \tag{3.4.19}$$

in order for the switching surface S to be nodally attractive to $\mathcal{S}$ locally.

3.4.1.2 Construction of nodally attracting switching surfaces

A method is now presented that given any function $H : \mathbb{R}^n \to \mathbb{R}^m$ defining a sliding manifold $\mathcal{M}$, constructs a set of switching surfaces that ensure nodal attractivity to the manifold $\mathcal{M}$, or determines that such set of switching surfaces does not exist. To design of the switching manifolds S, the attractivity condition in relation (3.4.13) is further simplified. Since the attractivity is a local property, it suffices to consider only linear surfaces. The function $\sigma : \mathbb{R}^m \to \mathbb{R}^m$ is defined as

$$\sigma(z) = K_S \cdot z \tag{3.4.20}$$

for some $K_S \in \mathbb{R}^{m \times m}$ that has full rank. A family of switching functions $S : \mathbb{R}^n \to \mathbb{R}^m$ is then defined as

$$S(x) = \sigma(H(x)). \tag{3.4.21}$$

By definition of S the intersection of the switching surfaces coincides with the sliding manifold

$$\mathcal{S} = \mathcal{M}, \tag{3.4.22}$$

so if sliding on $\mathcal{S}$, the sliding manifold $\mathcal{M}$ is stable. The partial derivative of S is

$$\partial_x S = \partial_z \sigma \cdot \partial_x H \tag{3.4.23}$$

$$= K_S \cdot \partial_x H. \tag{3.4.24}$$

Since H is a function defining a sliding manifold, the set

$$\{\partial_x H_i : i = 1, \ldots, m\} \tag{3.4.25}$$

is linearly independent. Since K_S has full rank, the set

$$\{K_S \cdot \partial_x H_i : i = 1, \ldots, m\} \tag{3.4.26}$$

is also linearly independent. Therefore, to construct a switching function resulting in nodally attractive switching surfaces, a matrix $K_S \in \mathbb{R}^{m\times m}$ with full rank must be constructed so that S satisfies the condition in relation (3.4.19). Using the mapping

$$z = H(x), \tag{3.4.27}$$

the attractivity condition is reduced to

$$\begin{aligned}&\exists \varepsilon > 0, \forall x \in \mathbb{R}^n : 0 < \|\sigma(z)\| < \varepsilon \Rightarrow \\ &\quad \left(\exists u \in \{0,1\}^m, \forall i \in \{1, \ldots, m\}, \exists \eta > 0 : \left(\partial_z \sigma_i \cdot \partial_x H(x^*) \cdot f(x^*, u)\right)\left(\partial_z \sigma_i \cdot z\right) < -\eta\right),\end{aligned} \tag{3.4.28}$$

where

$$\partial_z \sigma = K_S. \tag{3.4.29}$$

To further simplify the stability condition, the constraint on the norm of σ is expressed in terms of a constrain on z. Substituting by the definition of σ,

$$\|\sigma(z)\| = \|K_S \cdot z\| = \sqrt{z^T K_S^T K_S z}. \tag{3.4.30}$$

The matrix $K_S^T K_S$ is Hermitian and thus diagonalizable. Letting E be a matrix whose columns are eigenvectors of $K_S^T K_S$, and $\Lambda = \operatorname{diag}(\lambda_1, \ldots, \lambda_m)$ a diagonal matrix of the associated eigenvalues,

$$K_S^T K_S = E^{-1} \Lambda E \tag{3.4.31}$$

and therefore,

$$\|\sigma(z)\| = \sqrt{z^T E^{-1} \Lambda E z} \tag{3.4.32}$$

$$= \sqrt{\sum_{i=1}^{m} \lambda_i z_i^2} < \sqrt{K}\,\|z\|, \tag{3.4.33}$$

where

$$K = m \max\{\lambda_i : i \in \{1, \ldots, m\}\}. \tag{3.4.34}$$

Since $K_S^T K_S$ is a positive definite matrix, $\lambda_i > 0$ for all $i = 1, \ldots, m$ and $\sqrt{K}$ is well defined. Thus, for any $\varepsilon > 0$, there exists a $\varepsilon_z > 0$ such that

$$\|z\| < \varepsilon_z \Rightarrow \|\sigma(z)\| < \varepsilon. \tag{3.4.35}$$

The attractivity condition is therefore further simplified to

$$\exists \varepsilon > 0, \forall z \in \mathbb{R}^m : 0 < \|z\| < \varepsilon \Rightarrow \\ \left(\exists u \in \{0,1\}^m, \forall i \in \{1,\dots,m\}, \exists \eta > 0 : \left(\partial_z \sigma_i \cdot \partial_x H(x^*) \cdot f(x^*, u)\right)\left(\partial_z \sigma_i \cdot z\right) < -\eta\right), \quad (3.4.36)$$

and introducing the notation

$$v_H(u) = \partial_x H(x^*) \cdot f(x^*, u), \quad (3.4.37)$$

the stability condition is written as

$$\exists \varepsilon > 0, \forall z \in \mathbb{R}^m : 0 < \|z\| < \varepsilon \Rightarrow \\ \left(\exists u \in \{0,1\}^m, \forall i \in \{1,\dots,m\}, \exists \eta > 0 : \left(\partial_z \sigma_i \cdot v_H(u)\right)\left(\partial_z \sigma_i \cdot z\right) < -\eta\right). \quad (3.4.38)$$

The attractivity condition in relation (3.4.36) effectively requires that there is always a mode whose vector field points towards the the centre of the z projected space, and the vector filed has a finite speed so that the value of S reaches zero in finite time. Other configurations may lead to stable sliding as well [138], but the requirement of relation (3.4.36) is necessary for monotonic convergence in each individual sliding surface. This more strict requirement has the advantage that it prevents overshoot in the subspace spanned by the gradient vectors of the functions S_i.

The next step is the construction of the matrix K_S. Since the matrix K_S is non-singular, it has full rank, and thus for $\|z\| < \varepsilon$, the dot product $K_S \cdot z$ attains all possible combinations of sings in its components. This implies that the $K_S \cdot v_H(u)$ for $u \in \{0,1\}^m$ must also be able to attain all possible combinations of signs for each components by selecting an appropriate control input u for each z to ensure the condition

$$\forall i \in \{1,\dots,m\}, \exists \eta > 0 : \left(\partial_z \sigma_i \cdot v_H(u)\right)\left(\partial_z \sigma_i \cdot z\right) < -\eta \quad (3.4.39)$$

is satisfied. The vectors $v_H(u)$ define 2^m points in an m-dimensional space, one for each control input $u \in \{0,1\}^m$. Therefore, m hyperplanes are sufficient to separate the points $v_H(u)$ if such separation is possible. Let the $\{v_1,\dots,v_m\} \subset \mathbb{R}^{1\times m}$ be the set of vectors that define the planes which bisect the set of available modes $v_H(u)$. Furthermore, let $\mathrm{sg} : \{0,1\} \to \{-1,1\}$ be the function

$$\mathrm{sg}(x) = \begin{cases} -1, & x = 0 \\ 1, & x = 1. \end{cases} \quad (3.4.40)$$

An additional requirement is that for hyperplane v_i, all the points $\{v_H(u) : \mathrm{sg}(u_i) = x\}$ are on the same side of the hyperplane for $x \in \{-1,1\}$. This requirement can be formulated as the inequality

$$\forall u \in \{0,1\}^m : \mathrm{sg}(u_i)\left(v_i \cdot v_H(u)\right) \geq c \quad (3.4.41)$$

where $c > 0$ is any positive constant, as the magnitude of v_i is free to vary.

A set of optimization problems is then defined by requiring the solution maximizing the separation that the hyperplanes $\{v_1,\dots,v_m\} \subset \mathbb{R}^{1\times m}$ offer. These optimization problems are withing a wider class of problem called support vector machines. Support vector machines separate points into two classes using the hyperplane that maximizes the separation between

two sets of points [166]. In general, affine hyperplanes are used in support vector machines, so a modification to the problem defining the hyperplanes is necessary to ensure that the hyperplanes constructing by solving the problem pass through the origin. The problem defining the hyperplanes is an optimization problem requiring the maximization of the separation that each hyperplane offers. Defining the distance as

$$\rho(v_i) = \min_{u\in\{0,1\}^m:\mathrm{sg}(u_i)=1} \frac{v_i \cdot v_H(u)}{\|v\|} - \max_{u\in\{0,1\}^m:\mathrm{sg}(u_i)=-1} \frac{v_i \cdot v_H(u)}{\|v\|}, \tag{3.4.42}$$

the quantity being maximized is the distance $\rho(v_i)$.

$$\begin{aligned} \underset{v_i\in R^{1\times m}}{\text{maximize}} \quad & \rho(v_i) && \text{(3.4.43a)} \\ \text{subject to} \quad & \forall u \in \{0,1\}^m : \mathrm{sg}(u_i)\,(v_i \cdot v_H(u)) \geq c. && \text{(3.4.43b)} \end{aligned}$$

Without loss of generality, the value $c = 1$ can be selected for the constant. Since at least two points in each set will satisfy the constraint with an equality for optimal solutions, the quantity being maximized is reduced to

$$\rho(v_i) = \frac{2}{\|v_i\|}. \tag{3.4.44}$$

Thus, the maximization problem is reduced to

$$\begin{aligned} \underset{v_i\in R^{1\times m}}{\text{maximize}} \quad & \frac{2}{\|v_i\|} \\ \text{subject to} \quad & \forall u \in \{0,1\}^m : \mathrm{sg}(u_i)\,(v_i \cdot v_H(u)) \geq 1. \end{aligned}$$

The problem is intractable due to the non-convex objective function, but it can be reduced to the quadratic maximization problem,

$$\begin{aligned} \underset{v\in R^{1\times m}}{\text{minimize}} \quad & \frac{1}{2}\|v_i\|^2 && \text{(3.4.45a)} \\ \text{subject to} \quad & \forall u \in \{0,1\}^m : \mathrm{sg}(u_i)\,(v_i \cdot v_H(u)) \geq 1. && \text{(3.4.45b)} \end{aligned}$$

Quadratic optimization algorithms solve this optimization problem efficiently. Even better performance can be achieved by a number of problem specific optimization algorithms developed for the slightly extended version of this problem used in support vector machine training [166]. The benefit from more efficient algorithms is important in systems with a large number of switches, but for the trans-Z-source converter that has only two switches the quadratic optimization approach is sufficient.

Having solved the optimization problems for all values of $i = 1, \ldots, m$, the vectors $\mathcal{K} = \{v_1, \ldots, v_m\} \subset \mathbb{R}^{1\times m}$ are constructed if solutions to the optimization problem exist for every i. Given that the vectors in $\mathcal{K}$ are linearly independent, the matrix $K_S \in \mathbb{R}^{m\times m}$ is finally constructed as

$$K_S = \begin{pmatrix} \frac{1}{\|v_1\|} v_1 \\ \vdots \\ \frac{1}{\|v_m\|} v_m \end{pmatrix}. \tag{3.4.46}$$

In some cases multiplying the input vector by a matrix that is a column permutation of I_m, the

identity matrix of m rows, may convert a problem an unsolvable to a problem that is solvable. However, such cases are not considered here as the design of sliding surfaces for the impedance source converter is a directly solvable problem.

For the trans-Z-source converter there are two switches, $m = 2$, and so $K_S \in \mathbb{R}^{2\times 2}$. Furthermore, it is assumed that the design of the switching function is based on the ideal dynamics, since the non-ideal components are in general unknown during the design. According to relation (3.3.14) the function v_H for the ideal trans-Z-source converter is defined as,

$$v_H(u) = K_H \cdot f_{\text{id}}(x^*, u). \tag{3.4.47}$$

Solving the optimization problem, a surface that satisfies the constraints for the trans-Z-source converter, is determined by the matrix

$$K_S = \begin{pmatrix} 0.9997 & 0.0230 \\ -0.9959 & 0.0907 \end{pmatrix}. \tag{3.4.48}$$

This matrix defines two lines such that the first is perpendicular to the bisector of the angle $\angle(v_H(1,1), v_H(1,0))$ and the second defines a line that bisects the angle $\angle(v_H(0,1), v_H(0,0))$. The resulting normal vectors and the corresponding surfaces can be seen in fig. 3.8. The surface defined by K_S also offers maximal separation between the system modes. The maximal separation results in the greatest possible resilience to random perturbations in the dynamics of the system which are introduced by unmodeled non-ideal components.

3.4.2 Switching algorithms for the implementation of variable structure controllers with a hierarchy of switching surfaces

The sliding surfaces in a hierarchy enforce sliding in an ideal variable structure system. Practical switching algorithms are required to implement sliding a trans-Z-source converter. On a single stable sliding surface $\mathcal{S}_i$, sliding can be enforced by a hysteresis switching algorithm such as the one depicted in fig. 2.4b. In the intersection $\mathcal{S}_1 \cap \mathcal{S}_2$ of two stable sliding surfaces, $\mathcal{S}_1$ and $\mathcal{S}_2$, the combination of the hysteresis switching algorithms for each surface enforces sliding on the intersection. In the intersection $\mathcal{S}_1 \cap \mathcal{S}_2$ however, switching can be implemented with hysteresis with respect to the manifold $\mathcal{S}_1 \cap \mathcal{S}_2$ directly. In this case $\mathcal{S}_1$ and $\mathcal{S}_2$ do not need to be stable in order for sliding on their intersection to be stable.

However, other hysteresis options are available in an intersection of $\mathcal{S}_1 \cap \mathcal{S}_2$ of co-dimension two. A hysteresis switching algorithm is proposed here that operates by switching with respect to a distance metric from the surface $\mathcal{S}_1 \cap \mathcal{S}_2$ after the intersection is reached. The resulting dynamics in the boundary hysteresis layer are significantly different in the two switching approaches leading to different sliding dynamics. The first of the proposed switching algorithm uses two switching surfaces to enforce sliding on their intersection.

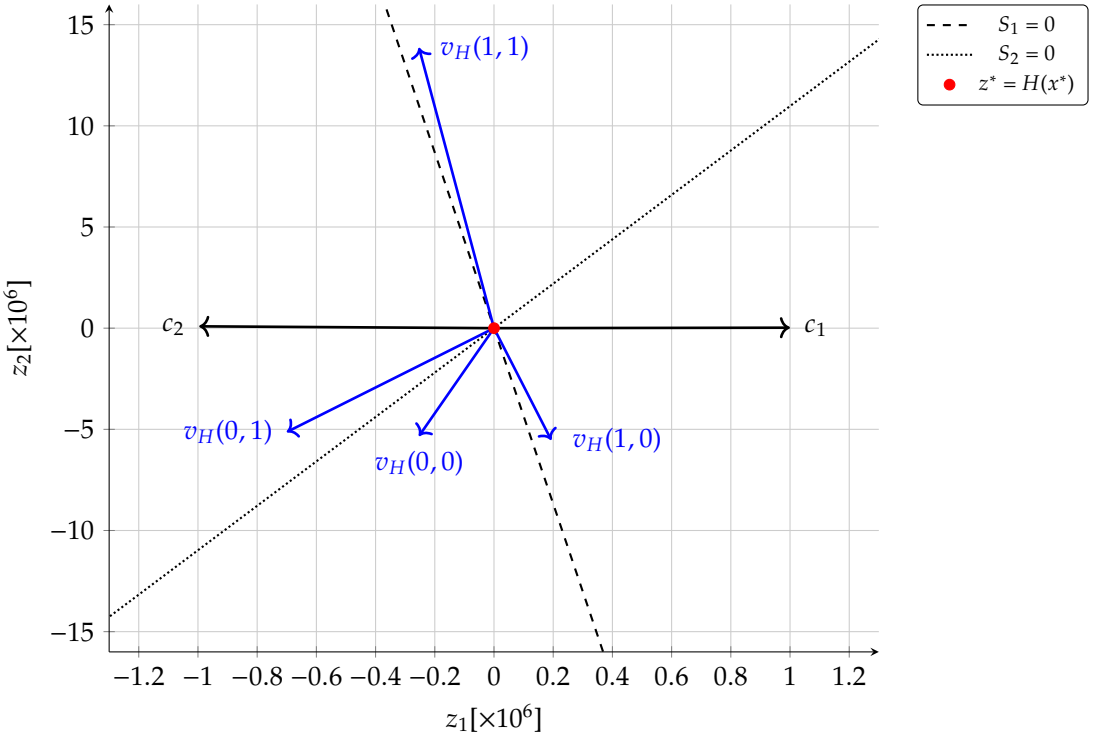

Figure 3.8: Selection of two switching surfaces that are nodally attractive. The vector function $v_H(u) = K_H \cdot f(x^*, u)$ determines the vector field for each control input. From the diagram it seems possible to select two surfaces $S_1 = 0$ and $S_2 = 0$ so that the system slides toward their intersection. The switching function $S = K_S \cdot z$ where K_S is defined in relation (3.4.48) is constructed by solving the optimization problem in section 3.4.1.2 for the trans-Z-source converter. The scaled gradient vector $c = \alpha \nabla_z S$ is also shown, where $\alpha = 4 \cdot 10^6$ was selected so that the vectors are visible in the scale of the plot.

3.4.2.1 Switching with hysteresis in the intersection of two independent co-dimension one switching surfaces

The first control algorithm designed for the trans-Z-source converter enforces sliding on a hierarchy of nodally attracting switching surfaces. Letting S be the switching function constructed for the trans-Z-source converter, sliding is enforced on any of the surfaces $\mathcal{S}_1$ and $\mathcal{S}_2$ whenever they are reached. Thus the sliding hierarchy is

$$\varnothing \rightarrow (\mathcal{S}_1 \rightarrow \mathcal{S}_1 \cap \mathcal{S}_2) \,|\, (\mathcal{S}_2 \rightarrow \mathcal{S}_1 \cap \mathcal{S}_2) \,. \tag{3.4.49}$$

The hierarchy is enforced by independent hysteresis switching on each of the surfaces $\mathcal{S}_1$ and $\mathcal{S}_2$ with hysteresis $\varepsilon_{\text{box}(1)} > 0$ and $\varepsilon_{\text{box}(2)} > 0$ respectively. In the intersection, the switching algorithm thus confines the system in a box-like region

$$\mathcal{S}_{\text{box}} = \left\{ x \in \mathbb{R}^n : |S_i(x)| \leq \varepsilon_{\text{box}(i)} \text{ for } i = 1, 2 \right\} . \tag{3.4.50}$$

The operation of the hysteresis switching hybrid automaton enforcing sliding is described in algorithm 1. Close to $S = 0$ where the two layers intersect, the hysteresis zone is the parallelogram on the range of the sliding function H which is depicted in fig. 3.10.

Algorithm 1 The algorithm describes a hysteresis switching automaton in the intersection of two independent co-dimension one switching surfaces. Given the state of the automaton $\mathrm{ST} = (\mathrm{ST}_1, \mathrm{ST}_2)$ with one binary digit for each switch, and the value of the switching function $s = S(x)$, the algorithm returns the next state and the input to the switches $\ell = (\ell_1, \ell_2)$ where ℓ_i is the input to the i^{th} switch.

function NEXTSTATE$_{\text{box}}$(ST, s)
  for $i \in \{1, 2\}$ **do**
    if $\mathrm{ST}_i = 0$ **then**
      if $s_i < -\varepsilon_{\text{box}(i)}$ **then**
        $\mathrm{ST}_i \leftarrow 1$
        $\ell_i \leftarrow 1$
      else
        $\ell_i \leftarrow 0$
      end if
    else
      if $s_i > \varepsilon_{\text{box}(i)}$ **then**
        $\mathrm{ST}_i \leftarrow 0$
        $\ell_i \leftarrow 0$
      else
        $\ell_i \leftarrow 1$
      end if
    end if
  end for
  return (ST, ℓ)
end function

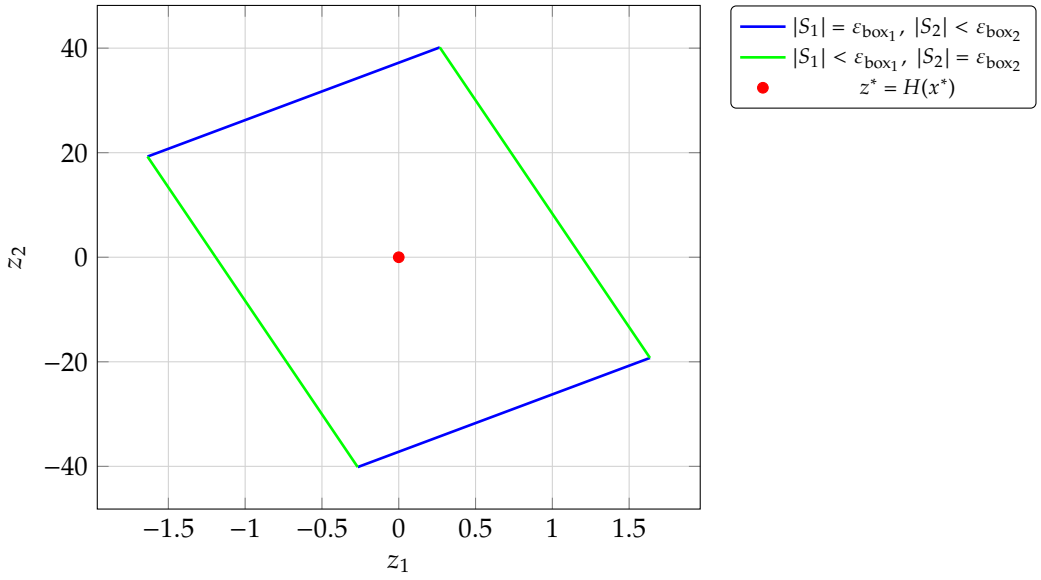

Figure 3.9: A hysteresis layer comprised by the intersection of two hysteresis layers around co-dimension one switching surfaces.

3.4.2.2 Switching with hysteresis with respect to a co-dimension two switching manifold

The second control algorithm designed for the trans-Z-source converter enforces sliding on a hierarchy of nodally attracting switching surfaces, but uses hysteresis switching with respect to the intersection of the surfaces when the intersection is reached. The sliding hierarchy used is

$$\varnothing \rightarrow \mathcal{S}_1 \rightarrow \mathcal{S}_1 \cap \mathcal{S}_2 \tag{3.4.51}$$

The switching in the intersection $\mathcal{S}_1 \cap \mathcal{S}_2$ is performed within a hysteresis layer at some distance from the intersection $\mathcal{S}_1 \cap \mathcal{S}_2$ which is a co-dimension two manifold. The switching layer for the system is determined by the equation

$$\mathcal{S}_{\text{ellipse}} = \left\{ x \in \mathbb{R}^n : V(x) \leq \varepsilon^2_{\text{ellipse}} \right\} \tag{3.4.52}$$

where $V : \mathbb{R}^3 \to \mathbb{R}$ and some $\varepsilon_{\text{ellipsis}} > 0$. The function V is constructed so that it is positive on R^3, except for the intersection $\mathcal{S}_1 \cap \mathcal{S}_2$ where it is zero. A quadratic function V is used defined as

$$V(x) = \frac{1}{2} H(x)^T \cdot A \cdot H(x), \tag{3.4.53}$$

where $A \in \mathbb{R}^{2\times 2}$ is some positive definite matrix, $A \succ 0$. A matrix A of the form

$$A = \begin{pmatrix} \alpha_1 & 0 \\ 0 & \alpha_2 \end{pmatrix} \tag{3.4.54}$$

where $\alpha_1, \alpha_2 > 0$ is used, resulting in a hysteresis layer forming an elliptical cylinder in $\mathbb{R}^3$ with its major and minor axis parallel to the z_1 and z_2 axis.

In the proposed algorithm, the components of the control vector u are no longer modulated independently of each other. This model of switching controllers has been used in the Lyapunov based control of power electronics [122], and is adjusted here to enforce sliding. While sliding on the intersection $\mathcal{S}_1 \cap \mathcal{S}_2$, to keep the system state within the hysteresis layer, whenever trajectory crosses $V(x) = \varepsilon^2_{\text{ellipse}}$, the vector field that moves the state faster towards the nominal state x^* is selected. The gradient of V is

$$\begin{aligned} \partial_x V &= \partial_x \left(H^T A H \right) && (3.4.55)\\ &= \frac{1}{2} \left(\left((\partial_x H)^T A H \right)^T + H^T A \partial_x H \right) && (3.4.56)\\ &= \frac{1}{2} \left(H^T A^T \partial_x H + H^T A \partial_x H \right) && (3.4.57)\\ &= \frac{1}{2} H^T \left(A^T + A \right) \partial_x H, && (3.4.58) \end{aligned}$$

and since A is symmetric,

$$\partial_x V = H^T A \partial_x H. \tag{3.4.59}$$

Therefore, by the chain rule the time derivative of V under ideal dynamics is

$$\begin{aligned} D_t V &= \partial_x V \cdot D_t x && (3.4.60)\\ &= \partial_x V \cdot f_{\text{id}}(x, u) && (3.4.61)\\ &= H(x) A \left(\partial_x H(x) \right)^T \cdot f_{\text{id}}(x, u). && (3.4.62) \end{aligned}$$

The switching input is calculated according to the ideal dynamics since the non-ideal behavior is unknown during the design of the controller. Thus the control input selected on the hysteresis

boundary when $V(x) = \varepsilon^2_{\text{ellipse}}$ is

$$w_{\text{el}}(x) = \arg\min_{u \in U} \left(H(x) A \left(\partial_x H(x)\right)^T \cdot f_{\text{id}}(x, u) \right). \tag{3.4.63}$$

The modulation algorithm for the selection of the control input is algorithm 2. A plot of the hysteresis layer projected around the intersection $\mathcal{S}_1 \cap \mathcal{S}_2$ in the range of the sliding function can be seen in fig. 3.10. The discrete states of the hysteresis controller are

$$\Sigma = \{L_{00}, L_{01}, L_{10}, L_{11}, V_{00}, V_{01}, V_{10}, V_{11}\}. \tag{3.4.64}$$

The auxiliary function subscript is defined over Σ as

$$\text{subscript}(x) = \begin{cases} s, & x = L_s \\ s, & x = V_s. \end{cases} \tag{3.4.65}$$

The modulation algorithm works by enforcing sliding first in a boundary layer around $\mathcal{S}_1$ until the state intersects the hysteresis layer around the the intersection $\mathcal{S}_1 \cap \mathcal{S}_2$; then switching occurs with hysteresis with respect to the intersection. To ensure that the two hysteresis layers merge as expected, a hysteresis layer of width $\varepsilon_{\mathcal{S}_1}$ is used around $\mathcal{S}_1$. The hysteresis width is defined as

$$\varepsilon_{\mathcal{S}_1} = \max \left\{ |S_1(x)| : x \in \overline{\mathcal{S}}_{\text{ellipse}} \right\} \tag{3.4.66}$$

where

$$\overline{\mathcal{S}}_{\text{ellipse}} = \left\{ x \in \mathbb{R}^n : V(x) = \varepsilon^2_{\text{ellipse}} \right\}. \tag{3.4.67}$$

The set $\overline{\mathcal{S}}_{\text{ellipse}}$ is closed and bounded, and the absolute value is a continuous function. Thus, according to the extreme value theorem, $\varepsilon_{\mathcal{S}_1}$ is well defined. In fact the resulting boundaries of the switching layer around $\mathcal{S}_1$ are tangent to the ellipsoid defined in $\mathbb{R}^3$ by $\overline{\mathcal{S}}_{\text{ellipse}}$.

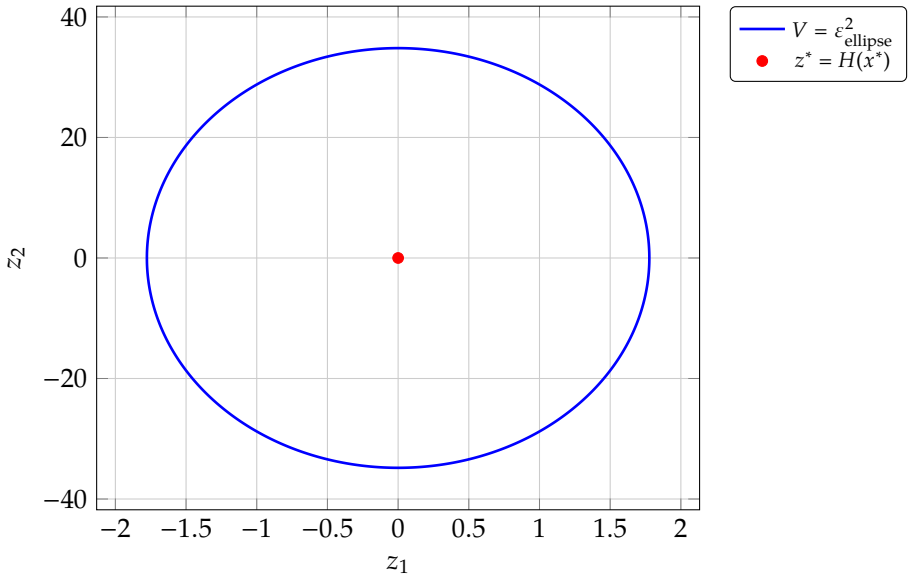

Figure 3.10: A hysteresis switching boundary comprised by a single elliptical hysteresis layer around a co-dimension two sliding surface.

Algorithm 2 The algorithm describes a hysteresis switching automaton in the intersection of two co-dimension one switching surfaces, where hysteresis is evaluated with respect to the intersection. Given the state of the automaton ST = (ST_1, ST_2) with one binary digit for each switch, and the system state x, the algorithm returns the next state and the input to the switches $\ell = (\ell_1, \ell_2)$ where ℓ_i is the input to the i^{th} switch.

function NextState$_{\text{ellipse}}$(ST, x)
  if ST $\in \{L_{00}, L_{01}, L_{10}, L_{11}\}$ **then**
    if $V(x) < \varepsilon^2_{\text{ellipsis}}$ **then**
      $\ell \leftarrow w_{\text{el}}(x)$
      ST $\leftarrow V_\ell$
    else if ST $= L_{00}$ **or** ST $= L_{01}$ **then**
      if $S_1(x) < -\varepsilon_{\mathcal{S}_1}$ **then**
        if $S_2(x) < 0$ **then**
          ST $\leftarrow L_{11}, \ell \leftarrow 11$
        else
          ST $\leftarrow L_{10}, \ell \leftarrow 10$
        end if
      else
        $\ell \leftarrow$ subscript(ST)
      end if
    else
      if $S_1(x) > \varepsilon_{\mathcal{S}_1}$ **then**
        if $S_2(x) < 0$ **then**
          ST $\leftarrow L_{01}, \ell \leftarrow 01$
        else
          ST $\leftarrow L_{11}, \ell \leftarrow 11$
        end if
      else
        $\ell \leftarrow$ subscript(ST)
      end if
    end if
  else
    if $V(x) < \varepsilon^2_{\text{ellipsis}}$ **then**
      $\ell \leftarrow$ subscript(ST)
    else
      $\ell \leftarrow w_{\text{el}}(x)$
      ST $\leftarrow V_\ell$
    end if
  end if
  return (ST, ℓ)
end function

3.4.3 Time domain simulations

The trans-Z-source converter was simulated for the two proposed control algorithms until reaching a steady state. The analysis of the switching algorithms focuses on steady state operation. During sliding on the manifold $\mathcal{M}$ the system trajectory remains constraint in the hysteresis switching layer. The system moves freely along the direction of the sliding manifold and eventually reaches a steady state limit cycle for both switching algorithms. For simplicity, the algorithm 1 will be called the box controller and algorithm 2 will be called the ellipse controller. The hysteresis parameters used in the two control algorithms are summarized in table 4.2b. In

the ellipse controller, the parameter α used in the definition of the hysteresis boundary is

$$\alpha = \begin{pmatrix} 384 \\ 1 \end{pmatrix}. \tag{3.4.68}$$

The parameter α was selected so that the ratio of the major and minor axes of the ellipse is close to the ratio of the diagonals of the box. In both the box and the ellipse controllers, the parameters were selected to ensure an average switching frequency of about 150 kHz. The selection was made through a trial and error approach.

Hysteresis width	
ε_{box}	$\begin{pmatrix} 1.42 \\ 11.4 \end{pmatrix}$
$\varepsilon_{\text{ellipse}}$	24.62

Table 3.5: Parameters for the sliding mode controller of the simulated voltage fed, DC-DC, trans-Z-source converter.

The time plots of the system state for the two controllers during steady state operation can be seen in fig. 3.11, and a projection of the steady state trajectory by H in fig. 3.12. The projection by the sliding function hides any variation along the sliding surface. In general, the box switching algorithm results in steady state cycle with a much larger period, fig. 3.12b, than the ellipse algorithm, fig. 3.12a. Let T be the period of the limit cycle. Over a single period $[t, t+T]$ of steady state operation the averaged value of the state is denoted as

$$\langle x \rangle = \frac{1}{T} \int_t^{t+T} x d\tau. \tag{3.4.69}$$

Furthermore, over a single period $[t, t+T]$ of steady state operation the ripple of the state is defined as

$$\Delta x_i = \max_{\tau \in [t, t+T]} x_i(\tau) - \min_{\tau \in [t, t+T]} x_i(\tau) \tag{3.4.70}$$

for $i = 1, 2, 3$. The averaged value of the converter states and their relative deviation from the ideal fixed point x^* can be found in table 3.6. The ripple of each of the states of the converter and its magnitude relative to the ideal fixed point can be found in table 3.7.

Both the box and the ellipse controller stabilize the system successfully. The output current ripple is relatively large in both controllers, but since the converter is connected to a DC voltage source, the current ripple can be filtered by a parallel capacitor. Regarding the steady state drift, both the box and the ellipse switching algorithm are acceptable. However, the box algorithm has a significantly smaller drift in the state of the impedance network (i_{L_m}, v_C).

3.5 Dynamics in the hysteresis boundary layer and jitter

In a hysteresis switched sliding mode controller, the converter follows some motion in the boundary layer that determines the dynamics along the sliding manifold. The regularized dynamics for hysteresis controllers are determined by the limit of the sliding dynamics as the

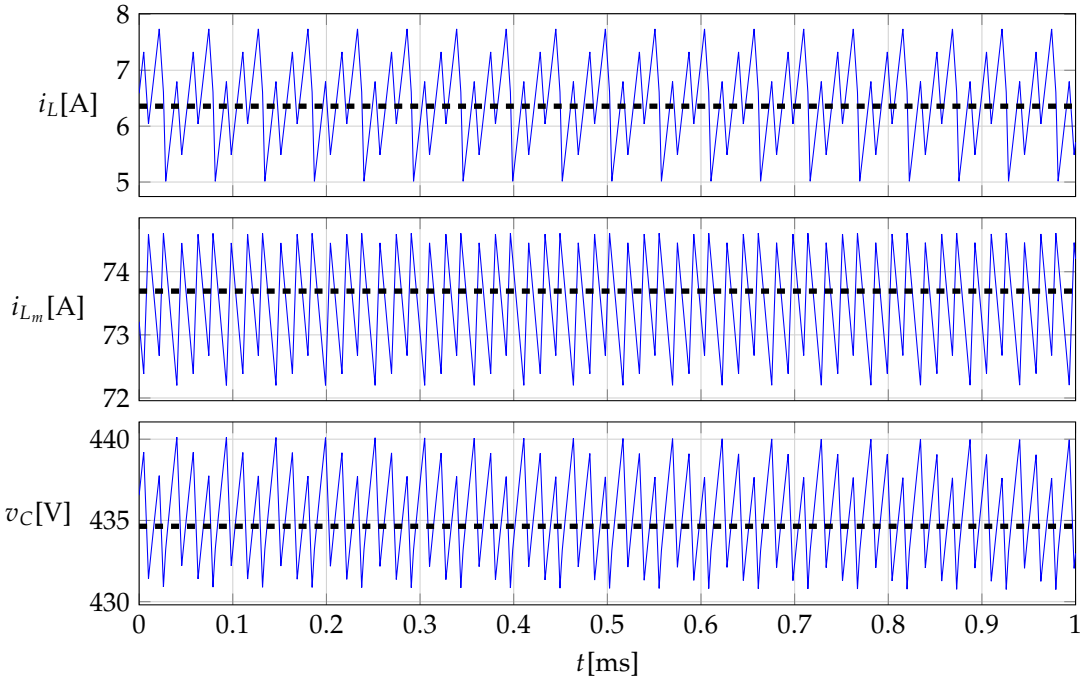

(a) Time plots for the controller operating in the $\mathcal{S}_{\text{ellipse}}$ hysteresis layer.

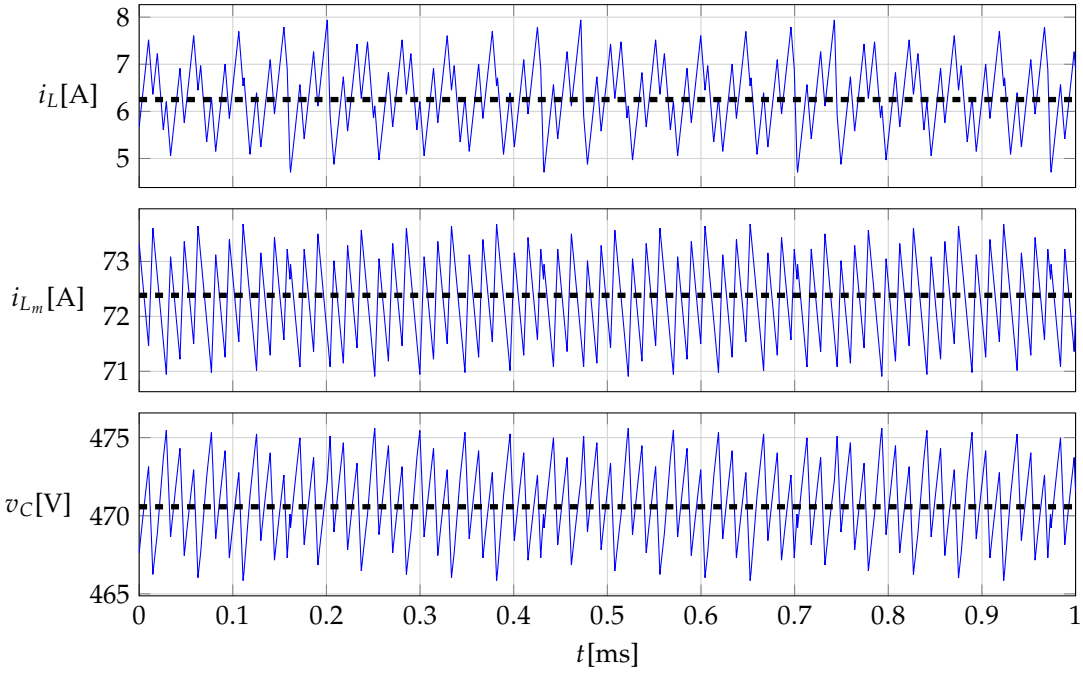

(b) Time plots for the controller operating in the $\mathcal{S}_{\text{box}}$ hysteresis layer..

Figure 3.11: Time plots of the state variables of the hysteresis modulates trans-Z-source converter in steady state operation. The tick dashed line corresponds to the mean value of the state over a steady state cycle. The hysteresis layer $\mathcal{S}_{\text{box}}$ results in a much higher period but smaller steady state drift from the hysteresis layer $\mathcal{S}_{\text{ellipse}}$.

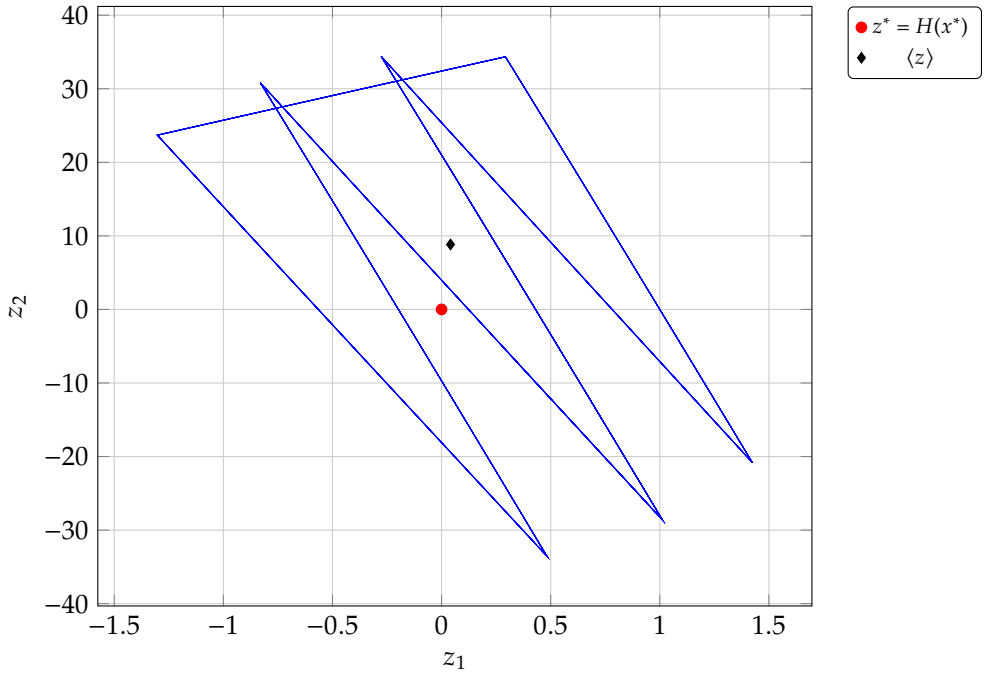

(a) Limit cycle in the $\mathcal{S}_{\text{ellipse}}$ hysteresis layer.

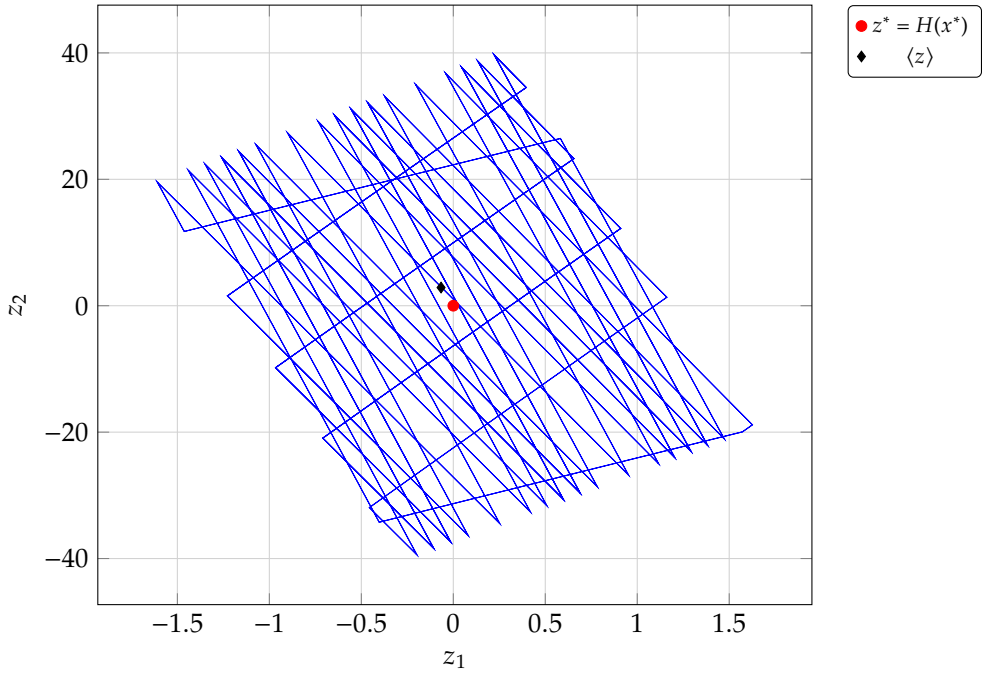

(b) Limit cycle in the $\mathcal{S}_{\text{box}}$ hysteresis layer.

Figure 3.12: Phase plots of the state variables of the hysteresis modulates trans-Z-source converter in steady state operation projecting on the space where the control objective take their values. The box hysteresis layer offers a much smaller steady state drift from the control objective. Note that, due to variation along the direction of the sliding manifold during the motion, the switching surface varies and its projection along the trajectory is not single curve.

	$\langle i_L \rangle$	$\langle i_{L_m} \rangle$	$\langle v_C \rangle$	$\frac{\langle i_L \rangle}{i_L^*}$	$\frac{\langle i_{L_m} \rangle}{i_{L_m}^*}$	$\frac{\langle v_C \rangle}{v_C^*}$
box	6.25 A	73.4 A	471 V	0.01	−0.005	0.02
ellipse	6.36 A	73.7 A	435 V	−0.006	−0.024	0.094

Table 3.6: Averaged value of the converter states during steady state operation and their relative deviation from the ideal fixed point x^*.

	Δi_L	Δi_{L_m}	Δv_C	$\frac{\Delta i_L}{i_L^*}$	$\frac{\Delta i_{L_m}}{i_{L_m}^*}$	$\frac{\Delta v_C}{v_C^*}$
box	3.24 A	2.77 A	9.75 V	0.512	0.039	0.02
ellipse	2.73 A	2.41 A	9.38 V	0.432	0.034	0.02

Table 3.7: Ripple of the converter states during steady state operation and the magnitude of the ripple relative to the ideal fixed point x^*.

width of the hysteresis layer tends to zero. In converters sliding on the intersection of two switching surfaces, the motion resulting from the regularization is equivalent to taking the projection of the converter dynamics on a surface that slices through the sliding manifold at the regularization point. Given that the hysteresis layer is small enough, the vector fields in the hysteresis layer are approximated by the vector field values as the regularization point of the sliding manifold. Letting the projected system evolve, if the proportion of time spent in each vector field converges, then multiplying the vector fields with their corresponding time proportions, results in the sliding vector field for the point where the dynamics of the system are regularized.

The regularization method for hysteresis switched controllers was first developed in [75] for systems sliding on the intersection of two switching surfaces. Furthermore, in [75] it was proven that the motion in a box hysteresis layer in the regularization limit where the vector fields are constant, always converges to an attractive or marginally stable limit cycle, and that the resulting dynamics are indeed tangent to the sliding manifold. However, similar results do not exist for the ellipse hysteresis layer or other families of hysteresis layers. In [139] it is demonstrated that multiple stable limit cycles exists in an elliptical hysteresis layer, and the limit cycle to which the solution converges depends on the initial conditions. When multiple solutions exists, the regularization limit is not unique, and there exists a set of possible sliding vector fields depending on the initial condition for the projected dynamics.

3.5.1 Projected dynamics in the regularized system

The regularization of the sliding dynamics requires the evaluation of the projection of the system dynamics on a surface perpendicular to the sliding manifold at the regularization point. The projection is evaluated using a coordinate transformation $T : \mathbb{R}^3 \to \mathbb{R}^3$, where

$$T(x) = \begin{pmatrix} H(x) \\ T_s(x) \end{pmatrix} \tag{3.5.1}$$

and H is linear function defining the sliding manifold $\mathcal{M}$, and the function $T_s : \mathbb{R}^3 \to \mathbb{R}$ is

$$T_s(x) = \overline{B}_{\mathcal{M}} \cdot (x - x^*) \tag{3.5.2}$$

where $\overline{B}_{\mathcal{M}}$ is defined in relation (3.3.47). The function T is indeed reversible. From the definition of T,

$$T(x) = \begin{pmatrix} H(x) \\ T_s(x) \end{pmatrix} \tag{3.5.3}$$

$$= \begin{pmatrix} K_H \\ \overline{B}_{\mathcal{M}} \end{pmatrix} \cdot (x - x^*)\,, \tag{3.5.4}$$

where the matrix

$$\begin{pmatrix} K_H \\ \overline{B}_{\mathcal{M}} \end{pmatrix} \tag{3.5.5}$$

is reversible according to the definitions of $\overline{B}_{\mathcal{M}}$ and K_H. Thus setting

$$R_T = \begin{pmatrix} K_H \\ \overline{B}_{\mathcal{M}} \end{pmatrix}^{-1} \tag{3.5.6}$$

the inverse transformation is

$$T^{-1}(x) = R_T \cdot x + x^*. \tag{3.5.7}$$

Furthermore, according to the definition of $\overline{B}_{\mathcal{M}}$, the function T_s projects any point $x \in \mathbb{R}^3$ on the sliding manifolds $\mathcal{M}$. Furthermore, since $\overline{B}_{\mathcal{M}}$ is normalized, the transformation T_s preserves distances along $\mathcal{M}$, therefore for any point $x \in \mathcal{M}$, $\|x - x^*\| = |T_s(x)|$.

According to the definition of $\overline{B}_{\mathcal{M}}$ a plane that is perpendicular to the sliding manifold $\mathcal{M}$ at the point $x \in \mathcal{M}$ is defined as

$$\mathcal{E}(y) = \left\{ v \in \mathbb{R}^3 : T_s(v) = y \right\} \tag{3.5.8}$$

where $y = T_s(x)$. Given any $x \in \mathcal{E}(y)$ let

$$z = H(x). \tag{3.5.9}$$

Then the dynamics of $z \in \mathbb{R}^2$ determine the projected dynamics of the systems on the plane $\mathcal{E}(y)$. Le the dynamics of x be given by a variable structure system

$$D_t x = f(x, u) \tag{3.5.10}$$

where $f : \mathbb{R}^3 \times \mathbb{R}^2 \to \mathbb{R}^3$ is a function smooth in its inputs. According to the chain rule,

$$D_t z = D_t H(x) \tag{3.5.11}$$

$$= \partial_x H \cdot f(x, u) \tag{3.5.12}$$

$$= \partial_x H \cdot f\left(T^{-1} \begin{pmatrix} z \\ y \end{pmatrix}, u \right) \tag{3.5.13}$$

where in the last equality the fact that $x \in \mathcal{E}(y)$ is used. Therefore, defining

$$f_{\text{proj}}(z, u; y) = \partial_x H \cdot f\left(T^{-1}\begin{pmatrix} z \\ y \end{pmatrix}, u\right), \tag{3.5.14}$$

the dynamics projected on $\mathcal{E}(y)$ are

$$D_t z = f_{\text{proj}}(z, u; y), \tag{3.5.15}$$

parametrized by $y \in \mathbb{R}$.

For any hysteresis modulation algorithm G, the dynamics of the system projected on the plane $\mathcal{E}(y)$ are determined by setting

$$x = T^{-1}\begin{pmatrix} z \\ y \end{pmatrix} \tag{3.5.16}$$

where the dynamics of z are determined by relation (3.5.14) for the constant term approximation where $z = 0$. Let $u : \mathbb{R} \to \{0,1\}^2$ be the control input produced for the projected system by the control algorithm G on the projection on the plane $\mathcal{E}(y)$. Then, the duty ratios for the enumeration κ of the control inputs in a system with two switches defined in relation (3.3.98) are

$$\gamma_{G_i}(y) = \lim_{\tau\to\infty} \frac{1}{\tau} \int_0^\tau \mathbb{I}(u(t) = \kappa_i)\, dt, \tag{3.5.17}$$

where $\mathbb{I}$ is the indicator function defined as

$$\mathbb{I}(A) = \begin{cases} 1, & \text{if } A \text{ is true} \\ 0, & \text{otherwise.} \end{cases} \tag{3.5.18}$$

Given that the limits γ_{G_i} are well defined, the sliding vector field in y is then

$$\hat{g}_G(y) = \sum_{i=1}^{4} \gamma_{G_i}(y) \left(\overline{B}_{\mathcal{M}} \cdot f\left(T^{-1}\begin{pmatrix} 0 \\ y \end{pmatrix}, \kappa_i\right)\right). \tag{3.5.19}$$

3.5.2 Jitter

When a converter system slides in the intersection of two switching surfaces, the limit cycle in the projected dynamics varies as the system moves along the intersection. Abrupt bifurcations appear in the limit cycle when the trajectory of the projected dynamics crosses the corners of the hysteresis box [75] resulting in changes in the sliding speed. This phenomenon is studied in detail in [76] where the abrupt variation in the sliding speed is called jitter. Abrupt variation in the sliding speed along the sliding surface appears for some realizations of the switching algorithm. In [76] it is shown that jitter appears for hysteresis switching, switching with time delays and in discrete systems with switching, where as it does not appear in smooth systems and systems with probabilistic switching.

The jitter is now demonstrated in a system with hysteresis switching. A system from [76] is used and its dynamics are sped down by a factor of 10^3 to simplify the notation. Let a discrete

variable structure system be defined by the function $f : \mathbb{R}^3 \times \mathbb{R}^2 \to \mathbb{R}^3$,

$$f(x,u) = G(u) \cdot x + g(u) \tag{3.5.20}$$

where $G : \mathbb{R}^2 \to \mathbb{R}^{3\times3}$ and $g : \mathbb{R}^2 \to \mathbb{R}^3$ are smooth auxiliary functions defined as

$$G(u) = (1-u_1)(1-u_2)A_{00} + u_1(1-u_2)A_{10} + (1-u_1)u_2A_{01} + u_1u_2A_{11} \tag{3.5.21}$$

and

$$g(u) = (1-u_1)(1-u_2)a_{00} + u_1(1-u_2)a_{10} + (1-u_1)u_2a_{01} + u_1u_2a_{11} \tag{3.5.22}$$

where

$$a_{00} = \begin{pmatrix} -\frac{20}{3} \\ -\frac{15}{8} \\ -\frac{10}{3} \end{pmatrix}, \qquad a_{01} = \begin{pmatrix} \frac{20}{3} \\ -\frac{15}{4} \\ -\frac{10}{3} \end{pmatrix}, \qquad a_{10} = \begin{pmatrix} -8 \\ -\frac{5}{2} \\ 5 \end{pmatrix}, \qquad a_{11} = \begin{pmatrix} \frac{2}{3} \\ \frac{5}{2} \\ \frac{5}{2} \end{pmatrix}, \tag{3.5.23}$$

and

$$A_{00} = \begin{pmatrix} 0 & -\frac{2}{3} & 0 \\ \frac{5}{8} & 0 & 0 \\ 0 & 0 & 0 \end{pmatrix}, \qquad A_{11} = \begin{pmatrix} 0 & 0 & \frac{2}{3} \\ 0 & 0 & 0 \\ -\frac{5}{6} & 0 & 0 \end{pmatrix}, \tag{3.5.24}$$

$$A_{10} = A_{01} = \mathbb{O}_3 \tag{3.5.25}$$

where $\mathbb{O}_3$ is the zero matrix in $\mathbb{R}^{3\times3}$. The function defining the sliding manifold is $H : \mathbb{R}^3 \to \mathbb{R}^2$ defined as

$$H(x) = \begin{pmatrix} x_1 \\ x_2 \end{pmatrix}. \tag{3.5.26}$$

A box type switching algorithm is used. Each of the switches u_i for $i = 1, 2$ is switched independently by a simple hysteresis switching algorithm defined in fig. 2.4b with switching function $S_i(x)$, where

$$S = H, \tag{3.5.27}$$

and a hysteresis width ε_i defined as

$$\varepsilon = \begin{pmatrix} 1 \\ 1 \end{pmatrix}. \tag{3.5.28}$$

The sliding variable is

$$y = T_s(x) \tag{3.5.29}$$

where $T_s : \mathbb{R}^3 \to \mathbb{R}$ is defined as

$$T_s(x) = x_3. \tag{3.5.30}$$

The regularized sliding dynamics are evaluated for the hysteresis switching algorithm over the range $y \in [6, 20]$. The resulting sliding vector field is plotted in fig. 3.13. The changes in the sliding speed are caused by bifurcations in the limit cycle of the regularized system. To demonstrate the range of variation of the sliding speed, the sliding speed is regularized with respect to the canopy solution and is plotted withing the regularized maximum and minimum

speed solutions in the minimal convex hull. Let g_{cp} be the canopy solution for the discrete variable structure system defined by relation (3.5.20). Furthermore, let g_{max} and g_{min} be the maximum and minimum sliding solutions in the minimal convex hull for the system. The normalized functions are defined as

$$\Delta\hat{g}_{box} = \hat{g}_{box} - g_{cp} \tag{3.5.31}$$

$$\Delta g_{min} = g_{min} - g_{cp}, \qquad \Delta g_{max} = g_{max} - g_{cp}, \tag{3.5.32}$$

and are plotted in fig. 3.14.

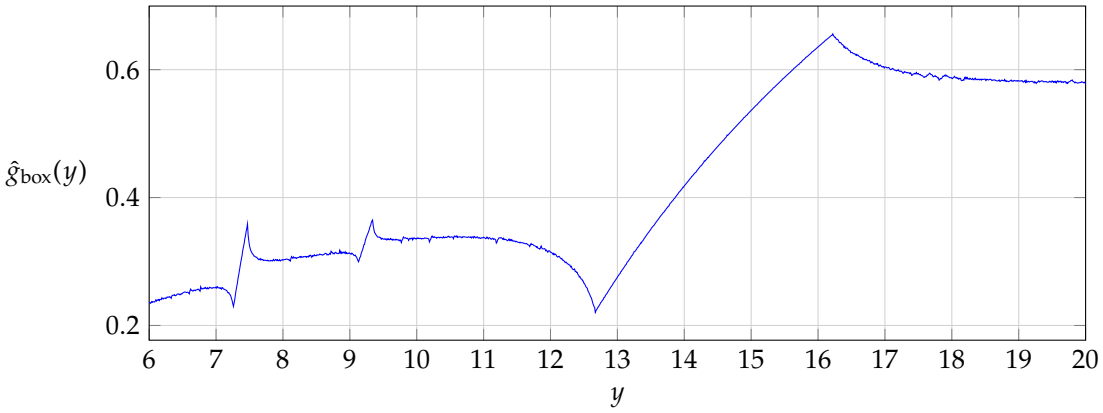

Figure 3.13: The sliding vector field for the regularized discrete variable structure system with dynamics defined by relation (3.5.20). The system slides in the intersection of two switching surfaces, and is actuated using hysteresis switching.

3.5.3 Sliding vector field in a practical system

Jitter also appears in the sliding mode controlled trans-Z-source converter with hysteresis switching. As a result, it is difficult to determine the exact sliding dynamics during the design phase single the sliding speed depends on the shape of the hysteresis region. The drift in the regularized dynamics persists even in the limit where the hysteresis region disappears. However, the hysteresis width has a finite size in a practical implementation of a hysteresis switched controller for the trans-Z-source converter to maintain a sufficiently small switching frequency. As a result, the constant term approximation for the sliding dynamics is not valid.

Given that the hysteresis width is sufficiently small, the dynamics in a projection on the a plane perpendicular to the sliding surface can be used to evaluate the sliding speed. The full projected dynamics in relation (3.5.15) are simulated for the box and ellipse control algorithms while the system is sliding. Thus, given a control input $u : \mathbb{R} \to \{0, 1\}^2$ evaluated by a control algorithm

$$G \in \{\text{ellipse}, \text{box}\} \tag{3.5.33}$$

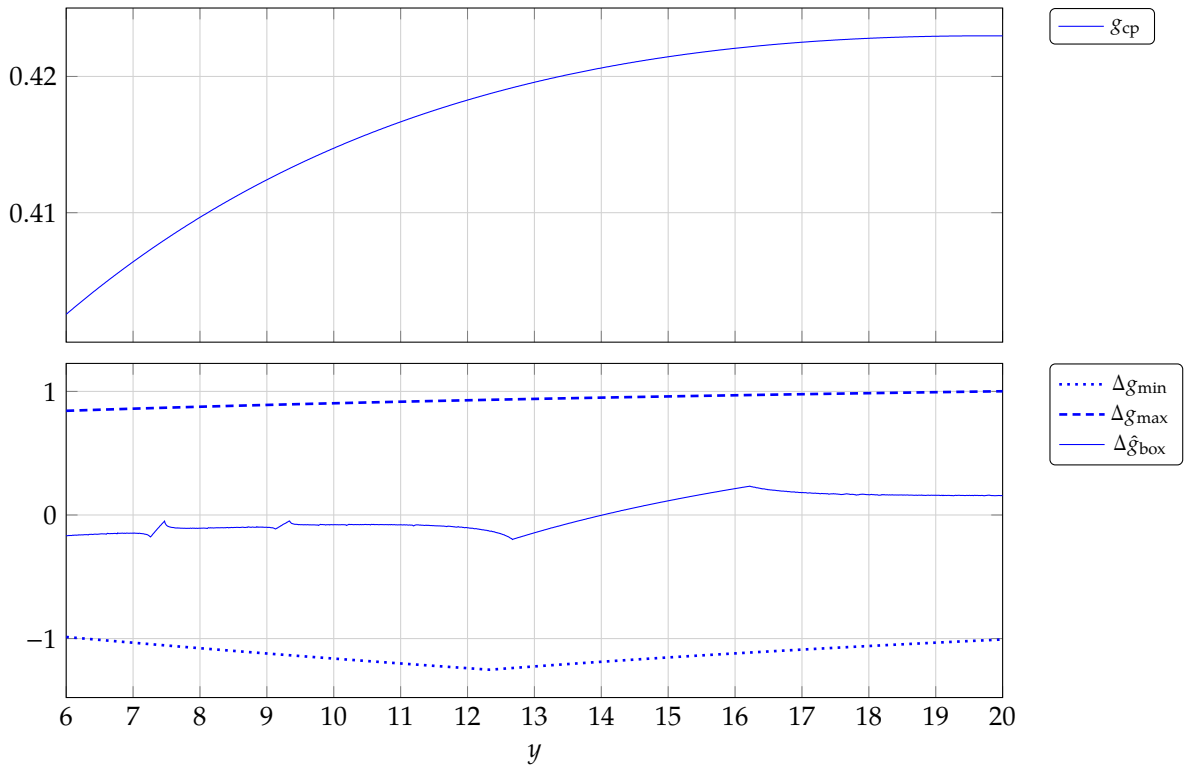

Figure 3.14: Plots of the canopy solution and the normalized regularized, and minimum and maximum sliding solutions for discrete variable structure system with dynamics defined by relation (3.5.20).

the averaged speed along the sliding surface is then evaluated as

$$\overline{g}_G(y) = \lim_{\tau\to\infty} \frac{1}{\tau} \int_0^\tau \overline{B}_{\mathcal{M}} \cdot f\left(T^{-1}\begin{pmatrix} z(t) \\ y \end{pmatrix}, u(t)\right) dt. \tag{3.5.34}$$

The averaged sliding speeds for the box and ellipse hysteresis regions as a function of the position along the sliding surface are depicted in fig. 3.15. The sliding dynamics for the modulation algorithm in the elliptical hysteresis region cross the y axis at about $y = -60$ resulting in a steady state relatively far from zero. In contrast, the box modulation algorithm crosses he y axis almost exactly at zero. The difference explains the larger drift in the impedance network states (i_{L_m}, v_C) that appears in the average steady state solution for ellipse algorithm in table 3.6.

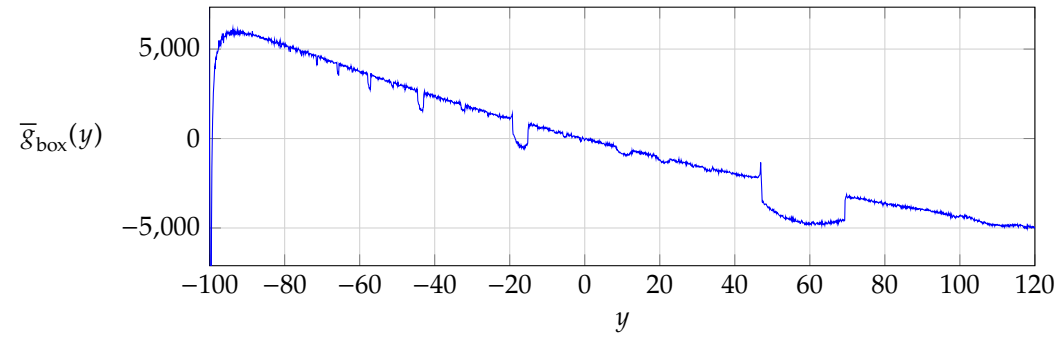

(a) Sliding speed for the box boundary hysteresis layer.

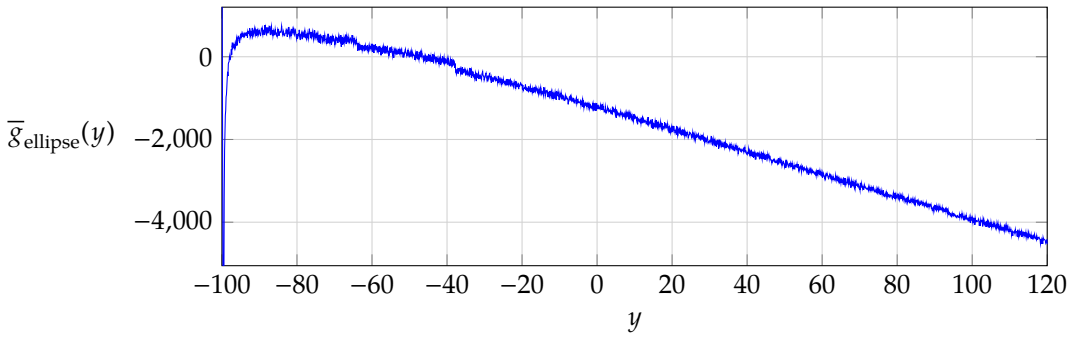

(b) Sliding speed for the elliptical boundary hysteresis layer.

Figure 3.15: Sliding vector fields for various hysteresis regions with different shape and switching logic around a co-dimension two sliding manifold.

3.5.4 Extended convex hull

When the hysteresis boundary is finite in size, the sliding speed of the regularized system can be outside the solution set predicted by the convex hull method. This happens as the sliding vector field is now composed by vector fields outside the sliding manifold as well. The effect can be seen in fig. 3.6, where the variations in the sliding solution due to jitter are larger than those allowed by the minimal convex hull in fig. 3.6. Thus, the minimal convex hull is extended with the all the possible values of the vector fields in the hysteresis zone to better describe the range of possible sliding dynamics in the trans-Z-source converter.

The minimal convex hull is extended to cover all the possible solutions within the finite hysteresis zone around the sliding surface. Considering a discrete variable structure system whose dynamics are determined by

$$D_t x = f(x, u) \tag{3.5.35}$$

where $f : \mathbb{R}^n \times \mathbb{R}^m \to \mathbb{R}^n$ is a continuous function, let $H : \mathcal{R}^n \to \Updownarrow$ for some $m < n$ be the function defining the manifold $\mathcal{M}$ where the system slides. If a hysteresis switching algorithm G constraints the system on some hysteresis zone $\mathcal{S}_G$ around $\mathcal{M}$ then the extended convex hull is defined over any $x \in \mathcal{M}$ as the set of solutions to the problem

$$f_s(x) = \sum_{u \in U} \gamma_u f(x_s, u) \tag{3.5.36}$$

where $\gamma : U \to \mathbb{R}$ and $x_s \in \mathbb{R}^n$ satisfy the constraints

$$C(H, x, \mathcal{S}_G) = \begin{cases} \sum_{u \in U} \gamma_u \left(\partial_x H(x_s) \cdot f_s(x_s) \right) = 0, & \text{(3.5.37a)} \\ \sum_{u \in U} \gamma_u = 1, & \text{(3.5.37b)} \\ \forall u \in U : 0 \leq \gamma_u \leq 1, & \text{(3.5.37c)} \\ x_s \in \mathcal{S}_G, & \text{(3.5.37d)} \\ \exists \epsilon \in \mathbb{R}^2 : x_s = x + (\partial_x H(x))^T \cdot \epsilon. & \text{(3.5.37e)} \end{cases}$$

To determined the range of the sliding speed appearing in the sliding mode controlled trans-Z-source converter, the maximum and minimum solutions are selected. Thus for a hysteresis switching algorithm G constraining the state on a set $\mathcal{S}_G$ around the sliding manifold $\mathcal{M}$, the maximum and minimum sliding speed given by

$$\max \overline{g}_G(x) = \max_{(\gamma, x_s) \in \Gamma(H, x, \mathcal{S}_G)} \sum_{u \in U} \gamma_u f(x_s, u), \tag{3.5.38}$$

and

$$\min \overline{g}_G(x) = \min_{(\gamma, x_s) \in \Gamma(H, x, \mathcal{S}_G)} \sum_{u \in U} \gamma_u f(x_s, u), \tag{3.5.39}$$

where Γ is the set of functions $\gamma : U \to \mathbb{R}$ satisfying the constraints defined in relation (3.5.37), or

$$\Gamma(H, V, \varepsilon) = \left\{ (\gamma, x_s) \in (U \to \mathbb{R}) \times \mathbb{R}^n : C(H, x, \mathcal{S}_G) \right\}. \tag{3.5.40}$$

A convex optimization algorithm was used to solve the problem of finding the minimum and maximum sliding speeds in the extended convex hull. For the box and ellipse hysteresis switching algorithms, the hysteresis zones $\mathcal{S}_{\text{box}}$ and $\mathcal{S}_{\text{ellipse}}$ are defined in relation (3.4.50) and relation (3.4.52) respectively. For both algorithms the constrain defining the hysteresis zone is convex, so efficient convex optimization algorithms can be used to determine the minimum and maximum sliding speeds. The variation of the sliding speeds from the canopy solution, and the upper and lower bounds on the difference from the canopy solution are depicted in fig. 3.16. The variation of the sliding speed from the canopy solution for a hysteresis algorithm G where

$$G \in \left\{ \text{ellipse}, \text{box} \right\}, \tag{3.5.41}$$

is defined as

$$\Delta\overline{g}_G(y) = \overline{g}_G(y) - g_{\text{cp}}(y). \tag{3.5.42}$$

Similarly, the deviations of the maximum and minimum sliding speed from the canopy solution are determined by

$$\max \Delta\overline{g}_G(y) = \max \overline{g}_G(y) - g_{\text{cp}}(y), \qquad \min \Delta\overline{g}_G(y) = \min \overline{g}_G(y) - g_{\text{cp}}(y), \tag{3.5.43}$$

respectively. Both the box and ellipse switching algorithms result in similar boundaries for the sliding speed. This is expected because there is significant overlap between the hysteresis zones of the two algorithms. Stable sliding solutions can be found for $y > y_{\text{ub}}$ where $y_{\text{ub}} \simeq -100$.

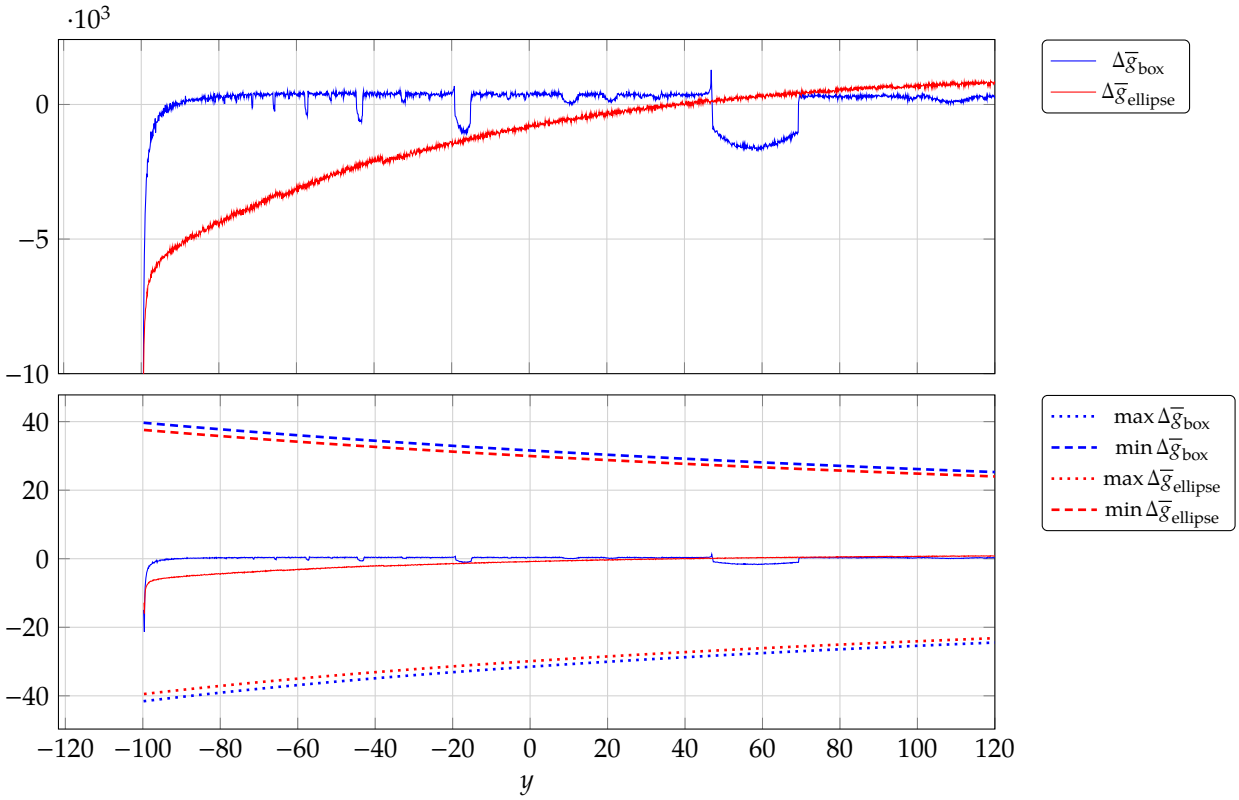

Figure 3.16: Plot of the sliding speed with a box and and elliptical hysteresis boundary. The extended convex hulls for each hysteresis boundary is also plotted demonstrating that the variation in the sliding speed remains within the limits predicted by extending the convex hull.

3.5.5 Sensitivity of jitter in system parameters

In the trans-Z-source converter jitter appears in the system controlled by the hysteresis controller with a box hysteresis region only, as it is demonstrated in the plot of fig. 3.16. The abrupt variations in the sliding speed are explained by the steady state limit cycles that appear in the projected dynamics in the boundary layer. A few trajectories for the hysteresis box controller are plotted in fig. 3.17a for a few values of y in the fig. 3.16. For values $y = -5$ and $y = 10$, stable limit cycles appear in the hysteresis layer with relatively high period. For the intermediate value $y = 0$, the solution trajectory is unstable resulting in a quasi-periodic trajectory. For systems

where the projected dynamics are constant for each control input, it was proven in [75] that only periodic trajectories exist. However, in the trans-Z-source converter the dynamics are not assumed to be constant resulting in additional dynamical behaviors.

Each steady state trajectory results in sliding dynamics with different sliding speed. As a trajectory is continuously transformed, the variation in the sliding speed is continuous. Abrupt changes in the sliding speed occur when the system transitions from one steady state trajectory to another. For instance, a few stable limit cycles are plotted in fig. 3.17b. As y increases the system enters in stable limit cycles with a large period plotted for $y = 40$, and a sliding speed relatively close to the canopy solution. As y increases furtherer, the trajectory transitions to a limit cycle with much lower periodicity plotted for $y = 60$ resulting in a sliding speed much different from the canopy solution. Finally, as y increases further, a limit cycle with high periodicity plotted for $y = 80$ appears again resulting in sliding speed close to the canopy solution.

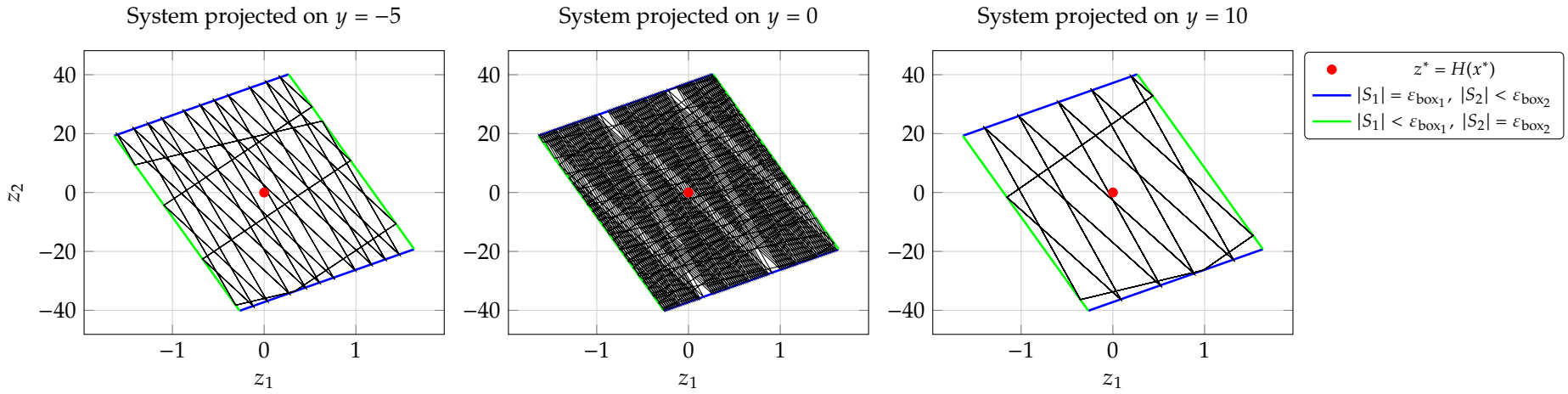

(a) A limit cycle transforms into a quasi-periodic solution for $y = 0$ and then to another limit cycle. Little variation from the canopy sliding speed can be observed.

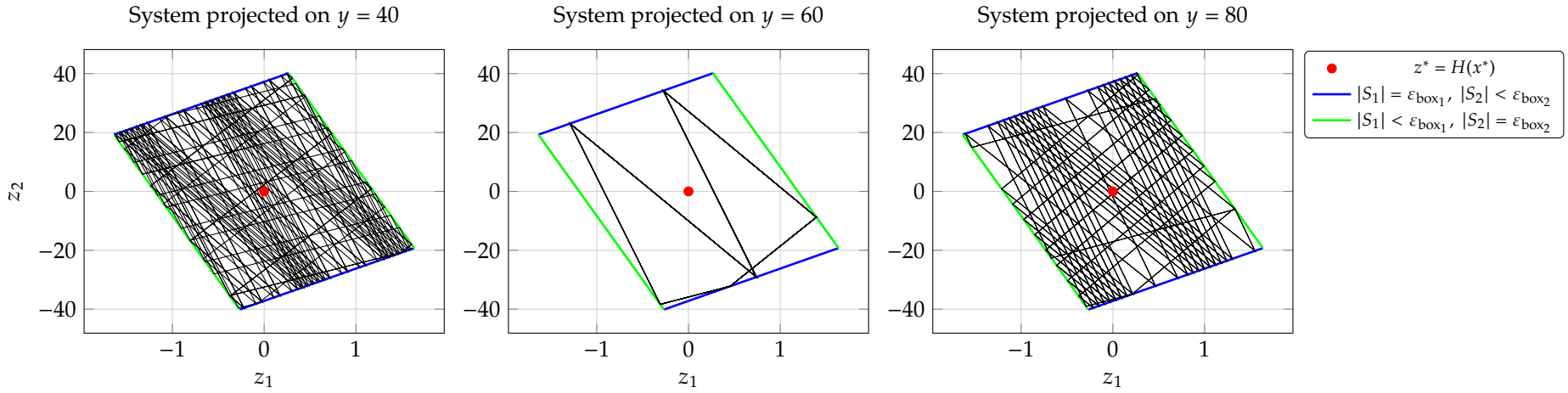

(b) A large period limit cycle jumps to a limit cycle with very low period and then to another limit cycle with large period. The low period limit cycle results in an abrupt decrease in the sliding speed relative to the canopy solution.

Figure 3.17: Limit cycles in a system with a box switching boundary for various positions along the sliding surface. Each limit cycle results in a different sliding speed. The higher periodicity limit cycles result into sliding speed that approach the canopy solution the closest.

In the hysteresis controller with an elliptical hysteresis boundary, a stable limit cycles appear for the whole length of the sliding surface. As demonstrated in fig. 3.18, the limit cycle depends on the initial conditions. To avoid jumping from one limit cycle to another due to variation in the initial condition, a continuation of the solution starting at $z(0) = (0, 0)^T$ at $y = 0$ for negative and positive values of y was used to evaluate the sliding speed. As demonstrated in fig. 3.19, the limit cycle starts with a large period which reduces as y increases. The transition from one limit cycle is smooth, in the sense that the periodicity of the solution changes by one in each bifurcation. The result is that only smooth changes in the sliding speed occur. Furthermore, as y increases simulations indicate that the limit cycle in the projected dynamics converges to a trajectory and no other topological changes occur. For instance the limit cycle is very similar for $y = 0$ and $y = 40$.

Jitter appears when bifurcations in the trajectory appearing in the boundary layer dynamics result in significantly different sliding speed. The bifurcation usually causes and abrupt variation in the sliding speed which lead to the use of the term jitter to describe the phenomenon [76]. There are some conditions that mush be satisfied in order for jitter to appear. Firstly, the convex hull must be non-flat. In a system with a flat convex hull a single sliding solution exists even if the duty ratios for each of the modes change due to bifurcations in the system trajectory. Secondly, changes bifurcations in the system trajectory must lead to different duty ratios for the system modes. For instance in the trans-Z-source converter with an ellipse hysteresis controller the bifurcations do not change the duty ratios for each mode leading to a smoothly varying sliding speed. In general though, to determine the sliding speed and detect jitter in systems sliding on the intersection of two switching surfaces simulations of the projected dynamics of the system in boundary layer are required to determine the duty ratios for each mode and the resulting sliding speed.

3.6 Conclusions

This section investigated the challenges in designing a sliding mode controller for a converter with multiple control inputs such as converter of the impedance source family. A method for selecting switching surfaces enforcing monotonic convergence to a sliding manifold was developed and tested with two hysteresis switching algorithms, each using a different sliding hierarchy. One of the controllers uses a box hysteresis surface and the other an elliptical hysteresis surface. The performance of the controllers is analyzed using numerical simulations. Both controllers stabilize the converter. Only the controller with the box hysteresis surface displays jitter. However, in the controller with the elliptical hysteresis surface there is a higher steady state drift and the sliding solution in sensitive to the initial condition in the hysteresis layer resulting in multiple steady state limit cycles.

The jitter in the sliding mode controlled trans-Z-source converter with a box hysteresis region is to our knowledge the first demonstration of jitter in a practical power electronic circuit. The regularization method for hysteresis switched systems sliding on the intersection of multiple sliding surfaces was first developed in [75] where abrupt variations in the sliding speed are attributed in bifurcations appearing in a projected motion in the boundary layer. The phenomenon is further studied in [76] where it is demonstrated that similar behavior appears

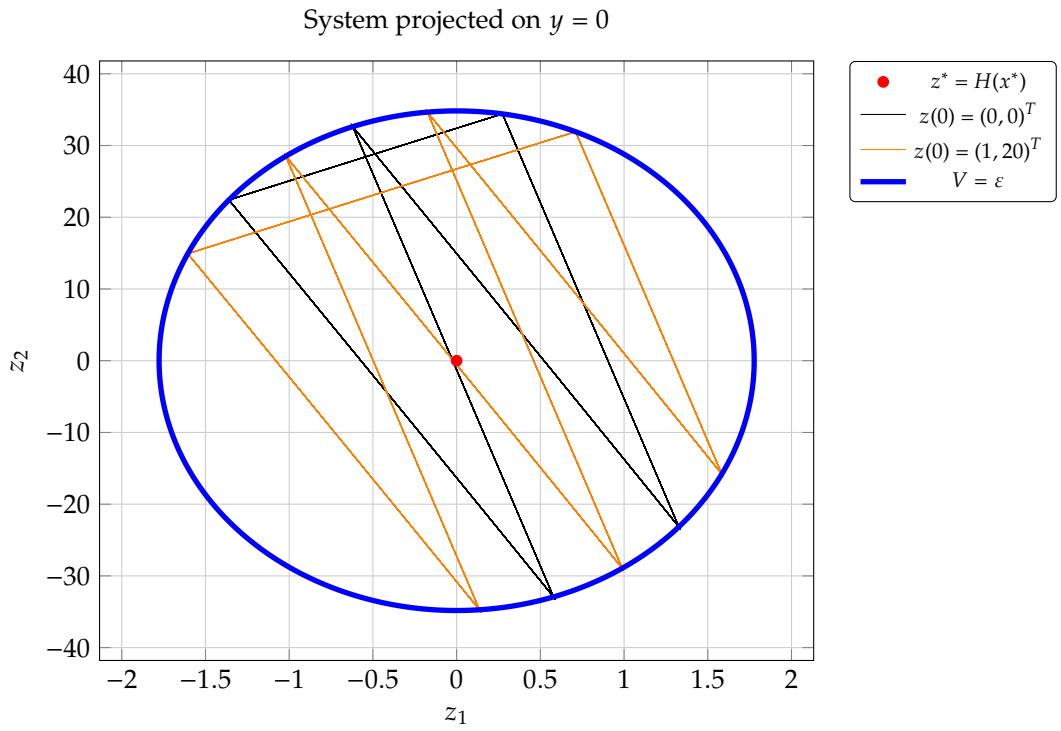

Figure 3.18: Demonstration of the sensitivity of the limit cycle that appears in the elliptical hysteresis layer to initial conditions. All simulations are initialized with control input $u = (1, 1)^T$, but one with initial condition $z(0) = (0, 0)^T$ and the other with $z(0) = (1, 20)^T$. The two solutions end up in different limit cycles.

for other switching algorithms except for hysteresis switching. In the case of sliding mode controller for the trans-Z-source converter, the finite size of the hysteresis region required to maintain a sufficiently small switching frequency affects the sliding speed increasing the sliding speed jitter the controller with a box hysteresis region.

The box hysteresis switching algorithm is simple in implementation, but jitter can negatively affect the performance of the converter. Jitter is undesirable in practical controllers as it leads to unpredictable performance for the controller on the sliding mode, and multiple fixed points if the jitters causes the sliding speed to reverse sign multiple times. Modifications of the switching logic resulting in a better control over the trajectory in the limit cycle may be possible. In particular the switching logic used in the elliptical switching algorithm is quite flexible. It is desirable to derive switching condition that result in sliding dynamics that are unique while displaying no jitter and minimal steady state drift.

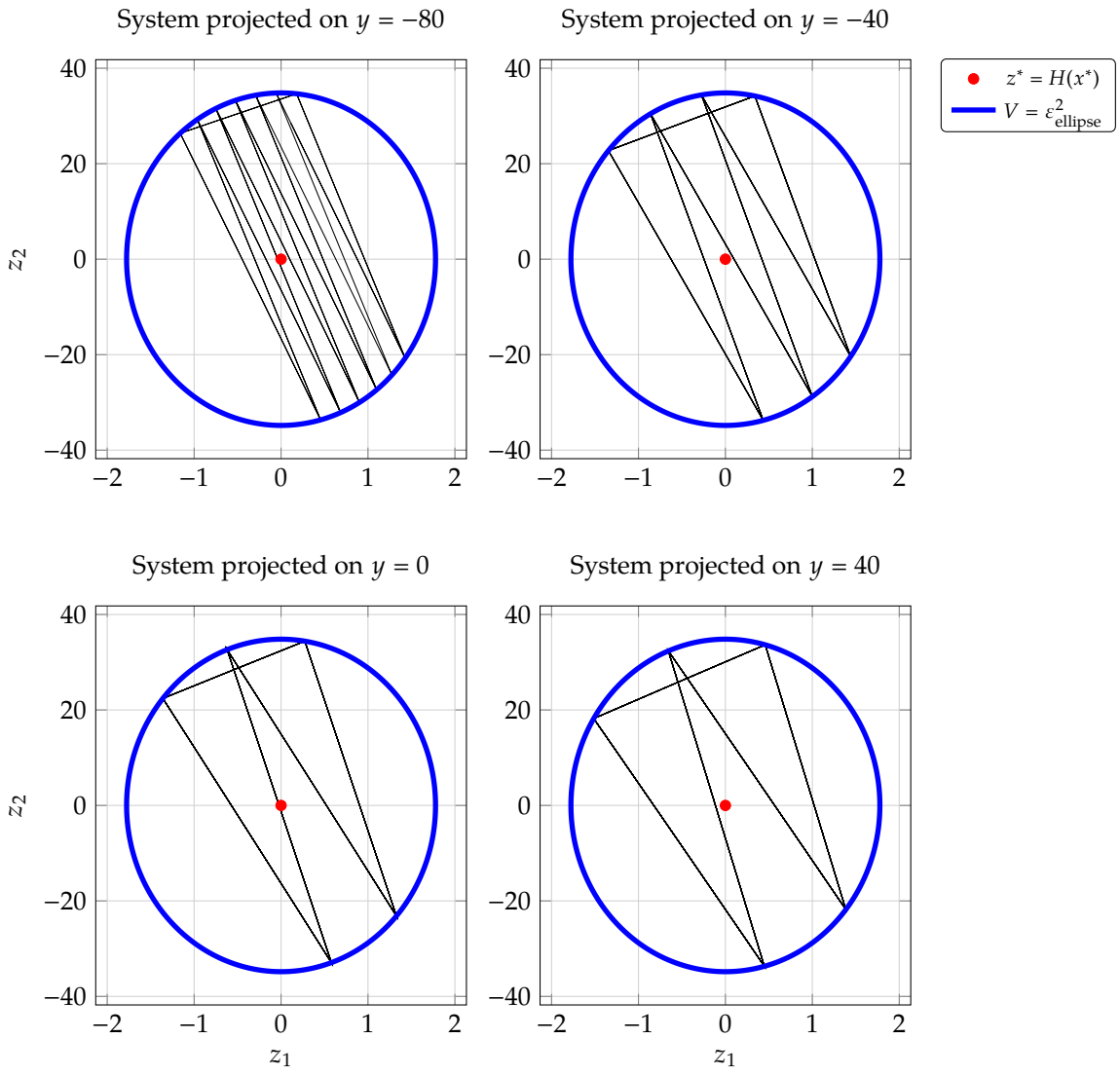

Figure 3.19: A limit cycle appears in the hysteresis layer of the modulation algorithm with an elliptical switching surface. The limit cycle varies smoothly as the system moves along the sliding surface.

Chapter 4

Incorporating the effect of sensor dynamics in the design of sliding mode controllers

Sensors introduce dynamics in converters that are not modeled during the design of sliding mode controllers. In the presence of sensors the sliding surface is unstable in the conventional sense, and a limit cycle appears in the system. In the stabilization problem for power converters, it is sufficient to impose a limit cycle close to the desired state in steady state operation. Given some constraints for the deviation from the ideal response of the controlled system, sensors of sufficient quality are required to ensure that the constraints are satisfied. In order to numerically determine the sensor configurations that result in a stable system, a converter with a sufficiently accurate model for the sensors is simulated. This section examines appropriate models for sensors in power electronics, and introduces a model for a buck converter with sensors. It is first proven that for the selected model the sliding surface is unstable. Then, numerical simulation determine the sensor configurations that result in a steady state limit cycle sufficiently close to the ideal solution. The resulting solution provides a range of sensors that can be used in the buck converter.

4.1 Introduction

The switching algorithm is a significant component that enforces the sliding mode of any sliding mode control algorithm for switched mode power electronic converter. Sliding mode controllers for power converters use properties of sliding modes, such as global stability [148] and the complete rejection of matched disturbances outside an invariant surface [112], [113] to deliver performance that is superior to linear averaged controllers in problems such as output stabilization [55], [130], [149], [167]–[169]. However, enforcing the sliding mode requires a switching algorithm with good performance, hindering the widespread adoption of sliding mode controllers [132].

The performance of power converters is sensitive to the switching frequency of the control algorithm. The filters used to remove the switching noise from the output of power converters

operate optimally at a short range of frequencies [84]. Hysteresis switching with respect to the sliding surface is used to enforce sliding, however, hysteresis switching algorithms display a variable switching frequency [93], [94]. To improve the performance of the controller over a wide range of operating conditions, switching algorithms with fixed frequency are being developed. Switching with a variable hysteresis width uses a hysteresis width that is evaluated algebraically [170] or dynamically [77], [129], [171] from the converter state to stabilize the switching frequency. Quasi sliding approaches, such as the zero averaged dynamics, allow the size of the boundary layer to vary dynamically, and enforce a constant switching frequency while the system remains on the sliding surface [78], [79]. Finally, sliding can be enforced with constant frequency pulse width modulation in integral sliding mode controllers, where the state remains always on the sliding surface [130].

Advances in electronics lead to the performance improvements for sliding mode controllers, but also to new challenges in the design of switching algorithms. Fast digital control [172] allows for fast real time execution of control algorithms, allows significantly higher switching frequencies and better control of the dynamics in the boundary layer of the sliding mode. Fixed frequency switching algorithms based on digital controllers have been developed for enforcing sliding, offering better performance than analogue implementations [79], [173], [174]. However, the introduction of wide band gap devices [175] that limit the duration of the switching transients, lead to compact converter designs that use higher switching frequencies. Constructing sliding mode controllers for converters with high switching frequency poses challenges.

As switching frequencies increase, fast dynamical behavior which is not modeled in the design of conventional sliding mode controllers is having a significant impact in the ability of the switching algorithms to enforce sliding. A typical example of such behavior is the dynamics of sensors. The regularization methods used to determine the ideal dynamics to which the system converges in the limit where the switching controller constrains the system closer to the sliding manifold assumes that non-modeled dynamics vanish the closer the system is constrained to the sliding surface [74]. The distortion introduced by the dynamics of the sensors, however, does not vanish [176], and as a result the effects of the sensors cannot be ignored in the regularization or the evaluation of solution in the minimal convex hull.

The design of high performance converters requires accurate sensor measurements. In some applications the sensors are explicitly designed to ensure the stability and accurate tracking of the sliding surface. A voltage sensor based on a trans-impedance amplifier was developed in [177]–[179] offering a stability margin sufficient for a buck converter with a 5 MHz switching frequency. When designing a custom sensor is impractical, a model of the sensor dynamics can in some cases inform the design of the switching algorithm. Analytic conditions guaranteeing the stability of the sliding mode in linear systems where the effects of the sensors are modeled as delays in the control input, are derived in [180], and a second order sliding mode controller stabilizing the system is constructed in [181].

In power electronic converters however, sensors are more accurately modeled by ordinary differential equations. Components such as low pass filters, which are used to reduce sensor sensitivity to noise, tend to dominate the dynamical behavior of sensors. This effect is particularly prominent in electrically isolated sensors where low pass filters are commonly used to filter and amplify a week signal passing through the isolation barrier [182]. Most low pass filters in electronics are effectively first order integrators. Therefore, many isolated sensors such as

current and voltage transducers are modeled by a first order integrator [182].

The main aim of this section is to develop a numerical analysis method for determining when sensors are of sufficient quality to implement a sliding mode controller for a buck converter with hysteresis switching. The converter analyzed is a buck converter with a hysteresis switching algorithm. The controller has access to measurements of the converter states provided by the sensors, but not to the states themselves. It is demonstrated that sliding does not exist in the conventional sense of definition 2.3.9 where the system state is constrained in an arbitrarily small neighborhood of the sliding surface. However, numerical simulations indicate the presence of an attractive limit cycle. By relaxing the requirement that the system is constrained arbitrarily close to the sliding surface, the limit cycle is numerically analyzed, and conditions on the sensor dynamics are derived ensuring that the system satisfies specific constraints on the output ripple during steady state operation.

The main contribution of this section is the use of a concrete dynamical model for the sensors to determine the constraints placed on the dynamics of the sensors by performance requirements for the converter. A linear integrator model for electrically isolated sensors is used to extend the dynamics of the buck converter to include the dynamics of the sensors. A formal proof is then derived that the sliding surface is no longer stable under a hysteresis switching algorithm. Numerical simulations of the converter extended with the dynamics of the sensors determine the range of parameters for the sensor dynamics that result in output ripple within some given specification. The resulting criterion is shown to be more accurate in the selection of sensors than conventional approaches based on the cut-off frequency of the sensors. This section is organized as follows:

- The effects of sensors in the performance of a buck converter are presented in section 4.2. The first order integrator model is used for electrically isolated sensors in the buck converter.
- A generic framework is developed in section 4.3 for introducing models for the sensor dynamics in the dynamics of the converter.
- Limitations of observer based sliding mode controllers for converters with sensors are discussed in section 4.4. When all states are accessible through sensor measurements only, observer based sliding mode controllers cannot be constructed.
- The stability of the sliding manifold in a buck converter, where the system states are accessible only through sensor measurements, is investigated in section 4.5, and it is demonstrated that the siding manifold is unstable.
- Finally, in section 4.6, the performance of a buck converter with sensors is analyzed numerically. The minimum requirement for the sensor gains, so that a set of performance criteria are met, is determined and the accuracy of the results is compared with constraints derived using a simple cutoff frequency.

4.2 Sensors in the buck converter

As the semiconductor switches and the control logic become faster, sensors are often the main source of non-ideal dynamical behavior in -power converters. This section demonstrates the

effects of the sensor dynamics in the performance of a buck converter with hysteresis modulated sliding mode control. The circuit diagram of the converter can be seen in fig. 4.1. It is assumed that the converter is implemented using synchronous rectification and that it always operates in continuous conduction mode. In the mathematical model of the buck converter, the state the converter, x_{sys}, is determined by the current trough the inductor, i_L, and the voltage across the capacitor, v_C, where

$$x_{\text{sys}} = \begin{pmatrix} i_L \\ v_C \end{pmatrix}. \tag{4.2.1}$$

The discrete control input u takes discrete values in the set $\{0, 1\}$. The dynamics are modeled by an ordinary differential equation linear in the control input [92],

$$D_t x_{\text{sys}} = f_{\text{sys}}(x_{\text{sys}}) + g_{\text{sys}}(x_{\text{sys}}) \cdot u, \tag{4.2.2}$$

where $f_{\text{sys}}, g_{\text{sys}} : \mathbb{R}^2 \to \mathbb{R}^2$ and

$$f_{\text{sys}}(x_{\text{sys}}) = \begin{pmatrix} 0 & -\frac{1}{L} \\ \frac{1}{C} & -\frac{1}{RC} \end{pmatrix} \cdot \begin{pmatrix} i_L \\ v_C \end{pmatrix}, \qquad g(x_{\text{sys}}) = \begin{pmatrix} \frac{E}{L} \\ 0 \end{pmatrix}. \tag{4.2.3}$$

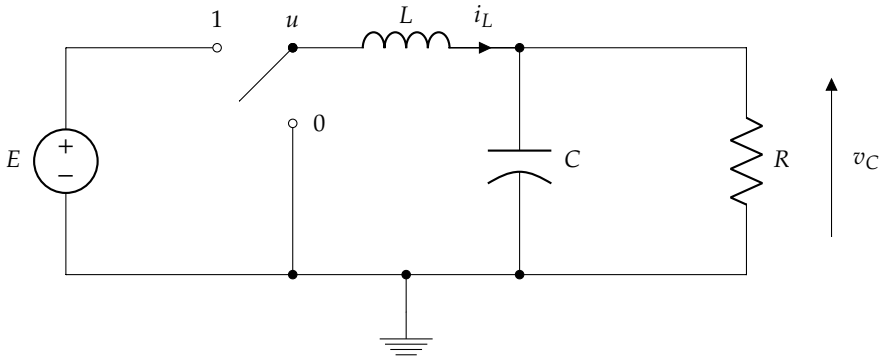

Figure 4.1: Circuit diagram of a continuous conduction buck converter. A bridge leg is used where two semiconductor switches operate complementary to implement the control input u. The position of the equivalent single pole double through switch for each control input, u, is indicated in the diagram.

4.2.1 Sliding mode control

A hysteresis switching algorithm is used to enforce sliding on the buck converter. The hysteresis switching controller with a switching function $S : \mathbb{R}^2 \to \mathbb{R}$ and hysteresis $\varepsilon > 0$ is given by the hybrid automaton in fig. 4.2. The hysteresis width ε is selected so that the switching frequency of the system is maintained within an acceptable range during steady state operation.

The effects of the sensors are investigated in the neighborhood of the ideal point x^*_{sys}. The ideal fixed point is the fixed point of the converter for the ideal continuous control input u^*, selected so that the output voltage attains the desired value

$$x^*_{\text{sys}_2} = v^*_C. \tag{4.2.4}$$

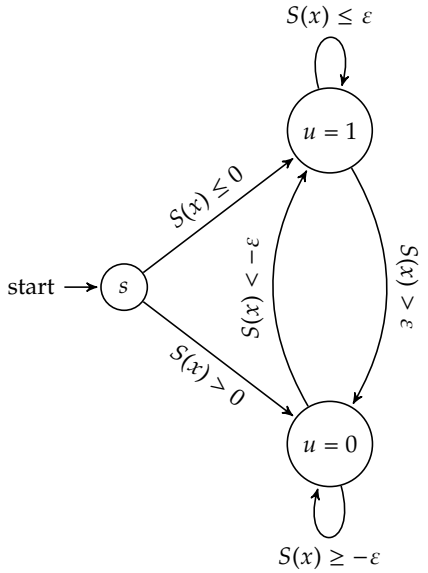

Figure 4.2: A hysteresis controller for actuating the switch u according to the switching function S with hysteresis $\varepsilon > 0$.

The fixed point and control input are thus determined by the solution of the system of equations

$$f_{\text{sys}}(x^*_{\text{sys}}) + g_{\text{sys}}(x^*_{\text{sys}}) \cdot u^* = 0, \qquad x^*_{\text{sys}_2} = v^*_C, \tag{4.2.5}$$

resulting in

$$x^*_{\text{sys}} = \begin{pmatrix} \frac{v^*_C}{R} \\ v^*_C \end{pmatrix}, \tag{4.2.6}$$

and

$$u^* = \frac{v^*_C}{E}. \tag{4.2.7}$$

The sliding manifold is the selected to ensure that the ideal fixed point x^*_{sys} resides on the sliding manifold so that x^*_{sys} is reachable by a sliding motion.

The effects of the sensors are demonstrated for a sliding manifold selected from a family of sliding manifolds. The manifolds are defined by family of functions $H : \mathbb{R}^2 \to \mathbb{R}$ defined as

$$H(x_{\text{sys}}) = \begin{pmatrix} \cos\phi & \sin\phi \end{pmatrix} \cdot \left(x_{\text{sys}} - x^*_{\text{sys}} \right), \tag{4.2.8}$$

and parametrized by $\phi \in [0, 2\pi)$. The parameter ϕ determines a normalized gradient vector

$$\partial_x H = \begin{pmatrix} \cos\phi & \sin\phi \end{pmatrix} \tag{4.2.9}$$

for each member of the family of sliding manifolds. The switching function in the hysteresis switching algorithm is then

$$S = H \tag{4.2.10}$$

so that the algorithm is uniquely determined by the parameter ϕ and a hysteresis width ε.

4.2.2 A linear integrator model for the converter sensors

In a buck converter with sensors, the converter state is not directly available to the controller. All state variables are measured by sensors which have dynamics of their own and provide a value for the measured state at their output. In power electronic circuits the first order integrator is a good model for electrically isolated voltage and current transducers over a wide range of signal frequencies [182, §2.3]. Also, in most cases it can be assumed that the sensors are dynamically independent from each other. Thus, a model where each sensor is model by a first order integrator is used for the buck converter with electrically isolated sensors. Letting $\hat{i}_L$ be the measured value of the inductor current and $\hat{v}_C$ the measured value of the capacitor voltage, the dynamics for the current and voltage sensors are determined respectively by

$$D_t \hat{i}_L = k_i \left(i_L - \hat{i}_L \right), \qquad D_t \hat{v}_C = k_v \left(v_C - \hat{v}_C \right). \tag{4.2.11}$$

In this model, the output of each sensor is the value of its internal state variable, so that the state variables $\hat{i}_L$ and $\hat{v}_C$ are directly available to the controller. One of the possible layouts for the position of these sensors can be seen in fig. 4.3.

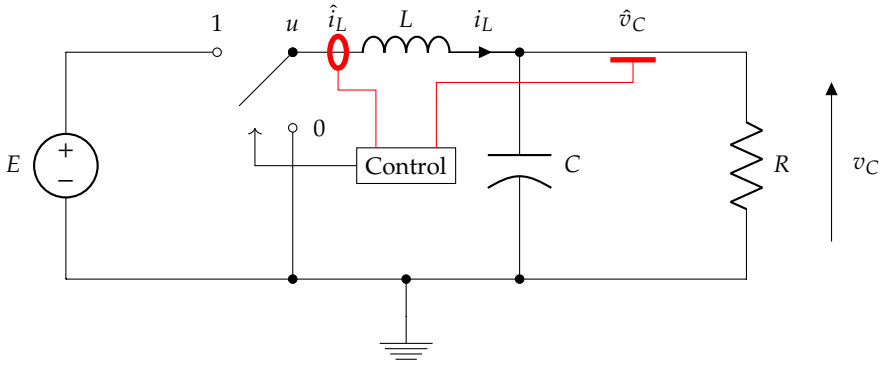

Figure 4.3: Circuit diagram of a continuous conduction buck converter with sensors. The position of the voltage and current sensors is depicted in the circuit diagram.

The dynamics of the system extended with sensors are expressed succinctly in vector form. The state of the sensors in vector form is

$$x_{\text{sen}} = \begin{pmatrix} \hat{i}_L \\ \hat{v}_C \end{pmatrix}, \tag{4.2.12}$$

and the dynamics are,

$$D_t x_{\text{sen}} = f_{\text{sen}}(x_{\text{sen}}, x_{\text{sys}}), \tag{4.2.13}$$

where

$$f_{\text{sen}}(x_{\text{sen}}, x_{\text{sys}}) = \begin{pmatrix} k_i & 0 \\ 0 & k_v \end{pmatrix} \cdot \left(x_{\text{sys}} - x_{\text{sen}} \right). \tag{4.2.14}$$

The dynamics of the buck converter extended to include the dynamics of the sensors are then determined by combining relations (4.2.2) and (4.2.13) in a single system,

$$D_t x_{\text{sys}} = f_{\text{sys}}(x_{\text{sys}}) + g_{\text{sys}}(x_{\text{sys}})u, \qquad D_t x_{\text{sen}} = f_{\text{sen}}(x_{\text{sen}}, x_{\text{sys}}). \tag{4.2.15}$$

The system is written into the canonical form for time invariant systems with a linear dependence on the control input by setting

$$x = \begin{pmatrix} x_{\text{sys}} \\ x_{\text{sen}} \end{pmatrix}, \tag{4.2.16}$$

Then the dynamics are given by

$$D_t x = f(x) + g(x) \cdot u, \tag{4.2.17}$$

where

$$f(x) = \begin{pmatrix} f_{\text{sys}}(x_{\text{sys}}) \\ f_{\text{sen}}(x_{\text{sen}}, x_{\text{sys}}) \end{pmatrix}, \qquad g(x) = \begin{pmatrix} g_{\text{sys}}(x_{\text{sys}}) \\ 0 \end{pmatrix}. \tag{4.2.18}$$

4.2.3 Effects of the sensors in the dynamics of the converter

During steady state operation, a buck converter with hysteresis switching converges into a limit cycle inside the hysteresis layer. Using a linear affine sliding surface with a given gradient vector, the size of the limit cycle depends only on the hysteresis width and determines the switching frequency, the state drift, and the ripple in the output current and voltage. To demonstrate the effects of the sensors in the steady state limit cycle a buck converter is simulated. The specifications of the converter are listed in table 4.1 and the specifications of the controller are listed in table 4.2. The parameters of the converter were selected to ensure a switching frequency lower than 10 kHz for a resistive load of 8 Ω. The input voltage is 48 V and the output voltage is 36 V.

The objective of the controller is to provide a constant output voltage v_C^* to a resistive load of fixed value R. Given the voltage v_C^*, the current i_L^* is determined by the solution of relation (4.2.5). Due to the variable structure nature of the system, there is some switching ripple in the actual current i_L and voltage v_C. Constraints are placed on the maximum amplitude of this ripple according to component limitations that constraint the output capacitor voltage, and thermal requirements that limit the peak current through semiconductor switches.

Component	Value
C	0.6 mF
L	1.7 mH
R	8 Ω
E	48 V

Table 4.1: Parameter values for the components of the buck converter. The parameters of the converter were selected to ensure a switching frequency lower than 10 kHz for a resistive load of 8 Ω.

To demonstrate the effects of the sensors, a buck converter with electrically isolated sensors modeled as first order integrators is simulated. Let T be the period of the resulting steady state limit cycle. Over a single period $[t, t+T]$ of steady state operation the averaged value of the state is denoted as

$$\langle x \rangle = \frac{1}{T} \int_t^{t+T} x d\tau. \tag{4.2.19}$$

Switching function parameters	
v_C^*	36 V
i_L^*	4.5 A
ϕ	$\frac{\pi}{4}$ rad

(a) Parameters for the switching function of the controller.

Hysteresis width	
ε	$\sqrt{0.1}$

(b) Hysteresis width for the hysteresis switching algorithm of the controller.

Table 4.2: Parameters of the sliding mode controller of the buck converter. The nominal output voltage is v_C^* and the resulting nominal output current i_L^* is determined by the solution of relation (4.2.5) for a resistive load $R = 8\,\Omega$.

for any $t \geq 0$, the ripple of the state is defined as

$$\Delta x_i = \max_{\tau \in [t, t+T]} x_i(\tau) - \min_{\tau \in [t, t+T]} x_i(\tau) \tag{4.2.20}$$

for $i = 1, 2$, and the maximum value as

$$\max x_i = \max_{\tau \in [t, t+T]} x_i(\tau) \tag{4.2.21}$$

for $i = 1, 2$. The integrator constants selected for the sensors are listed in table 4.3 and are typical for electrically isolated sensors[1]. The effects of the sensors in the system are demonstrated by the phase plots in fig. 4.6. In a system where the controller has direct access to the system state, the system state remains within the hysteresis boundary as seen in the system phase plot in fig. 4.6a. Furthermore, the constant harmonic component of the converter state $\langle x_{\text{sys}} \rangle_0$ is close to the ideal steady state x^*. Introducing the sensors dynamics into the system, the steady state limit cycle is altered. As demonstrated by the phase plot in fig. 4.6b, the limit cycle is now larger and overshoots the hysteresis boundary, resulting in a larger ripple in the output voltage and inductor current. Furthermore, the drift in the averaged components of the system steady state state $\langle x_{\text{sys}} \rangle$ is larger when the sensors dynamics are included in the model.

Sensor constant	Value
k_i	50×10^3
k_v	50×10^3

Table 4.3: Integration constants for the sensor model.

The limit cycle in the system where the controller has access only to sensor measurements has a lower frequency than the limit cycle in the system with direct access to the converter state. This is seen in the time plots of the ideal system and the system with sensors in fig. 4.4 and fig. 4.5 respectively. Also, in the presence of sensors the peak values and the ripple amplitude of the inductor current and the capacitor voltage are larger table 4.4a. The peak voltage is limited by the ratings of the capacitor and the peak current is limited by switch average power rating. Similarly, the peak current ripple is limited by loss constraints and the peak voltage ripple is typically limited by constraints in the harmonic emissions in the output of the converter.

In the presence of sensors, the sensor measurements of the state variables lag behind the

[1]For instance the current transducer LEM LA 55-P has a gain higher that $k_i = 32 \cdot 10^3$ according to its cutoff frequency.

value of the variable itself as it is demonstrated in fig. 4.5. As a result, the sensors underestimate the peak values and the ripple for the inductor current and the capacitor voltage. The estimations provided by the sensor measurements are summarized in table 4.4b. The ripple in the output voltage is small, and in a practical implementation it will be insignificant in comparison to ripple caused by the capacitor equivalent series resistance. So the sensors significantly affect the design of the controller in terms of the steady state drift for the capacitor voltage and the inductor current, and for the peak value and ripple of the inductor current.

	Ideal converter	Converter with sensors
T	0.1688 ms	0.2757 ms
$\max i_L$	4.946 A	5.219 A
$\max v_C$	36.009 V	35.912 V
Δi_L	0.894 A	1.473 A
Δv_C	0.0314 V	0.0846 V

(a) Steady state cycle period, peak value and ripple amplitude for the state variables of the ideal buck converter and a buck converter with sensors. The peak value and the ripple of the inductor current and the capacitor voltage are larger in the presence of sensors with non ideal dynamics.

Estimated variables	
$\max \hat{i}_L$	5.096 A
$\max \hat{v}_C$	35.906 V
$\Delta \hat{i}_L$	1.158 A
$\Delta \hat{v}_C$	0.077 V

(b) Peak values and amplitudes for the estimated state variables. The estimates consistently underestimate the peak current and the amplitude of the ripple for the inductor current and the capacitor voltage.

Table 4.4: Characteristics of the steady state periodic motion of the ideal buck converter and a buck converter with sensors.

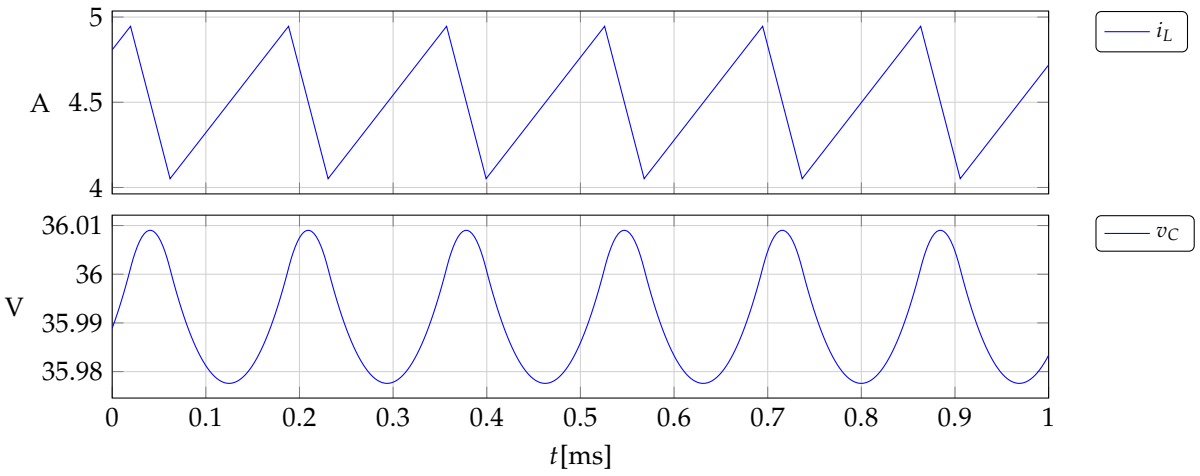

Figure 4.4: Time plot of the system state for the buck converter.

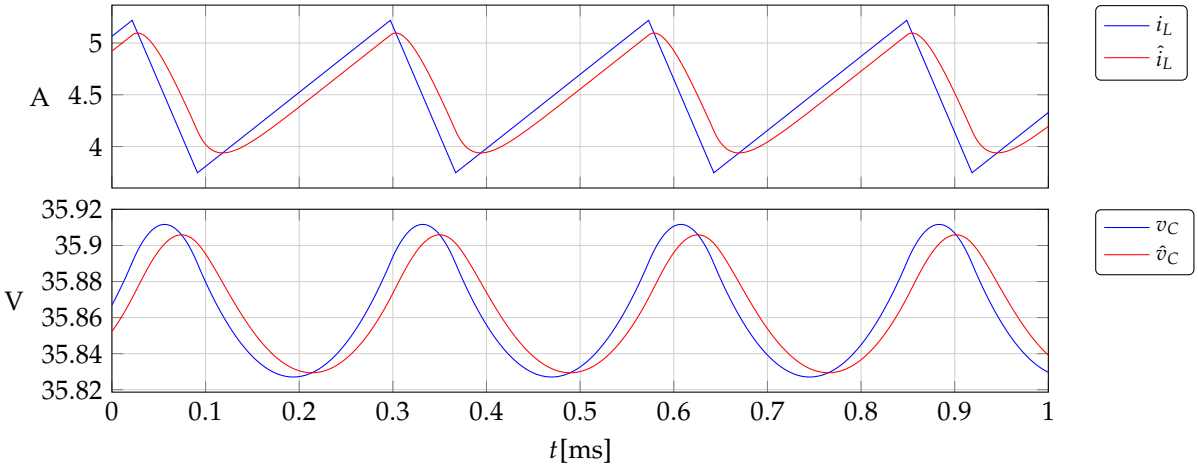

Figure 4.5: Time plot of the system state for a buck converter with sensors. The way the sensors estimates lag behind the system state is visible. This lag results in an underestimation of the peak values and the ripple for the inductor current and the capacitor voltage.

4.3 A generalized model for converters with sensors

Power converters with sensors are modeled as variable structure dynamical systems. In power converters and other systems linear with respect to their control input, the dynamics are determined by a differential equation

$$D_t x_{\text{sys}} = f_{\text{sys}}(x_{\text{sys}}) + g_{\text{sys}}(x_{\text{sys}}) \cdot u, \tag{4.3.1}$$

where x_{sys} is the state of the system taking values $x_{\text{sys}} \in \mathbb{R}^n$, $u \in \{0,1\}^m$ is the control input, and $f_{\text{sys}} : \mathbb{R}^n \to \mathbb{R}^n$ and $g_{\text{sys}} : \mathbb{R}^n \to \mathbb{R}^{n\times m}$ are smooth functions.

4.3.1 The sensor model

In a power converter with sensors, the states of the converter circuit are not directly accessible to the controller. Instead, measurements of the states are available, and these measurements are the output of the dynamical system of the sensors. The state x_{sen} of the sensors takes values in $x_{\text{sen}} \in \mathbb{R}^k$. The dynamics of the sensors are determined by the differential algebraic equation

$$f_{\text{sen}}(x_{\text{sen}}, D_t x_{\text{sen}}, x_{\text{sys}}) = 0, \tag{4.3.2}$$

where $f_{\text{sen}} : \mathbb{R}^k \times \mathbb{R}^k \times \mathbb{R}^n \to \mathbb{R}^k$ is a smooth function. The state of the converter circuit x_{sys} is an external input to the dynamical system of the sensors. The converter and the sensors combined form an *extended dynamical system*, whose dynamics are determined by the equations

$$D_t x_{\text{sys}} = f_{\text{sys}}(x_{\text{sys}}) + g_{\text{sys}}(x_{\text{sys}}) \cdot u, \qquad f_{\text{sen}}(x_{\text{sen}}, D_t x_{\text{sen}}, x_{\text{sys}}) = 0. \tag{4.3.3}$$

In this model the dynamics of the converter are independent of those of the sensors. This assumption is reasonable because the sensors are designed to draw small amounts of power

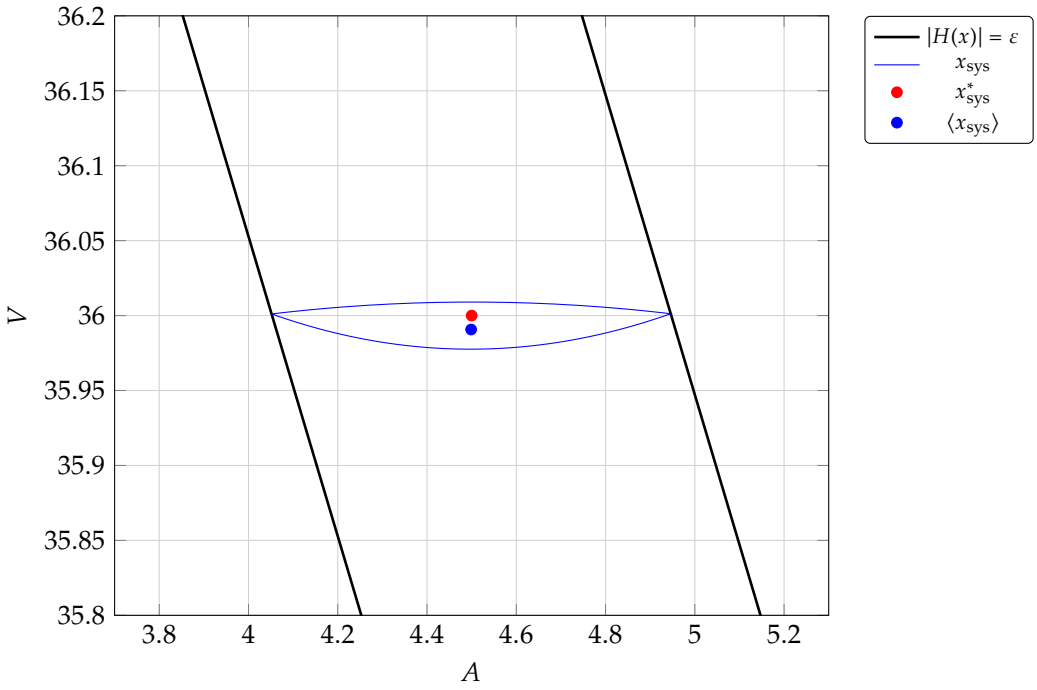

(a) State space trajectory of an ideal buck converter.

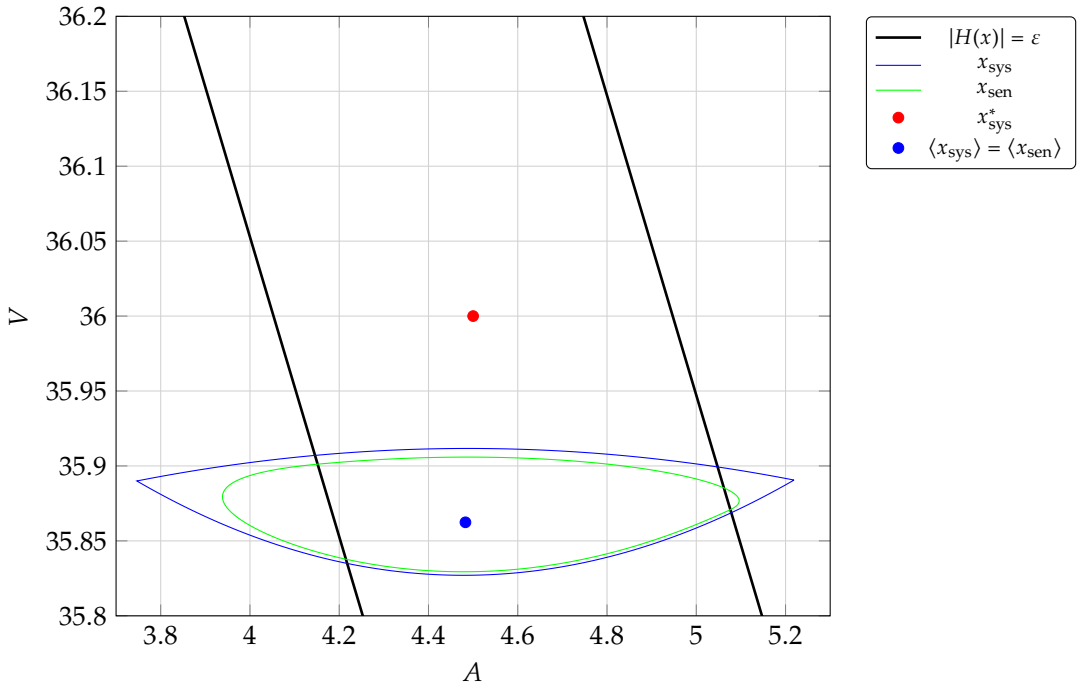

(b) State space trajectory of a converter with sensors, where the sensor gains are $k_i = 50 \times 10^3$ and $k_v = 50 \times 10^3$. Both the state and its measured value overshoot the hysteresis boundary.

Figure 4.6: Effects of sensor quality in trajectories in the phase space of the buck converter. Sensors with lower gain result in a steady state limit cycle with higher steady state drift and higher ripple. The hysteresis width $\varepsilon = 0.316$ is used.

from the converter circuit and thus they do not alter the circuit state significantly.

4.3.2 Canonical form

A canonical form is derived for the extended system by combining the dynamics of the system and the sensors. The state of the extended system is

$$x = \begin{pmatrix} x_{\text{sys}} \\ x_{\text{sen}} \end{pmatrix}, \tag{4.3.4}$$

where $x \in \mathbb{R}^{n+k}$, and the dynamics in canonical form are given by

$$f(x, D_t x, u) = 0, \tag{4.3.5}$$

where $f : \mathbb{R}^{n+k} \times \mathbb{R}^{n+k} \times \mathbb{R}^m \to \mathbb{R}^{n+k}$ and

$$f\left(\begin{pmatrix} x_{\text{sys}} \\ x_{\text{sen}} \end{pmatrix}, \begin{pmatrix} D_t x_{\text{sys}} \\ D_t x_{\text{sen}} \end{pmatrix}, u\right) = \begin{pmatrix} f_{\text{sys}}(x_{\text{sys}}) + g_{\text{sen}}(x_{\text{sys}}) \cdot u - D_t x_{\text{sys}} \\ f_{\text{sen}}(x_{\text{sen}}, D_t x_{\text{sen}}, x_{\text{sys}}) \end{pmatrix}. \tag{4.3.6}$$

4.3.3 Controller state variables and algebraic constraints

In many sliding mode controllers the dynamics of the converter circuit are extended with state variables that are internal to the controller, such as error integrals [130], [170]. In such cases sliding is enforced to the variable structure system of relation (4.3.1), where some of the system states x_{sys} are now internal to the controller. It is reasonable to assume that the controller has direct access to internal states. The differential algebraic equation model is an extension of the ordinary differential equation model, used for the buck converter in relation (4.2.13), which allows for the modeling of systems with algebraic constraints in the states of the sensors. Algebraic constraints are able to model states that are directly available to the controller. For instance, if x_{sys_i} is a system state, then the condition

$$f_{\text{sen}_i}(x_{\text{sen}}, D_t x_{\text{sen}}, x_{\text{sys}}) = x_{\text{sys}_i} - x_{\text{sen}_j}, \tag{4.3.7}$$

would make the state variable x_{sys_i} directly available to the controller through the sensor variable x_{sen_j}.

4.3.4 Switching surfaces for variable structure control

The sliding manifold, is defined by a function $H : \mathbb{R}^n \to \mathbb{R}^m$ acting in the state of converter without sensors. When sensors are included, the sliding surface is still defined over the converter variables, but the states available for the control are different. To separate the actual sliding surface from the surface perceived by the controller, two projections are defined over the state space extended with the state of the sensors, $M_{\text{sys}} : \mathbb{R}^{n+k} \to \mathbb{R}^n$ and $M_{\text{sen}} : \mathbb{R}^{n+k} \to \mathbb{R}^k$, where

$$M_{\text{sys}}\left(\begin{pmatrix} x_{\text{sys}} \\ x_{\text{sen}} \end{pmatrix}\right) = x_{\text{sys}}, \qquad M_{\text{sen}}\left(\begin{pmatrix} x_{\text{sys}} \\ x_{\text{sen}} \end{pmatrix}\right) = x_{\text{sen}}. \tag{4.3.8}$$

The function defining the sliding mode in the state space of the system extended with the dynamics of the sensors now is $H_{\text{sys}} : \mathbb{R}^{n+k} \to \mathbb{R}^m$, where

$$H_{\text{sys}}(x) = H(M_{\text{sys}}(x)), \tag{4.3.9}$$

resulting in the sliding manifold

$$\mathcal{M}_{\text{sys}} = \left\{ x \in \mathbb{R}^{n+k} : H_{\text{sys}}(x) = 0 \right\}. \tag{4.3.10}$$

The control objective is thus unaffected by the presence of the senors.

To determine the value of the control objective $H_{\text{sen}}(x)$ that is available to the controller, a function constructing a state of the system from the sensor measurements is defined. The function $h : \mathbb{R}^k \to \mathbb{R}^n$ with $k \geq n$, is an injective map from the state of the sensors to the converter state. Then for any $x_{\text{sen}} \in \mathbb{R}^k$,

$$x_{\text{sys}} = h(x_{\text{sen}}) \in \mathbb{R}^n \tag{4.3.11}$$

is the system state as measured by the sensors. Then, the value of the objective function as measured by the sensors is now

$$H_{\text{sen}}(x) = H(h(M_{\text{sen}}(x))), \tag{4.3.12}$$

and this is the value that is available to the controller. The state of the converter no longer determines directly the measured value of the objective as the controller does not have access to the converter state.

In many cases the sliding mode controller is implemented without taking into account the effects of the sensors. In these cases the switching algorithm is actuating the control input u according to the function H_{sen}. For instance, in a hysteresis switching algorithm the switching function S is then

$$S = H_{\text{sen}}. \tag{4.3.13}$$

Overall, the functions H_{sys} provides the control objective in the converter extended by the dynamics of the sensors, and the function H_{sen} determines how the control of the system is affected by the presence of sensors.

4.4 Asymptotic observer based sliding mode control

In many converters the controller has access to only a subset of the system states. The main difference from the sensor model is that the controller has direct access to a subset of the states, where as in the sensor model any state that is accessible is only accessible through a sensor measurement. For instance, a controller for a buck converter based on an inductor current observer is developed in [95]. The controller has access to the variable

$$y = h(x_{\text{sys}}) \tag{4.4.1}$$

where $h : \mathbb{R}^2 \to \mathbb{R}$ and

$$h(x_{\text{sys}}) = i_L. \tag{4.4.2}$$

A sliding mode controller based on an asymptotic state observer is presented in [95]. The observer reconstructs the system state based on a model of the system and the inductor current, and enforces sliding on a manifold in a state that includes the state reconstructed by the asymptotic observer. In the resulting sliding mode, the actual converter state converges asymptotically the the desired steady state.

A generic methodology for stabilizing dynamical systems with asymptotic observers was developed in [176]. By assuming that some of the system states are directly available to the controller, an observer based sliding mode controller that stabilizes the system is designed. Exact structural conditions on the system states that must be directly observable so that the observer based sliding mode controller can be constructed are presented in [183]. The controller can stabilize linear systems

$$D_t x = Ax + Bu \tag{4.4.3}$$

where $A \in \mathbb{R}^{n\times n}$ and $B \in \mathbb{R}^{n\times m}$, with sensors whose dynamics are modeled according a linear system

$$\mu D_t z = Dz + Hx \tag{4.4.4}$$

where $D \in \mathbb{R}^{q\times q}$, $H \in \mathbb{R}^{q\times n}$ and z is a positive scalar parameter determining the speed of the sensors. The control input u is a function of (x, z),

$$u_i(x, z) = \begin{cases} 1, & S_i(x, z) < 0 \\ 0, & S_i(x, z) > 0 \end{cases} \tag{4.4.5}$$

for $i = 1, \ldots, m$. Given a switching function

$$S = K_x x + K_z z, \tag{4.4.6}$$

where $K_x \in \mathbb{R}^{m\times n}$ and $K_z \in \mathbb{R}^{q\times n}$, sliding can be enforced if the matrix

$$K_x B \tag{4.4.7}$$

is non-singular. However, in a converter with electrical isolation, the converter does not have direct to system state, so K_x is the zero matrix. Thus, the structural constraints in dynamics of the system limit the applicability of observer base sliding mode controllers in power converters with electrically isolated senors.

4.5 Sliding stability in a buck converter with sensors

In systems converters where observer based sliding mode controllers cannot be constructed due to structural limitations, such as converters with electrically isolated sensors, a conventional sliding mode controller is used. The controller is designed assuming that the sensor dynamics are sufficiently fast so that any deviation from the ideal behavior is minimal. As controllers operate increasingly faster with respect to the sensors though, the disturbance introduced by the

sensors in many systems cannot be ignored. As a first step in analyzing the sensor dynamics, it is proven that in a back converter where all the state are accessible through sensors measurements, a sliding mode controller is unable to impose stable sliding using the sensor measurements.

The stability of the sliding surface in a buck converter with sensors is investigated locally in the neighborhood of the ideal fixed point. Let $\mathcal{M}$ be the sliding manifold defined by a function $H : \mathbb{R}^2 \to \mathbb{R}$ in an ideal buck converter without sensors, and let $x^*_{\text{sys}} \in \mathcal{M}$ be the ideal fixed point defined in relation (4.2.5). Sliding manifolds for the stabilization of the converter in x^*_{sys} are considered; such manifolds pass through the ideal fixed point so that the fixed point is reachable by sliding along $\mathcal{M}$, and thus

$$H(x^*_{\text{sys}}) = 0. \tag{4.5.1}$$

Furthermore, it is assumed that $\partial_x H(x^*)$ is a non-zero.

In the model of the buck converter extended with the dynamics of the current and voltlibrem 5age sensors, the sliding manifold exists within the extended state space that includes the state of the sensors. The dynamics of the extended system are determined in relation (4.2.17). The function $H_{\text{sys}} : \mathbb{R}^4 \to \mathbb{R}$ defining the sliding manifold is given by

$$H_{\text{sys}}(x) = H(M_{\text{sys}}(x)), \tag{4.5.2}$$

and its value measured by the sensors $H_{\text{sys}} : \mathbb{R}^4 \to \mathbb{R}$ is given by

$$H_{\text{sen}}(x) = H(h(M_{\text{sen}}(x))), \tag{4.5.3}$$

where in the buck converter with sensors

$$M_{\text{sys}}(x) = P_{\text{sys}} \cdot x, \qquad M_{\text{sen}}(x) = P_{\text{sen}} \cdot x, \tag{4.5.4}$$

with

$$P_{\text{sys}} = \begin{pmatrix} 1 & 0 & 0 & 0 \\ 0 & 1 & 0 & 0 \end{pmatrix}, \qquad P_{\text{sen}} = \begin{pmatrix} 0 & 0 & 1 & 0 \\ 0 & 0 & 0 & 1 \end{pmatrix}, \tag{4.5.5}$$

and the function $h : \mathbb{R}^2 \to \mathbb{R}^2$ is the identity operator

$$h(x) = x. \tag{4.5.6}$$

The function H_{sys} now defines a sliding manifold $\mathcal{M}_{\text{sys}} \subset \mathbb{R}^4$. The switching algorithm uses the measured value of the sliding manifold function to impose sliding, so the switching function is

$$S = H_{\text{sen}}. \tag{4.5.7}$$

It is assumed that only $O(t)$ changes or higher in the value of the switching function are detected.

In the systems extended with the dynamics of the sensors, a new ideal fixed point ensuring the desired output voltage is defined. The ideal fixed point $x^* \in \mathbb{R}^4$ is the fixed point of the extended converter dynamics defined in relation (4.2.17) for the ideal continuous control input

u^*, selected so that the output voltage attains the desired value

$$v_C = v_C^*. \tag{4.5.8}$$

The fixed point and control input are thus determined by the solution of the system of equations

$$f(x^*) + g(x^*) \cdot u^* = 0, \qquad x_2^* = v_C^*, \tag{4.5.9}$$

resulting in

$$x^* = \begin{pmatrix} \frac{v_C^*}{R} \\ v_C^* \\ \frac{v_C^*}{R} \\ v_C^* \end{pmatrix}, \tag{4.5.10}$$

and

$$u^* = \frac{v_C^*}{E}. \tag{4.5.11}$$

The ideal fixed point is on the sliding manifold in state space of the extended dynamics $x^* \in \mathcal{M}_{\text{sys}}$, as

$$H_{\text{sys}}(x^*) = 0, \tag{4.5.12}$$

and furthermore

$$H_{\text{sen}}(x^*) = 0. \tag{4.5.13}$$

Theorem 4.5.1 (Instability of the sliding surface in a buck converter with sensors)**.** *In a buck converter with sensors a switching algorithm using the switching function*

$$S = H_{\text{sen}} \tag{4.5.14}$$

cannot enforce sliding on the manifold $\mathcal{M}_{\text{sys}}$ defined by the function H_{sys}.

Proof. To prove that the switching algorithm is not enforcing sliding on H_{sys}, it is sufficient to prove that some state $x \in \mathbb{R}^4$ is reachable in the neighborhood of x^* so that $\|H(x)\| > 0$ is sufficiently large and the value of the switching function $S = H_{\text{sen}}$ has not deviated sufficiently from zero for the switching algorithm to detect the deviation in H_{sys}. The time derivative of H_{sys} is

$$D_t H_{\text{sys}} = \partial_x H \cdot P_{\text{sys}} \cdot f(x, u). \tag{4.5.15}$$

Let $\phi : \mathbb{R}^4 \times \mathbb{R} \to \mathbb{R}$ be a flow function of the system. Then, using the time derivative of H_{sys},

$$H_{\text{sys}}(\phi(x^*, t)) - H_{\text{sys}}(\phi(x^*, 0)) = \int_0^t \partial_x H \cdot P_{\text{sys}} \cdot f(\phi(x^*, \tau), u)\, d\tau \tag{4.5.16}$$

where it is assumed that the control input u is constant. Using the fact that $\phi(x^*, 0) = x^*$

$$H_{\text{sys}}(\phi(x^*, t)) = \int_0^t \partial_x H \cdot P_{\text{sys}} \cdot f(\phi(x^*, \tau), u)\, d\tau, \tag{4.5.17}$$

and using the Taylor expansion of f around $t = 0$,

$$H_{\text{sys}}(\phi(x^*, t)) = \partial_x H \cdot P_{\text{sys}} \cdot f(\phi(x^*, 0), u) \cdot t + O\left(t^2\right) \tag{4.5.18}$$
$$= \partial_x H \cdot P_{\text{sys}} \cdot f(x^*, u) \cdot t + O\left(t^2\right) \tag{4.5.19}$$
$$= \partial_x H \cdot f_{\text{sys}}(x^*_{\text{sys}}, u) \cdot t + O\left(t^2\right). \tag{4.5.20}$$

Similarly, the time derivative of H_{sen} is

$$D_t H_{\text{sen}} = \partial_x H \cdot P_{\text{sen}} \cdot f(x, u), \tag{4.5.21}$$

and therefore

$$H_{\text{sen}}(\phi(x^*, t)) - H_{\text{sen}}(\phi(x^*, 0)) = \int_0^t \partial_x H \cdot P_{\text{sen}} \cdot f(\phi(x^*, \tau), u)\, d\tau, \tag{4.5.22}$$

and using the Taylor expansion of f around $t = 0$,

$$H_{\text{sen}}(\phi(x^*, t)) = \partial_x H \cdot P_{\text{sen}} \cdot f(\phi(x^*, 0), u) \cdot t + O\left(t^2\right) \tag{4.5.23}$$
$$= \partial_x H \cdot P_{\text{sen}} \cdot f(x^*, u) \cdot t + O\left(t^2\right) \tag{4.5.24}$$
$$= O\left(t^2\right), \tag{4.5.25}$$

since

$$P_{\text{sen}} \cdot f(x^*, u) = \begin{pmatrix} 0 & 0 & 1 & 0 \\ 0 & 0 & 0 & 1 \end{pmatrix} \cdot \begin{pmatrix} -\frac{1}{L}\left(i_L^* - uE\right) \\ \frac{1}{C}\left(i_L^* - \frac{v_C^*}{R}\right) \\ 0 \\ 0 \end{pmatrix} = \begin{pmatrix} 0 \\ 0 \end{pmatrix}. \tag{4.5.26}$$

If the sliding surface is stable, the controller restricts the system state in a neighborhood such that $\left\|H_{\text{sen}}(\phi(x^*, t))\right\| < \varepsilon$, for some $\varepsilon > 0$. The gradient $\partial_x H$ is assumed to be non-zero. Thus, for at least one control input $u \in \{0, 1\}$,

$$\partial_x H \cdot f_{\text{sys}}(x^*_{\text{sys}}, u) \neq 0, \tag{4.5.27}$$

and thus according to relation (4.5.20) there is $t > 0$ such that

$$\left\|H_{\text{sen}}(\phi(x^*, t))\right\| > \varepsilon \tag{4.5.28}$$

for any sufficiently small $\varepsilon > 0$. At the same time the value of the switching function is

$$S = H_{\text{sen}}(\phi(x^*, t)) = O\left(t^2\right). \tag{4.5.29}$$

Thus the value of the switching function is not sufficiently different from zero to induce a change in the control input before the value of $\left\|H_{\text{sen}}(\phi(x^*, t))\right\|$ exceeds $\varepsilon > 0$. □

The instability of the sliding surface is related to the information that is available in the measured value of the switching function. In sliding mode controllers, information about the

state of the system is used to actuate the switches. For instance, in the hysteresis switching controller in fig. 4.2 the switching algorithm detects when the switching function S crosses the critical values

$$S = -\varepsilon, \qquad S = \varepsilon \tag{4.5.30}$$

for some hysteresis width $\varepsilon > 0$. When the switching function is evaluated according to measurements of the state variable by the sensors $S = H_{\text{sen}}$, the resulting deviation in the value of S for small deviations from x^* is not sufficient to cause the hysteresis switching algorithm to switch to a control input that rectifies the deviation of the system state from x^*. As a result, the deviation from the sliding manifold in the vicinity of x^* does not disappear as the system is constrained closer to $H_{\text{sys}} = 0$.

4.6 Designing of sliding mode controllers for converters with sensors

In a buck converter with sensors the motion in the boundary layer of the sliding manifold does not disappear in the regularization limit. Simulations reveal that a stable limit cycle appears in a hysteresis modulated converter. In applications, such as power electronics, where switching is necessary, it is sufficient to ensure that the converter state converges to a stable limit cycle in order to stabilize the system. Therefore, given that the limit cycle satisfies all design constraints regarding the switching frequency and state ripple, a switching function evaluated using the sensor measurements of the converter state is sufficient to stabilize the converter state.

The dimensions and frequency of the limit cycle however depend both on the hysteresis width and on the quality of the sensors. To determine a range of parameters for the sensor dynamics that result in an acceptable limit cycle for the stabilization of the converter, numerical simulations are used. Given a set of parameters for the sensor dynamics, the converter model with sensors is simulated until it converges to a steady state limit cycle. Then given some design constraints for the steady state performance of the converter, the space of parameters for the sensors is search to find all sensor parameters resulting in steady state limit cycles that satisfy the performance constraints.

For the selection of the admissible sensors parameters only the steady state operation of the converter is analyzed. In a realistic design task, the main performance constraints on the buck converter are:

- the switching frequency, f,
- the amplitude of the output inductor ripple, Δi_L,
- and the amplitude in the voltage of the output capacitor Δv_C.

An upper bound on the switching frequency is defined to limit the losses on the switches that scale proportionally to the switching frequency. Similarly, an upper bound is defined on the current ripple trough the inductor to limit the conduction losses in that scale proportionally to the square of the peak current. Finally, an upper bound on the ripple in voltage of the output capacitor is imposed by the voltage stability constraints for the load [84]. The steady state drift

introduced by hysteresis controllers is affected by the sensors, but it is limited and it can be compensated by the inclusion of a voltage error integrator that shifts the voltage target v_C^* such as the one designed in [130], [132], [184].

For the analysis of the converter with sensors, a periodic solution is detected numerically. The dynamics of the buck converter with sensors are defined in relation (4.2.17). Over a single period $[t, t+T]$ of the trajectory $x : \mathbb{R} \to \mathbb{R}^4$ of the system, the ripple is defined as

$$\Delta i_L = \max\{i_L(\tau) : \tau \in [t, t+T]\} - \min\{i_L(\tau) : \tau \in [t, t+T]\}, \tag{4.6.1}$$

and

$$\Delta v_C = \max\{v_C(\tau) : \tau \in [t, t+T]\} - \min\{v_C(\tau) : \tau \in [t, t+T]\} \tag{4.6.2}$$

respectively. The limit cycles that have been observed cross the hysteresis band of the switching function once every period, so the switching frequency is defined as

$$f = \frac{1}{T}. \tag{4.6.3}$$

The limit cycle is evaluated detecting the convergence of a Poincaré map on the sliding surface

$$H_{\text{sys}} = 0, \tag{4.6.4}$$

with a convergence threshold of $\varepsilon_{\text{map}} = 10^{-4}$. The quantities Δi_L, Δv_C and f are then evaluated numerically for the trajectory.

In the design of a buck converter with sensors, the specifications of the design are expressed as upper bounds on the performance measures Δv_C, Δi_L, and f. Thus given the upper bounds $\Delta v_{C\text{-ub}}$, Δi_L, and f_{ub}, the design problem is the the selection of all sensor parameters within a given range such that

$$\begin{cases} \Delta v_C < \Delta v_{C\text{-ub}}, & \text{(4.6.5a)} \\ \Delta i_L < \Delta i_{L\text{-ub}}, & \text{(4.6.5b)} \\ f < f_{\text{ub}}. & \text{(4.6.5c)} \end{cases}$$

The values for the upper bounds of the constraints selected for demonstrations purposes are summarized in table 4.5. The sensor dynamics are parametrized by $k_1, k_2 > 0$. A typical range for this parameters

$$k_1, k_2 \in [10^4, 10^5], \tag{4.6.6}$$

is searched to determine which pairs of sensor parameters result in a limit cycle that satisfies the design constraints. The resulting range of admissible sensor parameters can then be used to select a suitable set of current and voltage sensors to construct the converter.

Constraint	Value
f_{ub}	5 kHz
$\Delta i_{L\text{-ub}}$	2 A
$\Delta v_{C\text{-ub}}$	0.5 V

Table 4.5: Values for the constraints the buck converter.

The results of the time domain simulations are summarized in fig. 4.7. The system was simulated with the sensor gains k_1 and k_2 taking values in the interval $[10^4, 10^5]$ in a grid of resolution 10^3. The performance is more severely degraded for lower sensor gains, so only the range $[10^4, 5 \cdot 10^5]$ where the effects in the performance are more visible is plotted. The three performance measures, Δi_L, Δv_C and f, are affected mainly by the gain of the current sensor, with the gain of the voltage sensor having an effect about an order of magnitude less significant. Furthermore, from the three constraints in relation (4.6.5) the limit on the inductor ripple,

$$\Delta i_L < \Delta i_{L\text{-ub}}, \tag{4.6.7}$$

is the critical constraint, as the other two inequality constraints are satisfied for the whole range of sensor parameters. Thus, in the selection of the sensors only the current ripple is considered.

In fig. 4.8 the amplitude of the ripple in the current through the inductor is plotted. The constraint of the design specifications for the upper bound in the ripple is also plotted as the contour where $\Delta i_L = 2\,\text{A}$. The plot demonstrates that the inductor current ripple is primarily affected by the gain of the current sensor. Since the current ripple is the critical constraint, any combination of sensor gains that results in current ripple less than 2 A is an admissible design.

The set of admissible configurations for the sensor gains is summarized in fig. 4.9. The shaded areas is the set of gains for the sensor that result in a steady state limit cycle satisfying the design constraint for the current ripple. Given that the current ripple constraint is the critical constraint, the shaded set represents the solution of the design problem, that is the set of sensor gains that result in admissible performance.

4.6.1 Limitations and advantages of the analytical approach

The numerical method for determining the sensor configurations that satisfy the design constraints has some limitations. The method can be applied directly to other topologies with a single switch operating in continuous conduction mode, such as the boost and buck-boost converters. However, the design problem requires a search through the space of possible parameters for the sensor dynamics to numerically determine the admissible configurations. Therefore, the process is computationally intensive and sensitive to variation of other parameters in the converter. For instance, when the capacitance or the inductance in the converter change, the set of admissible sensor configurations for the sensors must be reevaluated.

Despite the high computational cost of the numerical analysis, it provides a more accurate description of the admissible sensor configuration compared to the cutoff frequency approach. The cutoff frequency determines a minimum gain for the sensors so that the resulting deviation between the sensor measurement and the actual state can be considered negligible. During steady state operation, the switching period of the converter is estimated using a constant approximation of the buck converter vector fields in steady state [74].

For $u = 0$:

$$T_0 = \frac{2\varepsilon}{\left|\partial_x H \cdot f_{\text{sys}}(x^*_{\text{sys}})\right|} \tag{4.6.8}$$

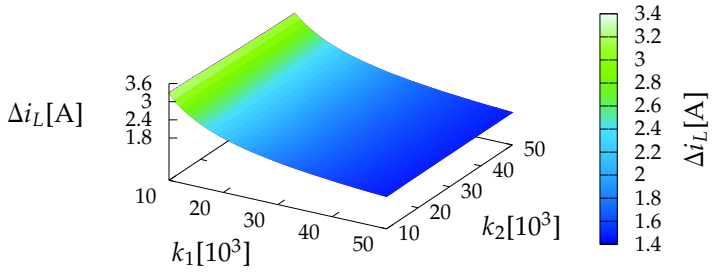

(a) The effect of the sensor gains in the ripple of the inductor current are significant. The ripple is mostly sensitive in the gain of the current sensor.

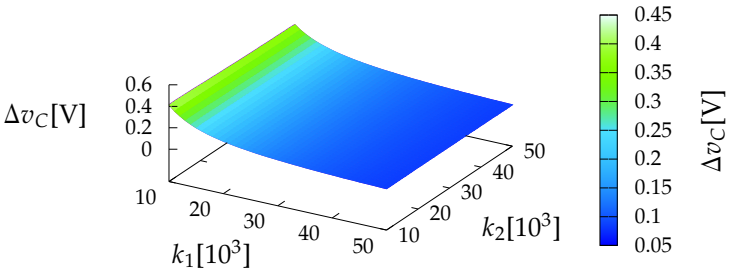

(b) The voltage ripple is impacted less severely by the sensor gains. The ripple is withing limits for the whole range of sensor gains meaning that the voltage is not a critical constraint in this model.

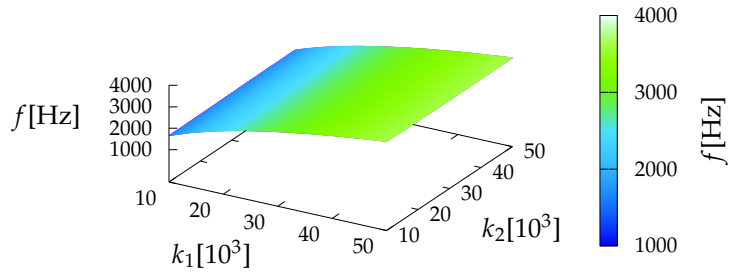

(c) The switching frequency is also within specification limits for the whole range of voltage gains and as a results it is not a critical parameter for the design.

Figure 4.7: A parametric analysis of the effects of the sensor dynamics was conducted trough time domain simulations. The system was simulated with the sensor gains k_1 and k_2 taking values in the interval $[10^4, 10^5]$ and a resolution of 10^3. The performance degradation is more severe for lower sensor gains, so only the range $[10^4, 5 \cdot 10^5]$ is plotted, where the effects in the performance are more visible.

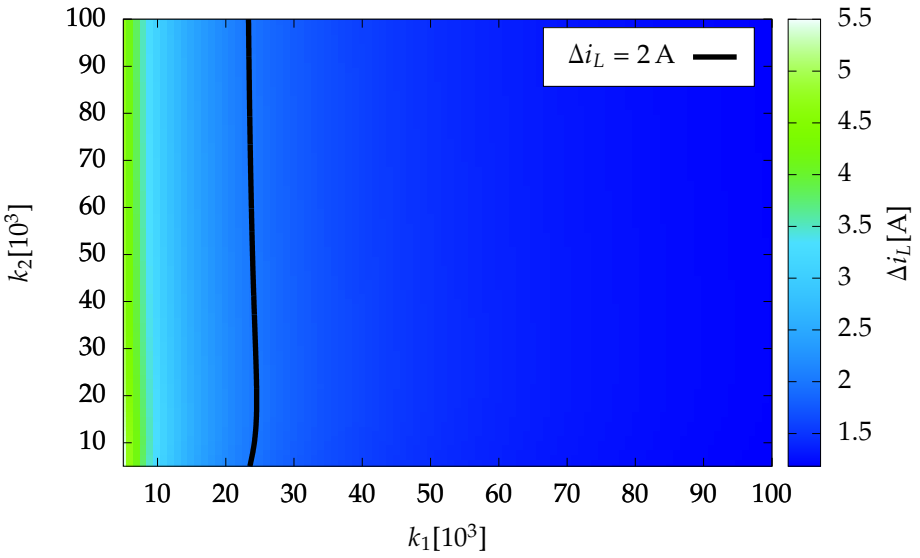

Figure 4.8: A plot of the ripple Δi_L of the inductor current in the steady state limit cycle with respect to different sensor gain configurations. The contour $\Delta i_L = 2$ A which corresponds to the maximum allowed current ripple in the design specifications is also plotted.

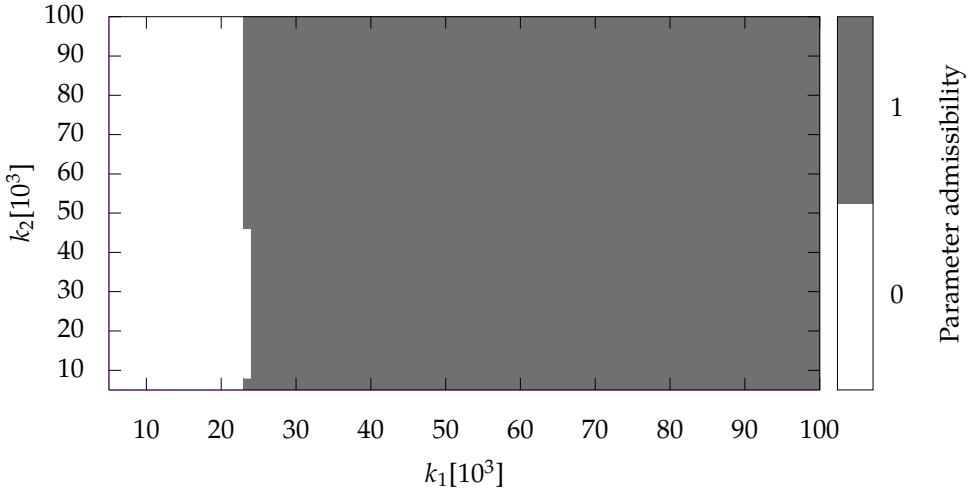

Figure 4.9: The shaded area is the solution to the design problem of relation (4.6.5). Configurations of the sensor gains in the shaded area result in a steady state limit cycle which satisfies the constraints for the design parameters in table 4.5.

For $u = 1$:

$$T_1 = \frac{2\varepsilon}{\left|\partial_x H \cdot \left(f_{\text{sys}}(x^*_{\text{sys}}) + g_{\text{sys}}(x^*_{\text{sys}})\right)\right|} \tag{4.6.9}$$

Therefore, the overall switching period is

$$T = T_0 + T_1, \tag{4.6.10}$$

and the resulting switching frequency

$$f = \frac{1}{T}. \tag{4.6.11}$$

Substituting the system parameters from table 4.2, the switching frequency is

$$f = 13.7\,\text{kHz}. \tag{4.6.12}$$

According to the definition of the sensor dynamics in relation (4.2.11), the sensors operate as low pass filters with time constants

$$\tau_i = \frac{1}{k_i}, \qquad \tau_v = \frac{1}{k_v}. \tag{4.6.13}$$

The resulting cutoff frequencies are

$$f_{c\text{-}i} = \frac{1}{2\pi\tau_i} = \frac{k_i}{2\pi}, \tag{4.6.14}$$

and similarly

$$f_{c\text{-}v} = \frac{k_v}{2\pi}. \tag{4.6.15}$$

To ensure that the system is controllable, the cutoff frequency of the sensors is selected to be larger that the switching frequency. Thus

$$f_{c\text{-}i} > f \tag{4.6.16}$$

$$\Rightarrow \quad k_i > 2\pi f \tag{4.6.17}$$

$$\Rightarrow \quad k_i > 85.8 \times 10^3, \tag{4.6.18}$$

and similarly,

$$k_v > 85.8 \times 10^3. \tag{4.6.19}$$

The constraints for the sensor gains are however very conservative. Especially for the voltage sensor, the numerical approach reveals that its performance is much less critical than the cutoff frequency method would suggest.

4.7 Conclusions

A numerical method is proposed for determining the range of admissible sensor configurations. The characteristic feature of this method is that the control algorithm has access to only measurements of the converter states by the sensors in order to evaluate the switching function. Due to this restriction, observer based sliding mode controllers cannot be used, as they rely on direct access to at least some of the converter states in order to stabilize the system.

In the converter with sensors the sliding surface is proven to be unstable. Numerical simulations reveal that an attracting steady state limit cycle exists. In applications, such as stabilization of power electronic converters, it is sufficient to enforce a limit cycle in steady state operation to stabilize the system. Given a set of constraints for the steady state operation, such as switching frequency and ripple, numerical simulations are used to filter the sensor configurations that result in an admissible steady state performance. The numerical method is shown to determine the set of admissible solutions much more accurately than heuristic approaches, such as the sensor cutoff frequency.

Despite the good performance of the numerical method, it is quite limited due to its computational complexity. New simulations are required every time any of the parameters of the converter are varied in order to determine the set of admissible sensor configurations. Analytical proofs for the existence and the characteristics of the steady state limit cycle could provide constraints for selecting sensor configuration resulting in admissible performance while being significantly less conservative than heuristic methods.

Chapter 5

Conclusions

The aim of this thesis was to analyze some of the phenomena in the dynamics of the boundary layer that affect the performance of stabilizing sliding mode controllers for power converters. The dynamics of the controlled system in the sliding mode are determined by the motion in the boundary layer around the sliding manifold. A sliding mode controller for the trans-Z-source DC-DC converter was designed, where the system slides in the intersection of two switching surfaces. An algorithm was developed that constructs the switching surfaces, given a control objective expressed as a set of invariant conditions. The resulting switching surfaces were used to construct a hysteresis modulated sliding mode controller.

Two hysteresis boundaries were investigated, a box boundary and a elliptical boundary. The regularization process determines the limit where the sliding speed converges as the boundary vanishes by projecting the system dynamics in the boundary perpendicular to the sliding manifold. In the projected dynamics, limit cycles appear that determine the average time the system spends in each of the four available modes and thus the resulting sliding speed. In the box boundary, jitter appears in the sliding speed, a phenomenon where the speed of sliding varies abruptly along the sliding manifold. The variation in the sliding speed is caused by changes in the limit cycle as the system moves along the sliding surface. The elliptical hysteresis layer does not display jitter, however there are multiple limit cycles resulting in multiple possible sliding speeds, and the limit cycle to which the system converges depends on the initial conditions on the projected dynamics.

Another source of dynamical behavior in the sliding layer, that degrades the performance of the sliding mode, is unmodeled dynamics. The effects of unmodeled dynamics on the sliding layer motion were investigated for a buck converter with sensors. A linear integrator was used to model isolated sensors used in power electronics. It was proven that in a system with sensors the sliding manifold is no longer stable. Numerical simulations indicate that a limit cycle appears during steady state operation. A relation between the quality of the sensors and the steady state ripple was derived numerically and was used to determine the minimum requirements for the sensor so that an acceptable performance is attained during steady state operation. This information is useful for the designer in selecting sensors so that design constraints in the switching ripple and frequency are satisfied.

5.1 Main contributions

The design of sliding mode controllers for power electronics has been an active research area [132]. With the introduction of new power converter topologies [29], [30] however, the design of the sliding dynamics that determine the performance of the controlled system is complicated. A more detailed analysis of the dynamics of systems sliding in the intersection of sliding surfaces conducted in [76] indicates that jitter may appear, a phenomenon which in hysteresis modulated controllers causes abrupt and unpredictable variation in the sliding speed.

In chapter 3 a new sliding mode controller for the stabilization of the voltage sourced trans-Z-source DC-DC converter was designed and simulated. An algorithm was developed that given a description of the control objective as a set of invariant surfaces constructs the switching surfaces of the sliding mode controller. The algorithm was used to construct a sliding mode controller that stabilizes both the output current of the trans-Z-source converter and the state of the impedance network. This is an improvement over conventional designs of sliding mode controllers for impedance source converters that use sliding mode control either for the output current [60] or the impedance network [61]–[64], in combination with an averaged controller for the objective not controlled using sliding. As a result, desirable properties of sliding mode controllers, such as complete rejection of disturbances outside the sliding manifold, are achieved only for part of the control objectives in these hybrid controllers. Some implementations of a sliding mode controller for the DC-DC Z-source converter circumvent the problem by using a single input and restricting the operating range of the converter to the maximum boost operation [72]. The algorithm designed in this thesis allows the control of the whole state of the converter without restrictions in the operating range. As a result, the proposed algorithm can be used with simple modulation methods such as hysteresis modulation without performance degradation.

The sliding mode control algorithm for the trans-Z-source converter enforces sliding in the intersection of two surfaces. A class of algorithms for enforcing sliding in the intersection of multiple surfaces is presented in [148]. Two hysteresis modulated algorithms where implemented for the trans-Z-source converter, one using a box hysteresis boundary and one using an elliptical hysteresis boundary. Numerical simulations of the controlled system on the sliding mode, indicate that jitter is present. This is the first demonstration of jitter in a practical system of which we are aware. The jitter appears to be sensitive in the selection of the switching surface and the control logic. The box switching layer results in jitter that can be explained by sudden topological changes in the dynamics that appear in the switching layer during sliding. Periodic and quasi periodic orbits appear in the hysteresis layer. Orbits that are quasi-periodic or periodic with high periodicity result in a sliding speed close to the canopy solution, a method used to construct a representative solution from the convex hull of available solutions [151]. Abrupt bifurcations that cause the appearance of low periodicity limit cycles seem to cause the largest deviations in the sliding speed. The elliptical switching surface does not display any measurable jitter. There are multiple limit cycles present in the elliptical boundary and the limit cycle in which the system converges depends on the initial conditions. Time domain simulations indicate that these limit cycles vary in a very predictable manner along the sliding surface resulting in a smooth variation in the sliding speed. However, the limit cycle where the solution converges depends on the initial conditions.

As part of the analysis of the sliding dynamics a method that describes the range of possible

sliding solutions in systems with a finite hysteresis boundary is constructed. Regularization conventionally assumes that the hysteresis layer vanishes; in this case the range of possible sliding solutions is determined accurately by the minimal convex hull of the vector fields on the sliding manifold. To describe the possible sliding vector fields in systems where the hysteresis layer is finite, the minimal convex hull of all vector fields in the finite hysteresis layer was used. Sliding solutions for the two proposed sliding mode control algorithms are within the range predicted by the extended convex hull.

Chapter-4 focuses on the effects of unmodeled dynamics in the performance of the modulation algorithm. The effect of sensor behavior in a buck converter with sensors was analyzed. A first order integrator model for the sensor dynamics is used to capture the behavior of isolated current and voltage sensors used in power electronic circuits. Analytical results exist for models where sensors are represented as time delays [180]. In systems where sensors are modeled as first order integrators it was proven analytically that the sliding manifold is no longer stable. Instead a limit cycle appears during steady state operation which determines the switching frequency and the ripple of the converter. As a means of deriving less conservative designs, the circuit was simulated numerically and a relation between the quality of the sensors and the ripple was derived. The simulations allow for a less conservative selection of sensors than the cut-off frequency criterion which is conventionally used for selecting the sensors.

5.2 Future research

In this thesis two cases were identified where dynamics in the switching layer affect the performance of sliding mode controllers in a manner that is difficult to regulate. In power converters with multiple inputs jitter can appear on a sliding mode located in the intersection of multiple sliding surfaces, or multiple sliding solutions may exist. In hysteresis modulated converters the jitter is significantly affected by the design of the switching surface and the switching logic. The exact effects of the surface topology have not been investigated analytically however. Limit cycles with predictable dynamics are present in the layer defined by an elliptical surface. If a cycle with the desired sliding dynamics can be detected, the switching logic in the ellipse can be selected so that the desired limit cycle changes smoothly, thus eliminating jitter.

A problem in the analysis of systems with multiple inputs is the lack of sufficient analytical conditions determining when ripple exists. Time domain simulations are at the moment the only reliable method to detect jitter in a system. Extending the convex hull method to include the variation of the vector fields in the hysteresis layer, less restrictive bounds for the sliding speed of hysteresis modulated system are evaluated numerically. These extended convex hull captures the effects of non-ideal components, but offers little information about jitter. A method that limits the convex hull to those solutions that are achievable with hysteresis modulation would provide a clear indication on whether jitter is present in the system.

The dynamics in the boundary layer of a buck convert with sensors were also analyzed. It was proven that the switching manifold in a buck with sensors is unstable, but simulations indicate there exists a limit cycle in the sliding layer. An analytical proof of the existence of the limit cycle could potentially provide conditions under which the limit cycle is stable. Furthermore, the limit cycle degrades the performance of the controller by increasing the switching ripple.

Determining the stability and amplitude of the limit cycle analytically could eliminate the need for time domain simulations of the system which are computationally expensive.

Overall, the dynamics in the boundary layer of the sliding manifold in power converters were analyzed. In conventional sliding modes, there is a direct relation between the sliding manifold and the boundary layer dynamics, and as a result the sliding dynamics are easily determined. Controllers that provide a direct link between the switching surface selection and the sliding dynamics in converter with more complex dynamics can make sliding mode controllers a viable choice in practical designs.

Bibliography

[1] K. A. Kim, Y.-C. Liu, M.-C. Chen, and H.-J. Chiu, "Opening the box: Survey of high power density inverter techniques from the little box challenge", *CPSS Transactions on Power Electronics and Applications*, vol. 2, no. 2, pp. 131–139, Aug. 2017.

[2] S. Haghbin, S. Lundmark, M. Alakula, and O. Carlson, "Grid-connected integrated battery chargers in vehicle applications: Review and new solution", *IEEE Transactions on Industrial Electronics*, vol. 60, no. 2, pp. 459–473, Feb. 2013.

[3] M. Calais, V. G. Agelidis, and M. Meinhardt, "Multilevel converters for single-phase grid connected photovoltaic systems: An overview", *Solar Energy*, vol. 66, no. 5, pp. 325–335, Aug. 1999.

[4] J. M. Carrasco, L. G. Franquelo, J. T. Bialasiewicz, E. Galvan, R. C. Portillo Guisado, M. A. M. Prats, J. I. Leon, and N. Moreno-Alfonso, "Power-electronic systems for the grid integration of renewable energy sources: A survey", *IEEE Transactions on Industrial Electronics*, vol. 53, no. 4, pp. 1002–1016, Jun. 2006.

[5] N. Pogaku, M. Prodanovic, and T. C. Green, "Modeling, analysis and testing of autonomous operation of an inverter-based microgrid", *IEEE Transactions on Power Electronics*, vol. 22, no. 2, pp. 613–625, Mar. 2007.

[6] A. N. A. Ali, M. H. Saied, M. Z. Mostafa, and T. M. Abdel-Moneim, "A survey of maximum PPT techniques of PV systems", in *IEEE Energytech*, May 2012, pp. 1–17.

[7] M. Kordestani, A. Mirzaee, A. A. Safavi, and M. Saif, "Maximum power point tracker (MPPT) for photovoltaic power systems-a systematic literature review", in *European Control Conference*, Jun. 2018, pp. 40–45.

[8] Y.-T. Hsiao and C.-H. Chen, "Maximum power tracking for photovoltaic power system", in *IEEE Industry Applications Conference*, vol. 2, Oct. 2002, pp. 1035–1040.

[9] R. Kot, M. Rolak, and M. Malinowski, "Comparison of maximum peak power tracking algorithms for a small wind turbine", *Mathematics and Computers in Simulation*, vol. 91, pp. 29–40, May 2013.

[10] M. J. Khan and L. Mathew, "Comparative study of maximum power point tracking techniques for hybrid renewable energy system", *International Journal of Electronics*, pp. 1–13, 2019.

[11] F. Zenith and S. Skogestad, "Control of fuel cell power output", *Journal of Process Control*, vol. 17, no. 4, pp. 333–347, Apr. 2007.

[12] O. E. Oni, I. E. Davidson, and K. N. I. Mbangula, "A review of LCC-HVDC and VSC-HVDC technologies and applications", in *IEEE International Conference on Environment and Electrical Engineering*, Jun. 2016, pp. 1–7.

[13] F. H. Gandoman, A. Ahmadi, A. M. Sharaf, P. Siano, J. Pou, B. Hredzak, and V. G. Agelidis, "Review of FACTS technologies and applications for power quality in smart grids with renewable energy systems", *Renewable and Sustainable Energy Reviews*, vol. 82, pp. 502–514, Jan. 2018.

[14] D. Garrido-Diez and I. Baraia, "Review of wide bandgap materials and their impact in new power devices", in *IEEE International Workshop of Electronics, Control, Measurement, Signals and their Application to Mechatronics*, May 2017, pp. 1–6.

[15] J. Millan, P. Godignon, X. Perpina, A. Perez-Tomas, and J. Rebollo, "A survey of wide bandgap power semiconductor devices", *IEEE Transactions on Power Electronics*, vol. 29, no. 5, pp. 2155–2163, May 2014.

[16] A. S. Morsy and P. N. Enjeti, "Comparison of active power decoupling methods for high-power-density single-phase inverters using wide-bandgap FETs for google little box challenge", *IEEE Journal of Emerging and Selected Topics in Power Electronics*, vol. 4, no. 3, pp. 790–798, Sep. 2016.

[17] G. Chen, M. Rentzch, F. Wang, D. Boroyevich, S. Ragon, V. Stefanovic, and M. Arpilliere, "Analysis and design optimization of front-end passive components for voltage source inverters", in *IEEE Applied Power Electronics Conference and Exposition*, vol. 2, Feb. 2003, pp. 1170–1176.

[18] F. Z. Peng, "Z-source networks for power conversion", in *IEEE Applied Power Electronics Conference and Exposition*, Feb. 2008, pp. 1258–1265.

[19] M. Mirjafari and R. S. Balog, "Multi-objective design optimization of renewable energy system inverters using a descriptive language for the components", in *IEEE Applied Power Electronics Conference and Exposition*, Mar. 2011, pp. 1838–1845.

[20] N. Simpson and P. H. Mellor, "Additive manufacturing of shaped profile windings for minimal AC loss in gapped inductors", in *IEEE International Electric Machines and Drives Conference*, May 2017, pp. 1–7.

[21] H. Hadim and T. Suwa, "Multidisciplinary design and optimization methodologies in electronics packaging: State-of-the-art review", *Journal of Electronic Packaging*, vol. 130, no. 3, Jul. 2008.

[22] F. Z. Peng, "A generalized multilevel inverter topology with self voltage balancing", in *IEEE Industry Applications Conference*, vol. 3, Oct. 2000, pp. 2024–2031.

[23] A. Lesnicar and R. Marquardt, "An innovative modular multilevel converter topology suitable for a wide power range", in *IEEE PowerTech*, vol. 3, Jun. 2003, pp. 272–277.

[24] S. Debnath, J. Qin, B. Bahrani, M. Saeedifard, and P. Barbosa, "Operation, control, and applications of the modular multilevel converter: A review", *IEEE Transactions on Power Electronics*, vol. 30, no. 1, pp. 37–53, Jan. 2015.

[25] J. Rodriguez, J.-S. Lai, and F. Z. Peng, "Multilevel inverters: A survey of topologies, controls, and applications", *IEEE Transactions on Industrial Electronics*, vol. 49, no. 4, pp. 724–738, Aug. 2002.

[26] F. Z. Peng, "Z-source inverter", *IEEE Transactions on Industry Applications*, vol. 39, no. 2, pp. 504–510, Mar. 2003.

[27] E. Babaei, M. S. Zarbil, and M. Sabahi, "A new structure of quasi z-source-based cascaded multilevel inverter", *Journal of Circuits, Systems and Computers*, vol. 26, no. 12, p. 1 750 203, Dec. 2017.

[28] A. Baghbany Oskouei, M. R. Banaei, and M. Sabahi, "Extended SVM algorithms for multilevel trans-z-source inverter", *Ain Shams Engineering Journal*, vol. 7, no. 1, pp. 265–274, Jan. 2016.

[29] Y. P. Siwakoti, F. Z. Peng, F. Blaabjerg, P. C. Loh, and G. E. Town, "Impedance-source networks for electric power conversion part i: A topological review", *IEEE Transactions on Power Electronics*, vol. 30, no. 2, pp. 699–716, Feb. 2015.

[30] O. Ellabban and A.-R. Haitahm, "Z-source inverter: Topology improvements review", *IEEE Industrial Electronics Magazine*, vol. 10, no. 1, pp. 6–24, Mar. 2016.

[31] E. Babaei, H. Abu-Rub, and H. M. Suryawanshi, "Z-source converters: Topologies, modulation techniques, and application - part i", vol. 65, no. 6, pp. 5092–5095, Jun. 2018.

[32] U. Badstuebner, J. Biela, and J. W. Kolar, "Design of an 99%-efficient, 5kw, phase-shift PWM DC-DC converter for telecom applications", in *IEEE Applied Power Electronics Conference and Exposition*, Feb. 2010, pp. 773–780.

[33] J. W. Kolar, J. Biela, and J. Minibock, "Exploring the pareto front of multi-objective single-phase PFC rectifier design optimization - 99.2% efficiency vs. 7kw/din3 power density", in *IEEE International Power Electronics and Motion Control Conference*, May 2009, pp. 1–21.

[34] J. W. Kolar, J. Biela, S. Waffler, T. Friedli, and U. Badstuebner, "Performance trends and limitations of power electronic systems", in *International Conference on Integrated Power Electronics Systems*, Mar. 2010, pp. 1–20.

[35] U. Badstuebner, J. Biela, D. Christen, and J. W. Kolar, "Optimization of a 5-kw telecom phase-shift DC–DC converter with magnetically integrated current doubler", vol. 58, no. 10, pp. 4736–4745, Oct. 2011.

[36] U. Badstuebner, A. Stupar, and J. W. Kolar, "Sensitivity of telecom dc-dc converter optimization to the level of detail of the system model", in *IEEE Applied Power Electronics Conference and Exposition*, Mar. 2011, pp. 585–592.

[37] I. D. Laird, X. Yuan, and N. McNeill, "A holistic approach to optimise the power density of a silicon carbide (sic) MOSFET based three-phase inverter", in *IEEE International Conference on Power Electronics and Drive Systems*, Jun. 2015, pp. 473–478.

[38] I. D. Laird, J. Scoltock, A. J. Forsyth, and X. Yuan, "A unified framework for computationally efficient power converter design optimisation", in *IET International Conference on Power Electronics, Machines and Drives*, Apr. 2016, pp. 1–6.

[39] I. D. Laird, X. Yuan, J. Scoltock, and A. J. Forsyth, "A design optimization tool for maximizing the power density of 3-phase DC–AC converters using silicon carbide (sic) devices", *IEEE Transactions on Power Electronics*, vol. 33, no. 4, pp. 2913–2932, Apr. 2018.

[40] S. Balachandran and F. C. Y. Lee, "Algorithms for power converter design optimization", *IEEE Transactions on Aerospace and Electronic Systems*, vol. 17, no. 3, pp. 422–432, May 1981.

[41] K. Rigbers, S. Schroder, T. Durbaum, M. Wendt, and R. W. De Doncker, "Integrated method for optimization of power electronic circuits", in *IEEE Power Electronics Specialists Conference*, vol. 6, Nov. 2004, pp. 4473–4478.

[42] A. T. Bryant, D. M. Jaeggi, G. T. Parks, and P. R. Palmer, "The influence of operating conditions on multi-objective optimization of power electronic devices and circuits", in *IEEE Industry Applications Conference*, vol. 2, Oct. 2005, pp. 1449–1456.

[43] S. Busquets-Monge, G. Soremekun, E. Hertz, C. Crebier, S. Ragon, D. Boroyevich, Z. Gurdal, M. Arpilliere, and D. K. Lindner, "Power converter design optimization", *IEEE Industry Applications Magazine*, vol. 10, no. 1, pp. 32–38, Jan. 2004.

[44] S.-J. Wang, Y. S. Lee, K. W. Siu, and X.-Z. Liu, "Expert system aided design, simulation and optimization of power converters", in *International Conference on Industrial Electronics, Control, and Instrumentation*, vol. 3, Nov. 1997, pp. 1016–1021.

[45] S.-J. Wang, K. W. Siu, and Y. S. Lee, "Applying expert system and fuzzy logic to power converter design", in *IEEE International Symposium on Circuits and Systems*, vol. 3, Jun. 1997, pp. 1732–1735.

[46] S.-J. Wang and Y. S. Lee, "Development of an expert system for designing, analyzing and optimizing power converters", in *Convention of Electrical and Electronics Engineers in Israel*, Oct. 1996, pp. 359–362.

[47] S. M. Chhaya and B. K. Bose, "Expert system based automated design technique of a voltage-fed inverter for induction motor drive", in *IEEE Industry Applications Society Annual Meeting*, vol. 1, Oct. 1992, pp. 770–778.

[48] ——, "Expert system based automated simulation and design optimization of a voltage-fed inverter for induction motor drive", in *Annual Conference of the IEEE Industrial Electronics Society*, vol. 2, Nov. 1993, pp. 1065–1070.

[49] B. K. Bose, "Expert system, fuzzy logic, and neural network applications in power electronics and motion control", *Proceedings of the IEEE*, vol. 82, no. 2, pp. 1303–1323, Aug. 1994.

[50] S. M. Chhaya and B. K. Bose, "Expert system aided automated design, simulation and controller tuning of AC drive system", in *Annual Conference of the IEEE Industrial Electronics Society*, vol. 1, Nov. 1995, pp. 712–718.

[51] G. W. Chang, "A new approach for optimal shunt active power filter control considering alternative performance indices", *IEEE Transactions on Power Delivery*, vol. 21, no. 1, pp. 406–413, Jan. 2006.

[52] Y. Guan, Y. Xie, Y. Wang, and B. Chen, "An optimal DC-link voltage control strategy of shunt active power filter", pp. 396–401, Oct. 2015.

[53] G. M. Vosters, T. J. Hassell, W. W. Weaver, and J. Wolfle, "Optimal control of power electronic converters for traction applications", in *IEEE Vehicle Power and Propulsion Conference*, Sep. 2011, pp. 1–5.

[54] S. Mariethoz, S. Almer, M. Baja, A. G. Beccuti, D. Patino, A. Wernrud, J. Buisson, H. Cormerais, T. Geyer, H. Fujioka, U. T. Jonsson, C.-Y. Kao, M. Morari, G. Papafotiou, A. Rantzer, and P. Riedinger, "Comparison of hybrid control techniques for buck and boost DC-DC converters", *IEEE Transactions on Control Systems Technology*, vol. 18, no. 5, pp. 1126–1145, Sep. 2010.

[55] G. Escobar, R. Ortega, H. Sira-Ramirez, J.-P. Vilain, and I. Zein, "An experimental comparison of several nonlinear controllers for power converters", *IEEE Control Systems*, vol. 19, no. 1, pp. 66–82, Feb. 1999.

[56] V. I. Utkin, "Sliding mode control design principles and applications to electric drives", *IEEE Transactions on Industrial Electronics*, vol. 40, no. 1, pp. 23–36, Feb. 1993.

[57] Y. Li, K. C. Ng, D. J. Murray-Smith, G. J. Gray, and K. C. Sharman, "Genetic algorithm automated approach to the design of sliding mode control systems", *International Journal of Control*, vol. 63, no. 4, pp. 721–739, Feb. 2007.

[58] Z.-m. Chen, W.-j. Meng, J.-g. Zhang, and J.-c. Zeng, "Scheme of sliding mode control based on modified particle swarm optimization", *Systems Engineering - Theory & Practice*, vol. 29, no. 5, pp. 137–141, May 2009.

[59] M. J. Mahmoodabadi, S. Momennejad, and A. Bagheri, "Online optimal decoupled sliding mode control based on moving least squares and particle swarm optimization", *Information Sciences*, vol. 268, pp. 342–356, Jun. 2014.

[60] F. Zare and J. A. Firouzjaee, "Hysteresis band current control for a single phase z-source inverter with symmetrical and asymmetrical z-network", in *Power Conversion Conference*, Nagoya, Japan, Apr. 2007, pp. 143–148.

[61] A. H. Rajaei, S. Kaboli, and A. Emadi, "Sliding-mode control of z-source inverter", in *Annual Conference of the IEEE Industrial Electronics Society*, Nov. 2008, pp. 947–952.

[62] U. K. Shinde, S. G. Kadwane, S. P. Gawande, M. J. B. Reddy, and D. K. Mohanta, "Sliding mode control of single-phase grid-connected quasi-z-source inverter", *IEEE Access*, vol. 5, pp. 10 232–10 240, May 2017.

[63] J. Liu, S. Jiang, D. Cao, X. Lu, and F. Z. Peng, "Sliding-mode control of quasi-z-source inverter with battery for renewable energy system", in *IEEE Energy Conversion Congress and Exposition*, Sep. 2011, pp. 3665–3671.

[64] Q. Sun and Y. Wang, "Integral sliding mode control of z-source inverter for motor drive system of electric vehicles", in *World Congress on Intelligent Control and Automation*, Jul. 2012, pp. 1196–1200.

[65] M. Shen, J. Wang, A. Joseph, F. Z. Peng, L. M. Tolbert, and D. J. Adams, "Maximum constant boost control of the z-source inverter", in *IEEE Industry Applications Conference*, vol. 1, Oct. 2004, pp. 142–147.

[66] F. Z. Peng, M. Shen, and Z. Qian, "Maximum boost control of the z-source inverter", *IEEE Transactions on Power Electronics*, vol. 20, no. 4, pp. 833–838, Jul. 2005.

[67] M. Shen, J. Wang, A. Joseph, F. Z. Peng, L. M. Tolbert, and D. J. Adams, "Constant boost control of the z-source inverter to minimize current ripple and voltage stress", *IEEE Transactions on Industry Applications*, vol. 42, no. 3, pp. 770–778, May 2006.

[68] W. Zhang and S. Sanders, "Minimum switching space vector modulation of the z-source inverter", in *IEEE Workshop on Control and Modeling for Power Electronics*, Jul. 2017.

[69] Y. P. Siwakoti, F. Z. Peng, F. Blaabjerg, P. C. Loh, G. E. Town, and S. Yang, "Impedance-source networks for electric power conversion part II: Review of control and modulation techniques", *IEEE Transactions on Power Electronics*, vol. 30, no. 4, pp. 1887–1906, Apr. 2015.

[70] A. Abdelhakim, F. Blaabjerg, and P. Mattavelli, "Modulation schemes of the three-phase impedance source inverters - part i: Classification and review", *IEEE Transactions on Industrial Electronics*, vol. 65, no. 8, pp. 6309–6320, Aug. 2018.

[71] ——, "Modulation schemes of the three-phase impedance source inverters - part II: Comparative assessment", *IEEE Transactions on Industrial Electronics*, vol. 65, no. 8, pp. 6321–6332, Aug. 2018.

[72] A. El Aroudi, R. Haroun, A. Cid-Pastor, K. Abdellah, and L. Martinez-Salamero, "A comparison between static and dynamic performances of a z-source and a dual-stage boost converter under SMC for PV energy applications", in *Energy Procedia*, ser. Mediterranean Green Energy Forum: Proceedings of an International Conference, vol. 42, Elsevier, Nov. 2013, pp. 587–596.

[73] A. F. Filippov, *Differential Equations with Discontinuous Righthand Sides*, F. M. Arscott, Ed., ser. Mathematics and its Applications. Springer, 1988, vol. 18, pp. X, 304.

[74] V. I. Utkin, *Sliding Modes in Control and Optimization*, ser. Communications and Control Engineering. Springer-Verlag, Jan. 1992, pp. XVI, 286.

[75] J. C. Alexander and T. I. Seidman, "Sliding modes in intersecting switching surfaces, II: Hysteresis", *Houston Journal of Mathematics*, vol. 25, no. 1, pp. 185–211, 1998.

[76] M. R. Jeffrey, G. Kafanas, and D. J. W. Simpson, "Jitter in piecewise-smooth dynamical systems with intersecting discontinuity surfaces", *International Journal of Bifurcation and Chaos*, vol. 28, no. 06, pp. 1–22, 2018.

[77] V. Repecho, D. Biel, J. M. Olm, and E. F. Colet, "Switching frequency regulation in sliding mode control by a hysteresis band controller", *IEEE Transactions on Power Electronics*, vol. 32, no. 2, pp. 1557–1569, Feb. 2017.

[78] E. Fossas, R. Grino, and D. Biel, "Quasi-sliding control based on pulse width modulation, zero averaged dynamics and the l2 norm", *Advances in Variable Structure Systems*, pp. 335–344, 2000.

[79] R. R. Ramos, D. Biel, E. Fossas, and F. Guinjoan, "A fixed-frequency quasi-sliding control algorithm: Application to power inverters design by means of FPGA implementation", *IEEE Transactions on Power Electronics*, vol. 18, no. 1, pp. 344–355, Jan. 2003.

[80] R. Strzelecki, M. Adamowicz, N. Strzelecka, and W. Bury, "New type t-source inverter", in *Compatibility and Power Electronics*, May 2009, pp. 191–195.

[81] W. Qian, F. Z. Peng, and H. Cha, "Trans-z-source inverters", *IEEE Transactions on Power Electronics*, vol. 26, no. 12, pp. 3453–3463, Nov. 2011.

[82] S. G. Nersesov, H. Ashrafiuon, and P. Ghorbanian, "On the stability of sliding mode control for a class of underactuated nonlinear systems", in *American Control Conference*, Jun. 2010, pp. 3446–3451.

[83] G. Kafanas, M. R. Jeffrey, and X. Yuan, "Variable structure control for active power decoupling topologies", in *IET International Conference on Power Electronics, Machines and Drives*, Apr. 2016, pp. 1–6.

[84] N. Mohan, T. M. Undeland, and W. P. Robbins, *Power Electronics: Converters, Applications, and Design*, 3rd ed. John Wiley & Sons, 2003, pp. XVII, 802.

[85] R. W. Erickson and D. Maksimovic, *Fundamentals of power electronics*, 2nd ed., ser. Circuits and Systems. New York: Springer, 2001, pp. XXI, 883.

[86] D. Liu, S. J. Hollis, H. C. P. Dymond, N. McNeill, and B. H. Stark, "Design of 370-ps delay floating-voltage level shifters with 30-v/ns power supply slew tolerance", *IEEE Transactions on Circuits and Systems II: Express Briefs*, vol. 63, no. 7, pp. 688–692, Jul. 2016.

[87] H. C. P. Dymond, J. Wang, D. Liu, J. J. O. Dalton, N. McNeill, D. Pamunuwa, S. J. Hollis, and B. H. Stark, "A 6.7-GHz active gate driver for gan FETs to combat overshoot, ringing, and EMI", *IEEE Transactions on Power Electronics*, vol. 33, no. 1, pp. 581–594, Jan. 2018.

[88] R. D. Middlebrook and S. Cuk, "A general unified approach to modelling switching-converter power stages", in *IEEE Power Electronics Specialists Conference*, Jun. 1976, pp. 18–34.

[89] S. Cuk and R. D. Middlebrook, "A general unified approach to modelling switching DC-to-DC converters in discontinuous conduction mode", pp. 36–57, Jun. 1977.

[90] S. Cuk, "Modelling, analysis, and design of switching converters", PhD thesis, California Institute of Technology, Nov. 1977.

[91] A. Girard, G. Pola, and P. Tabuada, "Approximately bisimilar symbolic models for incrementally stable switched systems", *IEEE Transactions on Automatic Control*, vol. 55, no. 1, pp. 116–126, Jan. 2010.

[92] V. I. Utkin, J. Guldner, and J. Shi, *Sliding Mode Control in Electro-Mechanical Systems*, 2nd ed., ser. Automation and Control Engineering. CRC Press, May 2009, vol. 34, pp. XVI, 503.

[93] L. Martinez-Salamero, A. Cid-Pastor, R. Giral, J. Calvente, and V. I. Utkin, "Why is sliding mode control methodology needed for power converters?", pp. 25–31, Sep. 2010.

[94] V. I. Utkin, "Sliding mode control of DC/DC converters", *Journal of the Franklin Institute*, vol. 350, no. 8, pp. 2146–2165, Oct. 2013.

[95] Y. M. Alsmadi, V. I. Utkin, M. A. Haj-ahmed, and L. Xu, "Sliding mode control of power converters: DC/DC converters", *International Journal of Control*, pp. 1–22, Apr. 2017.

[96] A. J. van der Schaft and J. M. H. Schumacher, *An Introduction to Hybrid Dynamical Systems*, ser. Lecture Notes in Control and Information Sciences. London: Springer-Verlag, 2000, vol. 251, pp. XIV, 174.

[97] R. Goebel, R. G. Sanfelice, and A. R. Teel, "Hybrid dynamical systems", *IEEE Control Systems Magazine*, vol. 29, no. 2, pp. 28–93, Apr. 2009.

[98] ——, *Hybrid Dynamical Systems: Modeling, Stability, and Robustness*. Princeton University Press, 2012.

[99] O. Maler, Z. Manna, and A. Pnueli, "From timed to hybrid systems", in *Real-Time: Theory in Practice*, ser. Lecture Notes in Computer Science. Berlin, Heidelberg: Springer, 1992, vol. 600, pp. 447–484.

[100] R. Alur, C. A. Courcoubetis, N. Halbwachs, T. A. Henzinger, P.-H. Ho, X. Nicollin, A. Olivero, J. Sifakis, and S. Yovine, "The algorithmic analysis of hybrid systems", *Theoretical Computer Science*, vol. 138, no. 1, pp. 3–34, Feb. 1995.

[101] C. J. Tomlin, J. Lygeros, and S. S. Sastry, "A game theoretic approach to controller design for hybrid systems", *Proceedings of the IEEE*, vol. 88, no. 7, pp. 949–970, Jul. 2000.

[102] J. Lygeros, G. Pappas, and S. S. Sastry, "An introduction to hybrid systems modeling, analysis, and control", in *Nonlinear Control Network Pedagogical School*, 1999, pp. 307–329.

[103] S. N. Simic, K. H. Johansson, J. Lygeros, and S. S. Sastry, "Towards a geometric theory of hybrid systems", *Dynamics of Continuous, Discrete and Impulsive Systems Series B: Applications and Algorithms*, vol. 12, no. 5-6, pp. 649–687, 2005.

[104] P. Collins, "A trajectory-space approach to hybrid systems", in *International Symposium on Mathematical Theory of Networks and Systems*, Leuven, Belgaium, Jul. 2004.

[105] ——, "Generalised hybrid trajectory spaces", in *International Symposium on Mathematical Theory of Networks and Systems*, Kyoto, Japan, Jul. 2006, pp. 2101–2109.

[106] M. di Bernardo, C. Budd, A. R. Champneys, and P. Kowalczyk, *Piecewise-smooth dynamical systems: theory and applications*, ser. Applied Mathematical Sciences. London: Springer-Verlag, 2008, vol. 163, pp. XXI, 482.

[107] C. Budd, F. Dux, and A. Cliffe, "The effect of frequency and clearance variations on single-degree-of-freedom impact oscillators", *Journal of Sound and Vibration*, vol. 184, no. 3, pp. 475–502, Jul. 1995.

[108] N. S. Namachchivaya and J. H. Park, "Stochastic dynamics of impact oscillators", *Journal of Applied Mechanics*, vol. 72, no. 6, pp. 862–870, Sep. 2004.

[109] H. Dankowicz and J. Jerrelind, "Control of near-grazing dynamics in impact oscillators", *Proceedings: Mathematical, Physical and Engineering Sciences*, vol. 461, no. 2063, pp. 3365–3380, Nov. 2005.

[110] S. W. Shaw, "On the dynamic response of a system with dry friction", *Journal of Sound and Vibration*, vol. 108, no. 2, pp. 305–325, Jul. 1986.

[111] M. R. Jeffrey, "On the mathematical basis of solid friction", *Nonlinear Dynamics*, vol. 81, no. 4, pp. 1699–1716, Sep. 2015.

[112] V. I. Utkin, "Variable structure systems with sliding modes", *IEEE Transactions on Automatic Control*, vol. 22, no. 2, pp. 212–222, Apr. 1977.

[113] J. Y. Hung, W. Gao, and J. C. Hung, "Variable structure control: A survey", *IEEE Transactions on Industrial Electronics*, vol. 40, no. 1, pp. 2–22, Feb. 1993.

[114] D. Liberzon, *Switching in Systems and Control*, ser. Systems & Control: Foundations & Applications. Birkhauser, 2003, pp. XIII, 233.

[115] M. E. Broucke and M. Ganness, "Reach control on simplices by piecewise affine feedback", *SIAM Journal on Control and Optimization*, vol. 52, no. 5, pp. 3261–3286, 2014.

[116] S. R. Sanders and G. C. Verghese, "Lyapunov-based control for switched power converters", *IEEE Transactions on Power Electronics*, vol. 7, no. 1, pp. 17–24, Jan. 1992.

[117] D. Liberzon and A. S. Morse, "Basic problems in stability and design of switched systems", *IEEE Control Systems*, vol. 19, no. 5, pp. 59–70, Oct. 1999.

[118] R. A. DeCarlo, M. S. Branicky, S. Pettersson, and B. Lennartson, "Perspectives and results on the stability and stabilizability of hybrid systems", *Proceedings of the IEEE*, vol. 88, no. 7, pp. 1069–1082, Jul. 2000.

[119] H. Sira-Ramirez, G. Escobar, and R. Ortega, "On passivity-based sliding mode control of switched DC-to-DC power converters", in *IEEE Conference on Decision and Control*, vol. 3, Dec. 1996, pp. 2525–2526.

[120] G. Escobar and H. Sira-Ramirez, "A passivity based-sliding mode control approach for the regulation of power factor precompensators", in *IFAC Symposium on Nonlinear Control Systems Design*, ser. IFAC Proceedings Volumes, vol. 31, Jul. 1998, pp. 529–534.

[121] ——, "A passivity based-sliding mode control approach for the regulation of power factor precompensators", in *IEEE Conference on Decision and Control*, vol. 3, Dec. 1998, pp. 2423–2424.

[122] M. Senesky, G. Eirea, and T. J. Koo, "Hybrid modelling and control of power electronics", in *Hybrid Systems: Computation and Control*, O. Maler and A. Pnueli, Eds., ser. Lecture Notes in Computer Science. Berlin, Heidelberg: Springer, Mar. 2003, vol. 2623, pp. 450–465.

[123] Y. Niu, Y. Gao, S. Guo, X. Lin-Shi, and B. Allard, "Sliding mode controller for switching mode power supply", in *Life System Modeling and Intelligent Computing*, ser. Lecture Notes in Computer Science. Berlin, Heidelberg: Springer, Jan. 2010, vol. 6328, pp. 416–424.

[124] H. Sira-Ramirez, "Sliding motions in bilinear switched networks", *IEEE Transactions on Circuits and Systems*, vol. 34, no. 8, pp. 919–933, Aug. 1987.

[125] ——, "A geometric approach to pulse-width modulated control in nonlinear dynamical systems", *IEEE Transactions on Automatic Control*, vol. 34, no. 2, pp. 184–187, Feb. 1989.

[126] E. M. Navarro-Lopez, D. Cortes, and C. Castro, "Design of practical sliding-mode controllers with constant switching frequency for power converters", *Electric Power Systems Research*, vol. 79, no. 5, pp. 796–802, Mar. 2009.

[127] D. Biel Sole and E. Fossas Colet, "SMC applications in power electronics", in *Variable Structure Systems: from principles to implementation*, ser. Control, Robotics & Sensors. Institution of Engineering and Technology, 2004, pp. 265–294.

[128] G. Spiazzi and P. Mattavelli, "Sliding-mode control of switched-mode power supplies", in *The Power Electronics Handbook*, T. L. Skvarenina, Ed., ser. Industrial Electronics. CRC Press, 2018, pp. 1–23.

[129] S.-C. Tan, Y. M. Lai, M. K. H. Cheung, and C. K. Tse, "On the practical design of a sliding mode voltage controlled buck converter", *IEEE Transactions on Power Electronics*, vol. 20, no. 2, pp. 425–437, Mar. 2005.

[130] S.-C. Tan, Y. M. Lai, and C. K. Tse, "A unified approach to the design of PWM-based sliding-mode voltage controllers for basic DC-DC converters in continuous conduction mode", *IEEE Transactions on Circuits and Systems I: Regular Papers*, vol. 53, no. 8, pp. 1816–1827, Aug. 2006.

[131] J.-F. Tsai and Y.-P. Chen, "Sliding mode control and stability analysis of buck DC-DC converter", *International Journal of Electronics*, vol. 94, no. 3, pp. 209–222, 2007.

[132] S.-C. Tan, Y. M. Lai, and C. K. Tse, "General design issues of sliding-mode controllers in DC-DC converters", *IEEE Transactions on Industrial Electronics*, vol. 55, no. 3, pp. 1160–1174, Mar. 2008.

[133] M. R. Jeffrey, *Hidden Dynamics: The Mathematics of Switches, Decisions and Other Discontinuous Behaviour*. Springer International Publishing, 2018, pp. XVIII, 521.

[134] Y. A. Kuznetsov, S. Rinaldi, and A. Gragnani, "One-parameter bifurcations in planar filippov systems", *International Journal of Bifurcation and Chaos*, vol. 13, no. 08, pp. 2157–2188, 2003.

[135] G. Teschl, *Ordinary Differential Equations and Dynamical Systems*, ser. Graduate studies in mathematics. American Mathematical Society, 2012, vol. 140, pp. XIV, 353.

[136] J. C. Alexander and T. I. Seidman, "Sliding modes in intersecting switching surfaces, i: Blending", *Houston Journal of Mathematics*, vol. 24, no. 3, pp. 545–569, 1998.

[137] L. Dieci and L. Lopez, "Sliding motion on discontinuity surfaces of high co-dimension. a construction for selecting a filippov vector field", *Numerische Mathematik*, vol. 117, no. 4, pp. 779–811, Feb. 2011.

[138] L. Dieci, C. Elia, and L. Lopez, "A filippov sliding vector field on an attracting co-dimension 2 discontinuity surface, and a limited loss-of-attractivity analysis", *Journal of Differential Equations*, vol. 254, no. 4, pp. 1800–1832, Dec. 2013.

[139] L. Dieci and F. Difonzo, "A comparison of filippov sliding vector fields in codimension 2", *Journal of Computational and Applied Mathematics*, vol. 262, pp. 161–179, May 2014.

[140] L. Dieci, C. Elia, and L. Lopez, "Sharp sufficient attractivity conditions for sliding on a co-dimension 2 discontinuity surface", *Mathematics and Computers in Simulation*, vol. 110, pp. 3–14, Apr. 2015.

[141] L. Dieci and C. Elia, "Piecewise smooth systems near a co-dimension 2 discontinuity manifold: Can one say what should happen?", *Discrete and Continuous Dynamical Systems - S*, vol. 9, no. 4, pp. 1039–1068, 2016.

[142] L. Dieci, "Sliding motion on the intersection of two manifolds: Spirally attractive case", *Communications in Nonlinear Science and Numerical Simulation*, vol. 26, no. 1, pp. 65–74, Sep. 2015.

[143] L. Dieci and F. Difonzo, "On the inverse of some sign matrices and on the moments sliding vector field on the intersection of several manifolds: Nodally attractive case", *Journal of Dynamics and Differential Equations*, vol. 29, no. 4, pp. 1355–1381, Dec. 2017.

[144] C. Edwards and S. K. Spurgeon, *Sliding Mode Control: Theory And Applications*, ser. Series in Systems and Control. CRC Press, Aug. 1998, pp. XVI, 237.

[145] G. Bartolini, A. Ferrara, and E. Usai, "Chattering avoidance by second-order sliding mode control", *IEEE Transactions on Automatic Control*, vol. 43, no. 2, pp. 241–246, Feb. 1998.

[146] Y. Feng, F. Han, and X. Yu, "Chattering free full-order sliding-mode control", *Automatica*, vol. 50, no. 4, pp. 1310–1314, Apr. 2014.

[147] F. Zare, "EMI issues in modern power electronic systems", *The IEEE EMC Society Newsletters*, vol. 221, pp. 53–58, 2009.

[148] W. Gao and J. C. Hung, "Variable structure control of nonlinear systems: A new approach", *IEEE Transactions on Industrial Electronics*, vol. 40, no. 1, pp. 45–55, Feb. 1993.

[149] R. Venkataramanan, "Sliding mode control of power converters", PhD thesis, California Institute of Technology, May 1986.

[150] H. E. Rose, *Linear Algebra: A Pure Mathematical Approach*. Birkhauser Basel, 2002, pp. XIV, 250.

[151] M. R. Jeffrey, "Dynamics at a switching intersection: Hierarchy, isonomy, and multiple sliding", *SIAM Journal on Applied Dynamical Systems*, vol. 13, no. 3, pp. 1082–1105, Jul. 2014.

[152] J. Anderson and F. Z. Peng, "A class of quasi-z-source inverters", in *IEEE Industry Applications Society Annual Meeting*, Oct. 2008, pp. 1–7.

[153] ——, "Four quasi-z-source inverters", in *IEEE Power Electronics Specialists Conference*, Jun. 2008, pp. 2743–2749.

[154] D. Vinnikov and I. Roasto, "Quasi-z-source-based isolated DC/DC converters for distributed power generation", *IEEE Transactions on Industrial Electronics*, vol. 58, no. 1, pp. 192–201, Jan. 2011.

[155] A. Chub, D. Vinnikov, F. Blaabjerg, and F. Z. Peng, "A review of galvanically isolated impedance-source DC–DC converters", *IEEE Transactions on Power Electronics*, vol. 31, no. 4, pp. 2808–2828, Apr. 2016.

[156] F. Evran and M. T. Aydemir, "Z-source-based isolated high step-up converter", *IET Power Electronics*, vol. 6, no. 1, pp. 117–124, Jan. 2013.

[157] M. Shen, Q. Tang, and F. Z. Peng, "Modeling and controller design of the z-source inverter with inductive load", in *IEEE Power Electronics Specialists Conference*, Jun. 2007, pp. 1804–1809.

[158] C. J. Gajanayake, D. M. Vilathgamuwa, and P. C. Loh, "Development of a comprehensive model and a multiloop controller for z-source inverter DG systems", *IEEE Transactions on Industrial Electronics*, vol. 54, no. 4, pp. 2352–2359, Aug. 2007.

[159] G. Sen and M. E. Elbuluk, "Voltage and current-programmed modes in control of the z-source converter", *IEEE Transactions on Industry Applications*, vol. 46, no. 2, pp. 680–686, Mar. 2010.

[160] O. Ellabban, J. Van Mierlo, and P. Lataire, "Control of a bidirectional z-source inverter for electric vehicle applications in different operation modes", *Journal of Power Electronics*, vol. 11, no. 2, pp. 120–131, 2011.

[161] ——, "A DSP-based dual-loop peak DC-link voltage control strategy of the z-source inverter", *IEEE Transactions on Power Electronics*, vol. 27, no. 9, pp. 4088–4097, Sep. 2012.

[162] Y. Tang, S. Xie, and C. Zhang, "Feedforward plus feedback control of the improved z-source inverter", in *IEEE Energy Conversion Congress and Exposition*, Sep. 2009, pp. 783–788.

[163] X. Ding, Z. Qian, S. Yang, B. Cuil, and F. Z. Peng, "A direct DC-link boost voltage PID-like fuzzy control strategy in z-source inverter", in *IEEE Power Electronics Specialists Conference*, Jun. 2008, pp. 405–411.

[164] S. Yang, X. Ding, F. Zhang, F. Z. Peng, and Z. Qian, "Unified control technique for z-source inverter", in *IEEE Power Electronics Specialists Conference*, Jun. 2008, pp. 3236–3242.

[165] S. K. Spurgeon, "Sliding mode control: A tutorial", in *European Control Conference*, Jun. 2014, pp. 2272–2277.

[166] C. Cortes and V. Vapnik, "Support-vector networks", *Machine Learning*, vol. 20, no. 3, pp. 273–297, Sep. 1995.

[167] P. Mattavelli, L. Rossetto, G. Spiazzi, and P. Tenti, "General-purpose sliding-mode controller for DC/DC converter applications", in *IEEE Power Electronics Specialists Conference*, Jun. 1993, pp. 609–615.

[168] S. K. Mazumder, A. H. Nayfeh, and D. Borojevic, "Robust control of parallel DC-DC buck converters by combining integral-variable-structure and multiple-sliding-surface control schemes", *IEEE Transactions on Power Electronics*, vol. 17, no. 3, pp. 428–437, May 2002.

[169] W.-T. Yan, C. N.-M. Ho, H. S.-H. Chung, and K. T. K. Au, "Fixed-frequency boundary control of buck converter with second-order switching surface", *IEEE Transactions on Power Electronics*, vol. 24, no. 9, pp. 2193–2201, Sep. 2009.

[170] S.-C. Tan, Y. M. Lai, C. K. Tse, and M. K. H. Cheung, "Adaptive feedforward and feedback control schemes for sliding mode controlled power converters", *IEEE Transactions on Power Electronics*, vol. 21, no. 1, pp. 182–192, Jan. 2006.

[171] V. Repecho, D. Biel, and E. Fossas, "Fixed switching frequency sliding mode control using an hysteresis band controller", in *International Workshop on Variable Structure Systems (VSS)*, Jun. 2014, pp. 1–6.

[172] S. Guo, L.-S. Xuefang, B. Allard, Y. Gao, and Y. Ruan, "Digital sliding-mode controller for high-frequency DC/DC SMPS", *IEEE Transactions on Power Electronics*, vol. 25, no. 5, pp. 1120–1123, May 2010.

[173] E. Vidal-Idiarte, G. Garcia, L. Martinez-Salamero, A. Marcos-Pastor, and A. Cid-Pastor, "Discrete-time sliding-mode-based digital pulse width modulation control of a boost converter", *IET Power Electronics*, vol. 8, no. 5, pp. 708–714, May 2015.

[174] F. E. Hoyos Velasco, N. T. Garcia, and Y. A. Garces Gomez, "Adaptive control for buck power converter using fixed point inducting control and zero average dynamics strategies", *International Journal of Bifurcation and Chaos*, vol. 25, no. 4, Apr. 2015.

[175] A. Leon-Masich, H. Valderrama-Blavi, J. M. Bosque-Moncusi, J. Maixe-Altes, and L. Martinez-Salamero, "Sliding-mode-control-based boost converter for high-voltage low-power applications", *IEEE Transactions on Industrial Electronics*, vol. 62, no. 1, pp. 229–237, Jan. 2015.

[176] A. G. Bondarev, S. A. Bondarev, N. E. Kostyleva, and V. I. Utkin, "Sliding modes in systems with asymptotic state observers", Russian, *Automation and Remote Control*, vol. 46, pp. 679–684, 6 Oct. 1985. [Online]. Available: http://mi.mathnet.ru/eng/at7028.

[177] A. Soto, P. Alou, and J. A. Cobos, "Non-linear digital control breaks bandwidth limitations", in *IEEE Applied Power Electronics Conference and Exposition*, May 2006, pp. 724–730.

[178] S. C. Huerta, P. Alou, J. A. Oliver, O. Garcia, J. A. Cobos, and A. M. Abou-Alfotouh, "Nonlinear control for DC-DC converters based on hysteresis of the c_OUT current with a frequency loop to operate at constant frequency", *IEEE Transactions on Industrial Electronics*, vol. 58, no. 3, pp. 1036–1043, Mar. 2011.

[179] S. C. Huerta, A. Soto, P. Alou, J. A. Oliver, O. Garcia, and J. A. Cobos, "Advanced control for very fast DC-DC converters based on hysteresis of the c_out current", *IEEE Transactions on Circuits and Systems I: Regular Papers*, vol. 60, no. 4, pp. 1052–1061, Apr. 2013.

[180] F. Gouaisbaut, W. Perruquetti, and J.-P. Richard, "A sliding mode control for linear systems with input and state delays", in *IEEE Conference on Decision and Control*, vol. 4, Nov. 1999, pp. 4234–4239.

[181] X. Li, X. Yu, and Q.-L. Han, "Stability analysis of second-order sliding mode control systems with input-delay using poincare map", *IEEE Transactions on Automatic Control*, vol. 58, no. 9, pp. 2410–2415, Sep. 2013.

[182] K. Sozanski, *Digital Signal Processing in Power Electronics Control Circuits*, 2nd ed., ser. Power Systems. London: Springer-Verlag, 2017, pp. XXI, 340.

[183] S. H. Zak, J. D. Brehove, and M. J. Corless, "Control of uncertain systems with unmodeled actuator and sensor dynamics and incomplete state information", *IEEE Transactions on Systems, Man, and Cybernetics*, vol. 19, no. 2, pp. 241–257, Mar. 1989.

[184] Y. Shtessel, C. Edwards, L. Fridman, and A. Levant, *Sliding Mode Control and Observation*, ser. Control Engineering. New York: Springer, 2013, pp. XVII, 356.

Appendices

Appendix A

Simulation software

A simulator of hybrid automate was designed for the simulations used in this thesis. The code and instructions on how to run the simulations can be found in the following web address.

Tans-Z-source converter: https://gitlab.com/gkaf/trans-Z-source,

Buck converter with sensors: https://gitlab.com/gkaf/buck-with-sensors.